Beam Space Signal Processing for Directional Transmission Phased Arrays

Ruiting Yang

Thesis submitted for the degree of

Doctor of Philosophy

School of Electrical & Electronic Engineering
Faculty of Engineering, Computer & Mathematical Sciences
The University of Adelaide
Adelaide, South Australia

June 2018

Contents

Abstract

Beam space (BS) processing is a spatial signal processing technique using beam output data. For example, the BS beamformer applies weights to a set of beam outputs, which are then summed to form a new output. In this way, advanced optimum spatial signal processing algorithms can be applied when the element outputs are not accessible. However, existing BS processing algorithms are based on a model that assumes a passive receiving system or for active systems that the transmission is omni-directional and can be ignored. When the transmission is directional as is typical for phased arrays that electronically scan over a given sector, such methods are mismatched and result in significant performance degradation.

The first part of this thesis presents a new formulation of BS processing for the scenario where relatively narrow beams are directionally transmitted and received and then scanned over a given sector of interest. New formulae are developed for this case and the performance of the new formulae is analysed.

The second part of this thesis is focused on the properties of directional transmission BS processing. When beams are formed in a sector of interest, problems related to the region outside the sector of interest are investigated, including analysing the output in the direction-of-arrival (DOA) of an interference lying outside the sector of interest, removing the high response in the region outside the sector of interest and mitigating a spurious output peak caused by the interference. Additionally, phased array errors cause the array response to be different from that being assumed and can seriously degrade the performance of the BS beamformer, a robust BS beamformer is developed to improve the tolerance to errors. Cramér–Rao Bounds (CRB) for DOA estimation for the directional transmission BS are derived and compared with the omni-directional element space (ES) and BS cases. The performance of the optimum BS beamformer for a non-stationary scatterer is evaluated.

The third part of this thesis deals with BS processing for coherent signals. The commonly used subarray algorithms for removing coherence in the ES processing cannot be applied to the BS problem directly. A method of reconstructing the ES signal subspace is developed for the omni-directional transmission BS case, and then existing methods, such as MUSIC, in ES processing can be applied. For the directional transmission BS case, a method is proposed to reconstruct a matrix which is a summation of weighted self-outer products of ES signal steering vectors, and this matrix allows the DOAs of coherent signals to be estimated regardless of coherence.

Finally, the developed algorithms are investigated by carrying out spatial processing on real experimental data containing stationary targets.

Declaration

I certify that this work contains no material which has been accepted for the award of any other degree or diploma in my name, in any university or other tertiary institution and, to the best of my knowledge and belief, contains no material previously published or written by another person, except where due reference has been made in the text. In addition, I certify that no part of this work will, in the future, be used in a submission in my name, for any other degree or diploma in any university or other tertiary institution without the prior approval of the University of Adelaide and where applicable, any partner institution responsible for the joint-award of this degree.

I give consent to this copy of my thesis, when deposited in the University Library, being made available for loan and photocopying, subject to the provisions of the Copyright Act 1968. I also give permission for the digital version of my thesis to be made available on the web, via the University's digital research repository, the Library Search and also through web search engines, unless permission has been granted by the University to restrict access for a period of time.

I acknowledge the support I have received for my research through the provision of an Australian Government Research Training Program Scholarship.

_____ _____

Signed Date

Acknowledgements

I would like to express my gratitude to those people who have given me support and assistance throughout my time as a PhD student.

First of all, I would like to express my deepest sense of gratitude and appreciation to my principal supervisor, Professor Douglas Gray. He keeps looking after me during these years in Adelaide. Several years ago, I finished my master by research degree under Doug's supervision and then worked for him. During the journey of this PhD, he guided me into this new area and spent a lot of time to teach me knowledge and skills for array processing. His ability to grasp the mathematical essence, insightful questions, knowledge, experience and invaluable advice keep me on the right track. It would have been impossible to finish this thesis without his constant guidance, encouragement, understanding and support.

Many thanks to my co-supervisor, Dr Waddah Al-Ashwal, whose knowledge and advice were great benefits for this thesis. He moved to another department of the University of Adelaide, but the continuous help and support he provided were more than I expected.

Many thanks also go to another co-supervisor, Dr Peter May. As an expert in radar meteorology, he always provides advice and insight from the aspect of weather applications. Unfortunately, not much work has been completed for weather radar applications in this thesis, but his insightful advice and careful review are valuable contributions. It is much appreciated that he offered the opportunity to visit Bureau of Meteorology and meet famous academics in the weather radar field.

Thanks to the team were involved in the ARC linkage weather radar project. Most ideas of this research were driven, inspired, and eventually tested by processing the experimental data collected by using the Phase Tilt Weather Radar for this project.

Thanks to other staff and students in the University of Adelaide Radar Research Centre, their kind help and suggestions were so beneficial. Those interesting discussions and leisure activities were so pleasant.

Finally, thanks must go to my family members, their consistent encouragement, understanding, patience and support helped my study so much. Their love is always the force driving me forward.

Publication

R. Yang, D. A. Gray and W. A. Al-Ashwal, "Formulation of optimum beam space processing for directional transmission phased array systems,"*2014 8th International Conference on Signal Processing and Communication Systems (ICSPCS)*, Gold Coast, QLD, 2014.

List of Figures

List of Tables

List of Symbols

Functions and Operators

$(\cdot)^*$	complex conjugate
$(\cdot)^H$	Hermitian transpose
$(\cdot)^T$	transpose
$()^+$	Moore-Penrose pseudoinverse
$\lfloor \cdot \rfloor$	integer part of the expression
$\circ$	Hadamard product
$\otimes$	Kronecker product
$\frac{d\boldsymbol{v}(\theta)}{d\theta}$	the first order derivative of $\boldsymbol{v}(\theta)$ respect to θ
$\frac{\partial \boldsymbol{v}(\theta_{sl})}{\partial \theta_{sl}}$	the first order partial derivative of $\boldsymbol{v}(\theta_{sl})$ regards to θ_{sl}
$\det(\cdot)$	determinant of a matrix
$\mathrm{E}\{\}$	expectation or ensemble averaging
$\exp(\cdot)$	exponential function
$ln(\cdot)$	natural logarithm, logarithm to the base e
$\mathrm{rank}(\cdot)$	rank of a matrix
$Re[\cdot]$	real part of a complex expression
$span\{\cdot\}$	form a space spanned by vectors
$\mathrm{tr}[\cdot]$	trace of a matrix
$\mathrm{unif}(\cdot)$	uniform distribution
$\mathrm{vec}\,[\cdot]$	stack the columns of a matrix on top of each other

Variables

α	Hermitian product of $\boldsymbol{w}(\theta_{s1})$ and $\boldsymbol{h}(\theta_{s2})$
$\beta(\theta_{s1}, \theta_{s2})$	Hermitian product of $\boldsymbol{h}(\theta_{s1})$ and $\boldsymbol{h}(\theta_{s2})$
$\beta_d(\theta_{s1}, \theta_{s2})$	Hermitian product of $\boldsymbol{v_y}(\theta_{s1})$ and $\boldsymbol{v_y}(\theta_{s2})$
γ	amplitude of correlation coefficient between two signals
δ_k	position error at the *k*-th element
ϵ	Maximum squared Euclidean distance from the assumed steering vector in an uncertainty set
θ	azimuthal angle
$\Delta\theta$	azimuthal angle difference of a non-stationary scatter between two adjacent pulses
Θ_s	DOAs of source signals
$\hat{\Theta}_s$	estimated DOAs of signals
Θ_B	azimuthal angles of transmit beam centres
Θ_{sc}	DOAs of coherent signals
Θ_{su}	DOAs of uncorrelated signals
λ	wavelength of transmit signal
λ_i	the *i*-th eigenvalue of ES covariance matrix
λ_{yi}	the *i*-th eigenvalue of BS covariance matrix
$\boldsymbol{\Lambda}$	A diagonal matrix with eigenvalue of ES covariance matrix on the diagonal
$\boldsymbol{\Lambda_y}$	A diagonal matrix with eigenvalue of BS covariance matrix on the diagonal
μ	Langrage multiplier
μ_k	complex gain error on the *k*-th element
ρ_{ij}	correlation coefficient between two signals $s_i(t)$ and $s_j(t)$

ρ_l'	weighted correlation coefficient in (6-26)
σ_I^2	power of interference
σ_n^2	power of noise
σ_s^2	combined power of a group of coherent signals
σ_{si}^2	power of the i-th signal
$\boldsymbol{\Sigma}$	Singular values
$\boldsymbol{\varphi}$	a vector, whose l-th element is $\pi sin\theta_{sl}$
$e^{j\varphi}$	random phase shift
ϕ_m	difference between the actual and assumed MRA of the m-th beam
$\omega(\theta)$	constrained optimisation function for MVDR
$B(\theta_1, \theta_2)$	Hermitian product of directional transmission BS steering vectors $\boldsymbol{v_y}(\theta_1)$ and $\boldsymbol{v_y}(\theta_2)$
$B_H\left(\theta_{1,}\, \theta_2\right)$	squared Hermitian product of $\boldsymbol{h}(\theta_1)$ and $\boldsymbol{h}(\theta_2)$
$bp(\theta', \theta)$	beam pattern at θ' when the MRA is at a look angle θ
$bp_l(\theta_m)$	beam pattern of the m-th transmitted beam at the DOA of the l-th signal
BW	beam width
c	number of constraints for LCMV
$\boldsymbol{C}$	matrix of c LCMV constraints
$\boldsymbol{C_e}(\Theta_s)$	covariance matrix of estimation errors
$\boldsymbol{C}_{CR}(\Theta_s)$	ES CRB for estimating Θ_s
$\boldsymbol{C}_{CR-\boldsymbol{h}}(\Theta_s)$	omni-directional transmission BS CRB for estimating Θ_s
$\boldsymbol{C}_{CR-\boldsymbol{Vy}}(\Theta_s)$	directional transmission BS CRB for estimating Θ_s
d	separation space between receivers
$\boldsymbol{d}_l$	the l-th column of $\boldsymbol{D}$, the first order partial derivative of ES steering vector, $\boldsymbol{v}(\theta_{sl})$, regards to θ_{sl}
$\boldsymbol{D}$	the first order derivative of $\boldsymbol{V_s}$

$\boldsymbol{D_H}$	the first order derivative of $\boldsymbol{H}$
$\boldsymbol{D_{Vy}}(\Theta_s)$	the first order derivative of $\boldsymbol{V_y}(\Theta_s)$
$\boldsymbol{e}$	a vector contains errors occur at different elements
$\boldsymbol{E_{IS}}$	oblique projection matrix
$\boldsymbol{E_n}$	noise subspace
$\boldsymbol{E_s}$	signal subspace
$\boldsymbol{\mathcal{F}}$	Fisher's information matrix
$\boldsymbol{g}$	vector of constraint values
$G(\theta)$	gain of conventional BS beamformer at θ
$\boldsymbol{h}(\theta)$	omni-directional transmission beam space steering vector at θ
$\boldsymbol{h}'(\theta)$	SFS BS steering vector
$\dot{\boldsymbol{h}}(\theta_{sl})$	the l-th column of $\boldsymbol{D_H}$
$\boldsymbol{h}(\Theta_{su})$	the uncorrelated signal vectors
$\boldsymbol{h_s}$	omni-directional transmission generalised coherent BS steering vector
$\boldsymbol{h_{sc}}$	omni-directional transmission generalised coherent BS steering vector(s)
$\boldsymbol{H}$	A matrix whose columns are the omni-directional BS steering vectors of signals
$H(\theta)$	squared Euclidean norm of BS steering vector $\boldsymbol{h}(\theta)$
H_c	the approximated constant value of $H(\theta)$
$H_y(\theta_s)$	squared Hermitian product of $\boldsymbol{h}(\theta_s)$ and $\boldsymbol{v_y}(\theta_s)$
$\boldsymbol{i}$	interference(s)
$\boldsymbol{I}$	identity matrix
$\boldsymbol{\Delta I}$	diagonal loading in a manner of identity matrix
$\boldsymbol{J}$	exchange matrix
$k_y(\theta)$	squared Euclidean norm of BS steering vector $\boldsymbol{v_y}(\theta)$

K	number of receivers
K_y	an approximated constant value of $k_y(\theta)$ in the sector of interest
L	number of signals
$L(\Theta_s)$	likelihood function
Lc	number of groups of coherent signals
$\boldsymbol{m_s}$	mean of signal component in receiver outputs
M	number of beams
$\boldsymbol{n}$	receiver noise
N	number of pulses (samples), number of averaging in spatial smoothing
N_e	number of extra virtual beams
$p_{\boldsymbol{x}\mid\Theta_s}$	probability density for a single snapshot vector
$p_{CB-ES}(\theta)$	output power of conventional ES beamformer at θ
$p_{MUSIC-BS}(\theta)$	BS MUSIC output at θ
$p_{MUSIC-ES}(\theta)$	ES MUSIC output at θ
$p_{MUSIC-Q_s}(\theta)$	MUSIC output at θ using singular vectors of $\boldsymbol{Q_s}$
$p_{MVDR-BS}(\theta)$	output power of optimum BS beamformer at θ
$p_{MVDR-ES}(\theta)$	output power of optimum ES beamformer at θ
$\boldsymbol{P}_{\boldsymbol{V_I}}^{\perp}$	orthogonal projection to $\boldsymbol{V_I}$
$\boldsymbol{q}_1(\theta_m)$	the principal eigenvector of $\boldsymbol{R_x}(\theta_m)$
$\boldsymbol{q}_{1s}$	the principal eigenvector the stacked ES covariance matrix
$\boldsymbol{q}_i$	eigenvector associated with the i-th eigenvalue of ES covariance matrix
$\boldsymbol{q}_{yi}$	eigenvector associated with the i-th eigenvalue of BS covariance matrix
$\boldsymbol{q}_{yc1}$	the principal eigenvector of BS coherent signal covariance matrix
$\boldsymbol{Q_s}$	summation of weighted self-outer products of ES signal steering vectors

$\widetilde{\boldsymbol{Q}}_{\boldsymbol{s}}$	estimated $\boldsymbol{Q}_{\boldsymbol{s}}$
$\boldsymbol{Q}_{\boldsymbol{y}}$	unitary matrix contains eigenvectors of BS covariance matrix
r_b	ratio between the target's location change and beam width
$\boldsymbol{R}_{FB}$	forward/backward spatially smoothed covariance matrix
$\widetilde{\boldsymbol{R}}_{\boldsymbol{n}}$	reconstructed ES noise covariance matrix
$\boldsymbol{R}_{\boldsymbol{s}}$	source signal covariance matrix
$\widehat{\boldsymbol{R}}_{\boldsymbol{s}}$	estimate of the source covariance matrix
$\boldsymbol{R}'_{\boldsymbol{s}}(\theta_m)$	source signal covariance matrix weighted by the beam patterns of the m-th transmission beam
$\boldsymbol{R}_{\boldsymbol{sc}}$	coherent source signal covariance matrix
$\boldsymbol{R}_{\boldsymbol{su}}$	uncorrelated source signal covariance matrix
$\boldsymbol{R}_{SS}$	forward spatially smoothed covariance matrix
$\boldsymbol{R}_u^f$	full rank $L \times L$ matrix generated by spatial smoothing
$\boldsymbol{R}_{\boldsymbol{x}}$	ES covariance matrix
$\boldsymbol{R}_{\boldsymbol{x}}(\theta_m)$	ES covariance matrix at the m-th directionally transmitted beam
$\boldsymbol{R}_{\boldsymbol{x}}^{(i)}$	ES covariance matrix of the i-th subarray
$\widetilde{\boldsymbol{R}}_{\boldsymbol{x}}$	reconstructed ES covariance matrix using matrix inverse
$\widetilde{\boldsymbol{R}}'_{\boldsymbol{x}}$	reconstructed ES covariance matrix from the BS principal eigenvector
$\overline{\boldsymbol{R}}_{\boldsymbol{x}}$	average over ES covariance matrices at different directional transmit beams
$\boldsymbol{R}_{\boldsymbol{xb}}^{(i)}$	covariance matrix of the i-th backward subarray
$\widetilde{\boldsymbol{R}}_{\boldsymbol{xc}}$	reconstructed ES coherent signal covariance matrix from the BS principal eigenvector
$\boldsymbol{R}_{\boldsymbol{xs}}$	stacked ES covariance matrix
$\boldsymbol{R}_{\boldsymbol{y}}$	BS covariance matrix
$\boldsymbol{R}_{\boldsymbol{y}(1)}$	BS covariance matrix for a single signal

$\boldsymbol{R}_{\boldsymbol{y}(1,2)}$	BS covariance matrix for two signals
$\boldsymbol{R}_{\boldsymbol{y}(2)}$	BS covariance matrix when only the second signal is incident
$\boldsymbol{R}_{\boldsymbol{y}\_1}$	BS covariance matrix for a non-stationary scatterer only
$\boldsymbol{R}_{\boldsymbol{y}\_2}$	BS covariance matrix for a stationary scatterer only
$\boldsymbol{R}_{\boldsymbol{y}-\mathrm{aug}}$	BS covariance matrix with virtual beams
$\boldsymbol{R}_{\boldsymbol{y}(\bar{l})}$	BS covariance matrix without the returns from the *l*-th scatterer
$\boldsymbol{R}_{\boldsymbol{yI}}$	Beam space covariance for a model with interference(s)
$\boldsymbol{R}_{\boldsymbol{y}(I)}$	BS covariance matrix for a single interference only
$\boldsymbol{R}_{\boldsymbol{y}}^{\boldsymbol{\perp I}}$	interference orthogonal projected covariance matrix
$\boldsymbol{R}_{\boldsymbol{yn}}$	directional transmission BS noise covariance matrix
$\boldsymbol{R}_{\boldsymbol{y}-ob}$	BS covariance matrix after oblique projection
$\boldsymbol{R}_{\boldsymbol{y}sfs}$	SFS BS covariance matrix
$\boldsymbol{s}$	source signals
$s_{cl}(t)$	part of a mixed signal and is correlated to the transmitted signal
$s_{ul}(t)$	part of a mixed signal and is uncorrelated to the transmitted signal
$s_T(\theta_m, \theta_{sl})$	signal transmitted to θ_{sl} through the sidelobe leakage of a beam whose MRA is at θ_m
$\boldsymbol{s}_{TR}(\theta_m, \theta_{sl})$	array outputs due to a reflected signal at θ_{sl}, which is transmitted through a sidelobe leakage of a beam whose MRA is at θ_m
t	time moment
U	linear transformation between stacked ES and BS covariance matrices
$\boldsymbol{U}_{\boldsymbol{sv}}$	matrix contains the left singular vectors
$\boldsymbol{v}(\theta)$	ES ULA steering vector at angle of θ
$\acute{\boldsymbol{v}}(\theta_{sl})$	ES steering vector at θ_{sl} but with errors
$\boldsymbol{v}_{\boldsymbol{p}}(\theta)$	stacked ES steering vector

$\boldsymbol{v_s}$	generalised coherent steering vector in ES
$\widetilde{\boldsymbol{v}}_{\boldsymbol{s}}$	reconstructed generalised coherent steering vector in ES
$\widetilde{\boldsymbol{v}}_{\boldsymbol{ss}}$	reconstructed stacked generalised coherent steering vector in ES
$\boldsymbol{v_x}(\theta_{si}, \theta_m)$	ES steering vector at θ_{si} when a signal is directionally transmitted by a beam whose MRA is at θ_m
$\boldsymbol{v_y}(\theta)$	directional transmission BS steering vector at θ
$\acute{\boldsymbol{v}}_{\boldsymbol{y}}(\theta_{sl})$	directional transmission BS steering vector at directional θ_{sl} but with errors
$\boldsymbol{v_{y-aug}}(\theta)$	directional transmission BS steering vector with virtual beams
$\boldsymbol{v_{ys}}$	generalised coherent signal steering vector in directional transmission BS
$\boldsymbol{V}$	matrix containing the ES steering vectors at directions of formed beams
$\boldsymbol{V'}$	SFS BS transformation matrix
$\boldsymbol{V_B}(\Theta_B)$	same as $\boldsymbol{V}$, formed beams centres are at Θ_B
$\boldsymbol{V_I}$	matrix contains the BS steering vector(s) for interference(s)
$\boldsymbol{V_s}(\Theta_s)$	matrix contains the ES steering vectors at DOAs
$\boldsymbol{V_{sv}}$	matrix contains the right singular vectors
$\acute{\boldsymbol{V}}_{\boldsymbol{s}}(\Theta_s)$	matrix contains the ES steering vectors at DOAs but with errors
$\boldsymbol{V_s^{(N)}}(\Theta_s)$	matrix containing all the source signal steering vectors in a subarray with N elements
$\boldsymbol{V_{\widehat{s}}}$	subspace to keep in the oblique projection
$\boldsymbol{V_x}(\Theta_s, \theta_m)$	matrix contains steering vectors of DOAs with a directional transmission beam whose centre is at θ_m
$\boldsymbol{V_y}(\Theta_s)$	matrix contains directional transmission BS steering vectors at different DOAs
$\boldsymbol{w}(\theta)$	beamformer weight vector at θ
$\boldsymbol{w_{MVDR-BS}}(\theta)$	optimum BS beamformer weights vector at θ
$\boldsymbol{w_{MVDR-ES}}(\theta)$	optimum ES beamformer weights vector at θ

$\boldsymbol{x}(t)$	element output vector at t
x_k	element output at the k-th element
$\boldsymbol{x}^{(i)}$	element output vector of the i-th subarray
$\boldsymbol{x}_b^{(i)}$	element output vector of the i-th backward subarray
$\boldsymbol{x}_s$	stacked element outputs over different transmit beam
$\boldsymbol{y}$	output vector of M conventional beams
$y(\theta)$	beamformer output in the direction at θ

Glossary

AIC	Akaike Information Criterion
BS	Beam Space
CRB	Cramér–Rao Bound
CRLB	Cramér–Rao Lower Bound
DOA	Direction-of-Arrival
DSTG	Defence Science and Technology Group
ES	Element Space
FBSS	Forward/Backward Spatial Smoothing
INR	Interference to Noise Ratio
IQ	In-phase and Quadrature
LCMV	Linear Constrained Minimum Variance
MDL	Minimum Description Length
MIMO	Multiple-Input and Multiple-Output
ML	Maximum Likelihood
MRA	Maximum Response Axis
MVDR	Minimum Variance Distortionless Response
PRF	Pulse Repetition Frequency
PTWR	Phase Tilt Weather Radar
RCS	Radar Cross Section
SFS	Sector Focused Stability
SNR	Signal to Noise Ratio

STF	System Test Facility
SVD	Singular Value Decomposition
Tx/Rx	Transmit/Receive
ULA	Uniform Linear Array
UCA	Uniform Circular Array

Chapter 1

Introduction

A signal can represent events, actions, sounds, acoustic or electromagnetic waves and other manners of changes. Different types of passive sensors, such as an antenna or a microphone, can be used to detect and convert the physical parameters or events into a signal and then record the signal waveforms. By using a single sensor, recorded waveforms in the time domain and spectral characteristics in the frequency domain can be used to measure properties of the signal and extract information. However, little spatial information, such as the direction-of-arrival (DOA) of a signal is contained in the data collected by a single sensor. To enhance the signal intensity and capture more spatial information, phased arrays, which normally contain multiple sensors in designed geometric array configurations, were developed and have been widely used since the early part of the 20th century [1].

Array signal processing methods (see [17] and [30]) have been well developed and provide an ability to extract spatial information from received signals, which would never be achieved by using only a single sensor. The major benefits of array processing include enhancing the power of signals from given directions, suppressing noise and clutter – particular interferences from other directions and allowing the directions of both desired signals and unwanted interferences to be estimated.

Array signal processing methods apply designed weights to the array element (sensor) outputs or other quantities derived from the element outputs, such as a covariance matrix, and this is normally called elements space (ES) processing. For example, an ES beamformer applies weights to different element outputs and then sums the weighted outputs as a beamformed output. The weights can be chosen according to different criteria for different purposes, for example, the conventional beamformer aligns the phase difference between elements and the null steering algorithm generates a beam pattern with nulls in given directions.

Alternatively, weights can be applied to the preformed beamformer outputs and the weighted outputs are then summed, this processing method is termed beam space (BS) processing. Different BS methods have been developed and used to achieve similar performance to ES processing, such as maximisation the signal-to-noise ratio (SNR) [25] and direction finding [27], [28] and [29]. Fundamentally, BS processing does not provide better performance than ES processing, but it can be used in cases where the element outputs are not available. Typically this occurs in low cost phased array radar or sonar systems, and also in some cases where only beamformed data has been recorded for post-processing. Additionally, some unique advantages are associated with BS processing. For example, when all the signals of interest are contained in one sector of

interest, a reduced dimension BS processing, whose number of beams is smaller than the number of elements, can achieve performance equivalent to that of ES processing but with less computation.

All the BS processing methods in the open literature are based on the assumption that signals incident on the elements of a phased array are generated by other transmitters or omni-directionally transmitted by the phased array itself (transmission with a broad beamwidth is usually considered to be near to omni-directional). Both scenarios lead to the same model, in which the transmission beam pattern is not taken into account in further spatial processing. However, to concentrate the transmission energy and obtain stronger returns, another type of transmission—directional transmission in an angular scanning fashion is widely used in practical phased array applications. The two different types of transmissions are illustrated in Figure 1-1. Omni-directional transmission radiates with a wide beam pattern near to equal energy in different directions over a wide angular region covering the sector of interest; whilst directional transmission with a narrow beam pattern scans across the sector of interest with most of its energy transmitted in the mainlobe and only some weak energy propagates to other directions through sidelobe leakage.

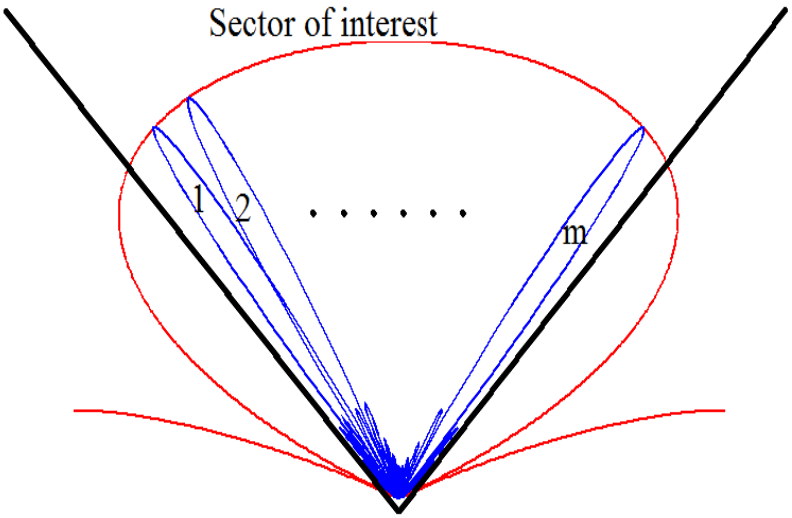

Figure 1-1: Two types of transmissions in phased array applications. The red curve represents an omni-directional transmission beam with a wide beam pattern; the blue curves show directional transmission beams with a narrow beam pattern scanning across a sector of interest.

This thesis focuses on BS spatial signal processing methods, especially for the latter case where the formed transmit/receive beams are directionally transmitted and scanned over a sector of interest. Whilst most of the new results presented in this thesis are for the directional transmission BS case, some gaps in the existing theory for the omni-directional transmission BS problems were identified in the course of the research and so some additional new results in this area are also presented.

1.1 Motivation

This research was initially driven by a project of applying spatial signal processing algorithms to a phase tilt weather radar (PTWR) system developed by Raytheon [94]. To radiate and receive greater power in chosen directions, this system was designed to transmit and receive narrow bandwidth signals in directional beams and only to record conventional beamformer outputs rather than receiver outputs. Typically, directional beams were formed and scanned over a sector of interest. For the post-processing of the recorded data, ES signal processing methods could not be applied and thus BS processing was the best option for spatial signal processing in this project. In this process, some gaps in the BS processing theory were found and became the motivation for this thesis.

1.1.1 Formulation of BS Processing for Directional Transmission Case

Existing standard BS processing formulae fail for directional transmission BS applications due to a mismatch between the omni-directional and directional transmission models. Surprisingly, although the directional transmission is commonly used in phased array operations, to the author's best knowledge, no BS processing method specifically for the directional transmission model has been investigated and developed. Possibly the reason is that the element outputs are available for most current phased array systems and the directional transmission can actually enhance the performance of ES processing, thus no extra modification is required for ES processing formulae. However, the directional transmission BS model is significantly different from that in the omni-directional transmission, and the standard BS processing formulae fail due to the mismatch issue. To solve this problem, new BS processing formulae for the directional transmission BS model are developed in this thesis.

1.1.2 Properties of Directional Transmission BS Processing

The properties of the directional transmission BS processing are not clear, especially for the case that directional transmit/receive beams are scanned over an angular region as a sector of interest. For example, as discussed in [31], [32], [39] and [42], interferences outside the sector of interest are attenuated or ignored in the existing BS processing literature, but little research has been carried out to determine if either the omni-directional or directional transmission forms of BS beamformers work well outside the sector of interest, where no beams are formed. Particular issues, such as if the interference can be detected and estimated by using the beams inside the sector of interest and if the interference would affect the estimation of signals, are addressed in this thesis.

Different types of errors commonly occur when using an imperfectly calibrated phased array, in addition to these errors in ES, errors in the beam directions can occur in BS problems. However, no solid work on increasing the tolerance of BS beamformers to such errors has been found in the literature. The modification of a robust ES beamforming technique for dealing with a variety of system errors to BS processing is proposed in this thesis.

1.1.3 Spatial Signal Processing of Coherent Signals in BS

Most current array processing methods are developed for models containing independent signals only, and coherent or highly correlated signals can seriously degrade the performance of these methods. DOA estimation of spatially coherent signals is a popular research topic in array processing. In ES processing, spatial coherence is normally removed by using decorrelation methods based on the concept of subarrays, such as spatial smoothing methods [47], [49] and [64] or for some special scenarios, such as using wideband signals [58], [59] or a moving array [61], [62].

The current existing ES decorrelation methods can't be directly applied to coherence problems in BS processing, as normally neither element nor beam outputs of subarrays are available. To the best of the author's knowledge, the coherence problem in BS processing is still an outstanding unsolved problem. Although the maximum likelihood method is a universal solution for estimating the DOAs of coherent signals, its high computational requirement makes it a prohibitive approach and quick signal decorrelation techniques together with subspace methods are often preferable. Thus one of the goals of this thesis has been to develop decorrelation methods for estimating the DOAs of coherent signals using subspace methods in both omni-directional and directional transmission BS cases.

1.2 Thesis Outline and Main Contributions

This thesis looks at the specific BS processing problems described in Section 1.1 and includes four parts.

The formulation of directional transmission BS processing algorithms is the main focus of the first part of this thesis. Following a review of the current standard BS processing methods, the directional transmission BS model is introduced. An analysis shows that unsatisfactory performance of applying the standard optimum BS beamformer to the directional transmission case. New formulae for the directional transmission BS processing are developed and presented.

Several properties of the directional transmission BS processing are investigated in the second part of this thesis. In this process, some techniques have been developed to solve unique problems in BS processing.

The third part of this thesis deals with spatially coherent signals in BS processing. An algorithm for reconstructing the ES signal subspace is developed and used together with a spatial smoothing technique to remove coherence for the omni-directional BS cases. A matrix is proposed to represent the coherent signals in the directional transmission BS case. This matrix can be estimated from the principal eigenvector of BS covariance matrix and it allows the DOAs of coherent signals can be estimated by existing subspace methods regardless of the signal coherence.

The final part of this thesis introduces the experiment using PTWR and presents some results of applying the developed BS algorithms to the real experimental data.

To summarise, the main novel contributions of this thesis include:

- **Derived expressions of the directional transmission BS model and developed new BS formulae for this case.**
- **Investigated the properties of the directional transmission BS processing and developed virtual beams and scaling methods to mitigate the high response of optimum BS beamformer in the region outside the sector of interest.**
- **Investigated the reason of a spurious peak of the optimum BS beamformer output power caused by an interference outside the sector of interest and applied oblique projection to eliminate it.**
- **Modified and extended a robust ES beamforming algorithm (robust Capon beamforming) to enhance the optimum BS beamformer tolerance to different types of errors.**
- **Derived CRB for DOA estimation in the directional transmission BS case and comparison with the CRBs for DOA estimation in the omni-directional transmission ES and BS cases.**
- **Developed a technique to reconstruct ES signal subspace from BS signal subspace, which enables the subarray methods to be used to estimate the DOAs of coherent signals in the omni-directional transmission BS case.**
- **Proposed to use a new expression matrix, which is the summation of self-outer products of ES steering vectors, to represent the coherent signals in the directional transmission BS case. This matrix allows the DOAs of coherent signals in the directional transmission case to be estimated regardless the coherence. A method has been developed to estimate the new expression matrix from BS signal subspace.**

1.2.1 Chapter Summaries

Chapter 2 Array Signal Processing Background

This chapter briefly reviews the concept and history of phased arrays and array signal processing. Some key concepts in phased arrays and typical ES array processing algorithms are introduced.

Chapter 3 Standard Beam Space Processing

This chapter reviews the standard BS processing algorithms and some examples are presented to compare the performance of ES and BS approaches. The number of beams required to give satisfactory performance of BS processing is discussed for the case where the beams span the whole angular space and for the other case where beams are only formed in a sector of interest. In case that the interference or an unexpected signal is incident out of the selected sector, the beamformer output power values at DOAs of the in sector signal and out of sector interference are analysed theoretically and numerically.

Chapter 4 Directional Transmission Beam Space Processing

This chapter analyses the mathematical model for both receiver and beam outputs for the directional transmission phased array. The performance degradation of the standard BS processing algorithm when applied to the directional transmission beam outputs, is investigated and quantified. New BS algorithms are derived for this model and the performance is analysed by theoretical analysis and numerical simulations.

The development of BS algorithms for the directional transmission BS processing is one of the major contributions of this thesis.

Chapter 5 Properties of Directional Transmission Beam Space Processing

This chapter investigates properties of the directional transmission BS processing and provides solutions to several unique problems that arise in BS processing. These include:

- A detailed analysis of the performance of BS processing outside the sector of interest.
- Mitigating the high response of the optimum BS beamformer in the region outside the sector of interest.
- Mitigating the spurious peak of the optimum BS beamformer output power when beams are formed in a sector of interest and an interference lies outside the sector of interest.
- Developing a robust BS beamformer to tolerate different types of array errors.
- Deriving CRB for DOA estimation in the directional BS case and comparing with the omni-directional ES and BS cases.
- Exploring the performance of the directional transmission optimum BS beamformer for the scenario containing a moving scatterer.

The main contributions in this chapter are:

- **Analysing properties and solve some unique problems in BS processing.**
- **Extending an ES robust beamforming algorithm to BS case.**
- **Deriving CRB for DOA estimation in the directional transmission BS case.**

Chapter 6 Beam Space Processing for Coherent Signals

This chapter is focused on the problem of coherent signals in BS processing. The BS model containing correlated signal is introduced and the performance degradation of BS algorithms is analysed. Following an analysis of the relationship between the ES and BS coherent signal subspaces, a technique for reconstructing the ES signal subspace is proposed which can be used together with spatial smoothing for DOA estimation in the omni-directional transmission BS case. For the directional transmission BS case, a vectorisation method is proposed to construct a matrix as a summation of weighted self-outer products of ES signal steering vectors. The rank of the constructed matrix is the same as the number of DOAs of signals and is not affected by the coherence thus allowing the DOAs to be readily estimated by using subspace methods. To estimate the DOAs of a mixture of coherent and uncorrelated signals in BS, oblique projection is used to separate coherent and uncorrelated signal BS subspace and to process each one separately. With a priori knowledge or estimation of the DOA, the LCMV BS beamformer is modified for the coherent signals.

Two main contributions for estimating DOAs of coherent signals in BS are included in this chapter. For coherent signals in the omni-directional transmission BS case, the method of reconstructing the ES coherent signal subspace is developed. For coherent signals in the directional transmission BS case, the new expression matrix to represent the coherent signals in an independent manner is proposed, and a method to estimate this matrix is developed.

Chapter 7 Application of Beam Space Processing to Real Experimental Data

This chapter describes a BS experiment and the collected data using PTWR that synchronously scans the directional transmit and receive beams over a sector of interest. Algorithms developed in this thesis are explored using the real experimental data collected with this array.

Chapter 8 Conclusion

This chapter provides a summary of the main work and results from the thesis and discusses potential work for future research.

Chapter 2

Array Signal Processing Background

2.1 Introduction to Phased Arrays

As mentioned in Chapter 1, data from a single sensor contains little spatial information. For example, the conventional parabolic dish radar is a typical single sensor. It only provides very limited directional information by mechanically scanning its beam over an angular sector of interest, usually, 360 degrees so providing range and Doppler information in different directions by appropriate analysis of the time and frequency domain data. Mechanically scanned radar systems have some disadvantages, such as long revisit time on regions of interest, beam smearing associated with the antenna rotation, and no capability for simultaneous multi-function operation.

To improve the performance and overcome the limitations of a single sensor, multiple sensors can be used in an array configuration. A typical phased array system has several separate elements (sensors) each with a phase shifter. Initially, phased arrays were used to enhance the transmission gain by shifting the phase of the signal transmitted from each element then combining them coherently. As described in [1], phased arrays were simply used as a combination of radiators in early radar systems at the turn of the twentieth century, such as the phased array developed for wireless telegraphy by Braun and Marconi. In the 1920s, the author in [2] proposed that the directive diagrams for transmission could be applied to the case of reception. In the 1930s, a phased array with mechanical phase shifters was developed to change steering angles for reception [3]. The advent of World War II accelerated the development of phased array radars. For example, Britain developed the Chain Home coast radar to detect and track aircraft and Germany developed the Klein Heidelberg radar for long-range air surveillance [4]; Luis Alvarez developed the first electronically scanned microwave phased array antenna and used it to help precision bombing and aircraft landing [5]. Since then, phased arrays have been applied in other fields such as sonar and radio astronomy. For modern radar applications, phased arrays have attracted more and more attention. The theory of phased array has been studied intensively and a series of phased array radar operational systems at different frequency bands have been built, such as the US naval S-band AN/SPY-1, the C-band PATRIOT, the X-band AN/SPY-3, and even a low cost phased array radar in the 77 GHz frequency band for the automotive industry [6].

Depending on the method of signal transmission, phased arrays can be simply categorised as active and passive arrays (which is different from the concept of active/passive electronically scanned arrays in [7]). Active phased arrays contain both transmitters and receivers. The obvious advantages include that more energy can be concentrated in the transmission direction and there is more freedom to look in a

direction of interest. Passive phased arrays contain only the receive part and one or more separate transmitters are used to radiate to the environment. The advantages of passive arrays include faster scanning as there is no need to switch between transmission and reception functions, lower cost and being concealed for covert operations.

Phased array processing depends heavily on the layout of the elements of the array. There are different types of array geometries that are commonly used, such as linear, circular and planar arrays. Arrays with a constant spacing between elements are known as uniform arrays, for example, the elements in a uniform circular array are evenly distributed in a circle. Non-uniform arrays deploy adjacent elements with different spatial separations, such as arrays in specially designed shapes, sparse linear arrays, and the very common case of a uniform array with missing or faulty elements. With a careful design, employing non-uniform arrays can achieve narrower beamwidths, lower sidelobes; moreover, they offer the potential to keep the same aperture and equivalent performance with fewer elements [117], [118].

As the array configuration and distances between elements are known, delays among elements for a signal from a given direction can be easily calculated. Modern electronically steered phased arrays, by applying the corresponding phase shifts to respective elements, allows agile beam steering. Additionally, phased arrays can rapidly steer beams or synthesise multiple beams simultaneously, thus they can perform multiple functions, and such radars are known as multi-function phased array radar (MPAR). An example is shown in [11], a phased array radar was used to both acquire weather data of a small storm and carry out detection and tracking of aircraft.

Furthermore, phased arrays contain both spatial and temporal information. Consequently, signal processing techniques were expanded and went beyond the methods for the single channel case. The first approach was conventional beamforming developed during the Second World War [17]. Later, adaptive beamforming methods, such as the Capon's method [18], were applied to resolve closely spaced sources, which achieve more accurate spatial spectrum estimation and also can be used for interference cancellation and clutter mitigation. Subspace based estimation techniques, such as MUSIC (MUltiple SIgnal Classification) [22], significantly improved the accuracy of signal DOA estimation. Many other array processing techniques were also developed, such as maximum likelihood estimation of signal parameters by maximising a likelihood function, array calibration and robust beamforming methods deal with arrays with errors, and space-time adaptive processing methods filter data in both the spatial and temporal domains, which is particularly useful for clutter mitigation.

Due to the obvious advantages of phased array systems and related array signal processing methods, they have been widely used in different areas and will appear more and more in both military and civilian applications. These applications include: radar, sonar [8], radio astronomy [9], seismology measurement [10], meteorological

observation [11], radio broadcasting [12], telecommunication [13], audio microphone arrays [14], optics and photonics [15], ultrasound and biomedical applications [16].

2.2 Model of Independent Signals Mixed with White Noise in ES

The research in this thesis is focused on scenarios where narrowband and far-field plane wave signals are transmitted, then reflected by point scatterers and received by phased arrays. The line of sight free space propagation model, which means signals travel in a direct path between the array and scatterers, is used and other complex issues like refraction, dispersion and absorption etc. are not considered. The receiver noise is modelled as Gaussian white noise and independent to the received signals. Except for the sections dealing with array errors in Chapter 5 and in Chapter 7, a perfect phased array model is used, where all receivers are exactly the same and no error occurs.

All methods described in this section are applicable to different types of arrays, but in this thesis, only the simplest case, a uniform linear array (ULA) is considered in the mathematical development for ease of notation. For a ULA containing K receivers with separation d, the steering vector for a narrowband signal incident on the array from an angle θ is given by

$$\boldsymbol{v}(\theta) = \begin{bmatrix} 1 & e^{j\frac{2\pi d}{\lambda}\sin\theta} & e^{j\frac{4\pi d}{\lambda}\sin\theta} & \cdots & e^{j\frac{2(K-1)\pi d}{\lambda}\sin\theta} \end{bmatrix}^T, \tag{2-1}$$

where $(\cdot)^{\mathrm{T}}$ denotes transpose and λ for the wavelength. At a given range, it is often assumed that there are L independent scatterers located at a set of angles $\Theta_s = \{\theta_{s1}, \theta_{s2}, \ \ldots \ \theta_{sL}\}$. Notice that for the spatial processing, it is assumed that the scatterers are in separate angular cells $(\theta_{si} \neq \theta_{sj})$ but in the same range bin. The reflected signals from these scatterers are called source signals and are denoted by an $L\times 1$ vector $\boldsymbol{s} = [s_1 \quad s_2 \quad \cdots \quad s_L]^T$. The amplitudes of these returns, which are proportional to their radar cross sections, at any receiver in the phased array can be denoted as $\{\sigma_{s1}, \sigma_{s2}, \ \ldots, \ \sigma_{sL}\}$. The source signal covariance matrix is given by

$$\boldsymbol{R_s} = \mathrm{E}\{\boldsymbol{s}\boldsymbol{s}^H\}. \tag{2-2}$$

where $(\cdot)^H$ denotes the Hermitian transpose, $\mathrm{E}\{\cdot\}$ denotes expectation, which can be estimated by ensemble averaging. For L uncorrelated scatterers, $\boldsymbol{R_s}$ can be written as

$$\boldsymbol{R_s} = diag\{\sigma_{s1}^2, \ \sigma_{s2}^2, \ \ldots, \ \sigma_{sL}^2\}. \tag{2-3}$$

The outputs of the K receivers at the t-th pulse is written in vector notation as

$$\boldsymbol{x}(t) = [x_1(t) \quad x_2(t) \quad \ldots \quad x_K(t)]^T. \tag{2-4}$$

where $x_k(t)$ is the output of the k-th receiver. As the main interest in this thesis is spatial signal processing, $\boldsymbol{x}(t)$ is often simply written as $\boldsymbol{x}$.

For a passive or active phased array system with an omni-directional transmitter, the receiver outputs are in direct proportion to the strength of the scattered signal. For the case of L plane waves in uncorrelated receiver noise incident on the phased array, a vector expression for the array outputs is given by

$$\boldsymbol{x} = \boldsymbol{V_s}(\Theta_s)\boldsymbol{s} + \boldsymbol{n}, \tag{2-5}$$

where the $K \times L$ matrix $\boldsymbol{V_s}(\Theta_s)$ contains the steering vectors corresponding to the DOAs of all the scatterer returns and given by

$$\boldsymbol{V_s}(\Theta_s) = [\boldsymbol{v}(\theta_{s1}) \quad \boldsymbol{v}(\theta_{s2}) \quad \ldots \quad \boldsymbol{v}(\theta_{sL})], \tag{2-6}$$

and $\boldsymbol{n}$ is a $K\times1$ vector of spatially uncorrelated receiver noise where it is assumed to be zero-mean Gaussian white noise and having the same power at each receiver element. The ES covariance matrix, $\boldsymbol{R_x}$, is given by

$$\boldsymbol{R_x} = \mathrm{E}\{\boldsymbol{x}\boldsymbol{x}^H\} = \boldsymbol{V_s}(\Theta_s)\boldsymbol{R_s}\boldsymbol{V_s}^H(\Theta_s) + \sigma_n^2\boldsymbol{I}, \tag{2-7}$$

where σ_n^2 is the noise power and $\boldsymbol{I}$ is the identity matrix.

Notice that only point scatterers whose sizes are smaller than the radar resolution cell are considered here, and the distributed target case is not included in this thesis. Also, the models and related spatial processing algorithms are based on the assumption that all returns are from the same range, thus propagation path loss effects are neglected.

2.3 Array Processing: ES

Array processing focuses on utilising the output of spatially distributed elements to detect and estimate parameters of signals and noises incident on the array, such as to estimate the number and DOAs of incident signals, to enhance the signal to noise ratio (SNR) and to suppress unwanted interferences. Typically, array processing applies different weights to the receiver outputs, covariance matrix or other expressions extracted from covariance matrix, such as a subspace, and to form a new output as the processed result. A diagram of a typical array processing – beamforming for a uniform linear array is presented in Figure 2-1. A far-field plane wave arrives at the receivers with different delays and a complex weight is applied to each receiver output, then the summation of these weighted receiver outputs is the beamformer output.

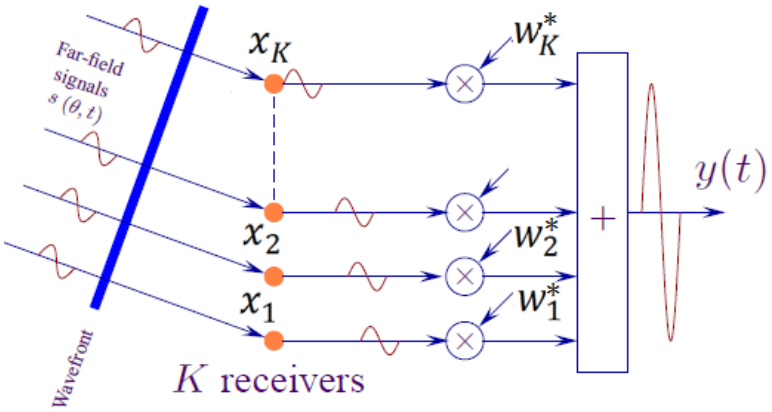

Figure 2-1: A diagram of beamforming for a signal incident on a uniform linear array.

Various algorithms have been developed for phased array spatial signal processing and a complete overview of the different approaches can be found in [30], only several formulae for typical array processing methods in ES are described here.

2.3.1 Conventional Beamforming

The conventional beamformer applies fixed weights to the receiver outputs and adds them to form the beamformer output. The set of weights used at a look angle θ is the Hermitian transpose of the steering vector at θ. Thus, this approach aligns the phases of a signal from the incident angle θ at different receivers, steering the maximum response axis (MRA) to θ. The output of a beam steered in the direction θ is given by

$$y(\theta) = \boldsymbol{v}^H(\theta)\boldsymbol{x}, \tag{2-8}$$

and the mean normalised output power of the conventional beamformer is given by

$$p_{CB-ES}(\theta) = \frac{1}{K^2}\boldsymbol{v}^H(\theta)\,\boldsymbol{R}_x\,\boldsymbol{v}(\theta). \tag{2-9}$$

The conventional beamformer reinforces a signal arriving from the look angle, θ, whilst signals from another direction θ' is still added but suppressed by an amount determined by the beam pattern which is given by

$$bp(\theta', \theta) = \frac{1}{K} exp\left(\frac{j(K-1)\pi d}{\lambda}\left(sin\,\theta' - sin\,\theta\right)\right)\left(\frac{sin\left(\frac{K\pi d}{\lambda}\left(sin\,\theta' - sin\,\theta\right)\right)}{sin\left(\frac{\pi d}{\lambda}\left(sin\,\theta' - sin\,\theta\right)\right)}\right) \tag{2-10}$$

It can be proved that for a single signal in uncorrelated receiver noise, the SNR gain of a conventional beamformer is *K*. Compared to many other array processing algorithms, conventional beamforming is robust to system errors and insensitive to correlation amongst the incident signals but its spatial resolution is limited by the width of the

mainlobe of the beam pattern and may not be able to resolve closely incident signals whose separation is less than that the width if the mainlobe.

2.3.2 Optimum Beamforming

Conventional beamformers use only the information about the location of elements to align the phase of a signal from a look direction at different elements. Optimum beamformers use the location information together with the received signals to achieve a better result, such as providing more suppression of noise, rejection of unwanted signals from other directions and a better directivity. Various array processing algorithms have been proposed to optimise the weights by different criteria. Since these criteria lead to the same or similar expressions, only the criterion of minimising power with a linear constraint is introduced here. The Minimum Variance Distortionless Response (MVDR) algorithm [18], also known as the Capon's method, applies a $K\times1$ vector $\boldsymbol{w}(\theta)$ to the receiver output vector, $\boldsymbol{x}$, such that the mean output power, given by $\boldsymbol{w}^H(\theta)\boldsymbol{R_x}\boldsymbol{w}(\theta)$, is minimised subject to maintaining a unity response to a unit amplitude signal arriving from the chosen look direction, θ. The optimisation is written as

$$\min \boldsymbol{w}^H(\theta)\boldsymbol{R_x}\boldsymbol{w}(\theta), \text{ subject to } \boldsymbol{w}^H(\theta)\boldsymbol{v}(\theta) = 1, \tag{2-11}$$

and using Lagrange multipliers, it can be shown the ES MVDR weight is given by

$$\boldsymbol{w}_{MVDR-ES}(\theta) = \frac{\boldsymbol{R_x^{-1}}\,\boldsymbol{v}(\theta)}{\boldsymbol{v}^H(\theta)\boldsymbol{R_x^{-1}}\,\boldsymbol{v}(\theta)}, \tag{2-12}$$

and the output power is given by

$$p_{MVDR-ES}(\theta) = \left(\boldsymbol{v}^H(\theta)\boldsymbol{R_x^{-1}}\,\boldsymbol{v}(\theta)\right)^{-1}. \tag{2-13}$$

The linear constrained minimum variance (LCMV) approach [19] adds extra constraints, such as nulls at the DOAs of interferences or unity responses in directions near to the steering vector. In this approach, the constraint is generalised to

$$\boldsymbol{w}^H\boldsymbol{C} = \boldsymbol{g}^H, \tag{2-14}$$

where $\boldsymbol{C}$ is a $K \times c$ matrix containing c constraints determined by the constraint vectors, i.e.,

$$\boldsymbol{C} = [\boldsymbol{v}_1 \quad \dots \quad \boldsymbol{v}_c], \tag{2-15}$$

and $\boldsymbol{g}$ contains the constraint values, i.e.,

$$\boldsymbol{g} = [g_1 \quad \dots \quad g_c]^H. \tag{2-16}$$

An example is directional constraints where

$$\boldsymbol{C}(\theta) = [\boldsymbol{v}(\theta) \quad \boldsymbol{v}(\theta + \Delta\theta) \quad \boldsymbol{v}(\theta - \Delta\theta)], \tag{2-17}$$

or a derivative constraint [20] where

$$\boldsymbol{C}(\theta) = \left[\boldsymbol{v}(\theta) \quad \frac{d\boldsymbol{v}(\theta)}{d\theta}\right]. \tag{2-18}$$

Similarly, other linear constraints, such as eigenvector constraints [21], can be used. These constraints are often applied to mitigate the loss in performance of optimum beamformers when the assumed and actual signal arrival directions are not exactly equal.

The optimal weight vector which minimises $\boldsymbol{w}^H\boldsymbol{R_x}\boldsymbol{w}$ subject to $\boldsymbol{w}^H\boldsymbol{C} = \boldsymbol{g}^H$ is given by

$$\boldsymbol{w}(\theta) = \boldsymbol{R_x}^{-1}\boldsymbol{C}(\theta)\left(\boldsymbol{C}^H(\theta)\boldsymbol{R_x}^{-1}\boldsymbol{C}(\theta)\right)^{-1}\boldsymbol{g}, \tag{2-19}$$

and the output power is given by

$$p_{LCMV-ES}(\theta) = \boldsymbol{g}^H\left(\boldsymbol{C}^H(\theta)\boldsymbol{R_x}^{-1}\boldsymbol{C}(\theta)\right)^{-1}\boldsymbol{g}. \tag{2-20}$$

2.3.3 Subspace Algorithms

Subspace methods utilise eigen-decomposition to separate the signal and noise components into different subspaces. Signal waveforms are normally designed with known shapes but can be random, such as signal waveforms used for noise radars or noise generated by a target in a passive context. Noise is generated by electronic devices (receivers), and is random in nature. The most common noise–thermal noise can be modelled as white Gaussian noise. As signals and noise are generated by different mechanisms, they are usually independent. In this situation, applying eigen-decomposition to the covariance matrix, the subspace spanned by the look direction vectors of the signals is the same subspace spanned by the eigenvectors corresponding to a set of the largest eigenvalues when the noise is spatially uncorrelated. When signals are independent of each other, the number of eigenvalues in this set is equal to the number of signals. The case of coherent or highly correlated signals, which has a different eigen-structure, will be discussed separately in Chapter 6.

Eigen-decomposition of the receiver covariance matrix can be expressed as

$$\boldsymbol{R_x} = \sum_{i=1}^{K}\lambda_i\boldsymbol{q}_i\boldsymbol{q}_i^H = \boldsymbol{Q}\boldsymbol{\Lambda}\boldsymbol{Q}^H, \tag{2-21}$$

$$\textit{where } \boldsymbol{\Lambda} = \begin{bmatrix} \lambda_1 & 0 & \dots & 0 \\ 0 & \lambda_2 & & \vdots \\ \vdots & & \ddots & 0 \\ 0 & \dots & 0 & \lambda_K \end{bmatrix} \text{ and eigenvalues } \lambda_1 \geq \lambda_2 \geq \cdots \geq \lambda_K,$$

$$\boldsymbol{Q} = [\boldsymbol{q}_1 \quad \dots \quad \boldsymbol{q}_L \quad \vdots \quad \boldsymbol{q}_{L+1} \quad \dots \quad \boldsymbol{q}_K], \tag{2-22}$$

where $\boldsymbol{q}_i$ is an eigenvector associated with the $i\text{–}th$ eigenvalue, λ_i. L is the number of independent signals and the signal subspace [22] is defined as

$$\boldsymbol{E_s} = [\boldsymbol{q}_1 \quad \cdots \quad \boldsymbol{q}_L], \tag{2-23}$$

where $\boldsymbol{E_s}$ is the set of eigenvectors corresponding to the largest L eigenvalues. The subspace spanned by these vectors is composed of signal as well as noise and this signal plus noise subspace is simply called the signal subspace. The remaining K-L eigenvectors span the noise subspace, which contains vectors of the noise process only and is given by

$$\boldsymbol{E_n} = [\boldsymbol{q}_{L+1} \quad \cdots \quad \boldsymbol{q}_K]. \tag{2-24}$$

There are different subspace methods for DOA estimation, and in general, DOAs are worked out by utilising the property that the signal and noise subspaces are orthogonal. The output of the most commonly used method—MUSIC [22], is given by

$$p_{MUSIC-ES}(\theta) = \frac{1}{\sum_{i=L+1}^{K} |\boldsymbol{v}^H(\theta)\boldsymbol{q}_i|^2}. \tag{2-25}$$

In the above expression, the output peaks over different azimuthal angles correspond to estimates of the signal arrival directions and the number of signals needs to be estimated before processing. There are some other variants including root-MUSIC [23], Esprit and TLS-Esprit [24] but they will not be discussed in this thesis.

2.4 Summary

This chapter provided a brief introduction to phased arrays and array signal processing methods. In Section 2.1, some basic concepts, history and different applications of phased arrays were briefly reviewed. In Section 2.2, the typical scenario that narrowband signals incident on a uniform linear phased array system was considered and its mathematical model in ES was described. Some key concepts were introduced, such as steering vector and covariance matrix. To focus on the spatial signal processing, some typical ES array processing algorithms were reviewed in Section 2.3.

Chapter 3

Standard Beam Space Processing

As mentioned in the previous chapter, ES array processing algorithms apply different weights to the element (receiver) outputs or covariance matrix extracted from the element outputs. However, in some cases, the ES processing algorithms cannot be applied directly, since the receiver outputs may not be accessible and only some beam outputs, such as outputs of conventional beamformer at different directions, are available or recorded. This problem occurs in some phased array radar and sonar systems which are limited by hardware and cost. For example, in the THAAD active electronically scanned array radar developed and built by Raytheon, the array operates with 72 subarrays, each containing 11 Tx/Rx element assemblies and each Tx/Rx element assembly contains 32 active T/R modules and radiating elements. All the receiver outputs from each subarray are combined through a beamformer and then sent to an analog-to-digital converter [99].

3.1 Introduction to BS Processing

For the above and similar systems, the outputs of preformed conventional beams only provide spatial samples of the conventional beamformer outputs at selected directions. To achieve better performance than simply interpolating these beam outputs, designed weights can be applied to these beam outputs and then summed to form a new output for each look angle; such a process is known as beam space (BS) beamforming. A schematic diagram of a BS beamformer is shown in Figure 3-1.

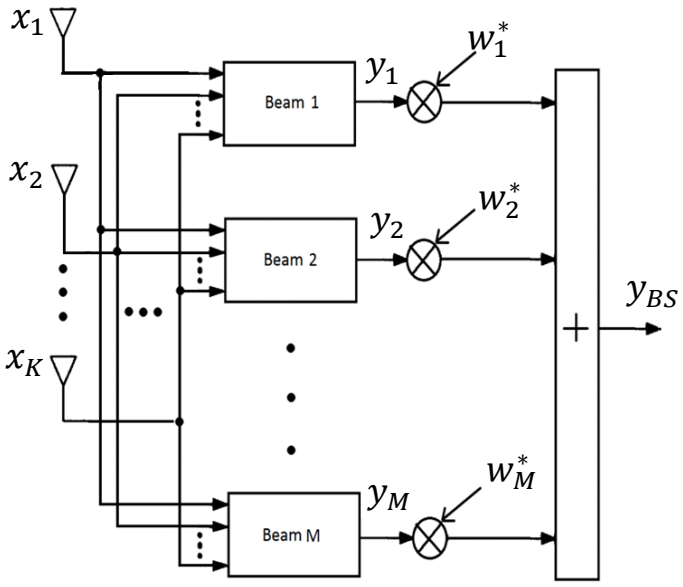

Figure 3-1: A diagram of BS beamformer

In this figure, x_k and y_m denote the k-th element output and the m-th beam output respectively and the complex weights $w_1, w_2, \ldots, w_M$ can be determined by an optimisation criterion, such as to maximise the SNR [25]. Furthermore, the beam outputs can be used to form a BS covariance matrix, and similarly, most other ES processing methods, such as MUSIC [27], [28], ESPRIT [29] can also be implemented in BS. All these approaches using beam outputs are termed BS processing. BS processing methods are mostly implemented in phased array radar and sonar systems but examples of applications are also found in other fields such as seismic data analysis [34], biomedical signal processing [35], [36] and potentially for radio astronomy [37].

In some cases, forming beams is a preliminary step to further processing, as some extra advantages are associated with using the beam outputs rather than the element outputs. Usually, the number of beams is smaller than the number of receivers, so BS processing has a lower dimensionality and fewer samples are required for estimation of the BS covariance matrix, thus reducing the required computational load. For example, to process sonar data from an array of 25 hydrophones, only 10 beams were used and achieved good performance in [26]. Furthermore, the averaging procedure in the preliminary beamformer brings some other benefits, such as a lower detection signal to noise ratio (SNR) threshold [26], [39], reduced sensitivity of high resolution methods to the noise distribution and to wavefront distortions [42], and reduced statistical variance of the estimated beam spectrum for small numbers of samples [26]. Also, by restricting the beams to lie within a given sector of interest, signals or interferences outside that sector only enter the beams through sidelobe leakage and hence are attenuated.

As shown in [28], the variance of DOA estimates using the BS subspace method is never smaller than that of ES methods for a large number of samples, thus, the performance of the BS processing is generally not superior to that of ES processing. Additionally, since the number of beams is generally smaller than the number of receivers and those beams are only formed in a sector of interest, there are some potential disadvantages of BS processing. These include:

- Missing unknown out of sector signals
- Reduced number of degrees of freedom
- Weaker capability for interference cancellation
- Reduced ability for noise suppression
- Reduced the maximum number of signals whose directions can be estimated.

In most cases, conventional beamformers are used as preformed beams in BS processing, but other beams can be considered. For example, in order to reduce out of sector interferences, low sidelobe beams such as Dolph-Chebychev and Hamming beams are suggested in [30]. Furthermore, special beams can be designed to minimise interfering sources located outside the sector, as discussed in [32] and [33]. In this thesis, the main interest is in general spatial signal processing and only further processing the outputs of

conventional beamforming is considered, thus to design beams in the pre-processing stage or BS processing for window weighted beams will not be discussed.

3.2 Standard BS Processing

In most BS processing literature, such as [25]–[31], phased arrays are commonly modelled as a passive receiving system or the transmitter is assumed to be omni-directional, and the directional characteristics of the transmission part are not incorporated. The BS processing methods based on this model are termed omni-directional transmission or standard BS processing. In this section, the formulae for standard BS processing are presented.

3.2.1 Standard BS Signal Model

A vector containing M conventional beam outputs is given by

$$\boldsymbol{y} = [y(\theta_1) \quad y(\theta_2) \quad \ldots \quad y(\theta_M)]^T. \tag{3-1}$$

where $y(\theta_m)$ is given by (2-8). The BS covariance matrix is given by

$$\boldsymbol{R_y} = \mathrm{E}\{\boldsymbol{y}\boldsymbol{y}^H\} = \boldsymbol{V_B^H R_x V_B}, \tag{3-2}$$

where $\boldsymbol{V_B}$ is a $K \times M$ matrix containing the steering vectors for each of the various M beams and is given by

$$\boldsymbol{V_B}(\Theta_B) = [\boldsymbol{v}(\theta_1) \quad \boldsymbol{v}(\theta_2) \quad \ldots \quad \boldsymbol{v}(\theta_M)], \tag{3-3}$$

where $\Theta_B = \{\theta_1, \quad \theta_2, \quad \cdots \quad \theta_M\}$ denotes the set of steering directions of the preformed beams. When no confusion occurs, a simpler notation $\boldsymbol{V}$ will be used instead of $\boldsymbol{V_B}(\Theta_B)$ in this thesis. In practice $\boldsymbol{R_y}$ can be estimated by

$$\widehat{\boldsymbol{R}}_{\boldsymbol{y}} = 1/N \sum_{t=1}^{t=N} \boldsymbol{y}(\mathrm{t})\boldsymbol{y}^H(\mathrm{t}), \tag{3-4}$$

where for an active system, e.g. a monostatic radar, the averaging is over N pulses contained in a coherent processing interval. The vector of beam outputs due to a single unit amplitude plane wave from direction θ is termed BS steering vector and is given by

$$\boldsymbol{h}(\theta) = \boldsymbol{V}^H \boldsymbol{v}(\theta). \tag{3-5}$$

For further processing, this vector will be needed as a processing vector or constraint vector at the angle θ.

3.2.2 Conventional BS Beamforming

The conventional BS beamformer is a weighted summation of beam outputs, and the weights are designed to align the phase of the signal from a chosen look direction for each beam, so that signal components from the same direction but in different beams are added in phase. Normalising the signal output to be the same as the output from a single receiver, the resulting output power at θ is given by

$$p_{CB-BS}(\theta) = \frac{1}{G(\theta)} \boldsymbol{h}^H(\theta) \boldsymbol{R_y} \boldsymbol{h}(\theta), \tag{3-6}$$

where the gain varies with the steering angle and depends on the beam pattern of each beam. The value of the gain is given by

$$G(\theta) = \|\boldsymbol{h}(\theta)\|^4. \tag{3-7}$$

Conventional BS beamforming is rarely used in practice, as its main effect is to interpolate the conventional ES beamformer outputs at different angles. When a sufficient number of beams are used, this approach becomes a valid interpolation mechanism. However when a small number of beams are used over a wide angular region, only very limited spatial information is obtained and the conventional BS beamformer output may be significantly different from the conventional ES beamformer output at some angles.

3.2.3 Optimum BS Beamforming

The optimum BS beamformer with MVDR criterion, which maintains unity gain in the look direction whilst minimising the total output power from a weighted set of beams, is given as the solution of the following problem (see [25] and Chapter 6 in [30])

$$\min \boldsymbol{w}^H(\theta) \boldsymbol{R_y} \boldsymbol{w}(\theta) \text{ subject to } \boldsymbol{w}^H(\theta) \boldsymbol{h}(\theta) = 1, \tag{3-8}$$

whose solution is given by

$$\boldsymbol{w}(\theta) = \frac{\boldsymbol{R_y^{-1}} \boldsymbol{V}^H \boldsymbol{v}(\theta)}{\boldsymbol{v}^H(\theta) \boldsymbol{V} \boldsymbol{R_y^{-1}} \boldsymbol{V}^H \boldsymbol{v}(\theta)}. \tag{3-9}$$

The output power of the optimum BS beamformer is given by

$$p_{MVDR-BS}(\theta) = \left(\boldsymbol{v}^H(\theta) \boldsymbol{V} \boldsymbol{R_y^{-1}} \boldsymbol{V}^H \boldsymbol{v}(\theta) \right)^{-1}. \tag{3-10}$$

Assuming zero-mean Gaussian white noise with power of σ_n^2 at each element and a single signal, whose DOA and amplitude are θ_s and σ_s, is incident on the array, with mutually orthogonal beams, it is easy to prove that the optimum BS beamformer output power at θ_s is given by

$$p_{MVDR-BS}(\theta_s) = \sigma_s^2 + \frac{K}{|\boldsymbol{h}(\theta_s)|^2} \sigma_n^2. \tag{3-11}$$

Similarly, LCMV algorithms can be implemented in BS by adding extra constraints, for example, to constrain the response in different directions. For this approach, the optimum weight vector for a steering angle, θ, is given by

$$\boldsymbol{w}(\theta) = \boldsymbol{R}_{\boldsymbol{y}}^{-1}\boldsymbol{C}(\theta)\left(\boldsymbol{C}^{H}(\theta)\boldsymbol{R}_{\boldsymbol{y}}^{-1}\boldsymbol{C}(\theta)\right)^{-1}\boldsymbol{g}(\theta). \tag{3-12}$$

Notice that $\boldsymbol{C}(\theta)$ is a constraint matrix containing a group of linear constraints in BS, such as a derivative constraint matrix can be given by $\boldsymbol{C}(\theta) = [\boldsymbol{h}(\theta) \quad \dot{\boldsymbol{h}}(\theta)]$ and different from the ES constraint in (2-19), and $\boldsymbol{g}(\theta)$ is a vector containing complex numbers denoting the response at the constraints in $\boldsymbol{C}(\theta)$ and

$$\boldsymbol{w}^{H}(\theta)\boldsymbol{C}(\theta) = \boldsymbol{g}^{H}(\theta). \tag{3-13}$$

The output power is given by

$$\begin{aligned} p_{LCMV-BS}(\theta) &= \boldsymbol{w}^{H}(\theta)\boldsymbol{R}_{\boldsymbol{y}}\boldsymbol{w}(\theta) \\ &= \boldsymbol{g}^{H}(\theta)\left(\boldsymbol{C}^{H}(\theta)\boldsymbol{R}_{\boldsymbol{y}}^{-1}\boldsymbol{C}(\theta)\right)^{-1}\boldsymbol{g}(\theta). \end{aligned} \tag{3-14}$$

3.2.4 BS Subspace Method

Subspace methods for DOA estimation in ES can be readily extended to BS. As mentioned before, noise from different receivers is commonly assumed to be spatially uncorrelated with zero mean and the same Gaussian distribution. For L uncorrelated plane waves incident with the uncorrelated receiver noise on the array, using equations (2-7) and (3-2), the BS covariance matrix is given by

$$\boldsymbol{R}_{\boldsymbol{y}} = \boldsymbol{V}^{\boldsymbol{H}}\boldsymbol{R}_{\boldsymbol{x}}\boldsymbol{V} = \sum_{\boldsymbol{l}=\boldsymbol{1}}^{\boldsymbol{L}} \sigma_l^2 \boldsymbol{h}(\theta_{sl})\boldsymbol{h}^{H}(\theta_{sl}) + \sigma_n^2 \boldsymbol{V}^{H}\boldsymbol{V}. \tag{3-15}$$

In most literature on BS processing, especially subspace methods, such as [27], [28], [38] and [42], the columns of matrix $\boldsymbol{V}$ are chosen to be mutually orthogonal and normalised by $1/\sqrt{K}$, thus $\boldsymbol{V}^{H}\boldsymbol{V} = \boldsymbol{I}$. Notice the normalisation ensures that the BS transformation is unitary but it does not affect the results of further processing, both $\boldsymbol{V}^{H}\boldsymbol{V} = \boldsymbol{I}$ and $\boldsymbol{V}^{H}\boldsymbol{V} = K\boldsymbol{I}$ are used in this thesis to represent the beam mutual orthogonality.

Eigen-decomposition of $\boldsymbol{R}_{\boldsymbol{y}}$ can be expressed as

$$\boldsymbol{R}_{\boldsymbol{y}} = \sum_{i=1}^{M} \lambda_{yi}\boldsymbol{q}_{yi}\boldsymbol{q}_{yi}^{H} = \boldsymbol{Q}_{\boldsymbol{y}}\boldsymbol{\Lambda}_{\boldsymbol{y}}\boldsymbol{Q}_{\boldsymbol{y}}^{H} \tag{3-16}$$

As shown in [27] and Appendix A, for orthogonal beams, a subset of the noise subspace eigenvectors of the ES covariance matrix, $\boldsymbol{q}_i$ are related to those noise eigenvectors of the BS covariance matrix, $\boldsymbol{q}_{\boldsymbol{y}i}$ by

$$\boldsymbol{q}_i = \boldsymbol{V}\boldsymbol{q}_{\boldsymbol{y}i}, (i = L+1, \dots, M). \tag{3-17}$$

For L uncorrelated signals from different DOAs and when $\boldsymbol{V}^H\boldsymbol{V} = \boldsymbol{I}$, the signal steering vectors $\{\boldsymbol{h}(\theta_{s1}), \dots, \boldsymbol{h}(\theta_{sL})\}$ span the same signal subspace as $\{\boldsymbol{q}_{\boldsymbol{y}1}, \cdots, \boldsymbol{q}_{\boldsymbol{y}L}\}$, therefore

$$\boldsymbol{h}^H(\theta_{sl})\boldsymbol{q}_{\boldsymbol{y}i} = 0, (l \le L, i = L+1, \dots, M), \tag{3-18}$$

and the output of BS MUSIC at angle θ is given by

$$p_{MUSIC-BS}(\theta) = \frac{1}{\sum_{i=L+1}^{M} |\boldsymbol{h}^H(\theta)\boldsymbol{q}_{\boldsymbol{y}i}|^2}. \tag{3-19}$$

Subspace methods require that the noise be spatially white. In ES processing, when the noise is spatially correlated, the eigenvectors corresponding to the largest L eigenvalues does not necessarily span the true signal subspace, and the signal and noise subspaces are not well separated. The standard subspace methods only work well for high SNR scenarios, thus pre-whitening for coloured noise with known covariance matrix is required or some other DOA estimation methods for unknown coloured noise models such as [43] and [44] can be considered.

For spatially white receiver noise $\boldsymbol{n}$, $E\{\boldsymbol{n}\boldsymbol{n}^H\} = \sigma_n^2\boldsymbol{I}$. By applying a linear transformation, the noise component in BS becomes $\boldsymbol{V}^H\boldsymbol{n}$. When $\boldsymbol{V}^H\boldsymbol{V} = \boldsymbol{I}$, the BS noise component is also white. When non-orthogonal beams are selected, i.e., $\boldsymbol{V}^H\boldsymbol{V} \neq \boldsymbol{I}$, the BS noise covariance matrix is coloured and the result is similar to the above ES coloured noise problem. To remove the correlation of the noise component caused by the linear transformation of $\boldsymbol{V}$, sector focused stability (SFS) BS processing [45] can be used to transform the beam steering vectors to be mutually orthogonal. The SFS BS transformation matrix is given by

$$\boldsymbol{V}' = \boldsymbol{V}(\boldsymbol{V}^H\boldsymbol{V})^{-1/2}, \tag{3-20}$$

and the SFS BS covariance matrix is written as

$$\boldsymbol{R}_{\boldsymbol{y}sfs} = \boldsymbol{V}'^H\boldsymbol{R}_{\boldsymbol{x}}\boldsymbol{V}' = (\boldsymbol{V}^H\boldsymbol{V})^{-1/2}\boldsymbol{R}_{\boldsymbol{y}}(\boldsymbol{V}^H\boldsymbol{V})^{-1/2}. \tag{3-21}$$

A comparison of the performance of the BS with non-orthogonal steered beams and SFS BS processing algorithms with both MVDR and MUSIC estimators can be found in [46].

3.3 Examples of Standard BS Processing

In this section, examples are presented to show the results of standard BS processing. A scenario is considered that two plane wave signals, whose power values are 10 and 6 dB above the noise power (considered as 0 dB) at any single receiver and DOAs are at azimuthal angles of 8° and 15° respectively, are incident on a phased array. This example of two sources will be used as a basic scenario in further BS processing in this thesis, because it is a general example where the two closely spaced sources are in a relative narrow sector but can be separated by conventional beamformer, also the angular difference between two sources are similar to the experimental data which will be described in Chapter 7. However, analysis based on this scenario would still be suitable for other general examples. The phased array is modelled as a horizontal (azimuthal) scanning uniform linear array of 64 elements spaced half a wavelength apart. An equal number of independent conventional beams spanning the full angular sector were modelled. The theoretical output power values of conventional and MVDR beamformers versus azimuthal angle for both ES and BS are compared in Figure 3-2 and the results of the ES and BS MUSIC algorithm are plotted in Figure 3-3.

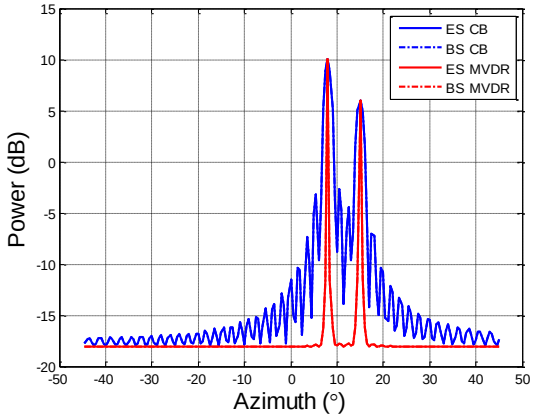

Figure 3-2: Theoretical output power values of conventional and optimum beamformers for both ES and BS versus azimuthal angle. *M* independent beams spanning the full angular space were used and *M*=*K*. Note: here and in subsequent figures, CB denotes the conventional beamformer.

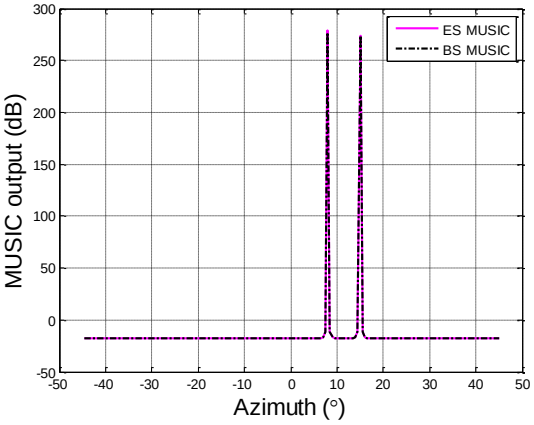

Figure 3-3: Theoretical output values of MUSIC algorithm for both ES and BS versus azimuthal angle. *M* independent beams spanning the full angular space were used and *M*=*K*.

Notice that the averaged power value of receiver noise is assumed as 0 dB here, and the output power values are referenced to the noise power, and the true numerical value of receiver noise depends on the noise level and sensitivity of receivers.

As expected, the BS and ES results of each algorithm are identical and overlap when the number of independent conventional beams scanning over the whole angular space is the same as the number of receivers. In this case, the ES and BS conventional beamformer output power values are exactly same and they are plotted on top of each and the same to the ES and BS MVDR, also ES and BS MUSIC outputs. Obviously, for both ES and BS processing, the performance of the optimum beamformers are superior to the conventional beamformers, as they provide a better angular resolution and a more accurate estimation of signal power. The strong and sharp peaks on the MUSIC output indicate the DOAs, due to the orthogonality between signal and noise subspaces, but these peaks values in the MUSIC output do not represent signal power.

Based on the theoretical ES covariance matrix, 128 pulses (i.e., receiver output samples) were simulated and used to estimate the ES covariance matrix in the normal fashion. At each pulse, conventional beamformer outputs in $M(M = K = 64)$ independent steering directions were formed, and then used together to estimate the BS covariance matrix as (3-4). Then, conventional, MVDR beamforming and MUSIC algorithms were applied to both ES and BS covariance matrices estimated by using the simulated data. The beamformer and MUSIC outputs are shown in Figure 3-4 and Figure 3-5.

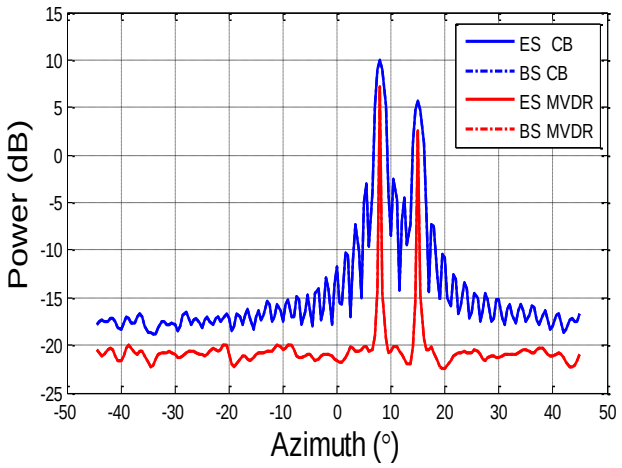

Figure 3-4: Simulated output power values of conventional and MVDR beamformers for both ES and BS versus azimuthal angle. *M* independent beams spanning the full angular space were used and *M=K*.

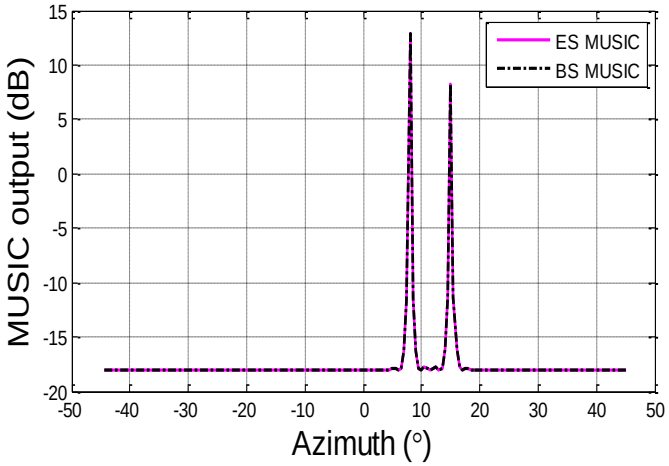

Figure 3-5: Simulated output values of MUSIC algorithm for both ES and BS versus azimuthal angle. *M* independent beams spanning the full angular space were used and *M*=*K*.

These results based on the simulated covariance matrix show the typical better resolution of the optimum ES and BS beamformers over the conventional beamformers, but the output power is slightly lower than the true SNRs. Both ES and BS MUSIC algorithms provide sharp peaks but the outputs at DOAs are not as strong as the theoretical numerical analysis. The optimum BS beamformer achieved nearly the same effective beamwidth as the theoretical numerical analysis.

The performance of BS MUSIC algorithm is normally not affected by the SNR significantly, as the signal and noise subspace are orthogonal to each other. However, for low SNRs, where the signal power is weaker than the noise power, the difficulty in separating the two subspaces is potentially increased, and this is especially obvious when a small number of samples are generated by simulation or collected by experiment. Notice in this example, that simulated covariance matrix is not exactly the same as the theoretical covariance matrix due to the number of samples (128), thus, the noise eigenvectors are not exactly orthogonal to the assumed signal steering vectors and the performance of MUSIC algorithm is not as outstanding as in the theoretical analysis. However, the performance would be improved by increasing the number of simulated samples averaged in the covariance matrix estimation. The MUSIC algorithm is based on the signal model of point scatterer, and its performance can be degraded when being applied to the extended targets (volume scatterers), as the distributed scatterers can be correlated and the number of the scatterers can be larger than the number of receivers/beams.

3.4 BS Processing with Different Number of Beams

As mentioned in Section 3.1, an important advantage of BS processing is its lower dimensionality when the number of beams, *M*, is smaller than number of receivers, *K*. However, when insufficient beams are formed in the full angular sector or a large angular sector, information loss happens in the transformation between the BS and ES

covariance matrices. In this section, the beamforming results using either a set of beams $(M < K)$ scanned over the full array manifold or only a sector of interest are discussed.

3.4.1 BS Beamformer in a Full Angular Sector

It has been proved in [25] and also shown by the example in Section 3.3, that performance of the optimum beamforming in BS and ES are equivalent when the number of independent beams spanning the full angular sector is the same as number of receivers, because the transformation matrix $\boldsymbol{V}$ is a $K \times K$ full rank invertible matrix, so $\boldsymbol{x} = (\boldsymbol{V}^H)^{-1}\boldsymbol{y}$. This indicates that, theoretically, the receiver outputs can be fully recovered and all the information in ES is fully retained in BS.

To obtain the maximum aperture without any grating lobes, most commonly, phased array elements are spaced half a wavelength of signal apart each other. In this case, if the number of beams spanning the full angular sector is smaller than the number of receivers, then these beams cannot adequately cover the whole angular region and some information in ES may not be fully recovered. In another case that the number of used beams is larger than K, it would cause the BS covariance matrix to become singular and degrade the performance of the optimum BS beamformer, unless a careful use of diagonal loading is made.

For wideband signals, the system may be designed to operate at the higher end of the frequency band, and so for signals at the lower end of the frequency band, the element spacing is smaller than half a wavelength. At these frequencies, it is not necessary to have the number of beams equals to the number of receivers.

Consider a phased array with 64 elements operating at a frequency where the element spacing is one quarter of the wavelength. In this example, only 32 independent beams are required to cover the full angular sector. The theoretical results of conventional and MVDR beamformers for both ES and BS cases are shown in Figure 3-6 and simulated results using 128 samples are shown in Figure 3-7. In both figures, the BS results closely approximate the ES results. As can be seen, due to the doubling of the angular beamwidth that occurs when d/λ=1/4, even using beams whose number is half of the receivers, the BS beamformers provide almost identical performance compared with the ES approaches. In fact, using all the element outputs for ES processing is spatially oversampling, as only 32 elements with a spacing of $\lambda/2$ between adjacent elements are required to cover the full array aperture. Thus, if only a group of element outputs in odd or even order were used for ES processing, the performance would be similar to this.

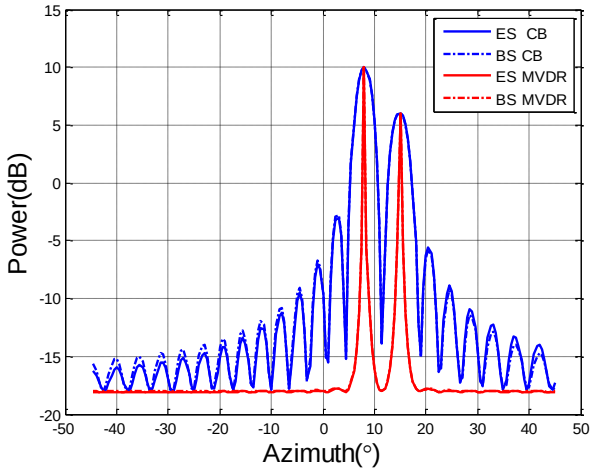

Figure 3-6: Theoretical output power values of conventional and optimum beamformers for both ES and BS versus azimuthal angle. 64 receivers are one quarter wavelength apart and 32 independent beams are used for BS processing.

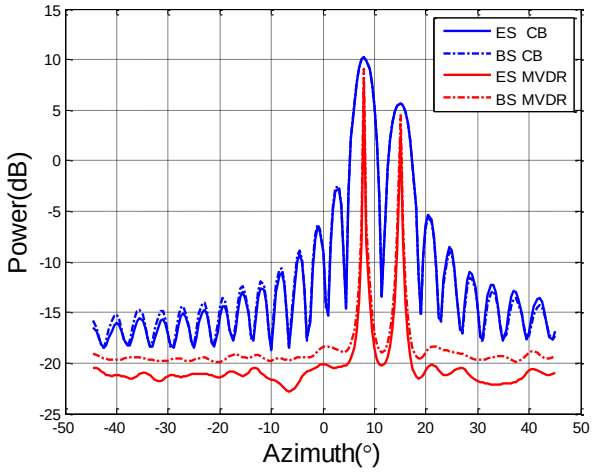

Figure 3-7: Simulated output power values of conventional and optimum beamformers for both ES and BS versus azimuthal angle. 64 receivers were one quarter wavelength apart and 32 independent beams are used for BS processing.

The above figures show there are small differences between BS and ES MVDR beamforming outputs when number of beams is half of the number of receivers, and this can be different by varying d/λ and its corresponding number of beams. As a general rule, beams are required to span the full angular space and the number of beams is given by $M = \lfloor 2Kd/\lambda \rfloor$, where $\lfloor \cdot \rfloor$ denotes the integer part of the expression. The averaged difference between BS and ES MVDR beamformer output power values at the two DOAs and over the whole region from -45° to 45° are plotted in Figure 3-8 respectively for different d/λ ($\frac{1}{16} \leq d/\lambda \leq \frac{1}{2}$). It shows that the differences between BS and ES beamformer output power values are small for all values of d/λ considered, especially for the output power values at DOAs, and the difference approaches zero when more beams formed.

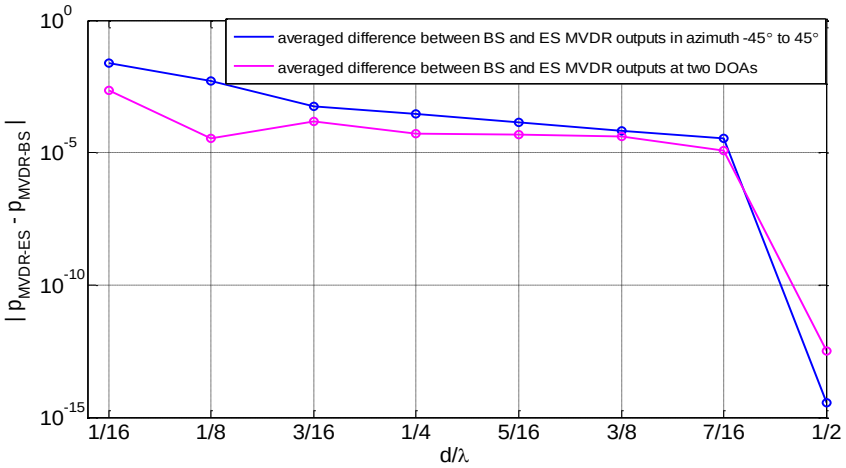

Figure 3-8: Averaged differences between output power values of BS and ES MVDR beamformers versus d/λ. Notice that number of beams at different d/λ changes as $M = \lfloor 2Kd/\lambda \rfloor$ and 64 receivers are used.

3.4.2 BS Beamformer in a Subsector

The above results are based on using independent beams that span the full angular sector, but often in many practical applications the signals of interest are located in a given subsector of the full angular region and so beams are usually only formed in that subsector. Also, in practical phased array operations, it is often hard to set or control all the beams to be fully orthogonal in a mathematical sense. However, with a sufficient number of beams covering the subsector, BS algorithms can still achieve satisfactory results when signals lie in the subsector and most information would be captured by the beams spanning that subsector.

The same scenario in Section 3.3 was considered but only 21 beams were formed at azimuthal angles ranging from -2° to 18° in 1° increments (note that the beams are not strictly orthogonal as in the previous scenario). Numerical evaluation of the output power values from conventional and optimum beamformer are plotted as a function of azimuthal angle in Figure 3-9, and a zoomed in view of the output in the sector of interest are shown in Figure 3-10. Notice that the conventional BS beamformer output is only meaningful at angles inside the subsector, and the output outside the subsector is dominated by some very high response values.

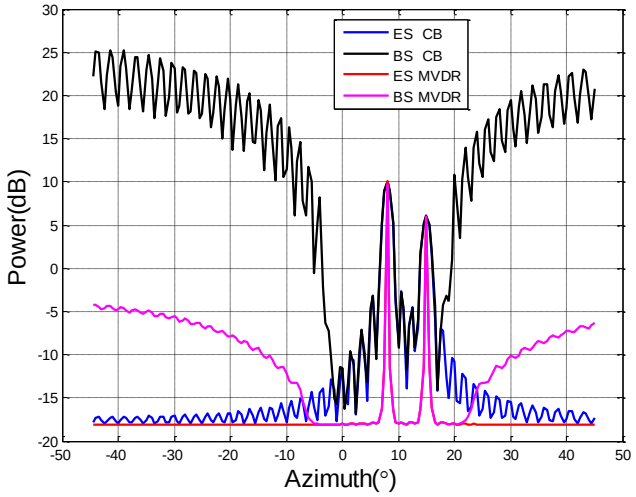

Figure 3-9: Theoretical output power values of conventional, optimum ES and subsector BS beamformers versus azimuthal angle. The DOAs of signals are 8° and 15° and 21 beams formed at azimuthal angles ranging from -2° to 18° in 1° increments.

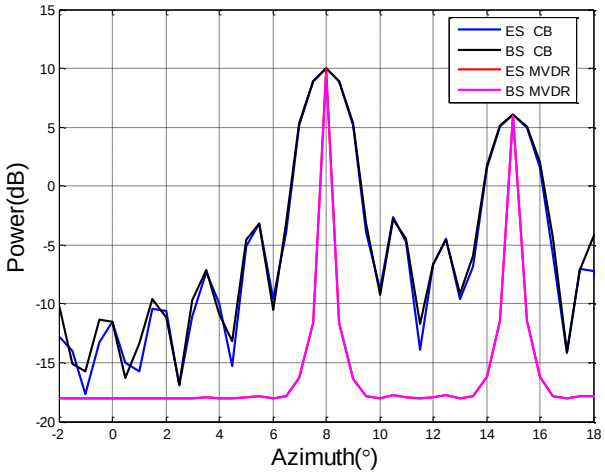

Figure 3-10: A zoomed in view of the theoretical output power of conventional, ES MVDR and subsector BS MVDR beamformers in the sector of interest.

The above figures indicate that both the ES and BS MVDR algorithms have very similar performance in the sector where beams were formed. Therefore, within a sector of interest, even the number of beams is smaller than the number of receivers, comparable performance can be achieved by the BS method. Notice, however, that outside the sector of interest spanned by the 21 beams, the response of the BS MVDR approach is significantly different from the ES MVDR beamformer; this is analysed in the following section. Although Tx/Rx beams with window functions can be used to reduce sidelobe level, the high response outside the sector of interest is still not avoided for subsector BS processing.

3.5 BS Processing in the Region outside the Sector of Interest

As shown in Figure 3-9, it is apparent that the subsector BS MVDR beamformer produces a strong response in the region not contained within the sector of interest. This is a unique problem for subsector BS processing and the region outside the sector of interest is normally treated as "not of interest", for example, in [32] and [33], the authors used the BS method for dimension reduction and rejection of interferences out of the sector of interest. In this section, the effect of interferences outside the sector of interest on the estimation of the signals within the sector of interest is studied. In addition, whether interferences lying out of the sector of interest can be identified using just beams spanning the sector of interest is investigated.

3.5.1 BS Model with an Out of Sector Interference

Out of sector signals in the omni-directional transmission BS model are received through sidelobes of beams. These signals can be reflections from strong scatterers outside the sector of interest; in the other case, these signals are from other transmitters, such as jamming signals towards a radar or acoustic signals from other ships in the sonar case. Consider L in sector signals incident on the array where the receiver outputs are given by equation (2-5) together with an independent interference from an azimuthal angle, θ_I. For this scenario the vector of conventional beam outputs is given by

$$\boldsymbol{y} = \boldsymbol{V}^H \boldsymbol{V}_{\boldsymbol{s}}(\Theta_s)\boldsymbol{s} + \boldsymbol{V}^H \boldsymbol{v}(\theta_I)\boldsymbol{i} + \boldsymbol{V}^H \boldsymbol{n}, \tag{3-22}$$

where $\boldsymbol{s}$, $\boldsymbol{i}$ and $\boldsymbol{n}$ denote the in sector signals, the out of sector interference and receiver noise respectively and the matrix $\boldsymbol{V}_{\boldsymbol{s}}(\Theta_s)$ containing the in sector steering vectors is given by

$$\boldsymbol{V}_{\boldsymbol{s}}(\Theta_s) = [\boldsymbol{v}(\theta_{s1}) \quad \boldsymbol{v}(\theta_{s2}) \quad \ldots \quad \boldsymbol{v}(\theta_{sL})]. \tag{3-23}$$

Denoting σ_I^2 as the power of the interference received by any single receiver, the BS covariance matrix is given by

$$\begin{aligned} \boldsymbol{R}_{\boldsymbol{yI}} &= \boldsymbol{V}^H \boldsymbol{V}_{\boldsymbol{s}}(\Theta_s)\boldsymbol{R}_{\boldsymbol{s}}\boldsymbol{V}_{\boldsymbol{s}}^H(\Theta_s)\boldsymbol{V} + \sigma_I^2 \boldsymbol{V}^H \boldsymbol{v}(\theta_I)\boldsymbol{v}^H(\theta_I)\boldsymbol{V} + \sigma_n^2 \boldsymbol{V}^H \boldsymbol{V} \\ &= \boldsymbol{R}_{\boldsymbol{y}} + \sigma_I^2 \boldsymbol{h}(\theta_I)\boldsymbol{h}^H(\theta_I), \end{aligned} \tag{3-24}$$

where $\boldsymbol{h}(\theta)$ is given by (3-5). With uncorrelated receiver noise, the BS covariance matrix for a single out of sector interference only is given by

$$\boldsymbol{R}_{\boldsymbol{y}(I)} = \sigma_I^2 \boldsymbol{V}^H \boldsymbol{v}(\theta_I)\boldsymbol{v}^H(\theta_I)\boldsymbol{V} + \sigma_n^2 \boldsymbol{V}^H \boldsymbol{V}. \tag{3-25}$$

3.5.2 Optimum BS Beamformer Output Power in the Presence of an Out of Sector Interference

Here the following analysis is restricted to a model containing a single scatterer within the sector of interest and a single interference outside the sector of interest. Denoting the DOAs of signals within and outside the sector of interest as θ_s and θ_I respectively, and σ_s^2 as the power of the in sector signal received by any single receiver, the BS covariance matrix is given by

$$\begin{aligned} \boldsymbol{R_{yI}} &= \sigma_s^2 \boldsymbol{h}(\theta_s)\boldsymbol{h}^H(\theta_s) + \boldsymbol{R_{y(I)}}\text{ , or} \\ \boldsymbol{R_{yI}} &= \sigma_I^2 \boldsymbol{h}(\theta_I)\boldsymbol{h}^H(\theta_I) + \boldsymbol{R_y}. \end{aligned} \tag{3-26}$$

3.5.2.1 Optimum BS Beamformer Output Power at the DOA of an In Sector Signal

When $\theta = \theta_s$, i.e., the optimum beam is steered directly at the signal of interest, the output power is given by

$$\begin{aligned} p_{MVDR-BS}(\theta_s)_I &= \left(\boldsymbol{h}^H(\theta_s)\boldsymbol{R}_{\boldsymbol{yI}}^{-1}\boldsymbol{h}(\theta_s)\right)^{-1} \\ &= \left(\boldsymbol{h}^H(\theta_s)\boldsymbol{R}_{\boldsymbol{y(I)}}^{-1}\boldsymbol{h}(\theta_s) - \frac{\sigma_s^2\boldsymbol{h}^H(\theta_s)\boldsymbol{R}_{\boldsymbol{y(I)}}^{-1}\boldsymbol{h}(\theta_s)\boldsymbol{h}^H(\theta_s)\boldsymbol{R}_{\boldsymbol{y(I)}}^{-1}\boldsymbol{h}(\theta_s)}{1+\sigma_s^2\boldsymbol{h}^H(\theta_s)\boldsymbol{R}_{\boldsymbol{y(I)}}^{-1}\boldsymbol{h}(\theta_s)}\right)^{-1} \\ &= \left(\boldsymbol{h}^H(\theta_s)\boldsymbol{R}_{\boldsymbol{y(I)}}^{-1}\boldsymbol{h}(\theta_s)\right)^{-1} + \sigma_s^2 \end{aligned} \tag{3-27}$$

Note that in (3-27) the estimate of the power of the desired signal, σ_s^2, is distorted by an amount $\left(\boldsymbol{h}^H(\theta_s)\boldsymbol{R}_{\boldsymbol{y(I)}}^{-1}\boldsymbol{h}(\theta_s)\right)^{-1}$ which is caused by leakage from the interference into the optimum beam. A mathematical representation of $\boldsymbol{R}_{\boldsymbol{y(I)}}^{-1}$ for the general case is not particularly illuminating, but when the steering beams are mutually orthogonal, i.e., $\boldsymbol{V^H V} = K\boldsymbol{I}$, then it is given by

$$\boldsymbol{R}_{\boldsymbol{y(I)}}^{-1} = \frac{\boldsymbol{I}}{K\sigma_n^2} - \frac{\frac{\sigma_I^2}{K\sigma_n^2}\boldsymbol{h}(\theta_I)\boldsymbol{h}^H(\theta_I)\frac{1}{K\sigma_n^2}}{1+\frac{\sigma_I^2}{K\sigma_n^2}\boldsymbol{h^H}(\theta_I)\boldsymbol{h}(\theta_I)} \tag{3-28}$$

Then, the bias term in the optimum BS beamformer output power in the beam steered at the DOA of the signal with an out of sector interference is given by

$$\left(\boldsymbol{h}^H(\theta_s)\boldsymbol{R}_{\boldsymbol{y(I)}}^{-1}\boldsymbol{h}(\theta_s)\right)^{-1} = \frac{K\sigma_n^2[H(\theta_I)\sigma_I^2 + K\sigma_n^2]}{H(\theta_s)K\sigma_n^2 + \left[H(\theta_s)H(\theta_I) - B_H\left(\theta_{s,}\,\theta_I\right)\right]\sigma_I^2}, \tag{3-29}$$

where H and B_H are defined as

$$\begin{aligned} H(\theta) &= \boldsymbol{h}^H(\theta)\boldsymbol{h}(\theta) = \|\boldsymbol{h}(\theta)\|^2 \\ B_H\left(\theta_1,\,\theta_2\right) &= \boldsymbol{h}^H(\theta_1)\boldsymbol{h}(\theta_2)\boldsymbol{h}^H(\theta_2)\boldsymbol{h}(\theta_1) = |\boldsymbol{h}^H(\theta_1)\boldsymbol{h}(\theta_2)|^2. \end{aligned} \tag{3-30}$$

The values of $H(\theta_s)H(\theta_I)$ and $B_H(\theta_{s,}\,\theta_I)$ are compared here. By using the previous scenario that 21 beams are formed at angles of -2° to 18° with 1° increments and the DOA of the interference is 25°. The values of $H(\theta_s)H(\theta_I)$ and $B_H(\theta_{s,}\,\theta_I)$ as a function of θ_s, i.e., the DOA of the in sector signal, are plotted in Figure 3-11.

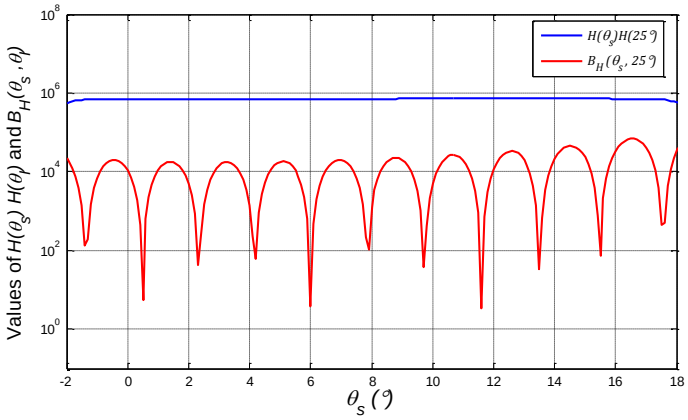

Figure 3-11: An example of values of $H(\theta_s)H(25^0)$ and $B_H(\theta_s, 25^0)$.

In this case the value of $H(\theta_s)H(\theta_I)$ is significantly larger than $B_H(\theta_{s,}\,\theta_I)$ and is approximately constant across the sector of interest. Thus when the DOAs of the signal and the interference are well separated, the beamformer output power at the DOA of the in sector signal, by substituting (3-29) in (3-27) and ignoring the relatively small part—$B_H(\theta_{s,}\,\theta_I)$, can be approximated as

$$p_{MVDR-BS}(\theta_s) \approx \sigma_s^2 + \frac{K\sigma_n^2}{H(\theta_s)} \tag{3-31}$$

Thus, in this case the optimum BS beamformer output power at the DOA of the in sector signal is only negligibly affected by the interference. Within the sector of interest, the noise component is attenuated, as the values of $\frac{K}{H(\theta_s)}$ are relatively small and plotted versus azimuthal angles in Figure 3-12.

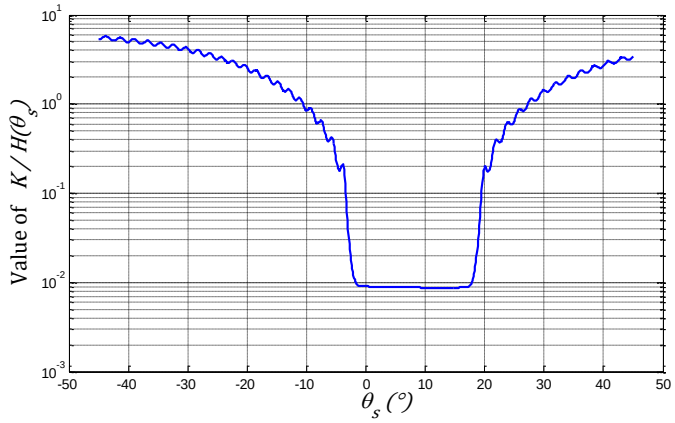

Figure 3-12: An example of value of $K/H(\theta_s)$.

However, when the DOAs of the signal and interference are spaced less than half beamwidth, the difference between values of $H(\theta_s)H(\theta_I)$ and $B_H(\theta_{s,}\,\theta_I)$ can be small. For example, when $\theta_s = 17.9°$ and θ_I is varied from 18° to 45°, the values of $H(\theta_s)H(\theta_I)$ and $B_H(\theta_{s,}\,\theta_I)$ are plotted in Figure 3-13. In this example, when the interference is at an azimuthal angle, $\theta_I \leq 18.5°$, the values of $H(\theta_s)H(\theta_I)$ and $B_H(\theta_{s,}\,\theta_I)$ are very close. In this case, the simplification leading to (3-31) is not valid anymore and the value of the beamformer output power depends on more parameters.

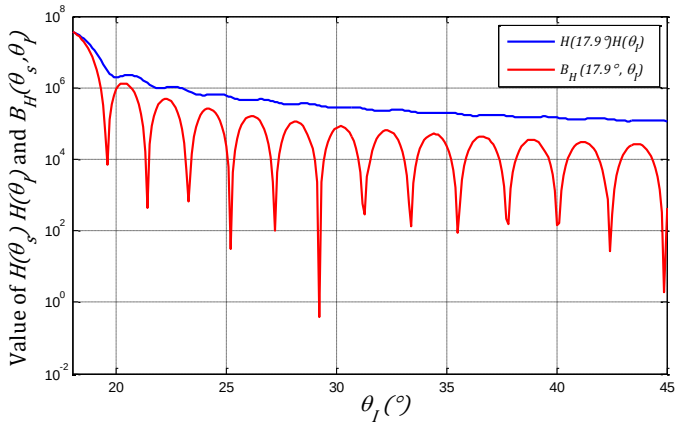

Figure 3-13: An example of values of $H(17.9^0)H(\theta_I)$ and $B_H(17.9^0, \theta_I)$.

3.5.2.2 Optimum BS Beamformer Output Power at the DOA of an Out of Sector Interference

When $\theta = \theta_I$, it can be shown by an argument similar to that used to derive (3-27), the optimum BS beamformer output power is given by

$$\begin{aligned} p_{MVDR-BS}(\theta_I) &= \left(\boldsymbol{h}^H(\theta_I)\boldsymbol{R}_{\boldsymbol{yI}}^{-1}\boldsymbol{h}(\theta_I)\right)^{-1} \\ &= \left(\boldsymbol{h}^H(\theta_I)\boldsymbol{R}_{\boldsymbol{y}}^{-1}\boldsymbol{h}(\theta_I)\right)^{-1} + \sigma_I^2 \end{aligned} \tag{3-32}$$

where the first term represents leakage of the in sector scatterer into the optimum beam steered at the interference. Similar to the derivation of (3-29) and using the second version of (3-26), the distortion term is given by

$$\left(\boldsymbol{h}^H(\theta_I)\boldsymbol{R}_{\boldsymbol{y}}^{-1}\boldsymbol{h}(\theta_I)\right)^{-1} = \frac{K\sigma_n^2(H(\theta_s)\sigma_s^2 + K\sigma_n^2)}{H(\theta_I)K\sigma_n^2 + \left(H(\theta_s)H(\theta_I) - B_H(\theta_{s,}\,\theta_I)\right)\sigma_s^2} \tag{3-33}$$

As analysed, when the DOAs of the signal and interference are well separated, $B_H(\theta_{s,}\,\theta_I)$ is much smaller than $H(\theta_s)H(\theta_I)$, thus, the output power can be approximated as

$$p_{MVDR-BS}(\theta_I) \approx \sigma_I^2 + \frac{K}{H(\theta_I)}\sigma_n^2. \tag{3-34}$$

It indicates the output power at the DOA of the interference is the sum of the interference power σ_I^2 and the noise power with a gain of $\frac{K}{H(\theta_I)}$. The results in Figure 3-12 can still be used here and show the value of $\frac{K}{H(\theta_I)}$ is a function of θ_I. As the gain is significantly larger than that inside the sector of interest, the noise component is amplified and the total output power given by (3-34) is significantly different from the interference power, σ_I^2.

3.5.2.3 Examples of Optimum BS Beamforming Output in the Region outside the Sector of Interest

In most cases, the DOAs of the signal and interference are not close, i.e., their angular separation is more than half a beamwidth. From (3-31) and (3-34), it is obvious that the BS MVDR beamformer output power at the DOA of either the in sector signal or the out of sector interference can be approximated as the sum of the signal/interference power and the noise power multiplied by the factor, $\frac{K}{H(\theta)}$. Thus, the identification and estimation of the signal and interference power depend on the ratio between two parts in the above equations (3-34), where in the second term the factor, $\frac{K}{H(\theta)}$, has been shown to be interpretable in terms of the array beam pattern. Note that the above analysis is based on the condition that the columns of the BS transformation matrix, $\boldsymbol{V}$, are mutually orthogonal, when this is not the case, the results may change.

Two examples are shown in Figure 3-14 and Figure 3-15, where the scenario is the same as that previously used in Figure 3-9 and the sector of interest is again from -2° to 18° in azimuth but an interference is at -5° with 10 dB interference to noise ratio (INR) (plotted in Figure 3-14) or at -10° with 10 dB INR (plotted in Figure 3-15). The optimum BS beamformer output power using a covariance matrix estimated using 128 samples simulated for the scenario in Figure 3-15 is plotted in Figure 3-16.

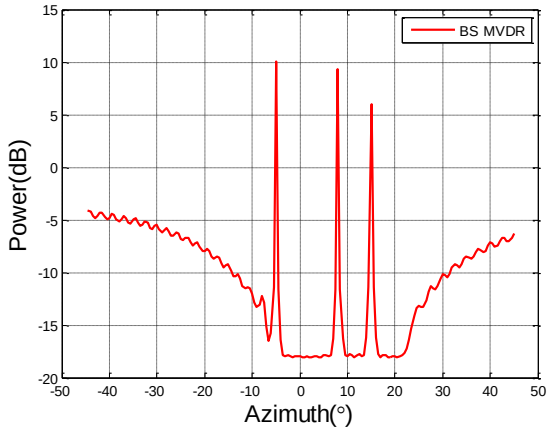

Figure 3-14: An example of subsector BS MVDR output power values with an interference at -5° with 10 dB INR.

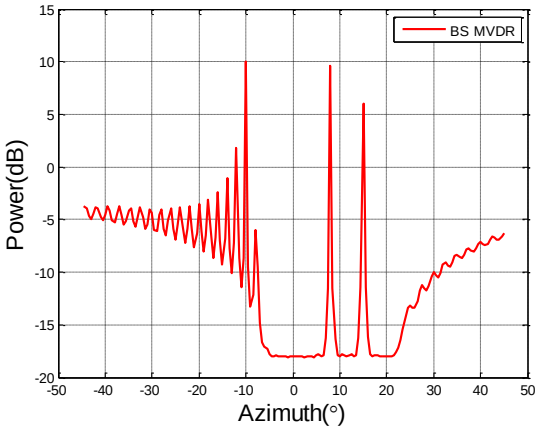

Figure 3-15: An example of subsector BS MVDR output power value versus azimuthal angle with an interference at -10° with 10 dB INR.

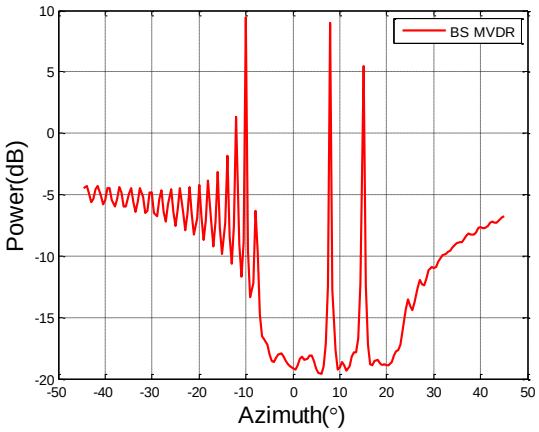

Figure 3-16: An example of simulated subsector BS MVDR output power values simulated with an interference at -10° with 10 dB INR.

As shown in the above examples, the optimum BS beamformer output power values in the sector of interest are not affected by the interference significantly and the interference outside of the sector of interest can be easily identified and well estimated when the interference intensity is reasonably strong compared with the noise term. However, as shown in Figure 3-15 and Figure 3-16, due to a weaker ability to suppress the power outside the sector of interest, there are some peaks around the DOA of the interference, which would potentially indicate wrong information.

According to equation (3-34), the output power at the DOA of the interference is the sum of the interference power σ_I^2 and the noise power with a gain of $\frac{K}{H(\theta_I)}$, which increases when the distance from θ_I to the sector of interest increases. Thus, when the INR is relatively small or the gain to noise power is very large, the interference is hard to identify using the BS MVDR method, especially when the number of interferers is unknown. For example, where the scenario is the same as that used in Figure 3-16, but the interference is located at -15° with 3 dB INR, the output power values of the

optimum BS beamformer based on a covariance matrix estimated by 128 simulated conventional beam samples are plotted in Figure 3-17. In this case, it is hard to identify and estimate the interference accurately. A more sophisticated method for a similar problem will be discussed later in Chapter 5.

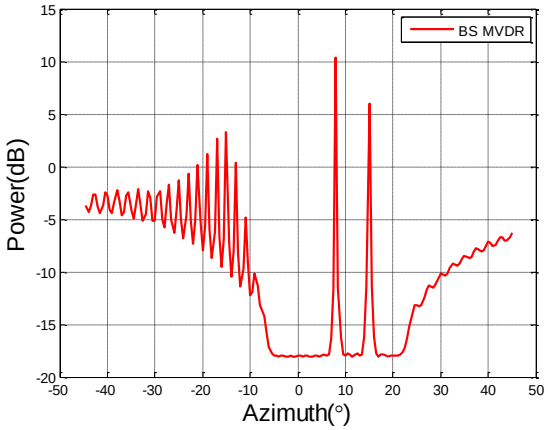

Figure 3-17: An example of subsector BS MVDR output with an interference at -15° with 3 dB INR.

3.6 Summary

In this chapter, some background and fundamental concepts of BS processing have been introduced in Section 3.1. In Section 3.2, the mathematical model of the omni-directional transmission BS and standard BS processing algorithms were briefly introduced. Some examples in Section 3.3 showed that ES equivalent performance can be achieved by the BS processing when the number of independent beams is the same as the number of receivers. In Section 3.4, the problems of using smaller numbers of beams for the optimum BS beamformer were considered. For ULAs, it was demonstrated that when $\frac{\lambda}{d} < \frac{1}{2}$ provided the beams overlap at the their 3 dB beam pattern points and span the full angular sector, a smaller number of beams $(M < K)$ is sufficient to achieve performance almost equivalent to that of the ES case. In another case, when the DOAs of signals lie inside an angular sector of interest, satisfactory performance can be achieved by the optimum BS beamformer when enough beams are formed to cover the angular subsector. The BS processing with an out of sector interference incident on the array was analysed in Section 3.5. It showed that in most cases where a signal and an interference are well separated, the optimum BS beamformer output power at the DOA of the signal (in sector) is only negligibly affected by the interference. On the other hand, identifying the interference according to optimum BS beamformer output is complicated and it depends on the INR and the DOA of the interference.

Chapter 4

Directional Transmission Beam Space Processing

As described earlier, most BS processing algorithms are formulated for either passive or active systems which assume that the transmitter is omni-directional. However, in many practical applications of the active systems, to transmit more energy to a concentrated area, directional transmission is widely used. The directional transmission can be a beam with a relatively large beamwidth fixed at an angle of interest, and focused on a sector determined by the transmit beamwidth; or it can be the case that a single transmit and receive beam with a relatively narrow beamwidth that are synchronously scanned over a wider sector of interest. Here only the second case is considered, as it is much more common in practice and the first case can be approximated as the omni-directional transmission. A schematic diagram of a beam scanning over a sector is drawn in Figure 4-1. In each beam direction *N* pulses are transmitted and then returns to the array after being reflected by scatterers either lying along the direction of the beam (main beam scatterers) or in other directions through sidelobe leakage (sidelobe scatterers).

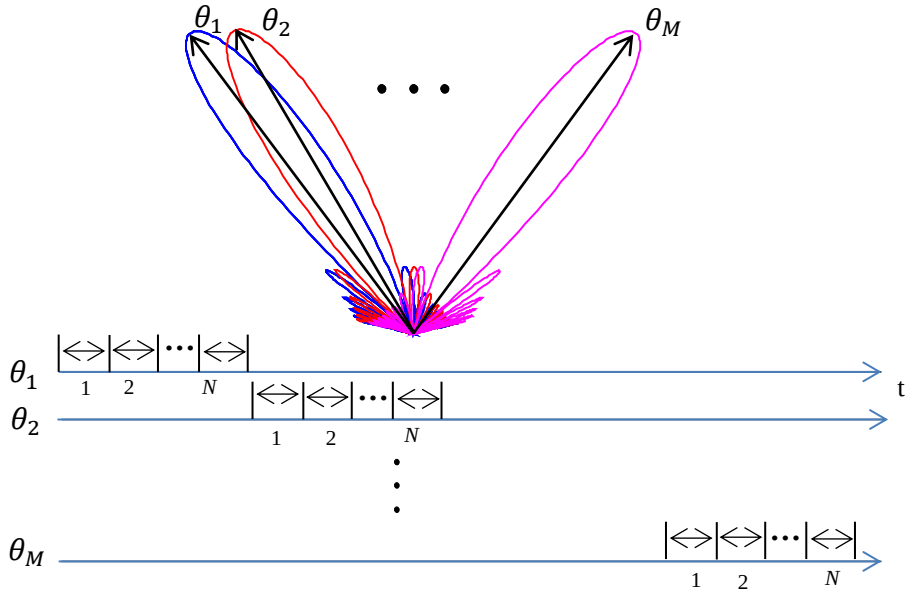

Figure 4-1: A diagram of a narrow beamwidth directional Tx/Rx beam scanning over a sector of interest. *M* sequential beams are formed in the sector of interest, and *N* Tx/Rx pulses are in each beam direction.

The omni-directional transmission model implies that the echo from any far-field scatterer at the receive array is statistically the same over the whole processing, and the difference among elements of the array is due to the propagation delay across the

aperture of the array. Thus for a stationary scatterer, the returns at the receive array do not vary when the receive beams are formed either simultaneously or sequentially. For the directional transmission case, the returns from such a scatterer will vary from transmit beam to transmit beam, as the amount of transmitted energy reaching the scatterer vary according to that scatterer's orientation relative to the MRA of the transmit beam. For example, the return from a scatterer located at broadside is maximum when the transmit beam is in the broadside direction but would be less if the transmit beam is at another angle. In this case, to model the receiver and beamformer responses to the scatterer, the beam patterns of both transmit and receive beam must be accounted for.

An example of such a phased array system is the phase tilt weather radar developed by Raytheon Integrated Defence Systems and produced by First RF Corporation [94]. This radar can scan electronically to ±45° in azimuth (the horizontal principal plane) and mechanically in elevation; only the conventional beamformer output power values are recorded for beams steered in directions of the scan sequence. A fixed number of pulses are transmitted and received before the Tx/Rx beam is switched to the next direction. More details about this phased array system will be further discussed in Chapter 7.

In the directional transmission case since the receiver outputs vary for different Tx/Rx beams, theoretical expressions for the ES and BS covariance matrices are different from those presented in Chapter 3. For ES approaches, the directional transmission does not pose a severe problem, since an ES covariance matrix can be estimated and used to derive the optimum set of array weights for each transmitted beam, provided that the sampling rate is fast enough. In the pulsed radar case, a sufficient number of pulses are transmitted for each beam, to allow a sufficient number of degrees of freedom to be used to estimate the covariance matrix. In fact, the directional transmission radiates less energy in the directions of scatterers out of main beam, which potentially enhances the performance of ES beamforming. For BS processing, the standard BS approaches assume that the phased array is passive or the transmission is omni-directional and as shown by equation (3-2), the BS covariance matrix is a linear transformation of an invariant ES covariance matrix. However, for the directional transmission where the receiver ES covariance matrix varies with the Tx/Rx beam, the linear transformation between BS and ES covariance matrices represented in (3-2) no longer exists; and as will be shown in Section 4.1.2, the performance of standard BS processing is degraded when it is applied to the directionally transmitted BS data.

In this chapter, the directional transmission ES/BS model is analysed and some examples are represented to illustrate shortcomings of the standard BS processing for the directional transmission BS model. Then new BS processing formulae for the directional transmission problem are derived by taking into account the directional nature of the transmitter. Finally, the performance of the new formulae for the directional transmission is analysed and evaluated. Notice that only the narrowband signal case is considered as the analysis can be readily adapted for the case of wide band signals.

4.1 Formulation of Directional Transmission BS Processing

When Tx/Rx beams are scanned over a sector of interest, each Tx/Rx beam dwells in a certain direction for a finite interval before switching to the next direction. The dwell duration depends on the pulse repetition frequency (PRF), number of collected samples and the beam scanning strategy. To process outputs of several beams whose MRAs lie in different directions together, an important assumption is that the scatterers remain stationary during the period over which the Tx/Rx beams scan across the sector of interest. With rapid electronic scanning of modern phased arrays, the directional Tx/Rx beam scanning can be completed in a very short time and most scatterers are near to stationary during this process. A special scenario containing a moving target will be specifically discussed later in Chapter 5.

4.1.1 Directional Transmission Model

Consider a scenario of an active phased array system where the transmit energy is beamformed in a certain direction and then scattered and reflected energy is received by a receive beam formed in the same direction. For a pulse in the *m*-th beam, most energy is transmitted through the mainlobe whose centre is at an azimuthal angle θ_m, and some energy is also transmitted via sidelobes. The transmitted energy reaches and is reflected by each of L scatterers located at a set of angles $\Theta_s = \{\theta_{s1}, \theta_{s2}, \ \ldots, \ \theta_{sL}\}$ in the same range bin. By transmitting a unit amplitude signal at the beam centre, θ_m, and ignoring any propagation loss, the amplitudes of the reflected signals, which are proportional to their radar cross sections (RCS), are written as an $L \times 1$ vector $[\sigma_{s1} \ \sigma_{s2} \ \ \ldots \ \ \sigma_{sL}]^T$. This scenario is illustrated in Figure 4-2.

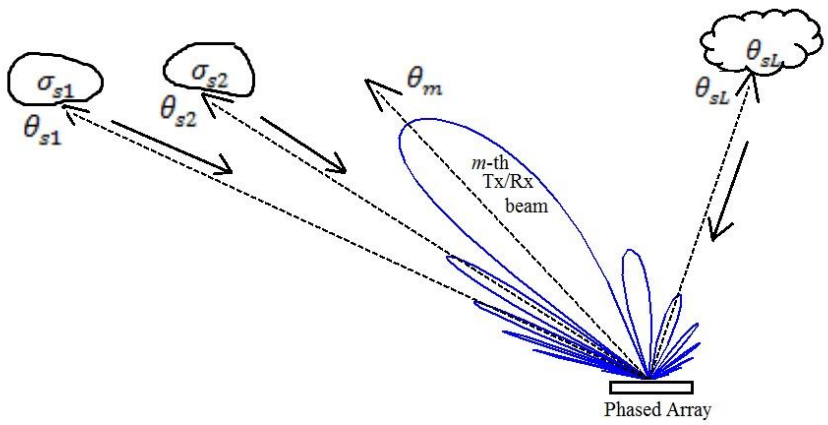

Figure 4-2: Plane wave propagation by using a directional Tx/Rx phased array.

For a signal $s(t)$ directionally transmitted by a phased array in a beam steered at an angle θ_m, the vector of transmit waveforms at the array elements is given by $s(t)\,\boldsymbol{v}^*(\theta_m)$. Assuming that unit signal energy is transmitted at the MRA in the

mainlobe, then at an azimuthal angle, θ_{sl}, the DOA of the l-th scatterer, energy is propagated through the mainlobe or a sidelobe of the transmit beam and is given by

$$s_T(\theta_m, \theta_{sl}) = s(t)\boldsymbol{v}^H(\theta_m)\boldsymbol{v}(\theta_{sl})/K\,. \tag{4-1}$$

This signal is reflected by the l-th scatterer, then received by those K elements of the phased array and the vector of receiver outputs is given by

$$\boldsymbol{s}_{TR}(\theta_m, \theta_{sl}) = \sigma_{sl}s(t)\boldsymbol{v}(\theta_{sl})\boldsymbol{v}^H(\theta_m)\boldsymbol{v}(\theta_{sl})/K, \tag{4-2}$$

where the additional $\boldsymbol{v}(\theta_{sl})$ term represents the phase delays across the receive array. In vector notation, the vector of receiver outputs due to the transmission of the m-th beam can be expressed as the summation of the signals reflected by different scatterers and receiver noise in this beam, and is given by

$$\begin{aligned}\boldsymbol{x}(\theta_m) &= \sum_{l=1}^{l=L} \boldsymbol{s}_{TR}(\theta_m, \theta_{sl}) + \boldsymbol{n}(\theta_m) \\ &= \boldsymbol{V_s}(\Theta_s)(\boldsymbol{V_s}^T(\Theta_s)\boldsymbol{v}^*(\theta_m)/K \circ \boldsymbol{s}) + \boldsymbol{n}(\theta_m),\end{aligned} \tag{4-3}$$

where $(\cdot)^*$ denotes complex conjugate; $\circ$ denotes the Hadamard product; $\boldsymbol{V_s}(\Theta_s)$ is given by equation (3-23); $\boldsymbol{s} = s(t)[\sigma_{s1} \quad \sigma_{s2} \quad \cdots \quad \sigma_{sL}]^{\mathrm{T}}$ and $\boldsymbol{n}(\theta_m)$ denotes the vector of receiver noise in the period when the m-th transmit beam is formed. A consequence of the sequential scanning strategy is that the noise can be assumed to be independent from beam to beam. The dependence of the receiver outputs on the transmit beam is made explicit in $\boldsymbol{x} = \boldsymbol{x}(\theta_m)$. The appearance of $\boldsymbol{V_s}(\Theta_s)$ twice reflects the fact that phase delays need to be accounted for both transmit and receive. Thus the ES covariance matrix is transmit beam dependent and can be shown to be given by

$$\boldsymbol{R_x}(\theta_m) = \boldsymbol{V_x}(\Theta_s, \theta_m)\boldsymbol{R_s}\boldsymbol{V_x}^H(\Theta_s, \theta_m) + E\{\boldsymbol{n}(\theta_m)\boldsymbol{n}^H(\theta_m)\}. \tag{4-4}$$

where
$$\boldsymbol{V_x}(\Theta_s, \theta_m) = [\boldsymbol{v_x}(\theta_{s1}, \theta_m) \quad \boldsymbol{v_x}(\theta_{s2}, \theta_m) \quad \cdots \quad \boldsymbol{v_x}(\theta_{sL}, \theta_m)], \tag{4-5}$$

and
$$\boldsymbol{v_x}(\theta_{si}, \theta_m) = \boldsymbol{v}(\theta_{si})\boldsymbol{v}^H(\theta_m)\boldsymbol{v}(\theta_{si})/K,\ i = 1, 2 \cdots L. \tag{4-6}$$

The vector containing the beamformer outputs corresponding to the M different transmit/receive beams is given by

$$\boldsymbol{y} = \begin{bmatrix} y(\theta_1) \\ y(\theta_2) \\ \vdots \\ y(\theta_M) \end{bmatrix} = \begin{bmatrix} \boldsymbol{v}^H(\theta_1)\boldsymbol{x}(\theta_1) \\ \boldsymbol{v}^H(\theta_2)\boldsymbol{x}(\theta_2) \\ \vdots \\ \boldsymbol{v}^H(\theta_M)\boldsymbol{x}(\theta_M) \end{bmatrix}, \tag{4-7}$$

where the dependence of each component of $\boldsymbol{y}$ on the particular chosen direction of the transmit beam is explicitly shown. The directional transmission BS steering vector,

which is the $M\times1$ vector of beam outputs for a single scatterer with a unit radar cross section at angle θ_{si}, is given by

$$\boldsymbol{v_y}(\theta_{si}) = \begin{bmatrix} \boldsymbol{v}^H(\theta_1)\boldsymbol{v}(\theta_{si})\boldsymbol{v}^H(\theta_1)\boldsymbol{v}(\theta_{si})/K \\ \boldsymbol{v}^H(\theta_2)\boldsymbol{v}(\theta_{si})\boldsymbol{v}^H(\theta_2)\boldsymbol{v}(\theta_{si})/K \\ \vdots \\ \boldsymbol{v}^H(\theta_M)\boldsymbol{v}(\theta_{si})\boldsymbol{v}^H(\theta_M)\boldsymbol{v}(\theta_{si})/K \end{bmatrix}. \tag{4-8}$$

For spatial and temporal white receiver noise, the receiver noise vectors due to different transmit beams are independent of each other, as those beams are formed at different times. Thus ES noise covariance matrices satisfy

$$\begin{gathered} E\{\boldsymbol{n}(\theta_m)\boldsymbol{n}^H(\theta_m)\} = \sigma_n^2\boldsymbol{I} \\ E\{\boldsymbol{n}(\theta_p)\boldsymbol{n}^H(\theta_q)\} = \boldsymbol{0}, p \neq q. \end{gathered} \tag{4-9}$$

Thus the directional transmission BS noise covariance matrix is given by

$$\begin{aligned} \boldsymbol{R_{yn}} &= \begin{bmatrix} \boldsymbol{v}^H(\theta_1)\boldsymbol{v}(\theta_1)\sigma_n^2 & & \boldsymbol{0} \\ & \boldsymbol{v}^H(\theta_2)\boldsymbol{v}(\theta_2)\sigma_n^2 & \\ \boldsymbol{0} & & \ddots \\ & & \boldsymbol{v}^H(\theta_M)\boldsymbol{v}(\theta_M)\sigma_n^2 \end{bmatrix} \\ &= K\sigma_n^2\boldsymbol{I}_{M\times M}. \end{aligned} \tag{4-10}$$

When there is only a single scatterer at angle θ_s and its amplitude is σ_s at any single receiver, the directional transmission BS covariance matrix is given by

$$\boldsymbol{R_{y(1)}} = \sigma_s^2\boldsymbol{v_y}(\theta_s)\boldsymbol{v_y^H}(\theta_s) + K\sigma_n^2\boldsymbol{I}_{M\times M}. \tag{4-11}$$

For L uncorrelated scatterers, $\boldsymbol{R_s} = diag\{\sigma_{s1}^2, \quad \sigma_{s2}^2, \quad \ldots, \quad \sigma_{sL}^2\}$ and

$$\boldsymbol{R_y} = \sum_{i=1}^{L}\sigma_{si}^2\boldsymbol{v_y}(\theta_{si})\boldsymbol{v_y^H}(\theta_{si}) + K\sigma_n^2\boldsymbol{I}. \tag{4-12}$$

In vector notation, the BS covariance matrix with directional Tx/Rx scanning is given by

$$\boldsymbol{R_y} = \boldsymbol{V_y}(\Theta_s)\boldsymbol{R_s}\boldsymbol{V_y^H}(\Theta_s) + K\sigma_n^2\boldsymbol{I}_{M\times M}. \tag{4-13}$$

where
$$\boldsymbol{V_y}(\Theta_s) = [\boldsymbol{v_y}(\theta_{s1}) \quad \boldsymbol{v_y}(\theta_{s2}) \quad \ldots \quad \boldsymbol{v_y}(\theta_{sL})]. \tag{4-14}$$

The above equation (4-13) for the BS covariance matrix also can be used for the case where signals are correlated but with a different expression for the source covariance matrix, $\boldsymbol{R_s}$, which will be discussed in Chapter 6.

4.1.2 Application of Standard BS Processing to Directionally Transmitted BS Data

As has been discussed, the steering vector for a directionally transmitted data is different from that of the standard omni-directional transmission. In this section, to check if the standard BS algorithms are adequate for the directional transmission problem, the standard optimum BS beamforming formula (3-10) is applied to the BS covariance matrix for the directional transmission case, i.e., (4-13).

There are two possible ways of applying the standard BS MVDR algorithm to the directional transmission model. In the first scenario, the MVDR weights are calculated using an omni-directional transmission BS covariance matrix. This can happen when observing a stationary environment with weights designed by using previous knowledge of the environment. However, as variations of the signals and noise are very common, this approach is only used for the conventional beamformer and will not be discussed here.

In the other case, the beamformer works in an online update fashion. The BS MVDR weights are calculated using the covariance matrix estimated from samples of the directionally transmitted BS data, which is then substituted directly into the standard BS expression for the beamformer weight and output power. This is more likely to happen and further discussion will be based on it.

In this way, the vector of BS MVDR beamforming weights at an angle θ is given by

$$\boldsymbol{w}(\theta) = \frac{\boldsymbol{R}_{\boldsymbol{y}}^{-1}\boldsymbol{V}^H\boldsymbol{v}(\theta)}{\boldsymbol{v}^H(\theta)\boldsymbol{V}\boldsymbol{R}_{\boldsymbol{y}}^{-1}\boldsymbol{V}^H\boldsymbol{v}(\theta)}, \tag{4-15}$$

and the output power can be expressed as

$$p_{MVDR-BS}(\theta) = \left(\boldsymbol{h}^H(\theta)\boldsymbol{R}_{\boldsymbol{y}}\boldsymbol{h}(\theta)\right)^{-1}. \tag{4-16}$$

For L uncorrelated signals, substituting the exact directional Tx BS covariance matrix given by (4-12) into $\boldsymbol{R}_{\boldsymbol{y}}$, the above expression can be written as

$$p_{MVDR-BS}(\theta) = \left(\boldsymbol{h}^H(\theta)\left(\sum_{i=1}^{L}\sigma_{si}^2\boldsymbol{v}_{\boldsymbol{y}}(\theta_{si})\boldsymbol{v}_{\boldsymbol{y}}^H(\theta_{si}) + K\sigma_n^2\boldsymbol{I}\right)^{-1}\boldsymbol{h}(\theta)\right)^{-1}. \tag{4-17}$$

The simplest case of a single scatter whose DOA is θ_s which lies inside the sector of interest and whose signal noise ratio (SNR) is σ_s^2/σ_n^2 is considered. The BS covariance matrix containing a single scatterer is given by (4-11), and using the matrix inversion

lemma, its inverse is given by

$$\boldsymbol{R}_{\boldsymbol{y}(1)}^{-1} = \frac{\boldsymbol{I}}{K\sigma_n^2}\left[\boldsymbol{I} - \boldsymbol{v_y}(\theta_s)\left(\boldsymbol{v}_{\boldsymbol{y}}^H(\theta_s)\boldsymbol{v_y}(\theta_s) + K\sigma_n^2/\sigma_s^2\right)^{-1}\boldsymbol{v}_{\boldsymbol{y}}^H(\theta_s)\right]. \tag{4-18}$$

By using the standard formula, the optimum BS beamformer output power at an azimuthal angle θ_s, i.e., when the optimum receive beam is pointed directly at the scatterer, is given by

$$\begin{aligned} p_{MVDR-BS}(\theta_s) &= K\sigma_n^2\left(\boldsymbol{h}^H(\theta_s)\left(\boldsymbol{I} - \boldsymbol{v_y}(\theta_s)\left(\boldsymbol{v}_{\boldsymbol{y}}^H(\theta_s)\boldsymbol{v_y}(\theta_s) + K\sigma_n^2/\sigma_s^2\right)^{-1}\boldsymbol{v}_{\boldsymbol{y}}^H(\theta_s)\right)\boldsymbol{h}(\theta_s)\right)^{-1} \\ &= \frac{K\sigma_n^2(k_y(\theta_s)\sigma_s^2 + K\sigma_n^2)}{\left(H(\theta_s)k_y(\theta_s) - H_y(\theta_s)\right)\sigma_s^2 + H(\theta_s)K\sigma_n^2}, \end{aligned} \tag{4-19}$$

where two scalars are defined as

$$\begin{aligned} k_y(\theta_s) &= \boldsymbol{v}_{\boldsymbol{y}}^H(\theta_s)\boldsymbol{v_y}(\theta_s), \\ H_y(\theta_s) &= \boldsymbol{h}^H(\theta_s)\boldsymbol{v_y}(\theta_s)\boldsymbol{v}_{\boldsymbol{y}}^H(\theta_s)\boldsymbol{h}(\theta_s), \end{aligned} \tag{4-20}$$

and $H(\theta_s)$has been given by (3-30) as $H(\theta_s) = \|\boldsymbol{h}(\theta_s)\|^2$. In this case the standard BS formula assumes the omni-directional transmission and only considers the receive beam pattern, and its assumed BS steering vector $\boldsymbol{h}(\theta_s)$ is mismatched with the actual BS steering vector $\boldsymbol{v_y}(\theta_s)$, which represents the response of an incident signal in different beam outputs. The actual array manifold is determined by $\boldsymbol{v_y}(\theta)$, but as the standard BS MVDR processor maintains a unity response for $\boldsymbol{h}(\theta_s)$, and the energy at the BS steering vector $\boldsymbol{v_y}(\theta_s)$, is suppressed. According to (4-19), the signal power at θ_s is attenuated to be $\frac{K\sigma_n^2 k_y(\theta_s)\sigma_s^2}{\left(H(\theta_s)k_y(\theta_s) - H_y(\theta_s)\right)\sigma_s^2 + H(\theta_s)K\sigma_n^2}$. The Cauchy–Schwarz inequality states $H(\theta_s)k_y(\theta_s) > H_y(\theta_s)$, then $\left(H(\theta_s)k_y(\theta_s) - H_y(\theta_s)\right)\sigma_s^2 > 0$, also $k_y(\theta_s) < H(\theta_s)$, thus the beamformer output power in (4-19) is smaller than the output for the omni-directional transmission model, which is given by (3-11), and the difference depends on the difference between $k_y(\theta_s)$ and $H(\theta_s)$.

The above expression (4-19) was evaluated for the example of a horizontal, ULA of 64 elements spaced half a wavelength apart. Only 21 beams were formed and spanned the azimuthal region of -2° to 18° with 1° separation. One scatterer whose return with SNR of 10 dB at any single receiver was located at the azimuthal angle 8°. The theoretical output power values of the ES conventional, ES MVDR beamformers, which assume the ES covariance matrices in different beams are accessible, and the standard BS MVDR for the directional transmission model using formula (4-16) are plotted in Figure 4-3. As the covariance matrices varied for each transmit beam, the ES results were obtained by

processing the 21 sectors separately. For any look angle, the covariance matrix corresponding to the nearest transmit beam centre was used to derive the output power.

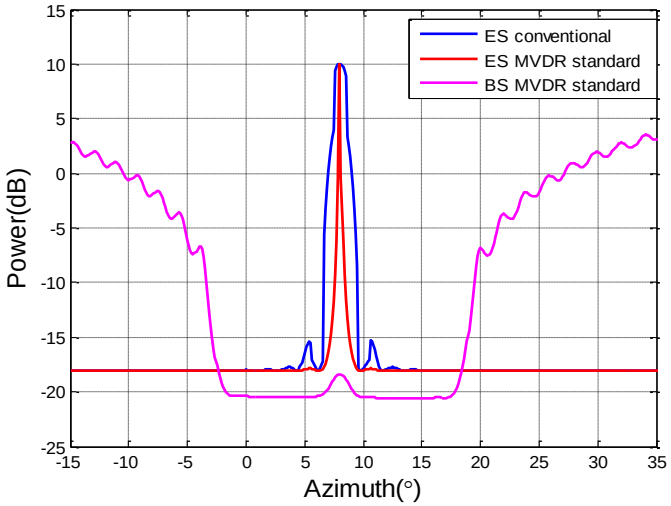

Figure 4-3: An example of applying the standard BS MVDR formula to the directional transmission model (single scatterer) and comparing with the normalised ES conventional and MVDR beamformers.

In this case, the results of using standard BS MVDR for the directional transmission model are unsatisfactory. It indicates the correct DOA but with a poor resolution and the output power value is much lower than the true power of the signal.

To check the impact of SNR, the standard BS MVDR beamformer output power (referenced to the noise level) at the DOA of the scatterer (8°) versus different SNR is plotted in Figure 4-4. As shown, below -5 dB the output power increases approximately linearly with input SNR but above -5 dB it plateaus. According to the MVDR optimisation criterion, the standard MVDR BS beamformer keeps unity response on $\boldsymbol{h}(\theta_s)$ at an angle θ_s and suppresses energy from other vectors, including other directions in the manifold and any mismatched steering vectors. Due to the mismatch between $\boldsymbol{h}(\theta_s)$ and the actual steering vector $\boldsymbol{v_y}(\theta_s)$, the signal component in $\boldsymbol{v_y}(\theta_s)$ is wrongly treated as an interference. With a low SNR, i.e., lower than 0 dB, the energy on the actual steering vector $\boldsymbol{v_y}(\theta_s)$ is only slightly higher than the noise level, so there is no strong suppression to $\boldsymbol{v_y}(\theta_s)$ by the beamformer and the output changes near linearly but slowly. When the SNR is higher, a deep null is formed to cancel the signal component specified by $\boldsymbol{v_y}(\theta_s)$ as it is treated as a strong interference and the beamformer output does not change significantly with further SNR increasing. In all cases the output power is significantly lower than the actual power of the signal.

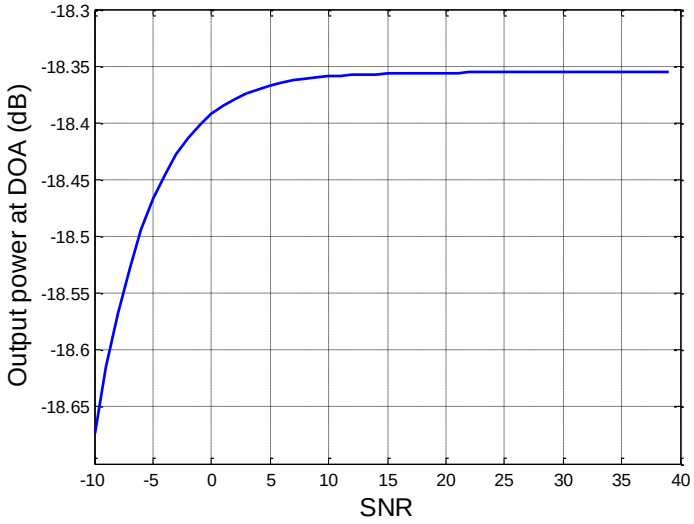

Figure 4-4: Beamformer output power versus SNR, when standard MVDR BS formula is applied to a directional transmission BS model containing only one signal.

To check if the DOA of the scatterer affects the performance of the standard BS MVDR algorithm, DOA of the signal is varied over a range of azimuthal angles, and then the corresponding beamformer output power at the DOA of the signal was evaluated. The results are shown in Figure 4-5 and indicate that the loss in signal power due to mismatch does not vary significantly with DOA within the sector.

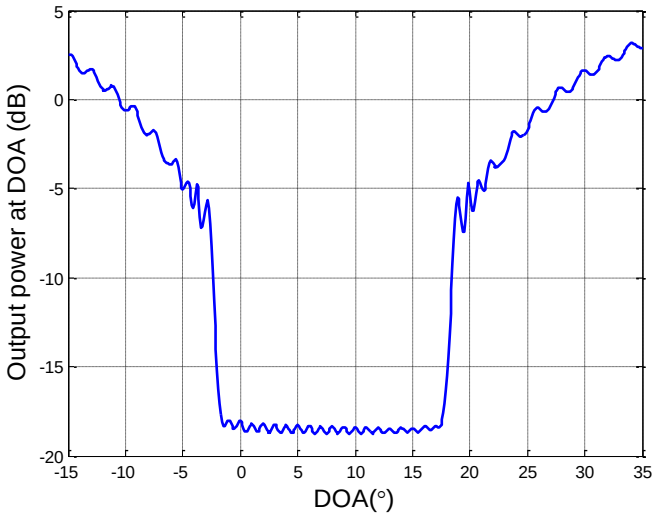

Figure 4-5: Beamformer output power value versus DOA of the in sector signal, when standard MVDR BS formula is applied to a directional transmission BS model containing only one signal.

To check if the number of scatterers affects the result, another scatterer whose return has an SNR of 6 dB at any single receiver and which is incident at an azimuthal angle of 15° was added. The output power values of the ES conventional, MVDR and standard BS MVDR beamformer are plotted versus azimuthal angle in Figure 4-6.

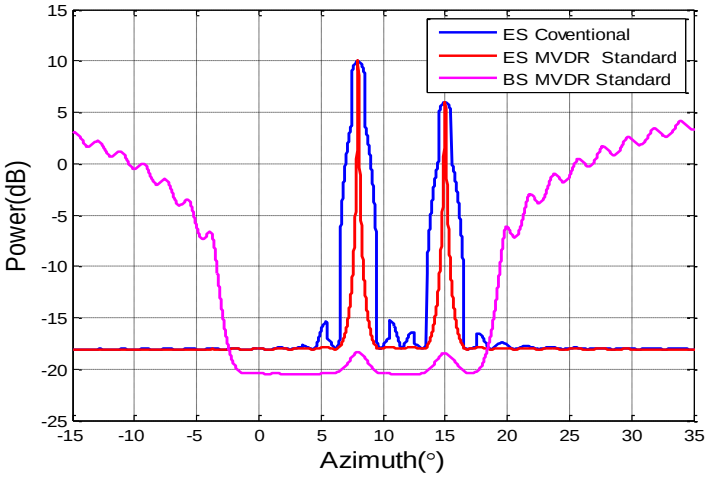

Figure 4-6: An example of applying the standard optimum BS formula to a directional transmission model (two targets) and comparing with the ES conventional and MVDR beamformers.

It can be seen from the above figure, although both DOAs of signals can be roughly estimated by the standard BS MVDR method, the mismatch has resulted in very low output power at DOAs of signals for the standard BS MVDR algorithm.

In summary, the standard BS MVDR beamforming formula does not provide adequate performance for the directional transmission BS case, since the mismatch between the assumed and actual BS steering vectors causes its performance to be significantly degraded. Significant performance losses are found for a range of incident angles, which indicate that the performance degradation is independent of DOAs and the poor performance with other variations also show it is almost independent of SNR and number of scatterers.

4.1.3 Formulation of Directional Transmission BS Processing

As shown in the last section, the performance of the standard MVDR BS formula when narrow beams are transmitted and scanned over a sector of interest is unsatisfactory due to a mismatch between the actual BS steering vector in the directional transmission model and the steering vector being used in the omni-directional transmission formula. To solve this problem, the proposed approach follows the thread of the standard BS processing method, which considers a linear transformation between the BS and ES covariance matrices and derives formulae based on this transformation. Referring to (3-2), which shows the linear transformation between the ES and BS covariance matrices and the formulae equations such as (3-9) and (3-10), are based on an invariant ES covariance matrix, in the sense that it is the same for all receive beams. However, for the directional transmission case, the ES covariance matrix varies as the transmit beam changes and so these formulae are no longer applicable.

The form of receiver outputs change with each transmit beam, and so each conventional receive beam output, which is the summation of the receiver outputs with appropriate phase alignment, will reflect this variation. To set up a linear transformation between ES and BS covariance matrices, all the receiver outputs in each of the *M* different transmit beams are stacked as a *KM*×1 vector

$$\boldsymbol{x}_s = \begin{bmatrix} \boldsymbol{x}(\theta_1) \\ \boldsymbol{x}(\theta_2) \\ \vdots \\ \boldsymbol{x}(\theta_M) \end{bmatrix}. \tag{4-21}$$

The corresponding *KM*×*KM* covariance matrix is given by

$$\begin{aligned} \boldsymbol{R}_{xs} &= E\{\boldsymbol{x}_s \boldsymbol{x}_s^H\} \\ &= E\left\{ \begin{bmatrix} \boldsymbol{x}(\theta_1)\boldsymbol{x}^H(\theta_1) & \boldsymbol{x}(\theta_1)\boldsymbol{x}^H(\theta_2) & \dots & \boldsymbol{x}(\theta_1)\boldsymbol{x}^H(\theta_M) \\ \boldsymbol{x}(\theta_2)\boldsymbol{x}^H(\theta_1) & \boldsymbol{x}(\theta_2)\boldsymbol{x}^H(\theta_2) & \dots & \boldsymbol{x}(\theta_2)\boldsymbol{x}^H(\theta_M) \\ \vdots & \vdots & \ddots & \vdots \\ \boldsymbol{x}(\theta_M)\boldsymbol{x}^H(\theta_1) & \boldsymbol{x}(\theta_M)\boldsymbol{x}^H(\theta_2) & \dots & \boldsymbol{x}(\theta_M)\boldsymbol{x}^H(\theta_M) \end{bmatrix} \right\}. \end{aligned} \tag{4-22}$$

The *M*×1 vector of beam outputs is given by

$$\boldsymbol{y} = \begin{bmatrix} y(\theta_1) \\ y(\theta_2) \\ \vdots \\ y(\theta_M) \end{bmatrix} = \begin{bmatrix} \boldsymbol{v}^H(\theta_1)\boldsymbol{x}(\theta_1) \\ \boldsymbol{v}^H(\theta_2)\boldsymbol{x}(\theta_2) \\ \vdots \\ \boldsymbol{v}^H(\theta_M)\boldsymbol{x}(\theta_M) \end{bmatrix} = \boldsymbol{U}^H \boldsymbol{x}_s, \tag{4-23}$$

where a *KM*×*M* linear transformation matrix is given by

$$\boldsymbol{U} = \begin{bmatrix} \boldsymbol{v}(\theta_1) & 0 & \cdots & 0 \\ 0 & \boldsymbol{v}(\theta_2) & \vdots & 0 \\ \vdots & \vdots & \ddots & \vdots \\ 0 & 0 & \cdots & \boldsymbol{v}(\theta_M) \end{bmatrix}. \tag{4-24}$$

The resulting *M*×*M* BS covariance matrix is given by

$$\boldsymbol{R}_{\boldsymbol{y}} = E\{\boldsymbol{y}\boldsymbol{y}^H\} = \boldsymbol{U}^H \boldsymbol{R}_{\boldsymbol{xs}} \boldsymbol{U}. \tag{4-25}$$

The *KM*×1 stacked ES steering vector $\boldsymbol{v}_{\boldsymbol{p}}(\theta)$ corresponding to a plane wave incident on the receive array from direction θ but taking into account the *M* different transmission beam patterns (see equation (4-2)) is given by

$$\boldsymbol{v}_{\boldsymbol{p}}(\theta) = \begin{bmatrix} \boldsymbol{v}(\theta)\boldsymbol{v}^H(\theta_1)\boldsymbol{v}(\theta)/K \\ \boldsymbol{v}(\theta)\boldsymbol{v}^H(\theta_2)\boldsymbol{v}(\theta)/K \\ \vdots \\ \boldsymbol{v}(\theta)\boldsymbol{v}^H(\theta_M)\boldsymbol{v}(\theta)/K \end{bmatrix} = \boldsymbol{v}(\theta) \otimes \left(\boldsymbol{V}^H \boldsymbol{v}(\theta)\right)/K, \tag{4-26}$$

where $\otimes$ denotes the Kronecker product and $\boldsymbol{V}$ is given by (3-3). The BS steering vector, $\boldsymbol{v_y}(\theta)$, which represents the M beam outputs when a wave with unit amplitude is incident (Tx/Rx) on the array from direction θ, is given by

$$\begin{aligned}\boldsymbol{v_y}(\theta) &= \boldsymbol{U}^H\boldsymbol{v_p}(\theta)\\ &= \frac{1}{K}\begin{bmatrix}\boldsymbol{v}^H(\theta_1)\boldsymbol{v}(\theta)\boldsymbol{v}^H(\theta_1)\boldsymbol{v}(\theta)\\ \boldsymbol{v}^H(\theta_2)\boldsymbol{v}(\theta)\boldsymbol{v}^H(\theta_2)\boldsymbol{v}(\theta)\\ \vdots\\ \boldsymbol{v}^H(\theta_M)\boldsymbol{v}(\theta)\boldsymbol{v}^H(\theta_M)\boldsymbol{v}(\theta)\end{bmatrix}\\ &= \boldsymbol{h}(\theta)\circ\boldsymbol{h}(\theta)/K\end{aligned} \tag{4-27}$$

The stacking process sets up the linear transformation between the stacked ES and BS covariance matrices, but processing in ES is actually not always necessary. To consider the problem in another way, the BS covariance matrix can be modelled from source signal to beam outputs directly, as given by equation (4-13), and the ES covariance matrix is not explicitly used. It also leads to the same expression for the directional transmission BS steering vector, but no receiver outputs or ES covariance matrices are required as an intermediate step.

The directional transmission BS beamformer output power is a linear combination of the preformed beam outputs and is given by $\boldsymbol{w}^H(\theta)\boldsymbol{R_y}\boldsymbol{w}\,(\theta)$ and minimising this subject to the constraint that $\boldsymbol{w}^H\boldsymbol{v_y}(\theta) = 1$, the vector containing the weights for an optimum beam steered at angle θ is given by

$$\boldsymbol{w}_{MVDR-BS}(\theta) = \frac{\boldsymbol{R_y^{-1}}\boldsymbol{v_y}(\theta)}{\boldsymbol{v_y^H}(\theta)\boldsymbol{R_y^{-1}}\boldsymbol{v_y}(\theta)} = \frac{\boldsymbol{R_y^{-1}}\boldsymbol{U}^H\boldsymbol{v_p}(\theta)}{(\boldsymbol{v_p^H}(\theta)\boldsymbol{U}\boldsymbol{R_y^{-1}}\boldsymbol{U}^H\boldsymbol{v_p}(\theta)}. \tag{4-28}$$

Substituting the weight vector into the expression, $\boldsymbol{w}^H(\theta)\boldsymbol{R_y}\boldsymbol{w}\,(\theta)$, the output power of the BS MVDR beamformer at θ is given by

$$p_{MVDR-BS}(\theta) = \left((\boldsymbol{v_p^H}(\theta)\boldsymbol{U}\boldsymbol{R_y^{-1}}\boldsymbol{U}^H\boldsymbol{v_p}(\theta)\right)^{-1}, \tag{4-29}$$

or

$$p_{MVDR-BS}(\theta) = \left(\boldsymbol{v_y^H}(\theta)\boldsymbol{R_y^{-1}}\boldsymbol{v_y}(\theta)\right)^{-1}. \tag{4-30}$$

The directional transmission BS conventional beamforming formula is given by

$$p_{CB-BS}(\theta) = \tfrac{1}{G(\theta)}\boldsymbol{v_y^H}(\theta)\boldsymbol{R_y}\boldsymbol{v_y}(\theta). \tag{4-31}$$

where

$$G(\theta) = \left\|\boldsymbol{v_y}(\theta)\right\|^4, \tag{4-32}$$

and the directionally dependent gain factor ensures that a unit amplitude signal from direction θ results in unit amplitude beam output power. Similarly to the conventional BS beamformer for the omni-directional transmission case, the approach can be

interpreted as simply performing an interpolation between the outputs of preformed directional Tx/Rx beams. So, it is of limited interest and mainly used as a baseline to check the performance of other BS processing algorithms.

For the omni-directional transmission case, the same or near to same gain is applied to scatterers in different directions, whilst for the directional transmission case, a signal transmitted and received through sidelobes has a lower gain than the return from a scatterer in the mainlobe. Thus, the BS conventional beamforming may achieve a better result than the omni-directional transmission, as less energy from scatterers whose DOAs lie outside the beam mainlobe is contained in the beam output. In some cases when high resolution is not required, the conventional beamformer can be used and it additionally provides some robustness to different types of steering vector mismatch, such as that caused by calibration errors.

To derive the MUSIC formula for the directional transmission BS case, the constraint vector $\boldsymbol{h}(\theta)$ in equation (3-19) is simply replaced by the directional transmission steering vector $\boldsymbol{v_y}(\theta)$ and the formula is given by

$$p(\theta)_{MUSIC-BS} = \frac{1}{\sum_{i=L+1}^{M} |\boldsymbol{v}_{\boldsymbol{y}}^{H}(\theta)\boldsymbol{q}_{\boldsymbol{y}i}|^2}. \tag{4-33}$$

where $\boldsymbol{q}_{\boldsymbol{y}i}, (L < i \leq M)$ are the set of eigenvectors of the BS covariance matrix, $\boldsymbol{R_y}$, corresponding to the *M-L* smallest eigenvalues and span the BS noise subspace. Notice that as shown in (4-10), for the directional transmission case, the white noise in each beam is independent as they occur at different times. Thus, no pre-whitening process is required anymore for BS processing and it is not necessary that these beams are mutually orthogonal.

4.2 Performance Evaluation of Directional Transmission Optimum BS Beamformer

In this section, the output expression of the directional transmission optimum BS beamformer using MVDR criterion is theoretically analysed, then, the performance of the algorithm verified by numerically evaluating the theoretical expression and then by applying the formula to a simulated BS data.

The simplest case is that directional Tx/Rx beams scan over a sector which only contains a single scatterer, and the optimum BS beamformer output at an azimuthal angle θ is analysed. For later use, the inner product of two directional transmission BS steering vectors at θ_1 and θ_2 is defined as

$$B(\theta_1, \theta_2) = \boldsymbol{v}_{\boldsymbol{y}}^{H}(\theta_1)\boldsymbol{v_y}(\theta_2). \tag{4-34}$$

The same scenario used for Figure 4-3 was used again, i.e., 21 directional ULA transmitted beams whose MRAs are at angles of -2° to 18° with 1° separation and a single scatterer whose return has SNR of 10 dB at any single receiver and whose DOA is 8°. The values of $k_y(\theta)$, defined in equation (4-20), and $|B(\theta, 8°)|$ are plotted as a function of θ in Figure 4-7. The blue curve indicates that the value of $k_y(\theta)$ is almost constant in the sector spanned by the beams, as it is the summation of the squared beam pattern values of different beams at angle θ. Denoting the mean value of $k_y(\theta)$ in the sector as K_y, then an approximation can be given by $k_y(\theta) \approx K_y$. The value of $k_y(\theta)$ drops dramatically when angle θ moves further away from the sector scanned by the beams. The value of $|B(\theta, 8^0)|$ decreases when the separation between θ and the DOA(8°) increases, and except for a non-interesting case that $\theta = 8^0$, for remaining angles within the sector scanned by the beams, $|B(\theta, 8^0)| \ll k_y(\theta)$.

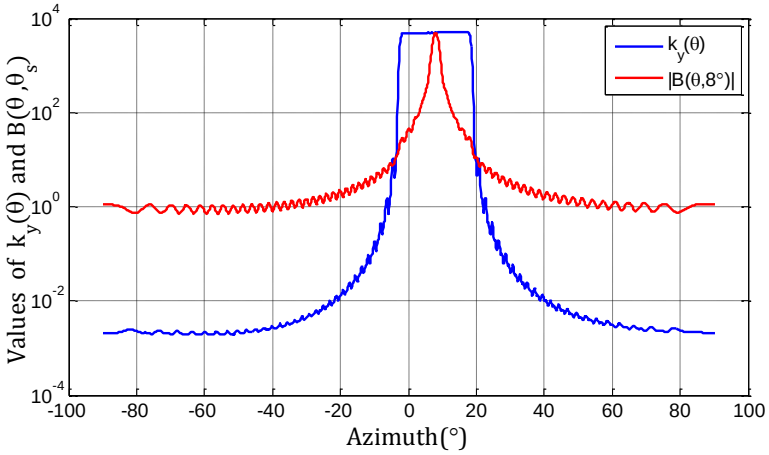

Figure 4-7: An example of values of $k_y(\theta)$ and $|B(\theta, 8^0)|$.

4.2.1 Theoretical Analysis

For the scenario of only a single scatterer, the covariance matrix is denoted by $\boldsymbol{R}_{\boldsymbol{y}(1)}$, and the optimum BS beamformer output power at angle θ is given by

$$\begin{aligned} p_{MVDR-BS}(\theta) &= \left(\boldsymbol{v}_{\boldsymbol{y}}^H(\theta)\boldsymbol{R}_{\boldsymbol{y}(1)}^{-1}\boldsymbol{v}_{\boldsymbol{y}}(\theta)\right)^{-1} \\ &= \frac{K\sigma_n^2(k_y(\theta_{s1})\sigma_{s1}^2 + K\sigma_n^2)}{k_y(\theta)K\sigma_n^2 + (k_y(\theta)k_y(\theta_{s1}) - |B(\theta,\theta_{s1})|^2)\sigma_{s1}^2}. \end{aligned} \tag{4-35}$$

When $\theta = \theta_{s1}$, i.e., the optimum beam is pointed directly at the DOA of the scatterer, $k_y(\theta) = k_y(\theta_{s1}) \approx K_y$ and $|B|^2 = k_y^2$, the above expression, (4-35), becomes

$$p_{MVDR-BS}(\theta_{s1}) \approx \sigma_{s1}^2 + \frac{K}{K_y}\sigma_n^2, \tag{4-36}$$

and confirms that the output power of a beam steered in the signal direction is independent of the DOA of the signal and also shows that the noise power is reduced by a factor of $\frac{K}{K_y}$.

When $\theta \neq \theta_{s1}$, but lies within the sector of interest where $k_y(\theta) \approx K_y$ and Figure 4-7 shows that $|B|^2 \ll K_y^2$, thus the above expression is approximately given by

$$p_{MVDR-BS}(\theta) \approx \frac{K}{K_y}\sigma_n^2, \tag{4-37}$$

which is the same amount of the attenuated noise power in equation (4-36).

In the second example where two uncorrelated scatterer returns are incident on the phased array, the BS covariance matrix is given by

$$\boldsymbol{R}_{\boldsymbol{y}(1,2)} = \boldsymbol{R}_{\boldsymbol{y}(1)} + \sigma_{s2}^2 \boldsymbol{v}_{\boldsymbol{y}}(\theta_{s2})\boldsymbol{v}_{\boldsymbol{y}}^H(\theta_{s2}) \tag{4-38}$$

and hence

$$\boldsymbol{R}_{\boldsymbol{y}(1,2)}^{-1} = \boldsymbol{R}_{\boldsymbol{y}(1)}^{-1} - \frac{\sigma_{s2}^2 \boldsymbol{R}_{\boldsymbol{y}(1)}^{-1}\boldsymbol{v}_{\boldsymbol{y}}(\theta_{s2})\boldsymbol{v}_{\boldsymbol{y}}^H(\theta_{s2})\boldsymbol{R}_{\boldsymbol{y}(1)}^{-1}}{1 + \sigma_{s2}^2 \boldsymbol{v}_{\boldsymbol{y}}^H(\theta_{s2})\boldsymbol{R}_{\boldsymbol{y}(1)}^{-1}\boldsymbol{v}_{\boldsymbol{y}}(\theta_{s2})} \tag{4-39}$$

The optimum BS beamformer output power at the DOA of the second signal is given by

$$\begin{aligned} p_{MVDR-BS}(\theta_{s2}) &= \left(\boldsymbol{v}_{\boldsymbol{y}}^H(\theta_{s2})\boldsymbol{R}_{\boldsymbol{y}(1,2)}^{-1}\boldsymbol{v}_{\boldsymbol{y}}(\theta_{s2})\right)^{-1} \\ &= \sigma_{s2}^2 + \frac{K\sigma_n^2\left(k_y(\theta_{s1})\sigma_{s1}^2 + K\sigma_n^2\right)}{k_y(\theta_{s2})K\sigma_n^2 + \left(k_y(\theta_{s1})k_y(\theta_{s2}) - |B(\theta_{s1},\theta_{s2})|^2\right)\sigma_{s1}^2} \\ &= \sigma_{s2}^2 + p_1(\theta_{s2}), \end{aligned} \tag{4-40}$$

where $p_1(\theta_{s2})$ is the optimum BS beamformer output power at θ_{s2} for the case that only a single scatterer at θ_{s1}, which is described in equation (4-35). Similarly, the output at the DOA angle of the first signal, whose DOA is θ_{s1}, is given by

$$\begin{aligned} p_{MVDR-BS}(\theta_{s1}) &= \left(\boldsymbol{v}_{\boldsymbol{y}}^H(\theta_{s1})\boldsymbol{R}_{\boldsymbol{y}(1,2)}^{-1}\boldsymbol{v}_{\boldsymbol{y}}(\theta_{s1})\right)^{-1} \\ &= \sigma_{s1}^2 + \left(\boldsymbol{v}_{\boldsymbol{y}}^H(\theta_{s1})\boldsymbol{R}_{\boldsymbol{y}(2)}^{-1}\boldsymbol{v}_{\boldsymbol{y}}(\theta_{s1})\right)^{-1}, \end{aligned} \tag{4-41}$$

where $\boldsymbol{R}_{\boldsymbol{y}(2)}$ is the covariance matrix when only the second signal is incident onto the array.

Similarly, the above approaches can be readily extended to the expression for the case of L independent signals and the optimum BS beamformer output power is given by

$$p_{MVDR-BS}(\theta_{sl}) = \left(\boldsymbol{v}_{\boldsymbol{y}}^H(\theta_{sl})\boldsymbol{R}_{\boldsymbol{y}(\bar{l})}^{-1}\boldsymbol{v}_{\boldsymbol{y}}(\theta_{sl})\right)^{-1} + \sigma_{sl}^2, \tag{4-42}$$

where $\boldsymbol{R}_{\boldsymbol{y}(\bar{l})}$ denotes the BS covariance matrix without the returned signal from the l-th scatterer and is given by

$$\boldsymbol{R}_{\boldsymbol{y}(\bar{l})} = \boldsymbol{R}_{\boldsymbol{y}} - \sigma_{sl}^2 \boldsymbol{v}_{\boldsymbol{y}}(\theta_{sl}) \boldsymbol{v}_{\boldsymbol{y}}^H(\theta_{sl}). \tag{4-43}$$

The above derivations and theoretical analysis describe the output of the directional transmission optimum BS beamformer inside the angular sector scanned by the beams, i.e., the sector of interest. For the scenario of a single scatterer, the optimum BS beamformer output power at the DOA of the scatterer is a summation of the signal power and the noise power attenuated by a factor of K/K_y. The output power value at one of other azimuthal angles inside the sector of interest is only the attenuated noise power. For a scenario of multiple independent scatterers, the output power at the DOA of a given scatterer is a summation of its power and the optimum BS beamformer output power at the angle where only returns from other scatterers incident, i.e., the BS covariance matrix becomes $\boldsymbol{R}_{\boldsymbol{y}(\bar{l})}$.

4.2.2 Numerical Analysis

The example in Figure 4-6 was used again and the directional transmission formula was numerically evaluated for the same signal model. The output power values of the directional transmission optimum BS beamformer, conventional and optimum ES beamformers using the exact form of the ES covariance matrices varying at each beam are plotted versus azimuth in Figure 4-8.

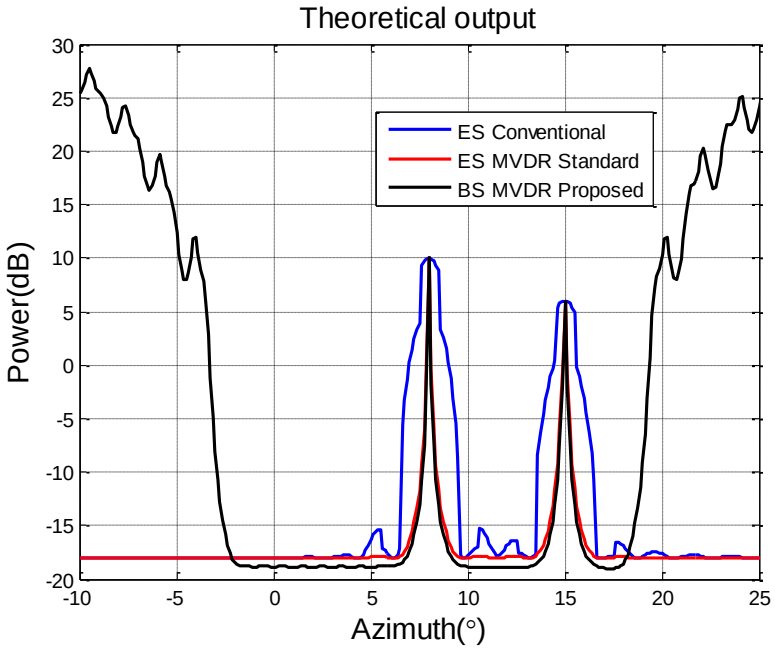

Figure 4-8: An example of applying the directional transmission optimum BS, conventional and optimum ES beamformers to the directional transmission model of two independent signals.

The performance of the directional transmission BS MVDR formula within the sector of interest is significantly better than the standard optimum BS beamformer results shown in Figure 4-6 and the high response outside the sector of interest will be discussed specifically in Chapter 5. The optimum BS beamformer output power values at the DOA of the signals are estimated accurately and the spatial resolution is much higher than the conventional ES beamforming and even slightly better than the standard ES MVDR, as the accumulated SNR gain from multiple directional transmission beams is higher than the gain applied by the optimum ES beamformer at one single beam.

4.2.3 Results on Simulated data

Based on the plane wave model described above, 128 realisations (pulses) were simulated. At each realisation, K element outputs and one beam output in each beam direction were simulated and those samples were then used to estimate the ES and BS covariance matrices. The result of applying the directional transmission optimum BS beamformer is shown in Figure 4-9, and the outputs of the conventional and optimum ES beamformers are also plotted. The plot indicates that the result is almost consistent with the numerical evaluation of the theoretical expressions. As shown in Figure 4-8, the numerical analysis result of the directional BS MVDR beamformer is slightly better than the standard ES MVDR, but for results using simulated data the BS MVDR algorithm has less suppression to the noise power. It indicates that the directional transmission optimum beamforming formula has a higher sensitivity of steering vector than the standard ES optimum beamformer and the performance would be improved by increasing the number of realisations.

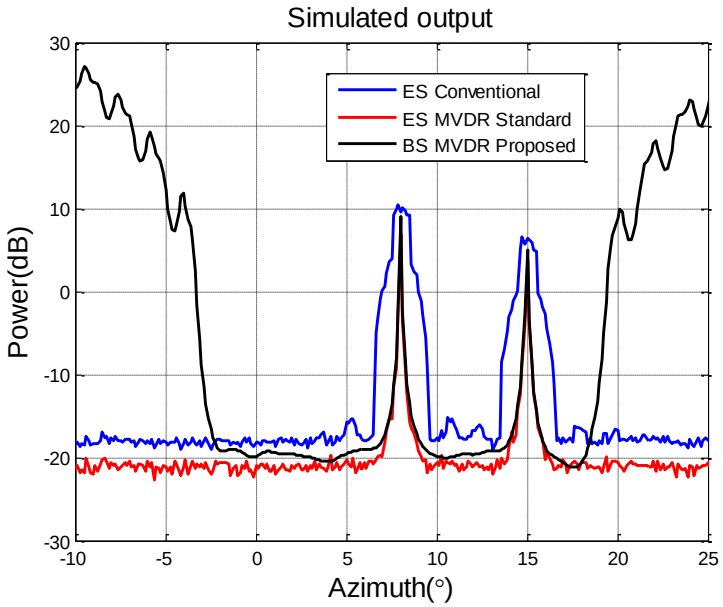

Figure 4-9: An example of applying the directional transmission BS MVDR formula to simulated directional transmission BS covariance matrix and comparing with the ES conventional and MVDR beamformers.

4.3 Summary

Phased arrays with relatively narrow scanning Tx/Rx beams are commonly used in practice, however few BS array processing algorithms have been developed for this specific case and the standard algorithms used for array processing always assume transmission is omni-directional or the transmitter directionality can be ignored. The standard ES array processing algorithms work well in each separate directional transmit beam, and even better than the omni-directional case, as the energy from scatterers which lie in the directions of sidelobes is attenuated. However, the standard BS algorithms fail when highly directional transmitters are used, due to the mismatch between the assumed omni-directional transmission and the actual directional transmission BS steering vectors. In many current phased array systems, sub-arrays are used on transmission, where the beam width is relatively wide. This is similar to the scenario illustrated in Figure 1-1, where the region of interest is approximately uniformly illuminated and in such cases standard ES or BS processing approaches are effective.

In this chapter, the BS model for the directional transmission case has been analysed. As the performance of applying the standard BS formula to the directional transmission covariance matrix is unsatisfactory, new BS algorithms specific for the directional transmission model were proposed. In Section 4.2, the theoretical optimum BS beamformer output power values inside the sector of interest were analysed and verified by numerical evaluation and simulation.

In conclusion, the proposed optimum BS beamforming algorithm for the directional transmission case modifies the steering vector to account for the various transmit beam pattern, and eliminates the mismatch with greatly improved results.

Chapter 5

Properties of Directional Transmission Beam Space Processing

In the previous chapter, new BS processing formulae, such as the directional transmission optimum BS beamforming, have been derived for phased arrays with relatively narrow directional transmission beams scanned over a sector of interest. In this chapter, some properties of such directional transmission BS processing are analysed.

Commonly, directional transmit/receive beams (main lobes) only scan over a sector. From the energy distribution perspective, the reflection of scatterers outside the sector may be not a significant issue as the energy radiated into this region is only through the sidelobe leakage. For the region outside the sector of interest, most related BS works in the literature treat it as "out of interest". Low sidelobe transmission beams, e.g., Dolph-Chebychev weighting, are suggested to be used to attenuate the returns from this region [30]. In [32], the transmit beams are specifically designed to increase the robustness to returns from outside of the region scanned by the preformed beams. However, in most practical systems the transmit beams are not specifically designed this way in advance and are either weighted by uniform or standard window functions. In some cases, scatterers outside the sector formed by conventional beams are sufficiently strong to return significant energy through sidelobes of the scanning Tx/Rx beams and there are three major unclear problems related to the region outside the sector of interest.

Firstly, it is not clear whether interferences lying outside the sector of interest, whose returns only propagate through sidelobes of those beams, can be detected and identified. Secondly, it has been noticed in Chapter 4, the optimum BS beamformer output power in the region outside the sector of interest is unexpectedly strong. This is a unique problem in BS processing and no discussion for this issue has been found in the literature. The reason for the high response is investigated and techniques for removing or avoiding the high response are developed. Thirdly, it is unknown if the interference outside the sector of interest would affect the optimum BS beamformer output power inside the sector.

In practice, different types of errors often occur in phased arrays due to imperfect calibration and limited precision of the hardware. These errors can seriously degrade the performance of both optimum ES and BS beamforming algorithms based on a perfect theoretical model. Some ES robust adaptive beamforming algorithms have been developed to increase robustness to such errors, but no solid work has been found for improving the robustness of the optimum BS beamformer. In this chapter, the directional transmission BS model with different errors is analysed and a typical robust ES

beamforming algorithm is modified and extended to the directional transmission BS case.

The Cramér–Rao bound (CRB) or Cramér–Rao lower bound (CRLB) describes the smallest variance achievable by any unbiased estimator. It is often discussed for different models and used to benchmark different estimation methods. The CRB for DOA estimation in the directional transmission BS case is derived and compared with the corresponding bounds for the omni-directional transmission ES and BS cases.

Developed BS processing algorithms are designed for stationary point scatterers, however these scatterers can be non-stationary or moving in practice. To check the usefulness of the algorithm for the moving scatterers, the performance of the directional BS beamformer under a scenario including a moving scatterer is analysed.

5.1 Directional Transmission BS Processing for the Region outside of the Sector of Interest

With directional Tx/Rx scanning beams, out of sector signals/interferences incident upon the array can be interferences from other transmitters or reflections of signals transmitted through sidelobe leakage. The first scenario is the passive phased array model and similar to the omni-directional transmission case discussed in Chapter 3. The second scenario needs to consider the beam pattern of the directional transmission beam and is further analysed in this chapter. Also, the analysis and methods for this problem can be readily applied to the first scenario by simply adjusting the transmission beam pattern.

5.1.1 Directional Transmission BS Model with an Out of Sector Interference

Consider an independent scatterer whose return is denoted by $\boldsymbol{i}$, located at an out of sector azimuth angle, θ_I, and it gives rise to the following vector of conventional beam outputs as

$$\boldsymbol{y} = \boldsymbol{V_y}(\Theta_s)\boldsymbol{s} + \boldsymbol{v_y}(\theta_I)\boldsymbol{i} + \boldsymbol{n}, \tag{5-1}$$

where for the directional transmission case considered here $\boldsymbol{V_y}(\Theta_s)$ is given by (4-14) and $\boldsymbol{v_y}(\theta)$ by (4-8). The directional transmission BS covariance matrix is given by

$$\begin{aligned}\boldsymbol{R_{yI}} &= \boldsymbol{V_y}(\Theta_s)\boldsymbol{R_s}\boldsymbol{V_y^H}(\Theta_s) + \sigma_I^2\boldsymbol{v_y}(\theta_I)\boldsymbol{v_y^H}(\theta_I) + K\sigma_n^2\boldsymbol{I} \\ &= \boldsymbol{R_y} + \sigma_I^2\boldsymbol{v_y}(\theta_I)\boldsymbol{v_y^H}(\theta_I),\end{aligned} \tag{5-2}$$

where σ_I^2 is the power of the interference received by any single receiver. The directional

transmission optimum BS beamformer output power is given by

$$p_{MVDR-BS}(\theta) = \left(\boldsymbol{v}_{\boldsymbol{y}}^{H}(\theta)\boldsymbol{R}_{\boldsymbol{yI}}^{-1}\boldsymbol{v}_{\boldsymbol{y}}(\theta)\right)^{-1}. \tag{5-3}$$

where $$\boldsymbol{R}_{\boldsymbol{yI}}^{-1} = \boldsymbol{R}_{\boldsymbol{y}}^{-1} - \frac{\sigma_I^2 \boldsymbol{R}_{\boldsymbol{y}}^{-1}\boldsymbol{v}_{\boldsymbol{y}}(\theta_I)\boldsymbol{v}_{\boldsymbol{y}}^{H}(\theta_I)\boldsymbol{R}_{\boldsymbol{y}}^{-1}}{1+\sigma_I^2 \boldsymbol{v}_{\boldsymbol{y}}^{H}(\theta_I)\boldsymbol{R}_{\boldsymbol{y}}^{-1}\boldsymbol{v}_{\boldsymbol{y}}(\theta_I)}. \tag{5-4}$$

5.1.2 Optimum BS Beamformer Output at the DOA of a Scatterer outside the Sector

When $\theta = \theta_I$, i.e., the optimum beam is steered at the DOA of the interference, recalling equation (4-42), the optimum beamformer output power is given by

$$p_{MVDR-BS}(\theta_I) = \sigma_I^2 + \left(\boldsymbol{v}_{\boldsymbol{y}}^{H}(\theta_I)\boldsymbol{R}_{\boldsymbol{y}}^{-1}\boldsymbol{v}_{\boldsymbol{y}}(\theta_I)\right)^{-1}. \tag{5-5}$$

As shown in the above equation, the significance of interference in the whole BS MVDR output spectrum depends on the ratio between the interference power i.e., the first part in (5-5) and the optimum BS beamformer output power without the interference at angle θ_I i.e., the second part in (5-5). Here consider the simplest case of a single scatterer inside the sector of interest, whose DOA is at an azimuthal angle θ_{s1} and recalling (4-35), the second part in (5-5) becomes

$$\left(\boldsymbol{v}_{\boldsymbol{y}}^{H}(\theta_I)\boldsymbol{R}_{\boldsymbol{y}}^{-1}\boldsymbol{v}_{\boldsymbol{y}}(\theta_I)\right)^{-1} = \frac{K\sigma_n^2\left(k_y(\theta_{s1})\sigma_{s1}^2 + K\sigma_n^2\right)}{k_y(\theta_I)K\sigma_n^2 + \left(k_y(\theta_I)k_y(\theta_{s1}) - |B(\theta_I,\theta_{s1})|^2\right)\sigma_{s1}^2}, \tag{5-6}$$

where k_y and B are defined by equations (4-20) and (4-34) respectively and the value of $k_y(\theta_{s1})$ inside the sector of interest is near to the constant K_y. As shown in Figure 4-7, as θ_I is outside the sector of interest, $k_y(\theta_I) \ll K_y$ and $|B(\theta_{s1},\theta_I)|^2 < k_y(\theta_I)K_y$, but the difference between $k_y(\theta_I)K_y$ and $|B(\theta_I,\theta_{s1})|^2$ varies at different θ_I and also causes the optimum BS beamformer output to change. For example, considering the scenario used in Figure 4-3 but with an extra scatterer outside the sector of interest, the values of $k_y(\theta)K_y$ and $|B(\theta,8°)|^2$ are plotted in Figure 5-1.

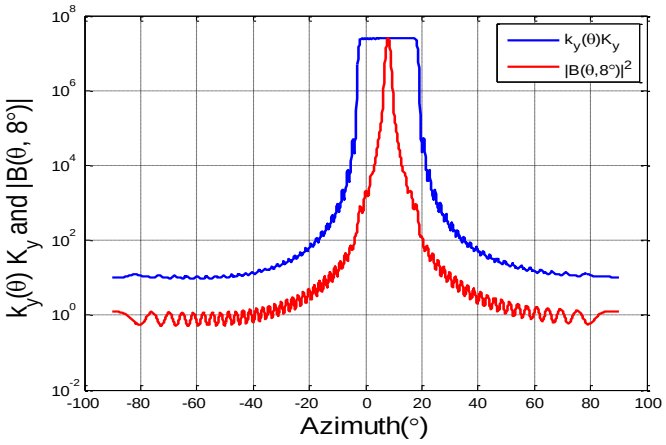

Figure 5-1: An example of inner product values of $k_y(\theta)K_y$ and $|B(\theta, 8°)|^2$.

Thus, when θ_I is close to the sector of interest, in this example, less than 10° away from the edge of the sector, $|B(\theta_{sl}, \theta_I)|^2 \ll k_y(\theta_I)K_y$ and the optimum BS beamformer output power can be approximated as

$$p_{MVDR-BS}(\theta_I) \approx \sigma_I^2 + \frac{K}{k_y(\theta_I)}\sigma_n^2. \tag{5-7}$$

As shown in Figure 4-7, at an angle outside of the sector scanned by the beams, the value of $k_y(\theta_I)$ is much smaller than K, thus the noise power at this region is amplified in the BS beamformer output.

An example is shown in Figure 5-2, where the scenario was the same as that used in Figure 4-8, but an interference at -5° with 10 dB INR was added. No obvious spectral peak can be found at -5° and it is impossible to identify the interference and estimate its power from the high optimum BS beamformer response outside of the sector.

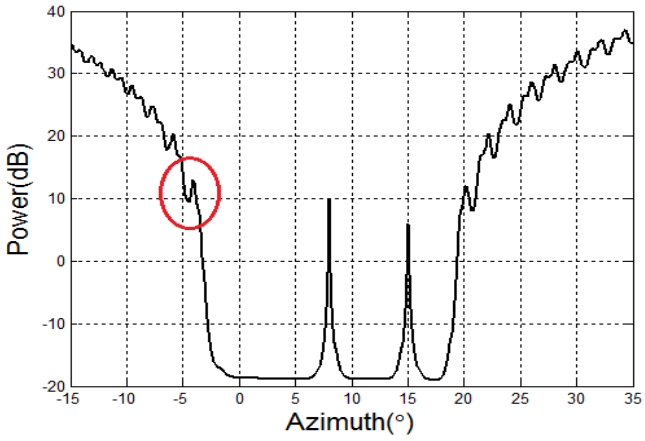

Figure 5-2: An example of subsector optimum BS beamformer output power values, where interference power is contaminated by the high response outside of the sector of interest.

Compared with Figure 3-14, which is a similar scenario but for the omni-directional transmission case, the directional transmission optimum BS beamformer provides a similar output power value at the DOA of the interference but the high response outside of the sector of interest is much stronger, since the value of $k_y(\theta_I)$ is much smaller than $H(\theta_I)$. This difference makes the detection and estimation of the interference for the directional transmission case more difficult.

In conclusion, the directional transmission optimum BS beamformer output power at the DOA of a scatterer (interference) outside the sector of interest can be approximated as a summation of the interference power and noise power multiplied by a factor of $\frac{K}{k_y(\theta_I)}$. In most cases, the noise component is amplified and dominates the output in this region, thus, it is difficult to identify and estimate the interference outside the sector of interest by using the optimum BS beamformer output directly.

5.1.3 Using MUSIC to Estimate the DOA of an Interference

As shown in Section 5.1.2, the general high optimum BS beamformer response outside the sector of interest prevents identifying and estimating the interference by using the optimum beamformer output. Notice that the high response is a result of the optimum BS beamformer and is not an inherent feature of the BS covariance matrix and so its eigen-decomposition into signal and noise subspaces is not affected by this effect.

Although the return from a scatterer outside the sector of interest is attenuated by propagation through sidelobes of both transmit and receive beams, its BS steering vector will still combine with the in sector signal steering vectors to determine the signal subspace, and since the power at DOA of the scatterer, $\left|\boldsymbol{v_y}(\theta_I)\right|^2\sigma_I^2 + \sigma_n^2$, is obviously larger than the noise power, this enables the signal and noise subspace to be separated. Therefore, BS subspace methods, such as MUSIC as described in equation (4-33), can still work effectively outside the sector of interest, as output values at the DOAs of both the signal and interference can be much larger than the high response caused by the impact of $K/k_y(\theta)$ and appear as peaks in the BS MUSIC output.

The results of applying the BS MUSIC algorithm to the scenario used to generate Figure 5-2 are plotted in Figure 5-3. It shows that the DOAs of both the signals and interference can be easily and accurately estimated by the sharp peaks in the BS MUSIC output. The high response in the region outside the sector of interest also appears, however, the values of MUSIC output at DOAs are significantly larger than the high response. Similar to the BS MVDR output, some fluctuations appear in the MUSIC output outside of the sector of interest, this is due to the variation of $k_y(\theta)$ at different azimuthal angles, but they are relatively weak and different from the sharp peaks which indicate DOAs.

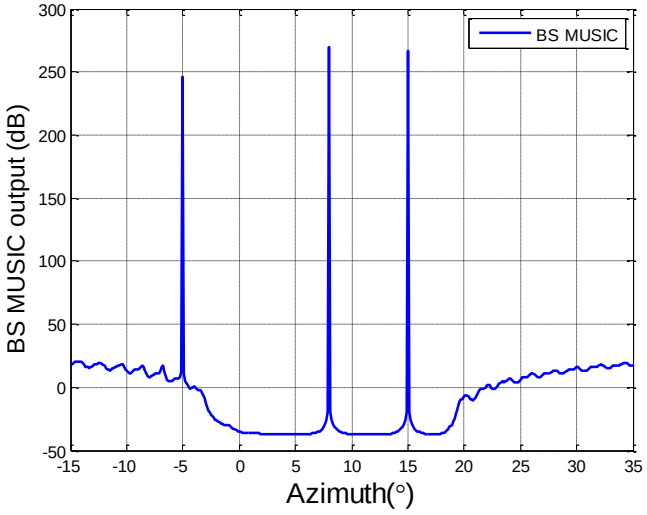

Figure 5-3: An example of applying BS MUSIC algorithm to a scenario with two independent signals and an interference with 10 dB INR at -5°. 21 directionally transmitted beams at angles of -2° to 18° with 1° separation.

5.2 Mitigation of the High Response outside the Sector of Interest

As mentioned before and shown in Figure 3-9 and Figure 4-9, the optimum BS beamformer generates a high response in the region outside the sector of interest. This is a unique problem to BS processing and happens for both the omni-directional and directional transmission cases. It can be argued that the high response is not an issue for the directional transmission case, as little energy is radiated in these directions and the region is not of interest. However there are potential problems with receiver noise whose angular spectrum (strictly wavenumber spectrum) is non-zero in the out of sector region and after optimum beamforming is large outside the sector of interest. Also, interferences can be incident upon the receive array from these directions, as shown in Section 5.1, this high response has dominated the output in the region outside the sector of interest and affected identifying and estimating the interference. Overall it is better to remove this high response.

5.2.1 High Response Mitigation Using Virtual Beams

The problem was first considered from the perspective of the optimum beamforming algorithm. As shown in Figure 4-7, the squared magnitude of the BS steering vector, i.e., $\left|\boldsymbol{v}_{\boldsymbol{y}}(\theta)\right|^2$ in the region outside the sector of interest is much smaller than that in sector, and so to keep the unity response at any angle in this region, the optimum BS beamformer needs to apply relatively large weights to those beam outputs, which potentially amplify the power from other directions rather than suppressing them. If extra

beams are formed in the out of sector, the region becomes a part of the sector of interest, thus, it can be predicted that the high response would not appear.

With an assumption that there is no interference in the out of sector region, N_e extra virtual beams at selected angles $\Theta_{\text{extra}} = [\theta_{M+1} \quad \theta_{M+2} \quad \cdots \quad \theta_{M+N_e}]$ in the region out of sector can be added. This ensures that the beams span the whole of the azimuthal region and these beams are assumed to contain uncorrelated noise only, where the noise level σ_n^2 can be chosen as the smallest or average noise eigenvalue of $\boldsymbol{R_y}$. The resulting ideally modified covariance matrix is given by

$$\boldsymbol{R}_{\boldsymbol{y}-\text{aug}} = \begin{bmatrix} \boldsymbol{R_y} & \boldsymbol{0} \\ \boldsymbol{0} & \sigma_n^2 \boldsymbol{I}_{N_e \times N_e} \end{bmatrix}. \tag{5-8}$$

Inspection of the above augmented BS covariance matrix indicates that the effect is to add additional eigenvalues at the noise level and the noise subspace is expanded to include the angular space outside the sector of interest. For the augmented system, the expanded steering vector becomes

$$\boldsymbol{v}_{\boldsymbol{y}-aug}(\theta) = \begin{bmatrix} \boldsymbol{v}^H(\theta_1)\boldsymbol{v}(\theta)\boldsymbol{v}^H(\theta_1)\boldsymbol{v}(\theta)/K \\ \boldsymbol{v}^H(\theta_2)\boldsymbol{v}(\theta)\boldsymbol{v}^H(\theta_2)\boldsymbol{v}(\theta)/K \\ \vdots \\ \boldsymbol{v}^H(\theta_{M+N})\boldsymbol{v}(\theta)\boldsymbol{v}^H\big(\theta_{M+N_e}\big)\boldsymbol{v}(\theta)/K \end{bmatrix}. \tag{5-9}$$

The optimum output power of the augmented system can be given by

$$p(\theta)_{MVDR-BS} = \left(\boldsymbol{v}_{\boldsymbol{y}-aug}^H(\theta)\boldsymbol{R}_{\boldsymbol{y}-aug}^{-1}\boldsymbol{v}_{\boldsymbol{y}-aug}(\theta)\right)^{-1}. \tag{5-10}$$

An example is shown in Figure 5-4, where the scenario was the same as that previously used in Figure 4-6, but an additional interference at -5° with 10 dB INR has been added. To be consistent with the separation between beams inside the sector of interest in the previous example, 180 beams at 1° separation and covering the full angular region were formed, the 160 beams outside the sector of interest were chosen as virtual beams and only spatial white noise was contained in each beam. The optimum BS beamformer output power using virtual beams is plotted versus azimuthal angle as the red curve.

Figure 5-4 shows that the high response out of sector has been effectively removed and the beamformer output power values at the DOAs of signals inside the sector of interest are almost the same as the outputs without virtual beams. The out of sector signal (interference at -5°) has been ignored completely by the virtual beam method.

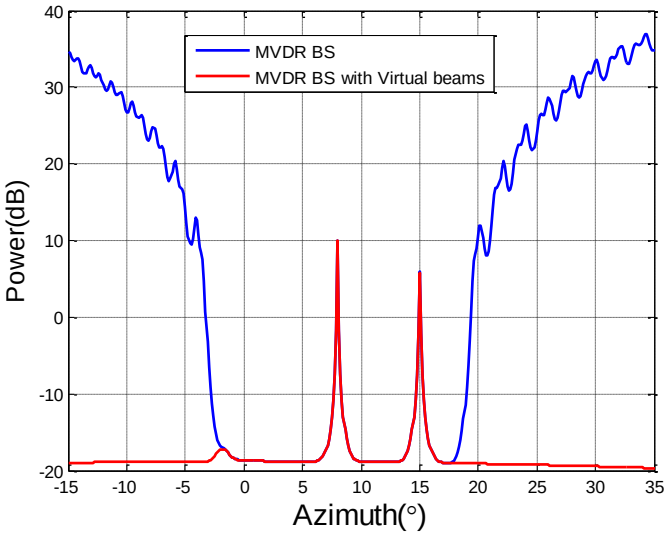

Figure 5-4: An example of using virtual beams to remove the optimum BS beamformer high response outside the sector of interest, with an interference whose INR = 10 dB, DOA at -5°.

By increasing the INR to 40 dB but keeping other parameters unchanged, the result versus azimuthal angle is plotted in Figure 5-5 and shows that the strong interference is also fully ignored by the virtual beam method.

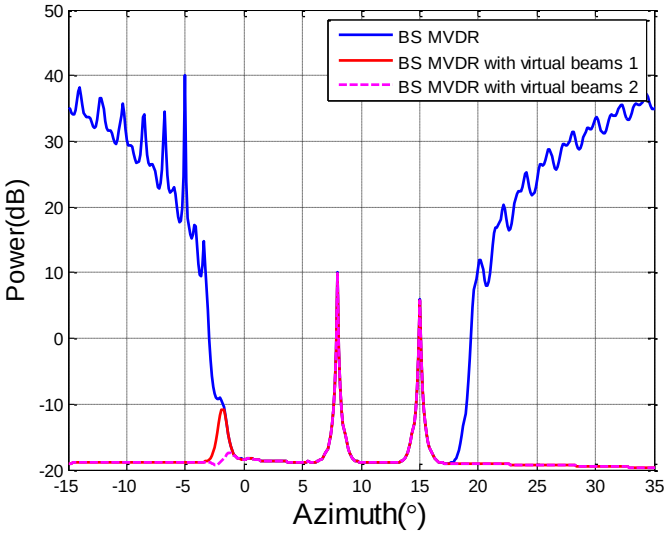

Figure 5-5: An example of using virtual beams to remove the optimum BS beamformer high response outside the sector of interest, an interference with 40 dB INR, DOA at -5°.

Notice that a spike appears at -2°, as the strong interference enhances the MVDR output at the edge of the sector of interest and the virtual beam only forces the output power outside the sector to be at the noise level. This spike does not indicate a signal there and it can be attenuated by changing the virtual beam near to the edge of the sector of interest. For example, changing the MRA of the virtual beam from -3° to -2.5°, the

output power of optimum BS beamformer with virtual beams is plotted as the magenta curve and the peak at -2° is significantly attenuated.

Varying the number of virtual beams, which are designed to be evenly distributed outside the sector of interest, the averaged output power in the out of sector is plotted versus the number of virtual beams in Figure 5-6.

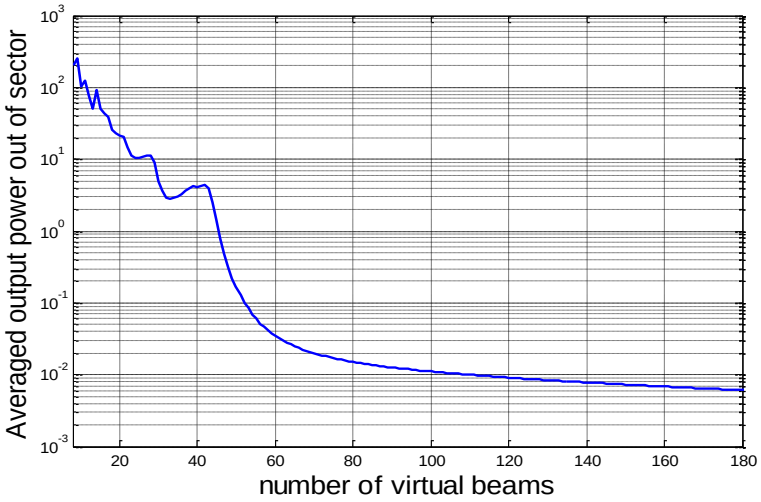

Figure 5-6: Averaged optimum BS beamformer output power values outside the sector of interest versus the number of virtual beams.

It can be seen, that the total power in this region decreases with increasing the number of virtual beams, but the change becomes insignificant when the virtual beams are more than the number of receivers. In this example, the virtual beams are simply designed to have an even separation as the case of beams inside the sector of interest, whilst the number and directions of the beams can be designed more sophisticatedly. The equivalent result may be achieved by using fewer beams, when mutually orthogonal virtual beams spanning the region outside the sector of interest are used.

5.2.2 High Response Mitigation by Scaling Optimum BS Beamformer Output Power

The directional transmission optimum BS beamformer output power values at all angles within the sector of interest are given by equations (4-36) and (4-37), and the output outside the sector of interest is given by equation (5-7). A general approximation for the directional transmission optimum BS beamformer output power can be given by

$$p_{MVDR-BS}(\theta) \approx \sigma_\theta^2 + \frac{K}{k_y(\theta)}\sigma_n^2, \tag{5-11}$$

where σ_θ^2 is the power of a signal or interference incident at an azimuthal angle, θ, and received by any single receiver, and it is zero when no signal/interference is incident.

Equation (5-11) shows that the noise gain, $\frac{K}{k_y(\theta)}$, varies with angle and affects the beamformer output at different azimuthal angles differently. As shown in Figure 4-7, the value of $k_y(\theta)$ is close to a constant K_y in the sector of interest and the noise gain $\frac{K}{k_y(\theta)} < 1$; for the angular region outside of the sector of interest, the value of $k_y(\theta)$ decreases dramatically as θ is moved away from the sector of interest, thus the noise gain $\frac{K}{k_y(\theta)}$ increases and causes a very high output.

The second method of removing the high response outside the sector of interest is to scale the optimum BS beamformer output to compensate for the variation of $k_y(\theta)$. With the prior knowledge of the DOAs of the signals/interferences, which could be worked out by the BS MUSIC algorithm as shown in Section 5.1.3, the directional optimum BS beamformer output power can be scaled as follows

$$p_{MVDR-BS}(\theta)=\begin{cases} k_y(\theta)/K_y\left(\boldsymbol{v}_y^H(\theta)\boldsymbol{R}_y^{-1}\boldsymbol{v}_y(\theta)\right)^{-1}, if\ \theta \notin \hat{\theta}_s \\ \left(\boldsymbol{v}_y^H(\theta)\boldsymbol{R}_y^{-1}\boldsymbol{v}_y(\theta)\right)^{-1} - \frac{K}{k_y(\theta)}\sigma_n^2, if\ \theta \in \hat{\theta}_s \end{cases}, \quad (5\text{-}12)$$

where $\hat{\theta}_s$ is the estimated set of DOA angles.

The same example used to produce Figure 5-2 was considered and after applying the above modified optimum BS beamforming algorithm, the beamformer output power values using (5-12) are shown in Figure 5-7.

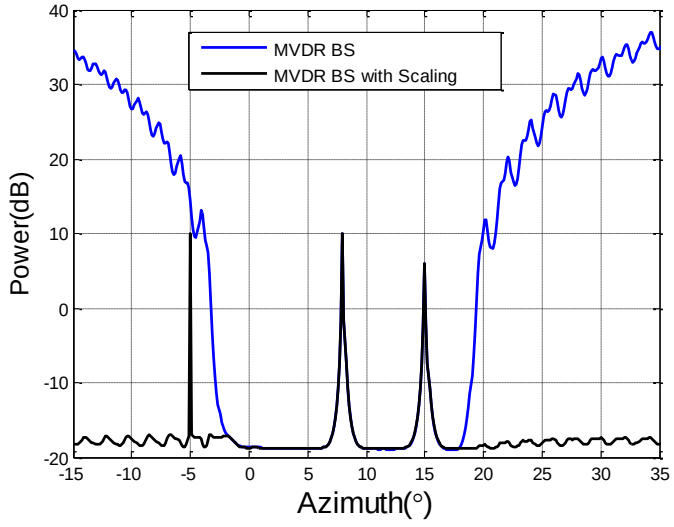

Figure 5-7: An example of using scaling algorithm to remove the optimum BS beamformer high response outside the sector of interest.

In this example, the power of the interference at -5° is 10 dB above the noise power, but it is fully hidden by the high response in the optimum BS beamformer output power, due

to the very high gain to the noise component. With scaling, the gain to noise is normalised, thus the high response outside the sector of interest is effectively mitigated and the power of the interference can be accurately estimated. This example shows that with effectively removing the high out of sector response, the output power at DOAs inside the sector of interest only changes slightly, as the reduced part, $\frac{K}{k_y(\theta)}\sigma_n^2$, is relatively small compared with signal power.

To check if the scaling method is robust for different signal intensities, especially for a weak INR, the beamformer output power at the DOA of the interference (-5°) versus different INR value is plotted Figure 5-8. It shows that the beamformer output power with the scaling methods is almost the same as the desired INR value, but when the INR is lower than 5 dB, the result is slightly higher than the true INR, but the difference is negligible.

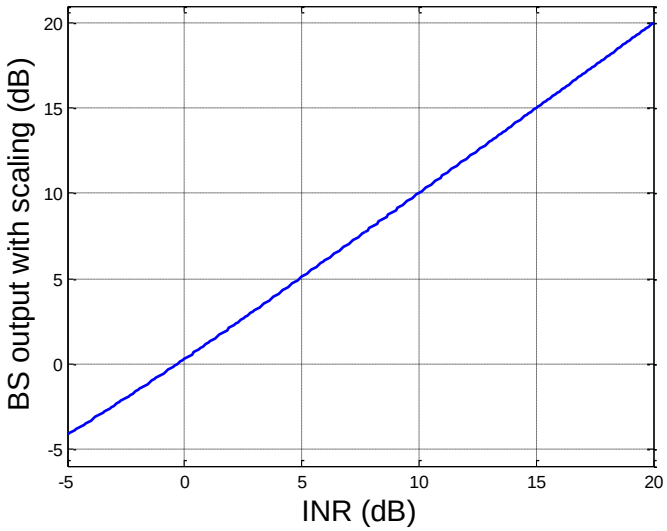

Figure 5-8: Optimum BS beamformer output power with scaling algorithm at the DOA of the interference versus different INR value.

It shows the scaling method can remove the high response and estimate the interference power very well, but it requires prior information of the DOAs, especially for an out of sector interference. However, for a weak interference far away from the sector of interest, as shown in Figure 5-1, the difference between $k_y(\theta)K_y$ and $|B(\theta, 8°)|^2$ is smaller and the value of $k_y(\theta)$ is very small, equation (5-11) can be biased seriously and provides a poor approximation, as a result, the estimation of the interference power can be inaccurate.

5.3 Directional Transmission BS Processing for the Region inside the Sector of Interest

To determine if the interference affects the optimum BS beamformer output within the sector of interest, the output power inside the sector of interest is analysed in this section.

5.3.1 Output at DOAs of Scatterers inside the Sector of Interest

Consider the simplest case of a single scatterer inside the sector of interest, whose DOA is at an azimuthal angle θ_{s1}. When $\theta = \theta_{s1}$, using equation (4-42), the output is given by

$$p_{MVDR-BS}(\theta_{s1}) = \left(\boldsymbol{v}_{\boldsymbol{y}}^{H}(\theta_{s1})\boldsymbol{R}_{\boldsymbol{y}(I)}^{-1}\boldsymbol{v}_{\boldsymbol{y}}(\theta_{s1})\right)^{-1} + \sigma_{s1}^{2} \tag{5-13}$$

where

$$\boldsymbol{R}_{\boldsymbol{y}(I)} = \sigma_I^2 \boldsymbol{v}_{\boldsymbol{y}}(\theta_I)\boldsymbol{v}_{\boldsymbol{y}}^{H}(\theta_I) + K\sigma_n^2 \boldsymbol{I} \tag{5-14}$$

Similarly to (4-35) but replacing $\boldsymbol{R}_{\boldsymbol{y}(1)}$ by $\boldsymbol{R}_{\boldsymbol{y}(I)}$, the first term of equation (5-13) is given by

$$\left(\boldsymbol{v}_{\boldsymbol{y}}^{H}(\theta_{s1})\boldsymbol{R}_{\boldsymbol{y}(I)}^{-1}\boldsymbol{v}_{\boldsymbol{y}}(\theta_{s1})\right)^{-1} = \frac{K\sigma_n^2\left(k_y(\theta_I)\sigma_I^2 + K\sigma_n^2\right)}{k_y(\theta_{s1})\left(k_y(\theta_I)\sigma_I^2 + K\sigma_n^2\right) - |B(\theta_{s1},\theta_I)|^2\sigma_I^2}, \tag{5-15}$$

where k_y and B are defined by equations (4-20) and (4-34), and the value of $k_y(\theta_{s1})$ in the sector scanned by the beams is near to the constant K_y.

When $\theta_{sl} \neq \theta_I$, which means DOAs of the interference and the signal are not overlapped, $|B(\theta_{sl}, \theta_I)|^2 \ll K_y k_y(\theta_I)$, and the output can be approximated as

$$p_{MVDR-BS}(\theta_{sl}) \approx \sigma_{s1}^2 + \frac{K\sigma_n^2}{K_y}, \tag{5-16}$$

where as shown in Figure 4-7, $K_y \gg K$, which indicates that the noise power is significantly attenuated.

In conclusion, optimum BS beamformer output power at the DOA of a scatterer within the sector of interest is only slightly affected by adding an extra insignificant amount of attenuated noise power. An exception is when DOAs of the signal and interference are too close to separate and identify, the approximation would not be valid. The resolution threshold between two scatterers depends on several factors including array size, number of beams, SNR, detailed discussions can be found in the literature, such as [27]. However, this case where the edge of the sector of interest is exactly between two closely spaced signals rarely happens, and will not be considered in this thesis.

5.3.2 Spurious Spectral Peak inside the Sector of Interest

As mentioned in Section 4.1.3, the optimum BS beamforming algorithm minimises the total power but keeps a unity response at the chosen look direction. Thus, for an interference with a high INR incident from an azimuthal angle near to the sector of interest, the optimum beamformer spends effort on manipulating the beam pattern and forming a deep null to suppress the interference. The resulting distortion of the beam pattern can give rise to spurious fluctuations which in the presence of noise and can be interpreted as an output peak inside the sector of interest, thus wrongly indicating a weak signal at around the noise level. In this section, the reason of the spurious spectral peak is investigated and a mitigation method is proposed.

5.3.2.1 Analysis of Spurious Spectral Peak

An example is shown in Figure 5-9, where the scenario was the same as that previously used in Figure 4-8, but no signal was included and only an out of sector interference was present at 20° with INR = 40 dB. The optimum BS beamformer output indicates, in addition to the peak at 20° corresponding to the DOA of the interference, a spurious peak at about 17°, which is inside the sector of interest and marked by a red circle in the figure. This can be a potential bad issue especially for the case of an unknown interference, returns from clutter or widespread strong volume scatterers such as heavy precipitation outside the sector of interest.

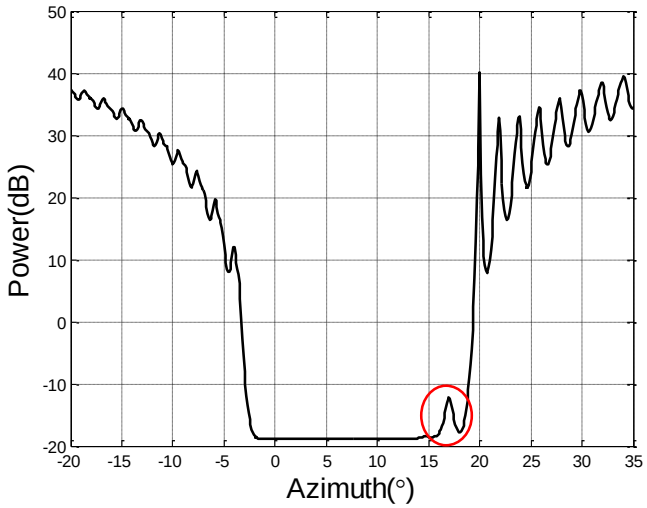

Figure 5-9: An example of applying the directional transmission BS MVDR formula to a model containing a strong interference as 40 dB INR near the sector edge. The spurious output peak is at 17° and marked by a red circle.

The eigen-spectrum of $\boldsymbol{R_y}$ is plotted in Figure 5-10, only one large eigenvalue exists and it clearly indicates a one dimensional signal subspace corresponding to the steering vector of the interference and no second signal component is included in the signal subspace. Additionally, as shown in Figure 5-11, even with a lower INR (20 dB), the

spurious peak still appeared but the power was slightly lower than the value in Figure 5-9. This indicates that the spurious peak is caused by the interference outside the sector of interest but its peak value is only slightly affected by the intensity of the interference.

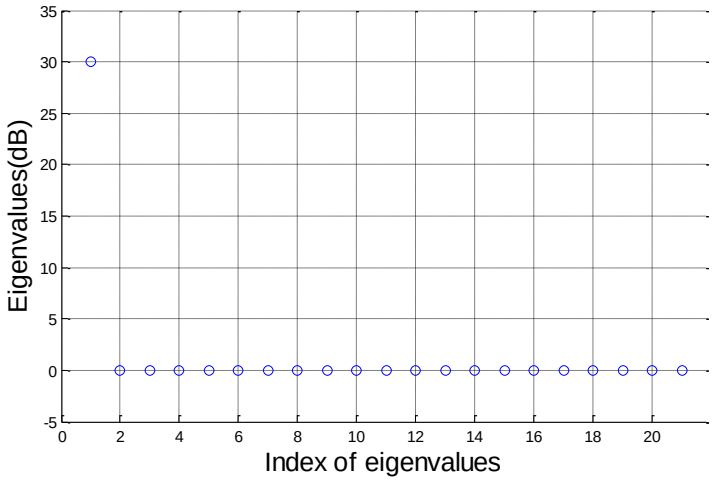

Figure 5-10: Eigen-spectrum of a BS covariance matrix for a single interference with 40 dB INR near the sector edge.

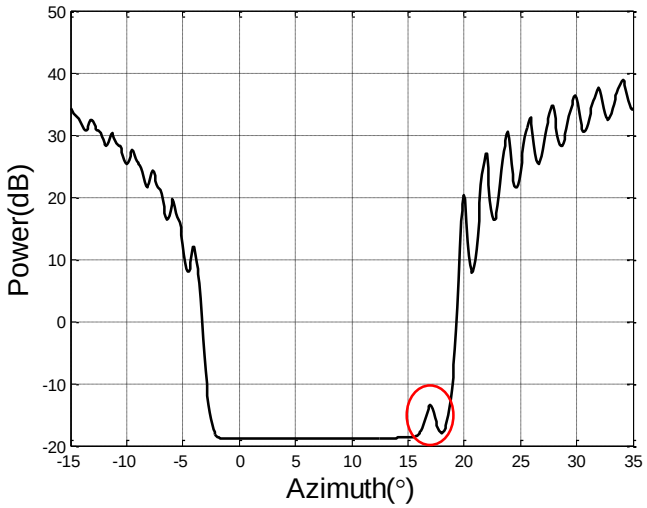

Figure 5-11: An example of applying the directional transmission BS MVDR formula to a model with an interference with 20 dB INR near the sector edge. The spurious output peak is at 17° and marked by a red circle.

The beam pattern of BS MVDR beamformer at the azimuthal angle of the spurious peak (17°) for the scenario of INR=20 dB is shown in Figure 5-12 and obviously, the algorithm manipulates the beam pattern to null the interference but the response in a very wide region around the spurious peak is around unity, thus giving rise to the spurious peaks in Figure 5-9 and Figure 5-11.

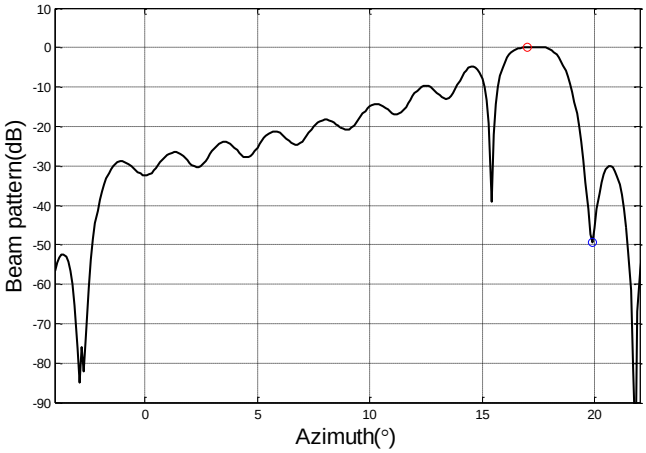

Figure 5-12: The beam pattern at the angle where a spurious peak appears, the blue circle denotes the deep nulls to cancel the interference and the red circle is the steering direction.

To investigate this problem mathematically, with a single interference at θ_I, the optimum BS beamformer output power at θ, which is inside the sector of interest, is, similarly to (5-15), given by

$$\left(\boldsymbol{v}_{\boldsymbol{y}}^{H}(\theta)\boldsymbol{R}_{\boldsymbol{y}(I)}^{-1}\boldsymbol{v}_{\boldsymbol{y}}(\theta)\right)^{-1} = \frac{K\sigma_n^2\left(k_y(\theta_I)\sigma_I^2 + K\sigma_n^2\right)}{\left(k_y(\theta)k_y(\theta_I) - |B(\theta,\theta_I)|^2\right)\sigma_I^2 + K\sigma_n^2} \tag{5-17}$$

The values of $k_y(\theta)$ and $|B(\theta, 20^0)|$ are plotted in Figure 5-13. It shows that the maximum value of $|B(\theta,\theta_I)|$ is inside the sector of interest rather than at θ_I. Using the Cauchy–Schwarz inequality, $k_y(\theta)k_y(\theta_I) \geq |B(\theta,\theta_I)|^2$, the optimum BS beamformer output power at θ, which is inside the sector of interest, increases when $|B(\theta,\theta_I)|^2$ increases, and the peak appears where $|B(\theta,\theta_I)|$ reaches its maximum value. Therefore, the out of sector interference causes a spurious peak value of optimum BS beamformer output power values inside the sector of interest.

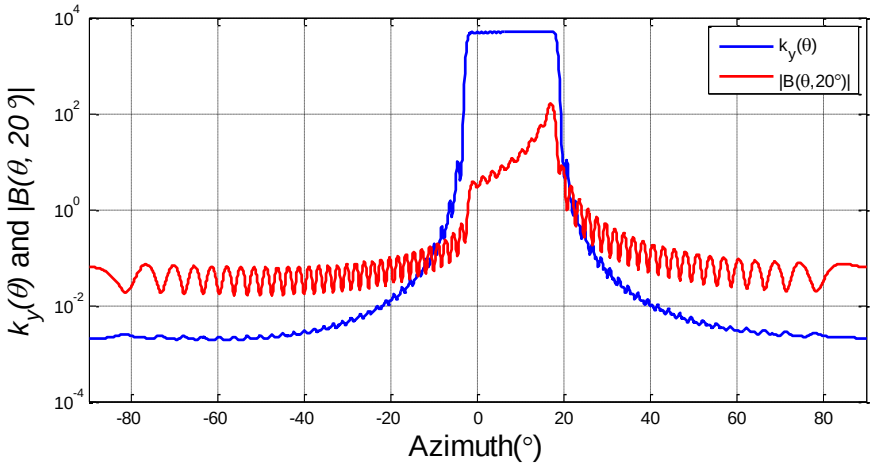

Figure 5-13: An example of inner product values of $k_y(\theta)$ and $|B(\theta, 20^0)|$.

The value of the spurious peak at 17° inside the sector of interest versus different INR is plotted in Figure 5-14. When the INR is below 0 dB, the peak is not obvious, as it is almost the same as the output at other azimuthal angles. The value of the spurious peak increases almost linearly with INR when the value of INR is between 5 to 25 dB. Then, with further INR increasing, the noise component becomes relatively negligible and the value of the peak progressively approaches its ultimate value. In this example, the value of the spurious peak remains almost the same at about -12.2 dB when INR is larger than 40 dB. As described in equation (5-17), when $\sigma_I^2 \gg K\sigma_n^2$, the beamformer output power approaches a value of $\frac{Kk_y(\theta_I)\sigma_n^2}{K_y k_y(\theta_I) - |B(\theta,\theta_I)|^2}$ and only the attenuated noise component contributes to this result.

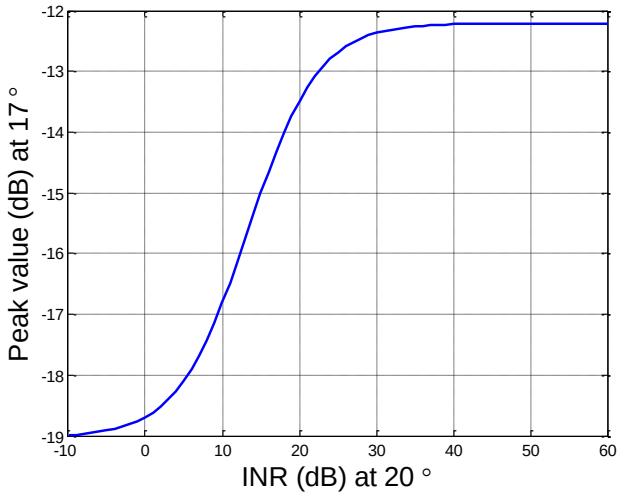

Figure 5-14: The value of the spurious peak inside the sector of interest at 17° versus INR at 20°.

A question arises whether the out of sector interference still causes a spurious peak when there are signals within the sector of interest. This question is answered by an example of a scenario of two signals at 8° and 15° with 10 dB and 6 dB SNRs and a single interference at 20° with 40 dB INR at any single receiver. The optimum BS beamformer output power value versus azimuthal angle for this scenario is plotted in Figure 5-15. It shows that the spurious peak still appears at the same azimuthal angle, whilst its value is slightly higher than the single interference only scenario, as more effort is required to null both signals and interference and less attenuation is on the noise component, but the difference is insignificant. In conclusion, adding signals inside the sector of interest neither avoids the spurious peak nor shifts its location, but is more likely to slightly increase the value of the spurious peak.

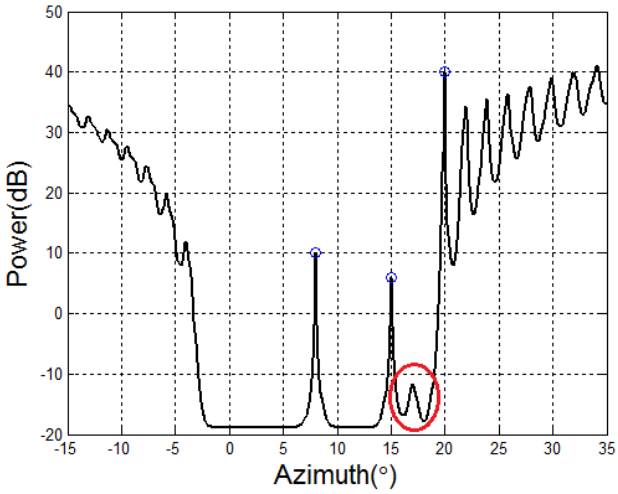

Figure 5-15: An example of applying the directional transmission BS MVDR formula to a model with two independent signals and a strong interference near the sector edge.

Generally, output peaks of subspace methods, such as MUSIC, indicate the DOAs. By selecting the principal eigenvector of the BS covariance matrix as the one dimensional signal subspace, it was expected that only one single peak for the eigen-spectrum described in Figure 5-10 would appear and the spurious peak would be rejected by using the result of the subspace method. However, to apply MUSIC to this scenario, as shown in Figure 5-16, apart from the strong output indicating the true DOA of the interference, a peak still appears at ~17° in the MUSIC output. Compared with the output at the true DOA, this spurious peak is much lower and can be ruled out by a threshold. However, the threshold method is not always absolutely secure and it may not work in the case of mismatch, such as small phase errors which can cause low MUSIC output values at the true DOAs. Therefore, it is better to mitigate the spurious peak rather than simply reject it according to the intensity of peaks. One approach for doing so is discussed in the following section.

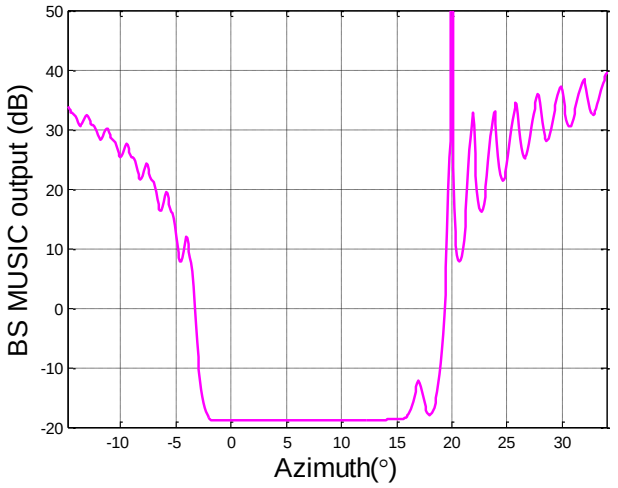

Figure 5-16: An example of BS MUSIC output contains a spurious peak.

5.3.2.2 Spurious Spectral Peak Mitigation by Projection

As discussed in the previous section, the spurious peak of the optimum BS beamformer output power values inside the sector of interest occurs because the beamformer manages to suppress the interference but not enough attenuation is applied to the noise. To eliminate this spurious peak, two kinds of projections have been investigated to null the interference.

Denote the matrix containing the BS steering vectors of interferences as $\boldsymbol{V_I}$, which are assumed to have been estimated by MUSIC in advance. Its orthogonal projection [95] is written as

$$\boldsymbol{P_{V_I}^{\perp}} = \boldsymbol{I} - \boldsymbol{V_I}(\boldsymbol{V_I^H V_I})^{-1}\boldsymbol{V_I^H}. \tag{5-18}$$

and the orthogonally projected covariance matrix is given by

$$\boldsymbol{R_y^{\perp I}} = \boldsymbol{P_{V_I}^{\perp}} \boldsymbol{R_{yI}} \boldsymbol{P_{V_I}^{\perp}}, \tag{5-19}$$

where $\boldsymbol{R_{yI}}$ is the BS covariance matrix containing both signal and interference components. Then, the optimum BS beamformer algorithm is applied to the projected covariance matrix and the output is given by

$$p(\theta)_{MVDR-BS} = \left(\boldsymbol{v_y^H}(\theta)\left(\boldsymbol{R_y^{\perp I}}\right)^{-1}\boldsymbol{v_y}(\theta)\right)^{-1}. \tag{5-20}$$

The same scenario as in Figure 5-15 was considered here but the BS covariance matrix is projected to be orthogonal to the interference, and the beamformer output power values versus azimuthal angle are shown in Figure 5-17.

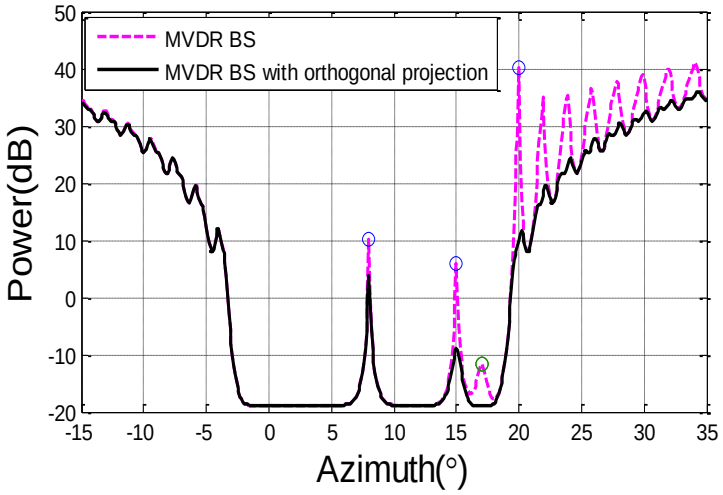

Figure 5-17: An example of using orthogonal projection to mitigate the spurious peak inside the sector of interest caused by an interference.

With the orthogonal projection, the spurious peak is eliminated completely, but unfortunately, the optimum BS beamformer output power values at the DOAs are also attenuated seriously. The example in Figure 5-17 shows the output power at 15° is about 15 dB lower than the optimum BS beamformer output power without projection. This is because a subspace orthogonal to the steering vector of the interference does not necessarily contain all the signal components.

It is desirable to mitigate the spurious peak without any change to the power estimations of the signals incident inside the sector of interest. Another method, oblique projection [38] was used. The steering vectors corresponding to the signals, interferences and spurious peak can be first estimated by using BS MUSIC. Then, two subspaces are chosen for different purposes. To apply beamforming at any angle inside the sector of interest, the interference components should be removed. The first subspace, $\boldsymbol{V_I}$, is chosen as the BS steering vector(s) of the interference(s), which could be determined by the BS subspace algorithm described above; the second subspace $\boldsymbol{V_{\tilde{S}}}$ includes the signal subspace and the steering vector at the angle where the spurious peak appears and its components will be fully kept. Additional vectors other than the interference steering vectors can be added in $\boldsymbol{V_{\tilde{S}}}$ to keep any potential information, and this process needs to satisfy a condition on the degrees of freedom that

$$\text{rank}\,(\boldsymbol{V_{\tilde{S}}}) + \text{rank}\,(\boldsymbol{V_I}) \leqslant \text{rank}\,(\boldsymbol{R_y}). \tag{5-21}$$

The oblique projection matrix is denoted by

$$\boldsymbol{E_{IS}} = \boldsymbol{V_{\tilde{S}}}(\boldsymbol{V_{\tilde{S}}^H P_{V_I}^{\perp} V_{\tilde{S}}})^{-1}\boldsymbol{V_{\tilde{S}}^H P_{V_I}^{\perp}}, \tag{5-22}$$

and the new covariance matrix after oblique projection is given by

$$\boldsymbol{R_{y-ob}} = \boldsymbol{E_{IS}^H R_{yI} E_{IS}}. \tag{5-23}$$

Then, the optimum BS beamformer is applied to the projected covariance matrix and the beamformer output power is given by

$$p(\theta)_{MVDR-BS} = \left(\boldsymbol{v_y^H}(\theta)\boldsymbol{R_{y-ob}^{-1}}\boldsymbol{v_y}(\theta)\right)^{-1}. \tag{5-24}$$

The same scenario as Figure 5-15 was considered and the BS covariance matrix was obliquely projected via equation (5-23), where $\boldsymbol{V_{\tilde{S}}}$ was chosen as a matrix containing steering vectors of 20 beams (-1° to 18° with 1° separation, the first beam at -2° was not included, since it was at the edge of the sector of interest and little energy was propagated through this beam) in the sector of interest. The new beam pattern at the azimuthal angle of the spurious peak and the output power versus azimuthal angle are shown in Figure 5-18 and Figure 5-19 respectively. The beamforming output indicates that the spurious peak caused by the interference is mitigated effectively without significant changes to the output power values at the DOAs of the signals.

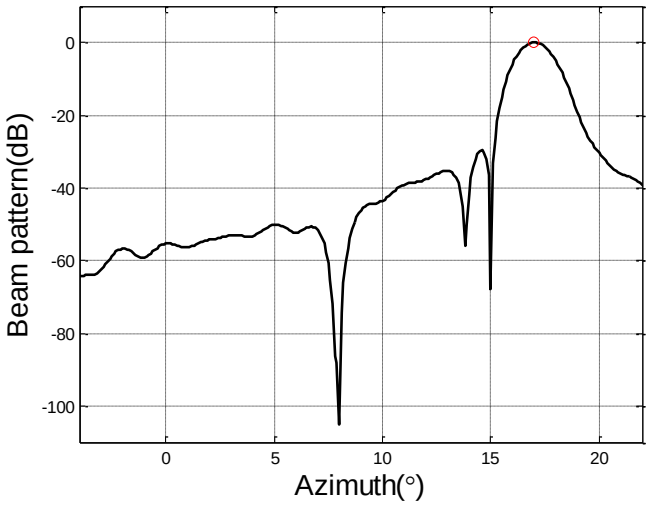

Figure 5-18: The beam pattern of optimum BS beamformer after oblique projection at the angle of the spurious peak.

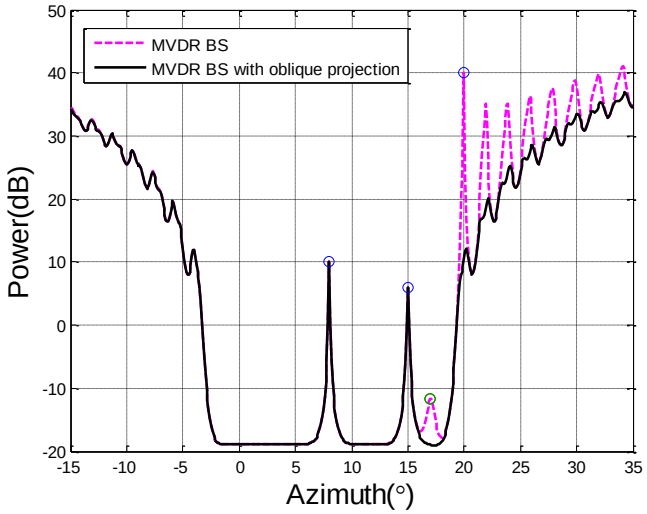

Figure 5-19: An example of using oblique projection to mitigate the spurious peak caused by the interference.

5.4 BS Processing with Array Errors

SNR gain and directivity (spatial resolution) are the most common parameters used to measure the performance of a phased array system or an array processing algorithm. Additionally, as errors often happen in practice and cause the array responses to be different from that being assumed, robustness to such errors is another measure of performance. Errors that typically occur in phased arrays can be array element gain and phase errors due to imperfect electronic components and imprecise positioning of the elements due to construction issues. With these errors, the array response is different from that assumed by the ideal model and the performance of array processing algorithms with weak robustness can be seriously degraded. An example has been

discussed in [78], where a small perturbation, such as random phase shifts in a few elements, can make the actual steering vector slightly mismatch the assumed steering vector, with the result that the response at the actual DOA is not constrained to be unity and the signal component is suppressed by the optimisation process.

The most straightforward way to deal with the errors is to carry out array calibration which avoids or compensates the errors. The calibration can be physically carried out on the phased arrays before use. Although phased arrays can be calibrated during manufacture, further system errors may occur whilst being used. For example, the phase and amplitude characteristics of most RF devices drift at different temperatures, which are not able to be corrected due to various system limitations. Another way of doing calibration is to apply correction or compensation to the collected data after use. However, it can be difficult to obtain the parameters for correction in practice.

Apart from the calibration, another way of dealing with the issue of array errors is to increase the robustness of beamformers. In this section, based on the directional transmission BS model, several types of potential errors are considered and then a robust BS beamformer, which is tolerant to such mismatch errors, is proposed.

5.4.1 Model of Directional Transmission BS with Errors

Each beam output is a linear combination of element outputs, so element errors are combined and passed to the BS model through this transformation. Also, there is another type of error that needs to be considered for BS processing. The actual MRAs of the preformed beams may be different from the designed directions or recorded inaccurately such as choosing the nearest angle value in a system direction control lookup table. Errors in both array elements and beam directions are considered in the directional transmission BS model here. For the directional Tx/Rx beam scanning case, as the same phase shifts are applied to both transmit and receive beams at the same angle, errors in transmission and receive beams are likely to be the same. In the presence of such errors, the vector of beam outputs is given by

$$\begin{aligned}\boldsymbol{y} &= \begin{bmatrix} y(\theta_1) \\ y(\theta_2) \\ \vdots \\ y(\theta_M) \end{bmatrix} \\ &= \begin{bmatrix} \boldsymbol{v}^H(\theta_1+\phi_1)\acute{\boldsymbol{V}}_{\boldsymbol{s}}(\Theta_s)\left(\acute{\boldsymbol{V}}_{\boldsymbol{s}}^T(\Theta_s)\boldsymbol{v}^*(\theta_1+\phi_1)/K \circ \boldsymbol{s}\right) + \boldsymbol{v}^H(\theta_1+\phi_1)\boldsymbol{n}_1 \\ \boldsymbol{v}^H(\theta_2+\phi_2)\acute{\boldsymbol{V}}_{\boldsymbol{s}}(\Theta_s)\left(\acute{\boldsymbol{V}}_{\boldsymbol{s}}^T(\Theta_s)\boldsymbol{v}^*(\theta_2+\phi_2)/K \circ \boldsymbol{s}\right) + \boldsymbol{v}^H(\theta_2+\phi_2)\boldsymbol{n}_2 \\ \vdots \\ \boldsymbol{v}^H(\theta_M+\phi_M)\acute{\boldsymbol{V}}_{\boldsymbol{s}}(\Theta_s)\left(\acute{\boldsymbol{V}}_{\boldsymbol{s}}^T(\Theta_s)\boldsymbol{v}^*(\theta_M+\phi_M)/K \circ \boldsymbol{s}\right) + \boldsymbol{v}^H(\theta_M+\phi_M)\boldsymbol{n}_M \end{bmatrix}. \end{aligned} \tag{5-25}$$

where ϕ_m is the angle difference between the actual and assumed MRA of the m-th transmit/receive beam and $\acute{\boldsymbol{V}}_{\boldsymbol{s}}(\Theta_s)$ denotes a matrix whose columns are array responses

to different DOAs of signals (signal steering vectors but with errors). For example, a steering vector of a signal incident from directional θ_{sl} but with errors is given by

$$\acute{\boldsymbol{v}}(\theta_{sl}) = \boldsymbol{v}(\theta_{sl}) \circ \boldsymbol{e} = \begin{bmatrix} \mu_1 e^{j2\pi\delta_1/\lambda sin(\theta_{sl})} \\ \mu_2 e^{j2\pi(d+\delta_2)/\lambda sin(\theta_{sl})} \\ \vdots \\ \mu_K e^{j2\pi((K-1)d+\delta_K)/\lambda sin(\theta_{sl})} \end{bmatrix} \tag{5-26}$$

where $\boldsymbol{e}$ is a vector contains errors occur at different elements; more specifically, μ_k represents a complex gain caused by the electronic component variations and it can change both the amplitude and phase of received signal at the *k*-th element; δ_k is the position error at the *k*-th element, which would cause a phase shift. Due to the phased array electronic scanning is normally finished quickly, the error $\boldsymbol{e}$ is assumed to be the same for all the Tx/Rx beams. Therefore, for a scatterer at an angle, θ_{sl}, the actual BS steering vector is given by

$$\acute{\boldsymbol{v}}_{\boldsymbol{y}}(\theta_{sl}) = \begin{bmatrix} \boldsymbol{v}^H(\theta_1+\phi_1)\acute{\boldsymbol{v}}(\theta_{sl})\boldsymbol{v}^H(\theta_1+\phi_1)\acute{\boldsymbol{v}}(\theta_{sl})/K \\ \boldsymbol{v}^H(\theta_2+\phi_2)\acute{\boldsymbol{v}}(\theta_{sl})\boldsymbol{v}^H(\theta_2+\phi_2)\acute{\boldsymbol{v}}(\theta_{sl})/K \\ \vdots \\ \boldsymbol{v}^H(\theta_M+\phi_M)\acute{\boldsymbol{v}}(\theta_{sl})\boldsymbol{v}^H(\theta_M+\phi_M)\acute{\boldsymbol{v}}(\theta_{sl})/K \end{bmatrix}. \tag{5-27}$$

Obviously, there is a mismatch between $\boldsymbol{v}_{\boldsymbol{y}}(\theta_{sl})$ and $\acute{\boldsymbol{v}}_{\boldsymbol{y}}(\theta_{sl})$, and as the actual steering vector is unknown and has uncertainty, the performance of the optimum BS beamformer using the assumed steering vector would be degraded. The performance degradation is similar to ES beamformers with errors, but can be worse due to the factor of extra beam steering angle errors.

5.4.2 Introduction to Robust Beamforming

Different methods have historically been proposed to improve the robustness of a beamformer. Additional linear constraints, such as linear constrained minimum variance (LCMV) approaches [19], [20] and [21], potentially increase robustness, as they normally broaden the beamwidth around the look direction. However, as errors are normally unknown, it is not clear how to find the best additional constraint to approximate the actual steering vector. Thus common constraints such as derivative constraints, only bring a very limited improvement. Also, adding extra constraints loses degrees of freedom and reduces the ability to suppress interferences. Projection methods, such as [80], remove noise, weak interferences and small perturbations, but are not robust to large errors in the steering vector. Simple diagonal loading ($\boldsymbol{R}_{\boldsymbol{y}} + \Delta\boldsymbol{I}$) has been commonly used and is equivalent to adding white noise to the covariance matrix. This method is less sensitive to perturbations whilst the system nulling capability is reduced. Quadratic constraints methods such as [21] and [79], actually add diagonal loading with different values of Δ to improve the robustness of the beamformer. However the required diagonal loading level is normally unknown and it is not clear how to choose the diagonal loading in these methods.

More recently robust beamformer research has focused on the uncertainty of the array steering vector. Several ES optimum beamforming with robustness techniques have been developed and are commonly called robust adaptive beamforming (RAB) in the literature. The worst-case performance optimisation method [82], and further developed methods in [83] and [87] constrain the absolute value of the array response in a multi-dimensional region around the look direction to lie above unity and minimise the beamformer output power. Such constraints guarantee that the distortionless response will be maintained for the true steering vector. Notice the uncertainty sets in these methods are different from the set in the LCVM method, whose constraints are only limited to a few given vectors and no recursive search and comparison are carried out. The method proposed by Lorenz and Boyd in [84] has a similar criterion to that proposed in [82] but considers a different uncertainty set which is anisotropic and uses the Lagrange multiplier technique to improve computation. The approach proposed by J. Li *et al.* in [85] and further extended in [86] searches for the largest output power by varying the steering vector in an uncertainty set around the look angle. All these methods are based on the same principle and belong to a class of diagonal loading approaches. In short, these typical robust beamforming algorithms assume the actual steering vector lies in an uncertainty set around the assumed steering vector and optimise the beamformer output subject to constraints on the set.

5.4.3 Robust BS Beamforming

When used as a pre-processing step, the BS transformation itself increases robustness. As described in [42] and [45], conventional and sector focused stability BS beamformers are inherently robust to small system errors, as small errors and noise can be potentially reduced in the process of beamforming, however the robustness is very limited.

There is very little literature on robust adaptive beamforming techniques in BS processing. In [88], beams are designed as vectors which span the complementary set of a pre-selected angular sector of interest, and then a robust beamforming method in [87] is applied to estimate the actual BS steering vector. In this process, the BS transformation is mainly used to remove the signal of interest and obtain a signal free covariance matrix, but it does not really solve the robustness problem in BS processing for preformed beams.

Here the robust beamforming algorithm in [85] is extended to the directional transmission BS steering vector mismatch problem. Similar to the ES method in the literature, an uncertainty set in BS is chosen around the assumed BS steering vector at θ, $\boldsymbol{v_y}(\theta)$, as $\left\|\acute{\boldsymbol{v}}_{\boldsymbol{y}}(\theta) - \boldsymbol{v_y}(\theta)\right\|^2 \leq \epsilon$. The optimisation problem of finding the maximal output power value around the assumed BS steering vector can be formulated as

$$\min \acute{\boldsymbol{v}}_{\boldsymbol{y}}^{H}(\theta)\boldsymbol{R}_{\boldsymbol{y}}^{-1}\acute{\boldsymbol{v}}_{\boldsymbol{y}}(\theta), \text{ subject to } \left\|\acute{\boldsymbol{v}}_{\boldsymbol{y}}(\theta) - \boldsymbol{v_y}(\theta)\right\|^2 \leq \epsilon. \tag{5-28}$$

The solution to (5-28) can be found by introducing a Langrage multiplier μ and minimising the function

$$f = \acute{\boldsymbol{v}}_{\boldsymbol{y}}^{H}(\theta)\boldsymbol{R}_{\boldsymbol{y}}^{-1}\acute{\boldsymbol{v}}_{\boldsymbol{y}}(\theta) + \mu\left(\left\|\acute{\boldsymbol{v}}_{\boldsymbol{y}}(\theta) - \boldsymbol{v}_{\boldsymbol{y}}(\theta)\right\|^{2} - \epsilon\right). \tag{5-29}$$

The process of solving the Lagrange multiplier μ is similar to that described in [85] and will not be discussed in detail here. The output of the robust optimum BS beamformer is given by

$$p(\theta)_{Robust-BS} = \frac{1}{\boldsymbol{v}_{\boldsymbol{y}}^{H}(\theta)\boldsymbol{Q}_{\boldsymbol{y}}\boldsymbol{\Lambda}_{\boldsymbol{y}}\left(\mu^{-2}\boldsymbol{I} - \frac{2}{\mu}\boldsymbol{\Lambda}_{\boldsymbol{y}} + \boldsymbol{\Lambda}_{\boldsymbol{y}}^{2}\right)^{-1}\boldsymbol{\Lambda}_{\boldsymbol{y}}^{H}\boldsymbol{Q}_{\boldsymbol{y}}^{H}\boldsymbol{v}_{\boldsymbol{y}}(\theta)}, \tag{5-30}$$

as defined in (3-16), $\boldsymbol{Q}_{\boldsymbol{y}}$ is the matrix whose columns contain the eigenvectors of $\boldsymbol{R}_{\boldsymbol{y}}$ and the main diagonal elements of $\boldsymbol{\Lambda}_{\boldsymbol{y}}$ are the corresponding eigenvalues. In [85] for the ES case, the value of ϵ is normally the same for all steering directions. Notice that for the directional transmission BS case, as different transmission beam patterns are applied to each look direction and the magnitude of the BS steering vector, $\boldsymbol{v}_{\boldsymbol{y}}(\theta)$, varies with the look angle, θ. Thus, although the array element perturbation $\boldsymbol{e}$ is assumed to be the same at different Tx/Rx beams, the value of $\left\|\acute{\boldsymbol{v}}_{\boldsymbol{y}}(\theta) - \boldsymbol{v}_{\boldsymbol{y}}(\theta)\right\|$ is slightly different at different azimuthal angles. Therefore, a fixed value of ϵ would not be the best choice and an adjustment for the value of ϵ according to the BS steering vector may be necessary, for example ϵ at θ is chosen as $\epsilon(\theta) \propto \left\|\boldsymbol{v}_{\boldsymbol{y}}(\theta)\right\|^{2}$.

5.4.4 Examples of Robust BS Beamforming

As an example, a scenario was considered that 20 directionally transmitted beams in a sector of azimuthal angles of 1° to 20° with 1° separation and a ULA with 64 half a wavelength separated receivers and two scatterers whose return SNRs were 30 dB and 16 dB at any single receiver and whose DOAs were 8.23° and 15.44° respectively. The perturbations included:

(a) Random element complex gain errors μ_k ($|\mu_k| \sim \text{unif}(0.75, 1.25)$ and $\angle\mu_k \sim \text{unif}(-\frac{\pi}{3}, \frac{\pi}{3})$),
(b) Random array element location errors $\delta_k \sim \text{unif}(-0.05d, 0.05d)$,
(c) Random independent steering beam centre angle (MRA) errors $\phi_m \sim \text{unif}(-0.3°, 0.3°)$.

Perturbations (a) and (b) represent errors of the receiver elements and they are random and independent at each element and unchanged for all the beams; perturbation (c) represents the steering angle errors which are random and independent for each beam. The details of the perturbations are described in Appendix B. The outputs of directional transmission conventional, MVDR BS beamformers and robust beamformer with an

uncertainty parameter $\epsilon(\theta) = 0.11\|\boldsymbol{v_y}(\theta)\|^2$ are plotted versus azimuthal angle in Figure 5-20. In this example, the conventional BS beamformer output is not seriously affected by the perturbations but as usual its resolution is coarse; the directional transmission BS MVDR beamformer can provide good estimation of the DOAs of the scatterers, but the estimated power values are incorrect and the directivity is unsatisfactory; whilst the directional transmission robust MVDR BS beamformer estimates the peak power with accurate values at the correct DOAs but the width of the main lobe response of the beamformer output power spectrum is broader than the optimum beamformer result with the error-free model.

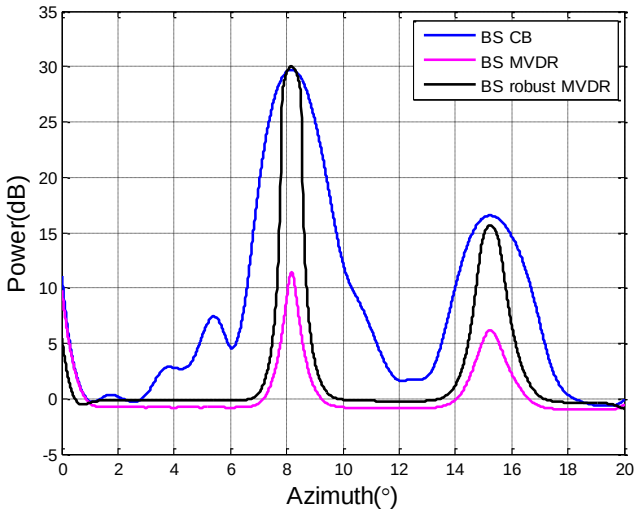

Figure 5-20: An example of applying robust BS beamforming to a scenario of the directional transmission BS model containing perturbations.

A scenario identical as that in Figure 5-20 was simulated. Based on the BS covariance matrix with random, 128 conventional beamformer output pulse samples (with the same perturbations) were generated for each beam. Then those beam output samples were used to estimate a covariance matrix and the robust BS beamformer with the same uncertainty set as the above example, i.e., $\epsilon(\theta) = 0.11\|\boldsymbol{v_y}(\theta)\|^2$, was applied. The results of the directional transmission conventional, MVDR and robust MVDR BS beamformers are plotted in Figure 5-21. Similar to the theoretical analysis, the performance of optimum BS beamformer is seriously degraded, but the superior performance of the robust BS beamformer indicates its satisfactory robustness to the mismatch caused by different errors.

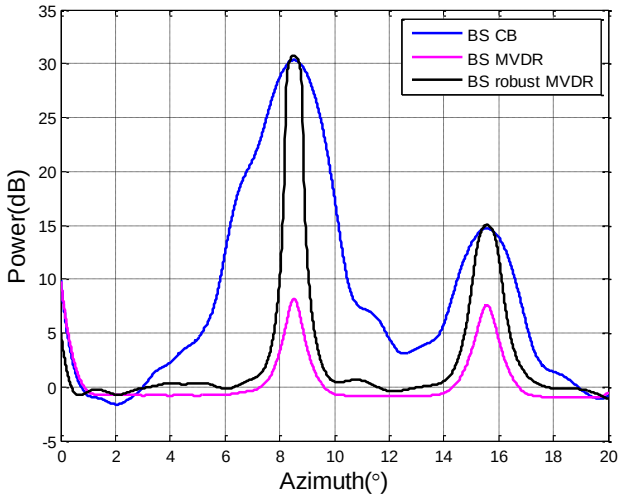

Figure 5-21: An example of applying robust BS beamforming to a simulated data using a directional transmission BS model containing perturbations.

To check the performance with more simulations, 512 independent realisations of the BS data simulation were carried out. Each realisation was similar to the above simulation and had different independent random perturbations but lying in the same range as the previous perturbations conditions (a), (b) and (c), and the robust BS beamformer with $\epsilon(\theta) = 0.11\left\|\boldsymbol{v}_{\boldsymbol{y}}(\theta)\right\|^2$ was applied. The mean and mean plus one standard deviation of the output power values versus azimuth are plotted in Figure 5-22. The variance of output power values in the region not containing incident signals is relatively small, as the output is at the noise level only and the output is almost not affected by the array and beam responses. In those two narrow regions around the DOAs of signals, the averaged output power values are very close to the true signal intensities; and the analysis of the output powers showed that statistically 95% of the robust beamformer output power values at DOAs of signals were within 3 dB of the correct value.

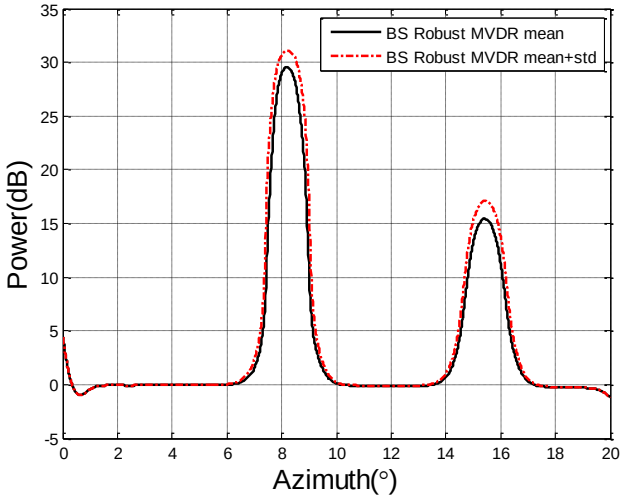

Figure 5-22: An example of statistics of robust BS beamformer output power values with 512 independent realisations of simulated data based on a directional Tx BS model containing perturbations.

As the values of errors are unknown in advance, the uncertainty set needs to be adjusted for each robust beamformer, and it can be difficult to find the best value of ϵ. A small value of ϵ may not be able to fully compensate the steering vector mismatch, whilst a large value of ϵ reduces the spatial resolution and requires more unnecessary computation.

5.5 Cramér–Rao Bounds for DOA Estimation

Parameters are estimated by using samples, and due to the random nature of receiver noise and, in some cases, the incident signal, different realisations drawn from the same ensemble of sample values normally generate different estimates of the parameters of interest. Two commonly used measures are the mean and variance of the estimated parameters. For an unbiased estimator, a smaller variance indicates more accurate estimates. In estimation theory, the CRB expresses a bound on the variance of estimators. It is the smallest variance that any unbiased estimator can achieve in practice and the lowest possible mean squared error among all unbiased estimators.

Using data collected by a phased array, different parameters can be estimated, such as the range and velocity of a target. Among these parameters, the DOA estimation is a popular topic and its CRB has attracted a lot of research interest. With an assumption that the number of signals is known in advance, both ES and BS CRBs for DOA estimation in the omni-directional transmission case are reviewed in Section 5.5.1, then the BS CRB for DOA estimation in the directional transmission case is derived and analysed in Section 5.5.2.

5.5.1 CRBs for DOA Estimation in Omni-directional ES and BS Cases

The derivation of the CRB for the ES DOA estimation can be found in [30], [71] and [72], some details of which are also described in Appendix C. Briefly, when the signal vector is a sample of Gaussian random process, the ES CRB for estimating DOAs, i.e., $\Theta_s = \{\theta_{s1} \quad \theta_{s2} \quad \cdots \quad \theta_{sL}\}$, is given by

$$\boldsymbol{C}_{CR}\left(\Theta_s\right) = \frac{\sigma_n^2}{2N}\left\{Re\left[\left(\boldsymbol{D}^H \boldsymbol{P}_{\boldsymbol{V}_s}^{\perp} \boldsymbol{D}\right) \circ \left(\boldsymbol{R}_{\boldsymbol{s}} \boldsymbol{V}_{\boldsymbol{s}}^H \boldsymbol{R}_{\boldsymbol{x}}^{-1} \boldsymbol{V}_{\boldsymbol{s}} \boldsymbol{R}_{\boldsymbol{s}}\right)^T\right]\right\}^{-1}, \tag{5-31}$$

where N is the number of samples; $\boldsymbol{R}_{\boldsymbol{s}}$ is the source covariance matrix defined in equation (2-2); $\boldsymbol{V}_{\boldsymbol{s}}$ is the matrix whose columns are the steering vectors of the L signals and defined in equation (2-6) and

$$\boldsymbol{P}_{\boldsymbol{V}_s}^{\perp} = [\boldsymbol{I} - \boldsymbol{V}_{\boldsymbol{s}}(\boldsymbol{V}_{\boldsymbol{s}}^H \boldsymbol{V}_{\boldsymbol{s}})^{-1} \boldsymbol{V}_{\boldsymbol{s}}^H],$$

$$\boldsymbol{D} = \dot{\boldsymbol{V}}_{\boldsymbol{s}} = \left[\frac{\partial \boldsymbol{v}(\theta_{s1})}{\partial \theta_{s1}} \quad \frac{\partial \boldsymbol{v}(\theta_{s2})}{\partial \theta_{s2}} \quad \ldots \quad \frac{\partial \boldsymbol{v}(\theta_{sL})}{\partial \theta_{sL}}\right]^T, \tag{5-32}$$

where $\frac{\partial \boldsymbol{v}(\theta_{sl})}{\partial \theta_{sl}}$ can be denoted as $\boldsymbol{d}_l$.

When the signal vector is deterministic, $\boldsymbol{s}(n)$, the n-th snapshot of the signals, becomes a non-random $L\times 1$ complex signal vector, the CRB is given by

$$\begin{aligned}\boldsymbol{C}_{CR}(\Theta_s) &= \frac{\sigma_n^2}{2}\left\{\sum_{n=1}^{N} Re\left[\boldsymbol{s}^H(n)\boldsymbol{D}^H\boldsymbol{P}_{\boldsymbol{V}_s}^{\perp}\boldsymbol{D}\boldsymbol{s}(n)\right]\right\}^{-1} \\ &= \frac{\sigma_n^2}{2N}\left\{Re\left[\left(\boldsymbol{D}^H\boldsymbol{P}_{\boldsymbol{V}_s}^{\perp}\boldsymbol{D}\right)\circ\widehat{\boldsymbol{R}}_{\boldsymbol{s}}^{T}\right]\right\}^{-1},\end{aligned} \tag{5-33}$$

where $\widehat{\boldsymbol{R}}_{\boldsymbol{s}}$ is an estimate of the source covariance matrix and given by

$$\widehat{\boldsymbol{R}}_{\boldsymbol{s}} = \frac{1}{N}\sum_{n=1}^{N}\boldsymbol{s}(n)\boldsymbol{s}^H(n). \tag{5-34}$$

In most active radar systems, the waveform is known and a matched filter is usually used before further processing, therefore, the signal is normally deterministic and the second expression for the CRB, i.e., (5-33), is often used.

In the omni-directional transmission case, the BS CRB for DOA estimation can be easily derived from the ES CRB, and as shown in [92] and [93], the only modification is to replace $\boldsymbol{V}_{\boldsymbol{s}}$ and $\boldsymbol{D}$ in equation (5-33) by their linear transformed expressions in BS, i.e., $\boldsymbol{H}$ and $\boldsymbol{D}_{\boldsymbol{H}}$ defined below. For a uniform linear phased array BS processing where a narrowband deterministic signal is considered, the BS CRB is given by

$$\boldsymbol{C}_{CR-\boldsymbol{h}}(\Theta_s) = \frac{\sigma_n^2}{2N}\left\{Re\left[\left(\boldsymbol{D}_{\boldsymbol{H}}^H\boldsymbol{P}_{\boldsymbol{H}}^{\perp}\boldsymbol{D}_H\right)\circ\widehat{\boldsymbol{R}}_{\boldsymbol{s}}^{T}\right]\right\}^{-1}, \tag{5-35}$$

where terms are defined as follows

$$\begin{gathered}\boldsymbol{H} = \boldsymbol{V}^H\boldsymbol{V}_{\boldsymbol{s}}(\Theta_s), \\ \boldsymbol{P}_{\boldsymbol{H}} = \boldsymbol{H}(\boldsymbol{H}^H\boldsymbol{H})^{-1}\boldsymbol{H}^H, \\ \boldsymbol{P}_{\boldsymbol{H}}^{\perp} = \boldsymbol{I} - \boldsymbol{P}_{\boldsymbol{H}}, \\ \boldsymbol{D}_{\boldsymbol{H}} = \dot{\boldsymbol{H}} = [\dot{\boldsymbol{h}}(\theta_{s1}) \quad \dot{\boldsymbol{h}}(\theta_{s2}) \quad \ldots \quad \dot{\boldsymbol{h}}(\theta_{sL})]^T, \\ \dot{\boldsymbol{h}}(\theta_{sl}) = \frac{\partial \boldsymbol{h}(\theta_{sl})}{\partial \theta_{sl}} = \boldsymbol{V}^H\dot{\boldsymbol{v}}(\theta_{sl}).\end{gathered} \tag{5-36}$$

5.5.2 CRB for DOA Estimation in Directional Transmission BS Case

According to the directional transmission BS model described in Section 4.1.1, a matrix $\boldsymbol{V}_{\boldsymbol{y}}(\Theta_s)$ containing the directional transmission BS signal steering vectors, i.e.,

$\boldsymbol{v_y}(\theta_{sl}) = \boldsymbol{h}(\theta_{sl}) \circ \boldsymbol{h}(\theta_{sl})$, is given by equation (4-14), thus the first order derivative of $\boldsymbol{V_y}(\Theta_s)$ is given by

$$\begin{aligned} \boldsymbol{D_{Vy}} &= \dot{\boldsymbol{V}}_{\boldsymbol{y}}(\Theta_s) \\ &= \left[\frac{\partial\, \boldsymbol{v_y}(\theta_{s1})}{\partial\theta_{s1}} \quad \frac{\partial\, \boldsymbol{v_y}(\theta_{s2})}{\partial\theta_{s2}} \quad \dots \quad \frac{\partial\, \boldsymbol{v_y}(\theta_{sL})}{\partial\theta_{sL}}\right] \\ &= 2[\boldsymbol{h}(\theta_{s1}) \circ \dot{\boldsymbol{h}}(\theta_{s1}) \quad \boldsymbol{h}(\theta_{s2}) \circ \dot{\boldsymbol{h}}(\theta_{s2}) \quad \dots \quad \boldsymbol{h}(\theta_{sL}) \circ \dot{\boldsymbol{h}}(\theta_{sL})] \\ &= 2[\,(\boldsymbol{V}^H\boldsymbol{v}(\theta_{s1})) \circ (\boldsymbol{V}^H d_1) \quad (\boldsymbol{V}^H\boldsymbol{v}(\theta_{s2})) \circ (\boldsymbol{V}^H d_2) \quad \dots \quad (\boldsymbol{V}^H\boldsymbol{v}(\theta_{sL})) \circ (\boldsymbol{V}^H d_L)]. \end{aligned} \tag{5-37}$$

Notice here a factor of $\frac{1}{K}$ has been removed from the expression of $\boldsymbol{v_y}(\theta_{sl})$, defined in (4-8) and $\boldsymbol{h}(\theta_{sl})$ is normalised, i.e., $\boldsymbol{V}^H\boldsymbol{V}$=$\boldsymbol{I}$. This normalisation avoids the different ES and BS gains for signals and allows an easier comparison between ES and BS CRBs. Assuming deterministic signals are transmitted and received, the CRB derivation for DOA estimation in the directional transmission BS case is similar to the above omni-directional transmission BS case. The modification is to replace $\boldsymbol{V_s}$ and $\boldsymbol{D}$ by their corresponding expressions in the directional transmission BS case $\boldsymbol{V_y}(\Theta_s)$ and $\boldsymbol{D_{Vy}}$ in both (5-32) and (5-33), and for DOA estimation in the directional transmission BS case is given by

$$\boldsymbol{C}_{CR-Vy}(\Theta_s) = \frac{\sigma_n^2}{2N}\left\{Re\left[\left(\boldsymbol{D}_{Vy}^H P_{Vy}^{\perp} \boldsymbol{D}_{Vy}\right) \circ \widehat{\boldsymbol{R}}_{\boldsymbol{s}}^T\right]\right\}^{-1}. \tag{5-38}$$

A scenario consisting of two uncorrelated signals at DOAs of 8.23° and 9.44°, and whose SNRs were 10 dB and 5 dB respectively, 64 receivers, d=0.5λ, with variable number of beams evenly spaced in angle over the sector of [1°, 20°] was considered. Both the omni-directional transmission and directional Tx/Rx scanning cases have been considered. The CRBs for DOA estimation in the omni-directional transmission ES, BS and the directional transmission BS cases at $\theta_{s1} = 8.23°$ are compared by varying the number of snapshots (samples) in Figure 5-23 and Figure 5-24, where the number of beams used was 8 and 20 respectively.

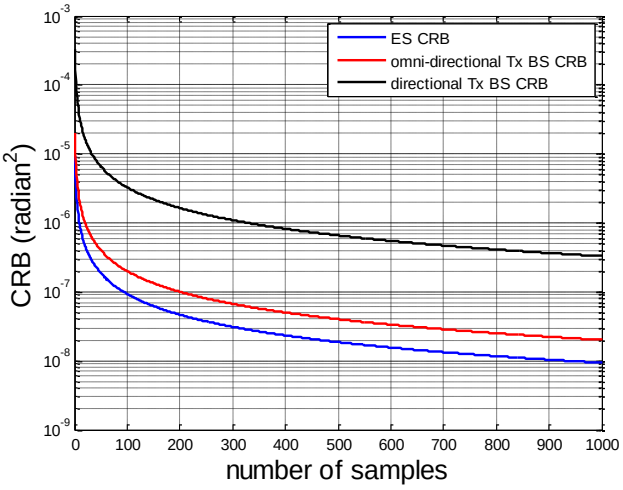

Figure 5-23: The CRBs for DOA estimation in the omni-directional transmission ES, BS and directional transmission BS cases versus the number of snapshots. The number of beams is 8.

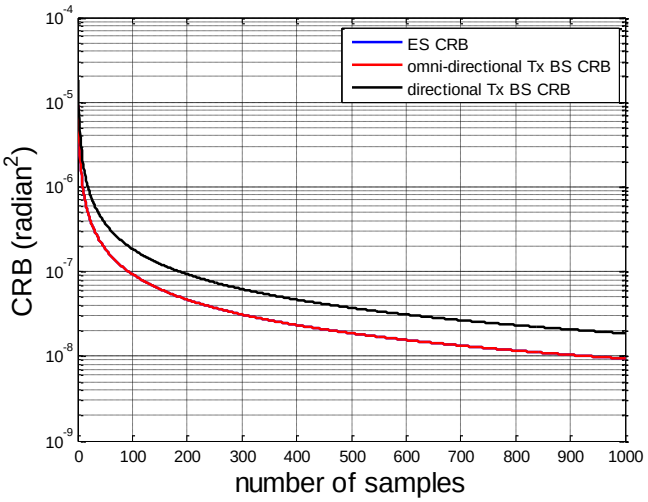

Figure 5-24: The CRBs for DOA estimation in the omni-directional transmission ES, BS and directional transmission BS cases versus the number of snapshots. The number of beams is 20.

For a fixed number of samples as 1000, the results are also compared as a function of the number of beams in Figure 5-25. To keep the gain unchanged in ES and BS processing, the SFS method was used to make beams mutually orthogonal and with unit magnitude, i.e., $\boldsymbol{V}^H\boldsymbol{V}=\boldsymbol{I}$.

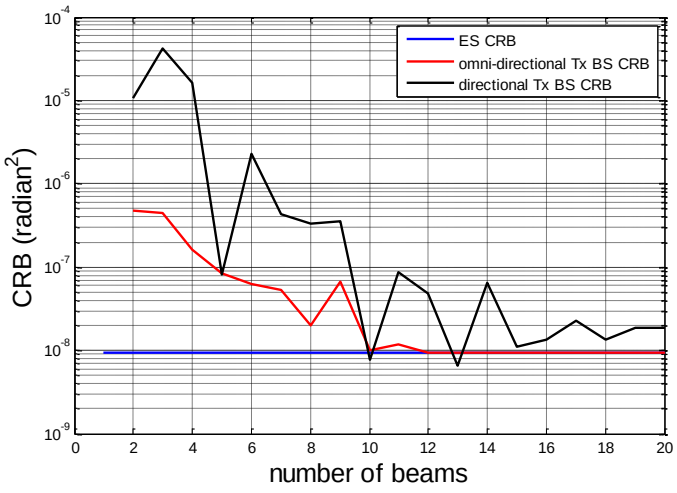

Figure 5-25: The CRBs for DOA estimation in the omni-directional transmission ES, BS and directional transmission BS versus the number of beams, where the number of snapshots is 1000.

The BS CRBs for estimation DOA of a single signal are determined by several factors together, including: the number of samples, the number of beams, array aperture, SNR and DOA. Generally, more samples, larger array aperture and higher SNR will produce lower CRBs. For the omni-directional transmission case, Figure 5-23 shows that for this scenario with 8 beams, $\boldsymbol{C}_{CR-\boldsymbol{h}}(\Theta_s) > \boldsymbol{C}_{CR}(\Theta_s)$; whilst as shown in Figure 5-24, when the number of beams is 20, the ES and BS results are identical. Figure 5-25 shows that with increasing the number of beams, the omni-directional transmission BS CRB for DOA

estimation approaches the ES CRB and they become the same when the number of beams is larger than 13, where the separation between adjacent beam centres is less than half a beamwidth. A theoretical proof can be found in [92] that the omni-directional transmission BS CRB is never smaller than the ES CRB, and the equality appears if and only if

$$\begin{aligned} \boldsymbol{V}\boldsymbol{V}^H\boldsymbol{P}_{\boldsymbol{V}_s}^{\perp}\boldsymbol{D} &= \boldsymbol{P}_{\boldsymbol{V}_s}^{\perp}\boldsymbol{D}, \\ \boldsymbol{V}\boldsymbol{V}^H\boldsymbol{V}_s &= \boldsymbol{V}_s. \end{aligned} \tag{5-39}$$

Figure 5-23 and Figure 5-24 show that the directional transmission BS CRB, $\boldsymbol{C}_{CR-\boldsymbol{V}\boldsymbol{y}}(\Theta_s)$, is obviously higher than that for the omni-directional transmission BS case. However, considering the very low CRB values, for example, the largest value of the directional transmission BS CRB in Figure 5-23 is smaller than 10^{-4}radian^2, which indicate the standard derivation is about 0.6°. Also, with increasing the number of beams, the CRBs values become much smaller and with a large number of samples, the difference between the directional transmission BS CRB and omni-directional transmission BS for DOA estimation is very insignificant. Figure 5-25 shows that the directional transmission BS CRB drops when the number of beams increases but with some fluctuation, as the DOAs may fall at the beam centre and produce very low CRB values. Generally, CRB for DOA estimation in the directional transmission BS case is larger than that of the omni-directional transmission BS case but this is not always the case, when DOAs coincidently at the centre of beam, $\boldsymbol{C}_{CR-\boldsymbol{V}\boldsymbol{y}}(\Theta_s)$ can be lower than $\boldsymbol{C}_{CR-\boldsymbol{h}}(\Theta_s)$ and $\boldsymbol{C}_{CR}(\Theta_s)$.

Signal correlations or system perturbations change the steering vector and signal model, their effects on the CRB for DOA estimation in the directional transmission BS case are similar to the omni-directional ES model, which can be found in [30] and will not be discussed here.

5.6 Optimum BS Beamforming with a Moving Scatterer

In all the previous descriptions of array processing, it has been assumed that the scatterers remain stationary, but non-stationary scatterers are quite common in practice. Rapidly moving interferences will degrade the algorithm performance and a projection algorithm has been proposed in [96], [97] to overcome this problem via artificial widening of adaptive pattern nulls for a moving interference. The application of the BS MVDR algorithm to moving sources has been reported in [91], where the main purpose of using BS processing is to reduce the covariance matrix dimension as the number of data snapshots in a non–stationary environment is limited. Little performance degradation was reported for a slowly moving source but significant performance degradation for fast moving sources. To check how the motion of a scatterer affects the performance of the directional transmission optimum BS beamformer, a scenario containing both stationary and non-stationary scatterers was considered. In this example,

only a short period is considered, where a target was moving at a constant speed and at the same range, thus eliminating the need to consider the range and Doppler effects.

The beam scanning strategy will have an impact on the algorithm's performance against a moving target. The example considered was where a burst of *N* pulses is transmitted at each steering angle of a phased array. The initial azimuthal angle of a non-stationary scatterer is θ_{s1} and the scatterer moves an angle $\Delta\theta$ during the interval between adjacent pulses. In this problem, only the scenario where the DOA of the moving scatterer always remains within the sector of interest was considered. The BS covariance matrix is estimated by

$$\boldsymbol{R}_{\boldsymbol{y}} = E\{\boldsymbol{y}\boldsymbol{y}^H\} = \frac{1}{N}\sum_{n=1}^{N}\boldsymbol{y}(n)\boldsymbol{y}^H(n), \tag{5-40}$$

where $\boldsymbol{y}(n)$ denotes a vector which contains all the beam outputs at the *n*-th pulse for each beam. The covariance matrix is a composite of stationary scatterers, non-stationary scatterers and noise components, given by

$$\boldsymbol{R}_{\boldsymbol{y}} = \boldsymbol{R}_{\boldsymbol{y}\_1} + \boldsymbol{R}_{\boldsymbol{y}\_2} + K\sigma_n^2\boldsymbol{I}, \tag{5-41}$$

where $\boldsymbol{R}_{\boldsymbol{y}\_1}$ and $\boldsymbol{R}_{\boldsymbol{y}\_2}$ are the non-stationary and stationary scatterers components respectively. For a single non-stationary scatterer whose complex amplitude is σ_{s1}, the *i*, *j* entry of matrix $\boldsymbol{R}_{\boldsymbol{y}\_1}$ is given by

$$\left(\boldsymbol{R}_{\boldsymbol{y}\_1}\right)_{ij} = \frac{\sigma_{s1}^2}{N}\sum_{n=1}^{N}\boldsymbol{v}_{\boldsymbol{y}}\left(\theta_{s1} + \left((i-1)N + n - 1\right)\Delta\theta\right)\boldsymbol{v}_{\boldsymbol{y}}^H\left(\theta_{s1} + \left((j-1)N + n - 1\right)\Delta\theta\right). \tag{5-42}$$

To demonstrate the performance of the directional transmission BS MVDR beamformer for the non-stationary scatterer, a scenario similar to that in Figure 4-6, two returns from scatterers are uncorrelated, but including one stationary and one moving scatterer, was considered. The first scatterer with 10 dB SNR at any single receiver and initially at an azimuthal angle at 8° was moving at a fixed speed in azimuth. The second scatterer was stationary and located at 15°. The ratio of the moving scatterer's location change during an interval between two adjacent beams to a beam width, *BW* (here the beamwidth was about 1.6° at broadside in this example), is defined as

$$r_b = N\Delta\theta/BW, \tag{5-43}$$

and it indicates the fraction (or multiple) of a beamwidth that the scatterer moves when the transmitted/received beams change from one steering direction to the next. The value of r_b was chosen as 0.05, 0.1, 0.2 and 0.5, which correspond to angular changes of the scatterer's azimuthal location over the total assumed "coherent processing interval" of 1.67°, 3.33°, 6.66° and 16.65° respectively. The processing results with different r_b are shown in Figure 5-26, which indicates that the received signal reflected by the slow moving scatterer, i.e., $r_b = 0.05$, can still be effectively beamformed and hence detected

but the location of the peak values, i.e., 8.8° is biased to the midway of its motion; with increasing speed, i.e., $r_b = 0.1$ the non-stationary scatterer can be detected when it is in the mainlobe of a beam but the sharp peak is widened by motion of the scatterer. Increasing the speed to $r_b = 0.2$ adds some spurious peaks, as the moving scatterer is detected several times and wrongly identified as different targets. When the speed is increased to $r_b = 0.5$, the non-stationary scatterer is moving too fast to be detected, as it could not be captured by in the mainlobe of any of the beams and has run out of the sector before the scanning finished. The processing result of the stationary scatterer is not affected unless the non-stationary and stationary scatterers fall into the same beam.

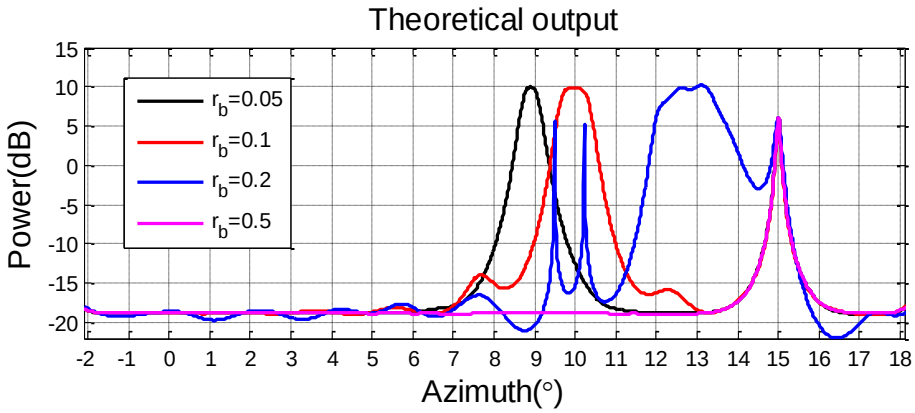

Figure 5-26: The output power values of the directional transmission BS MVDR beamformer for a stationary scatterer and a non-stationary scatterer with different moving speeds.

To improve the performance of the beamfomer for non-stationary scatterers, a faster beam scanning strategy and algorithms which would detect and compensate for the scatterer motion can be considered. Some related works for this problem in ES can be found in [89] or a similar problem of stationary sources but with a moving array is addressed in [90].

5.7 Summary

The directional transmission BS processing takes into account the transmission beam pattern and some properties are different from the standard BS processing. When beams are formed in a sector of interest, investigations for problems related to the region outside the sector of interest have been carried out covering three aspects. Firstly, the optimum BS beamformer output power at the DOA of an interference lying out of sector was analysed. It was shown that it is hard to identify the interference according to the optimum BS beamformer output power, as it is hidden by the high response of the BS MVDR beamformer in the region out of sector. Secondly, compared with the omni-directional transmission case, the BS MVDR response out of sector is much higher, and two methods have been proposed to mitigate this high response. The first method using virtual beams effectively mitigated the high response but also removed the interference. The second scaling beamforming method removed the high response and kept the

interference, but the DOAs need to be estimated in advance and the method can fail when the DOA of interference is far away from the sector. Thirdly, the interference outside the sector of interest almost has no effect on the optimum BS beamformer output power at the DOAs of signals inside the sector of interest, but can cause a spurious peak within the sector. To eliminate the spurious peak but keep the output power values at DOAs of signals unchanged, an oblique projection method was proposed.

In Section 5.4, different array perturbations in BS processing were analysed and an ES robust beamforming algorithm was extended to improve the robustness of the directional transmission optimum BS beamformer.

The CRB for DOA estimation in the directional transmission BS case was derived and compared with the CRBs for DOA estimation in the omni-directional transmission BS an ES cases in Section 5.5.

As moving targets commonly occur in practice, to investigate how the motion of a scatterer affects the performance of the directional transmission optimum BS beamformer, the proposed BS algorithm was applied to a scenario containing both stationary and non-stationary scatterers in Section 5.6.

Notice that the work completed in this chapter was mainly based on the directional transmission BS model, but some properties and proposed methods can also be directly applied the omni-directional BS case.

Chapter 6

Beam Space Processing for Coherent Signals

In previous chapters, different BS processing algorithms have been introduced and developed. All these algorithms are based on the assumption that signals and interferences are fully independent. This typically happens when the received signals from different directions are random or with different unique features, e.g. different waveforms, unique coding etc. For passive array systems, the received signals, which are self-generated by targets, such as vibrations from a ship, are normally random and independent of signals from other directions. For active phased array systems, the transmitted signal waveforms are reflected by targets and with modifications both in amplitude and phase. The modifications often change with time or variation of the position of the target and these disturbances give rise to random return signals which can be modelled as being independent of each other. For example, the phase of the return from a weather phenomenon is random, and with a large number of returned samples in each beam direction, the reflected signals from different directions are independent. So, in these cases, the above assumption is valid.

However in practice, signals from different DOAs can be correlated. For example, multipath often happens; signals which scatter off a target can be then reflected and bounced off adjacent objects such as roads, buildings and superstructures to produce multiple returns from different directions with different phase delays and amplitudes. In another case, a smart jammer, which generates interferences coherent with the desired signal, can be used to interrupt signal detection and estimation, e.g. retransmitting the received source signal back to the source by multiple propagation paths such as direct and terrain bounce in the case of hot clutter. Even more, for an active system, where the same signal is transmitted in different directions, the returns from large, stationary targets or a clutter at the same range can be coherent.

In the scenario where Tx/Rx beams are synchronously scanned across a sector, the same signal is transmitted through different beams (with different main lobe axes). For targets at the same range which are stationary during the whole scan period, two kinds of correlations occur. Firstly, the returns from different DOAs can be highly correlated for each single transmit beam, although the directional transmission radiation pattern applies different gains to different DOAs. Secondly, returns from the same DOA but in different beams can be highly correlated, as the same signal is transmitted at M different times, although the Tx/Rx beam pattern applied to the signal varies due to the MRA changes at each beam. In BS processing, the outputs from different beams are used together for further processing, both of the two kinds of correlations occur, thus the correlated nature of the return signals must be taken into consideration.

The model of correlated signals is different from the model used in previous chapters to derive BS processing algorithms and this mismatch can degrade the performance of BS processing. A large body of work for direction finding of correlated signals in ES has been completed. However, no work for the correlated signals in BS has been found in the literature. In this chapter, the performance degradation of the BS processing algorithms caused by signal correlation is analysed and methods for estimating DOAs and intensities of correlated signals are proposed.

6.1 Impact of Signal Correlation on the Performance of BS Processing

The correlation coefficient between two signals $s_i(t)$ and $s_j(t)$ is written as

$$\rho_{ij} = \frac{E\{s_i(t)s_j^*(t)\}}{\sqrt{E\{s_i(t)s_i^*(t)\}E\{s_j(t)s_j^*(t)\}}}, \tag{6-1}$$

which is a complex number and can be located in any position in or on the unit circle. When $|\rho_{ij}|$=1, the two signals are fully correlated, which is also called coherent; $|\rho_{ij}|$=0 is for the case that two signals are uncorrelated and $0 < |\rho_{ij}| < 1$ means the two signals are partially correlated. When signals are correlated, the signal covariance matrix is different from the case containing uncorrelated signals only, and will affect the results of BS processing.

6.1.1 Model of Correlated Signals

Consider a ULA consisting of *K* identical elements and receiving *L* narrowband signals. These signals are denoted as $\boldsymbol{s} = \{s_1(t),\ s_2(t),\ \ldots,\ s_L(t)\}$ and their DOAs are denoted as $\Theta_s = \{\theta_{s1},\ \theta_{s2},\ \ldots,\ \theta_{sL}\}$. Assuming a transmitted unit amplitude narrowband signal is denoted as $s_0(t)$, $\sigma_{s0} = 1$, and a received signal at θ_{sl}, $s_l(t)$, can be a mixture of signals correlated or uncorrelated with $s_0(t)$. As discussed earlier, the reflected signal from a stationary scatterer, $s_{cl}(t)$, is fully correlated to the transmitted signal; the uncorrelated part can be the return from non-stationary scatterers, which generate a random phase, or, an uncorrelated jamming signal transmitted and received from the same direction, θ_{sl}. By ignoring propagation delays, $s_l(t)$ can be given by

$$s_l(t) = s_{cl}(t) + s_{ul}(t), \tag{6-2}$$

where $s_{cl}(t)$ and $s_{ul}(t)$ are independent with each other, so

$$E\{s_{cl}(t)s_{ul}^*(t)\} = 0. \tag{6-3}$$

The powers of $s_{cl}(t)$, $s_{ul}(t)$ and $s_l(t)$ at any single receiver are given by

$$\begin{aligned} E\{s_{cl}(t)s_{cl}^*(t)\} &= \sigma_{scl}^2, \\ E\{s_{ul}(t)s_{ul}^*(t)\} &= \sigma_{ul}^2, \\ E\{s_l(t)s_l^*(t)\} &= \sigma_{sl}^2 = \sigma_{scl}^2 + \sigma_{ul}^2. \end{aligned} \tag{6-4}$$

Thus, ρ_l, the correlation coefficient between $s_l(t)$ and $s_0(t)$, is given by

$$\begin{aligned} \rho_l &= \frac{E\{s_l(t)s_0^*(t)\}}{\sqrt{E\{s_l(t)s_l^*(t)\}E\{s_0(t)s_0^*(t)\}}} \\ &= \frac{E\{s_{cl}(t)s_0^*(t)\}}{\sqrt{\sigma_{sl}^2\sigma_{s0}^2}} \\ &= \frac{E\{s_{cl}(t)s_0^*(t)\}}{\sqrt{(\sigma_{scl}^2+\sigma_{ul}^2)\sigma_{s0}^2}} \end{aligned} \tag{6-5}$$

since $s_{cl}(t)$ is coherent with $s_o(t)$, thus

$$\left|\frac{E\{s_{cl}(t)s_0^*(t)\}}{\sqrt{E\{s_{cl}(t)s_{cl}^*(t)\}E\{s_0(t)s_0^*(t)\}}}\right| = \left|\frac{E\{s_{cl}(t)s_0^*(t)\}}{\sqrt{\sigma_{scl}^2\sigma_{s0}^2}}\right| = 1, \tag{6-6}$$

substituting $\sigma_{s0} = 1$ into (6-5) and (6-6), it shows that $|\rho_l| < 1$ and the expression of $s_l(t)$ can be rewritten as

$$s_l(t) = \sigma_{sl}\rho_l s_0(t) + s_{ul}(t), \tag{6-7}$$

Therefore, the correlated parts of these L returns are replicas of the same transmitted (source) signal, $s_0(t)$, but with different amplitudes and phases. All the L signals at one moment t are incorporated in a vector and written as

$$\boldsymbol{s}(t) = \begin{bmatrix} \rho_1\sigma_{s1}s_0(t) + s_{u1}(t) \\ \rho_2\sigma_{s2}s_0(t) + s_{u2}(t) \\ \vdots \\ \rho_L\sigma_{sL}s_0(t) + s_{uL}(t) \end{bmatrix}, \tag{6-8}$$

as no temporal signal processing (except for estimating the covariance matrix) will be considered, the symbols $\boldsymbol{s}(t)$, $s_0(t)$, $s_l(t)$ and $s_{ul}(t)$ can be simply denoted as $\boldsymbol{s}$, s_0, s_l and s_{ul} respectively. Since $E\{s_0 s_{ul}^*\} = 0, 1 \le l \le L$ and $E\{s_{ui}s_{ul}^*\} = 0, i \ne l$, the covariance matrix of these signals is given by

$$\boldsymbol{R_s} = E\{\boldsymbol{s}\boldsymbol{s}^H\} = \begin{bmatrix} \sigma_{s1}^2 & \rho_{12}\sigma_{s1}\sigma_{s2} & \cdots & \rho_{1L}\sigma_{s1}\sigma_{sL} \\ \rho_{12}^*\sigma_{s1}\sigma_{s2} & \sigma_{s2}^2 & \cdots & \rho_{2L}\sigma_{s2}\sigma_{sL} \\ \vdots & \vdots & \ddots & \vdots \\ \rho_{1L}^*\sigma_{s1}\sigma_{sL} & \rho_{2L}^*\sigma_{s2}\sigma_{sL} & \cdots & \sigma_{sL}^2 \end{bmatrix}, \tag{6-9}$$

where ρ_{ij} is the correlation coefficient between the *i*-th and *j*-th signals. When all signals are fully uncorrelated or partially correlated, the above source covariance matrix $\boldsymbol{R_s}$ is full rank; when all *L* signals are fully correlated, $|\rho_l| = |\rho_{ij}| = 1$, the uncorrelated part is zero and the l-th signal can be written as $s_l = \sigma_{sl}\rho_l s_0$, then the rank of the above source covariance matrix, $\boldsymbol{R_s}$, is one.

The phased array receiver output vector is given by

$$\boldsymbol{x}(t) = \sum_{l=1}^{L} s_l(t)\boldsymbol{v}(\theta_{sl}) + \boldsymbol{n}(t), \tag{6-10}$$

For the omni-directional transmission or passive phased array cases, the ES covariance matrix is given by

$$\boldsymbol{R_x} = \boldsymbol{V_s}(\Theta_s)\boldsymbol{R_s}\boldsymbol{V_s}^H(\Theta_s) + \sigma_n^2\boldsymbol{I} \tag{6-11}$$

and the corresponding BS covariance matrix becomes

$$\begin{aligned}\boldsymbol{R_y} &= \boldsymbol{V}^H(\Theta_B)\boldsymbol{R_x}\boldsymbol{V}(\Theta_B)\\ &= \boldsymbol{H}(\Theta_s)\boldsymbol{R_s}\boldsymbol{H}^H(\Theta_s) + \boldsymbol{V}^H(\Theta_B)\boldsymbol{V}(\Theta_B)\sigma_n^2,\end{aligned} \tag{6-12}$$

where from (5-36), $\boldsymbol{H}(\Theta_s) = \boldsymbol{V}^H(\Theta_B)\boldsymbol{V_s}(\Theta_s)$.

With a directional transmission transmitter, the ES covariance matrix varies with each Tx beam, and for the *m*-th beam with a steering angle θ_m, it is given by

$$\boldsymbol{R_x}(\theta_m) = \boldsymbol{V_x}(\Theta_s, \theta_m)\boldsymbol{R_s}\boldsymbol{V_x}^H(\Theta_s, \theta_m) + \sigma_n^2\boldsymbol{I}, \tag{6-13}$$

and the corresponding directional transmission BS covariance matrix is given by

$$\boldsymbol{R_y} = \boldsymbol{V_y}(\Theta_s)\,\boldsymbol{R_s}\boldsymbol{V_y}^H(\Theta_s) + K\sigma_n^2\boldsymbol{I}, \tag{6-14}$$

where $\boldsymbol{V_x}(\Theta_s, \theta_m)$ and $\boldsymbol{V_y}(\Theta_s)$ are given by (4-5) and (4-14) respectively.

6.1.2 Conventional BS Beamformer Output with Correlated Signals

When the signals are correlated, the output of the conventional BS beamformer is different from that of the case containing uncorrelated signals only. Here the simplest case is considered; two correlated signals s_1 and s_2 arriving from θ_{s1} and θ_{s2}, incident on a passive or omni-directional transmission phased array. The receiver output vector is $\boldsymbol{x}(t) = s_1(t)\boldsymbol{v}(\theta_{s1}) + s_2(t)\boldsymbol{v}(\theta_{s2}) + \boldsymbol{n}(t)$, thus the BS covariance matrix is given by

$$\boldsymbol{R_y} = [\boldsymbol{h}(\theta_{s1}) \quad \boldsymbol{h}(\theta_{s2})]\begin{bmatrix}\sigma_1^2 & \rho_{12}\sigma_1\sigma_2\\ \rho_{12}^*\sigma_1\sigma_2 & \sigma_2^2\end{bmatrix}[\boldsymbol{h}(\theta_{s1}) \quad \boldsymbol{h}(\theta_{s2})]^H + \sigma_n^2\boldsymbol{V}^H\boldsymbol{V}. \tag{6-15}$$

According to formula (3-6) and the normalisation in (3-7), the output power of a conventional BS beamformer at the DOA of one of the correlated signals is given by

$$\begin{aligned} p_{CB-BS}(\theta_{s1}) &= \frac{1}{G(\theta_{s1})}\boldsymbol{h}^{\boldsymbol{H}}(\theta_{s1})\boldsymbol{R}_{\boldsymbol{y}}\boldsymbol{h}(\theta_{s1}) \\ &= \frac{1}{G(\theta_{s1})}\Bigg(\boldsymbol{h}^H(\theta_{s1})[\boldsymbol{h}(\theta_{s1}) \quad \boldsymbol{h}(\theta_{s2})]\begin{bmatrix}\sigma_{s1}^2 & \rho_{12}\sigma_{s1}\sigma_{s2}\\ \rho_{12}^*\sigma_{s1}\sigma_{s2} & \sigma_{s2}^2\end{bmatrix}[\boldsymbol{h}(\theta_{s1}) \quad \boldsymbol{h}(\theta_{s2})]^H\boldsymbol{h}(\theta_{s1}) \\ &\qquad + \sigma_n^2\boldsymbol{h}^H(\theta_{s1})\boldsymbol{V}^H\boldsymbol{V}\boldsymbol{h}(\theta_{s1})\Bigg) \\ &= \frac{1}{G(\theta_{s1})}\Big(\big(\boldsymbol{h}^H(\theta_{s1})\boldsymbol{h}(\theta_{s1})\big)^2\sigma_{s1}^2 + \boldsymbol{h}^H(\theta_{s1})\boldsymbol{h}(\theta_{s2})\boldsymbol{h}^H(\theta_{s1})\boldsymbol{h}(\theta_{s1})\rho_{12}^*\sigma_{s1}\sigma_{s2} \\ &\qquad + \boldsymbol{h}^H(\theta_{s1})\boldsymbol{h}(\theta_{s1})\boldsymbol{h}^H(\theta_{s2})\boldsymbol{h}(\theta_{s1})\rho_{12}\sigma_{s1}\sigma_{s2} + |\boldsymbol{h}^H(\theta_{s1})\boldsymbol{h}(\theta_{s2})|^2\sigma_{s2}^2 \\ &\qquad + \sigma_n^2\boldsymbol{h}^H(\theta_{s1})\boldsymbol{V}^H\boldsymbol{V}\boldsymbol{h}(\theta_{s1})\Big) \end{aligned} \tag{6-16}$$

As defined in (4-20), $H(\theta) = \boldsymbol{h}^H(\theta)\boldsymbol{h}(\theta)$ and the inner product of the two BS steering vectors whose DOAs are θ_{s1} and θ_{s2} is denoted as

$$\beta(\theta_{s1}, \theta_{s2}) = \boldsymbol{h}^H(\theta_{s1})\boldsymbol{h}(\theta_{s2}), \tag{6-17}$$

and can be simply denoted as β for the two signals case. Also since $G(\theta_{s1}) = H^2(\theta_{s1})$, then for the scenario of two coherent signals, the BS conventional beamformer output power at one of the DOAs is given by

$$p_{CB-BS}(\theta_{s1}) = \sigma_{s1}^2 + \frac{\sigma_{s1}\sigma_{s2}}{H(\theta_{s1})}(\beta\rho_{12}^* + \beta^*\rho_{12}) + \frac{|\beta|^2}{H^2(\theta_{s1})}\sigma_{s2}^2 + \frac{\sigma_n^2\boldsymbol{h}^H(\theta_{s1})\boldsymbol{V}^H\boldsymbol{V}\boldsymbol{h}(\theta_{s1})}{H^2(\theta_{s1})}. \tag{6-18}$$

The variation of $H(\theta)$ with angle decreases with an increasing number of beams in the sector of interest, and when the separation between beam centres is less than half of the 3 dB beamwidth, the value of $H(\theta)$ is almost constant and $H(\theta) \approx H_c$. The value of β decreases dramatically with an increasing separation between the two DOAs. For example, consider the scenario used before, 21 directional ULA transmitted beams at angles of -2° to 18° with 1° separation. The value of $H(\theta)$ and $|\beta(\theta, 8°)|$ versus θ are plotted in Figure 6-1.

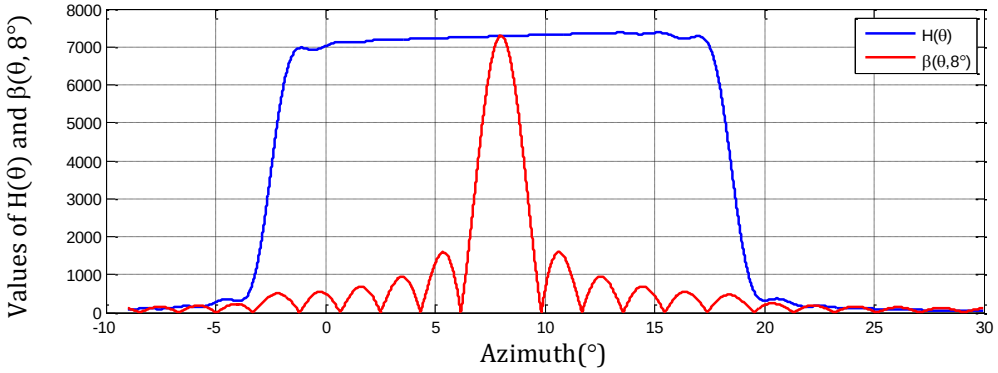

Figure 6-1: An example of values of $H(\theta)$ and $|\beta(\theta, 8°)|$.

In expression (6-18), setting $\rho_{12} = 0$ gives the conventional BS beamformer output power for the case of independent signals, and the second part of (6-18) shows that the extra power caused by the correlation, $\frac{\sigma_{s1}\sigma_{s2}}{H(\theta_{s1})}(\beta\rho_{12}^{*} + \beta^{*}\rho_{12})$, which depends on both the correlation between signals and the correlation between two steering vectors. When the separation between θ_{s1} and θ_{s2} is larger than half a beamwidth, the value of $\frac{|\beta|}{H_c}$ becomes relatively small and the correlation between signals only affects the output at θ_{s1} slightly. Otherwise, the extra power can be significant. Therefore, the correlation causes a different beamformer output from the result for the model containing independent signals only and can potentially shift the angles of the conventional beamformer output power peaks.

6.1.3 Optimum BS Beamformer Output with Correlated Signals

The optimum BS beamformer (MVDR) algorithm minimises the total power under the constraint of unity response at the look direction. With this criterion, the process of optimisation manipulates correlated signals to partially or completely cancel the desired signal at the look angle, which distorts the output power seriously. More detailed description of the performance degradation of optimum ES beamformer in the presence of correlated signals can be found in [50], [104] and [105]. In this section, only the effect on BS processing is analysed.

6.1.3.1 Optimum BS Beamformer Output Power at DOAs of Correlated Signals in Omni-directional Transmission Case

The output power of the standard optimum BS beamformer at the DOA of one of the correlated signals, e.g., θ_{s1} is derived in Appendix D, where it is shown that the optimum BS beamformer output power at θ_{s1} is given by

$$\begin{aligned} p_{MVDR-BS}(\theta_{s1}) \approx{}& \sigma_{s1}^{2} \\ &+ \frac{1}{(H_c^2 - \beta^{*}\beta)\sigma_{s2}^{2} + KH_c\sigma_n^2}\left(|\rho_{12}|^2\sigma_{s1}^{2}\sigma_{s2}^{2}(\beta^{*}\beta - H_c^2) \right. \\ &\left. + K\sigma_n^2\left(\frac{\beta^{*}\beta\sigma_{s2}^{2}}{H_c} + \sigma_{s1}\sigma_{s2}(\beta^{*}\rho_{12} + \beta\rho_{12}^{*})\right)\right) + \frac{K}{H_c}\sigma_n^2 \end{aligned} \tag{6-19}$$

Therefore, the optimum BS beamformer output power values at the DOAs of the correlated signals can be significantly different from the corresponding independent signals case and the output at the DOA, θ_{s1}, is seriously attenuated. When the SNR of $s_1(t)$ is very high ($\sigma_{s1}^2 \gg \sigma_n^2$), equation (6-19) can be simply approximated as

$$p_{MVDR-BS}(\theta_{s1}) \approx \sigma_{s1}^{2}(1 - |\rho_{12}|^2) \tag{6-20}$$

In this case, the output power depends only on the signal power at DOA θ_{s1} and the correlation coefficient between the two signals. The higher correlation causes more attenuation to the output power, and a weak but coherent interference may cancel a strong signal.

When two DOAs are very closely spaced, $\boldsymbol{h}(\theta_{s1}) \approx \boldsymbol{h}(\theta_{s2})$ and $\beta^*\beta \approx H^2$, then the optimum BS beamformer output power approaches to $\sigma_{s1}^2 + \sigma_{s2}^2 + \frac{1}{H}\sigma_{s1}\sigma_{s2}(\beta^*\rho_{12} + \beta\rho_{12}^*) + \frac{K}{H}\sigma_n^2$, where K is the number of receivers. In this case, the optimum BS beamformer works similar to a conventional BS beamformer.

6.1.3.2 Optimum BS Beamformer Output Power at DOAs of Correlated Signals in Directional Transmission Case

With a similar derivation in Appendix D, for the directional transmission case, the optimum BS beamformer output power at one of the DOAs of coherent signals is given by

$$p_{MVDR-BS}(\theta_{s1}) \approx \sigma_{s1}^2 + \frac{1}{({K_y}^2 - |\beta_d|^2)\sigma_{s2}^2 + K_y K\sigma_n^2}\left(|\rho_{12}|^2\sigma_{s1}^2\sigma_{s2}^2(|\beta_d|^2 - K_y^2) + K\sigma_n^2\left(\frac{|\beta_d|^2\sigma_{s2}^2}{K_y} + \sigma_{s1}\sigma_{s2}(\beta_d^*\rho_{12} + \beta_d\rho_{12}^*)\right)\right) + \frac{K}{K_y}\sigma_n^2 \quad (6\text{-}21)$$

where $k_y(\theta_{s1})$ has been defined in (4-20) and its value is near the constant K_y when θ_{s1} is inside the sector scanned by formed beams; $\beta_d = \boldsymbol{v}_y^H(\theta_{s1})\boldsymbol{v}_y(\theta_{s2})$, which was earlier denoted as $B(\theta_{s1}, \theta_{s2})$ in (4-34). Comparing equations (6-19) and (6-21), the expressions are very similar and lead to the same conclusion, i.e., output SNR can be attenuated by correlation, for example, a weak multipath signal can result in the cancellation of the direct path signal.

An example of the directional transmission BS beamformer output for two fully correlated signals, where $\rho_{12} = j$, i.e., the direct path and reflected signals are 90° out of phase, was considered. A ULA containing 64 elements spaced half of a wavelength apart and 20 Tx/Rx beams were formed scanning over the azimuthal region of 1° to 20° with 1° separation. The returns from two scatterers have SNRs of 10 dB and 6 dB at any single receiver and they were incident from azimuthal angles 8° and 15° respectively. The theoretical output power values of the conventional and MVDR BS beamformers are plotted versus azimuthal angle in Figure 6-2. In this example, the conventional BS beamformer output power is only slightly affected by the coherence. Considering the array aperture size, the two targets were reasonably separated in azimuth, but the output of optimum beamformer can be seriously degraded by the coherence.

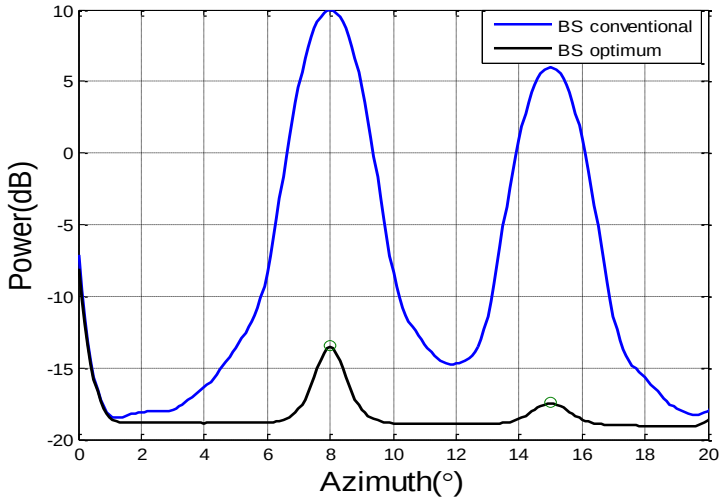

Figure 6-2: An example of outputs of the directional transmission conventional and optimum BS beamformers for a model of two coherent signals. The green circles are the output power calculated using (6-21).

To further quantify the performance of this example, the output SNR of the optimum BS beamformer in direction θ_{s1} =8° is plotted versus the actual SNR of that signal at a single receiver in Figure 6-3. It shows that when the SNR of the signal $s_1(t)$ at θ_{s1} is weaker than the SNR of the signal in the other direction θ_{s2}, i.e., 6 dB, it is almost fully cancelled and the optimum BS beamformer output power at θ_{s1} is approximately $\frac{K}{K_y}\sigma_n^2$; when the SNR of $s_1(t)$ is equal or larger than the SNR of the signal in direction θ_{s2}, the optimum BS beamformer output power is near to a linear function of the SNR of $s_1(t)$, but with a shift (i.e., loss) of about -25 dB.

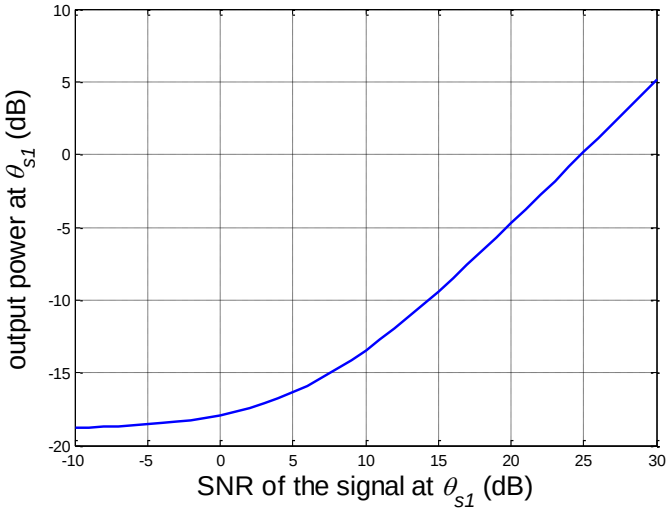

Figure 6-3: Directional transmission optimum BS beamformer output power value at the DOA of the signal ($\theta_{s1} = 8°$) versus different SNR. The SNR of the second signal is 6 dB, DOA = 15° and $\rho_{12} = j$.

The optimum BS beamformer output power is also plotted versus SNR of the other signal in Figure 6-4. It shows that the output at θ_{s1} decreases with an increasing of the SNR of the other signal. When the SNR of the signal from θ_{s2} reaches the same intensity of the signal at $\theta_{s1,}$ i.e., 10 dB, the output curve becomes flatter and the output at θ_{s1} is more than 25 dB lower than the SNR of $s_1(t)$.

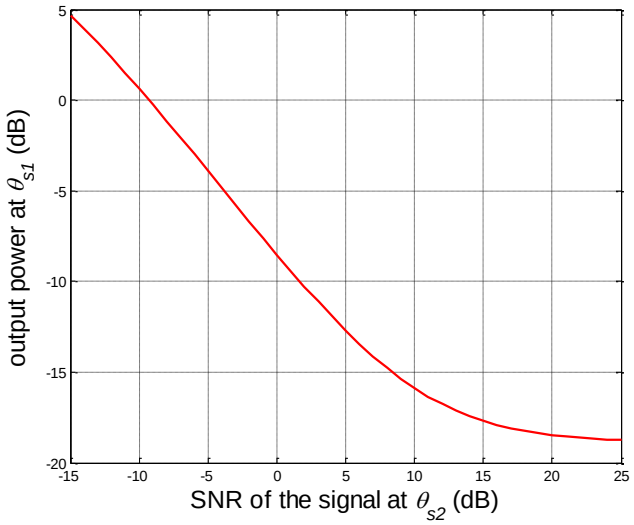

Figure 6-4: Directional transmission optimum BS beamformer output power value at the DOA of the signal ($\theta_{s1} = 8°$) versus the SNR of the other signal whose DOA is 15° and $\rho_{12} = j$.

The optimum BS beamformer output power at θ_{s1} is plotted as a function of amplitude of the correlation coefficient between two signals in Figure 6-5, where $\rho_{12} = \gamma j, 0.1 \leq \gamma \leq 1$. By increasing the value of $|\rho_{12}|$, the optimum BS output at θ_{s1} is attenuated more significantly and falls dramatically when $|\rho_{12}| > 0.9$.

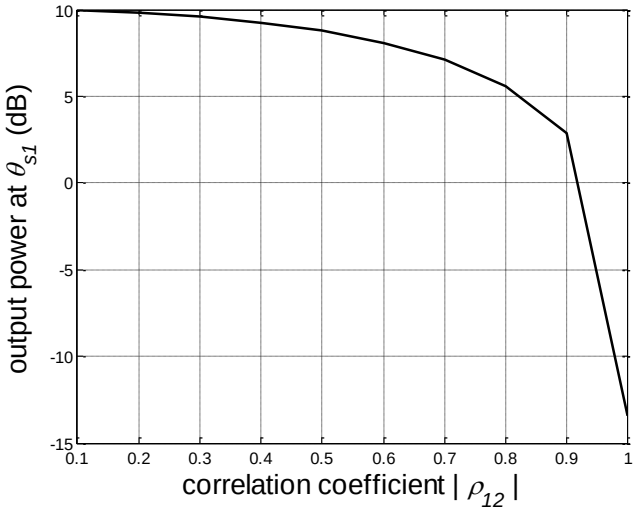

Figure 6-5: Directional transmission BS MVDR beamformer output power value at the DOA of the signal ($\theta_{s1} = 8°$) versus correlation coefficient $\rho_{12} = \gamma j, 0.1 \leq \gamma \leq 1$. The SNR of the signal at $\theta_{s1} = 8°$ is 10 dB and the SNR of the signal at $\theta_{s2} = 15°$ is 6 dB.

6.1.4 Eigen-decomposition of a BS Covariance Matrix for the Case of a Group of Coherent Signals

Subspace methods are based on eigen-decomposition of the covariance matrix to separate the eigenvectors for signal and noise subspaces. When signals are uncorrelated or partially correlated, the source signal covariance matrix is non-singular and its rank depends on the number of signals L and number of beams M and is given by

$$rank(\boldsymbol{R_s}) = \min(L, M). \tag{6-22}$$

All the steering vectors from the DOAs of signals span the signal subspace and are orthogonal to the noise subspace; therefore, the DOAs can be estimated by using subspace methods. Notice that for partially correlated signals, their DOAs can be correctly indicated by the peaks of the MUSIC output, but the values of the peaks are significantly lower than the uncorrelated signals case.

However, when a group of signals are completely coherent, the steering vectors at different DOAs are added with different weights in the receiver outputs and thus form a new generalised vector. Thus, the signal subspace covariance matrix becomes rank deficient. In the omni-directional transmission case, the receiver output vector containing a group of L coherent signals is given by (6-10) and the beam output vector is given by

$$\begin{aligned} \boldsymbol{y}(t) &= \boldsymbol{V}^H \left(\sum_{l=1}^{L} s_l(t)\boldsymbol{v}(\theta_{sl}) + \boldsymbol{n}(t) \right) \\ &= \sum_{l=1}^{L} \rho_l \sigma_{sl} s_0(t) \boldsymbol{V}^H \boldsymbol{v}(\theta_{sl}) + \boldsymbol{V}^H \boldsymbol{n}(t) \\ &= s_0(t) \sum_{l=1}^{L} \rho_l \sigma_{sl} \boldsymbol{h}(\theta_{sl}) + \boldsymbol{V}^H \boldsymbol{n}(t). \end{aligned} \tag{6-23}$$

where $s_0(t)$ is the transmitted unit amplitude narrowband signal. Here a generalised BS steering vector, which contains BS steering vectors of those coherent signals, can be defined as

$$\boldsymbol{h_s} = \sum_{l=1}^{L} \rho_l \sigma_{sl} \boldsymbol{h}(\theta_{sl}), \tag{6-24}$$

and it is easy to verify that the following relationship between the principal eigenvector of the BS covariance matrix, $\boldsymbol{q_{y1}}$, and the generalised BS steering vector, $\boldsymbol{h_s}$, is

$$\boldsymbol{q_{y1}} = \frac{\boldsymbol{h_s}}{\|\boldsymbol{h_s}\|} e^{j\varphi}, \tag{6-25}$$

where $e^{j\varphi}$ is a random phase shift. Thus, the principal eigenvector of $\boldsymbol{R_y}$ is a linear combination of the L coherent signal steering vectors and it can be written as

$$\begin{aligned}\boldsymbol{q}_{\boldsymbol{y}1} &= \rho_1'\boldsymbol{h}(\theta_{s1}) + \rho_2'\boldsymbol{h}(\theta_{s2}) + \cdots + \rho_L'\boldsymbol{h}(\theta_{sL}) \\ &= \boldsymbol{V}^H\left(\rho_1'\boldsymbol{v}(\theta_{s1}) + \rho_2'\boldsymbol{v}(\theta_{s2}) + \cdots + \rho_L'\boldsymbol{v}(\theta_{sL})\right),\end{aligned} \tag{6-26}$$

where $\rho_l' = \frac{\rho_l\sigma_{sl}e^{j\varphi}}{\|\boldsymbol{h}_s\|}$. Provided that $\boldsymbol{V}^H\boldsymbol{V} = \boldsymbol{I}$, the rest of the eigenvalues are given by $\lambda_2 = \lambda_3 = \cdots = \lambda_M = \sigma_n^2$, and the corresponding eigenvectors, $\boldsymbol{q}_{\boldsymbol{y}i}$, $i = 2,3,\cdots M$, span the noise subspace, and the signal subspace being of rank one, which is rank deficient.

Because of their Vandermonde structure, ES steering vectors for a ULA at different angular positions are linearly independent, and the same conclusion is applied to the BS case, i.e., no steering vector in the BS array manifold can be represented as a linear combination of the other BS steering vectors, when $M < K$. Thus the generalised BS steering vector is never coherent with a BS steering vector at any azimuthal angle. Since if $\boldsymbol{h}_s = \rho_{L+1}\boldsymbol{h}(\theta_{L+1})$, then

$$\boldsymbol{V}^H\left(\rho_1'\boldsymbol{v}(\theta_{s1}) + \rho_2'\boldsymbol{v}(\theta_{s2}) + \cdots + \rho_L'\boldsymbol{v}(\theta_{sL}) - \rho_{L+1}'\boldsymbol{v}(\theta_{L+1})\right) = 0 \tag{6-27}$$

As columns of $\boldsymbol{V}$ are linearly independent, the above equation can only be satisfied by

$$\rho_1'\boldsymbol{v}(\theta_{s1}) + \rho_2'\boldsymbol{v}(\theta_{s2}) + \cdots + \rho_L'\boldsymbol{v}(\theta_{sL}) - \rho_{L+1}'\boldsymbol{v}(\theta_{L+1}) = 0, \tag{6-28}$$

and since $\boldsymbol{v}(\theta_l)$ is linearly independent of each other, only ρ_i=0 for $i = 1, 2, \ldots, L+1$.

Hence $\boldsymbol{q}_{\boldsymbol{y}1} = \frac{\boldsymbol{h_s}}{\|\boldsymbol{h_s}\|}e^{j\varphi}$ is a linear combination of the BS steering vectors of the coherent signals, but it is not coherent with any BS steering vector. Thus, it is not able to separate the signal and noise subspaces as that for the model containing independent signals only. Consequently, eigen-decomposition methods, such as MUSIC, fail in DOA estimation, as no sharp output peaks would appear in the array manifold to indicate the DOAs.

6.2 Direction-of-Arrival Estimation for Coherent Signals

The problem of DOA estimation for coherent signals has received considerable attention, and for ES approaches most methods rely on using the outputs from different subarrays to recover the rank loss of the "signal subspace". In these approaches, slight differences between the covariance matrices of different subarrays are exploited to address the rank deficiency problem. For example, the spatial smoothing method [47], [48], [49] or its extensions, such as [77], are used to restore the rank of signal covariance matrix and methods in [50], [51] and [52] form a new Toeplitz matrix whose elements are the correlations among receivers, and the rank is the same as the number of signals.

There are some other methods for estimating the DOAs of coherent signals in the literature, such as utilising different frequencies for wideband signals [58], [59] or relying on a moving array [61], [62]. However, these methods are based on special conditions and not applicable to the most common scenario of narrowband signals incident on a stationary phased array.

To implement the known spatial smoothing methods requires either receiver outputs or the ES covariance matrix. However, in BS processing, when the ES data is not accessible, the standard subarray methods cannot be applied. To the best of author's knowledge, no method in the literature has been proposed to remove the coherence for BS processing. In [63], the authors suggested performing spatial smoothing in ES then further processing in BS, but this method requires the exact ES covariance matrix to be known and is not applicable to the case where only beam data is available.

After reviewing the spatial smoothing method in Section 6.2.1, a technique for reconstructing an ES coherent signal subspace from the omni-directional transmission BS outputs is proposed in Section 6.2.2. In Section 6.2.3, a special matrix which allows the DOAs of the coherent signals to be estimated is proposed, and a method of estimating this matrix from the directional transmission BS data is developed.

6.2.1 Spatial Smoothing

Spatial smoothing methods have been developed to reduce signal correlations and force the signal covariance matrix to be non-singular. Forward spatial smoothing [47] can be summarised as averaging over several subarray covariance matrices, enabling the rank of signal subspace to be increased until it is of full rank. This process removes the coherence between coherent signals and allows the subspace methods to work. The forward spatially smoothed covariance matrix formed by using N subarrays is given by

$$\boldsymbol{R}_{SS} = \frac{1}{N}\sum_{i=1}^{i=N} \boldsymbol{R}_{\boldsymbol{x}}^{(i)}, \tag{6-29}$$

where $\boldsymbol{R}_{\boldsymbol{x}}^{(i)}$ is covariance matrix of the i-th subarray and is given by

$$\boldsymbol{R}_{\boldsymbol{x}}^{(i)} = E\{\boldsymbol{x}^{(i)}\boldsymbol{x}^{(i)H}\}, \tag{6-30}$$

where $\boldsymbol{x}^{(i)}$ is the receiver output vector of the i-th subarray and given by

$$\boldsymbol{x}^{(i)} = [x_i \quad x_{i+1} \quad \dots \quad x_{i+K-N}]^T. \tag{6-31}$$

After spatial smoothing, the forward averaged subarray covariance matrix can be expressed as

$$\boldsymbol{R}_{SS} = \boldsymbol{V}_{\boldsymbol{s}}^{(N)}(\theta_s)\boldsymbol{R}_u^f\boldsymbol{V}_{\boldsymbol{s}}^{(N)H}(\theta_s), \tag{6-32}$$

where $\boldsymbol{V}_{\boldsymbol{s}}^{(N)}(\Theta_s)$ is a matrix containing all the source signal steering vectors but the length of each steering vector is reduced to *K-N+1* and $\boldsymbol{R}_u^f$ is a full rank $L \times L$ matrix. Thus $\boldsymbol{R}_{SS}$ has exactly the same form as the covariance matrix for the case of *L* incoherent signals, and then the subspace methods can be applied to estimate the DOAs regardless of the coherence. A detailed description and analysis of $\boldsymbol{R}_u^f$ and $\boldsymbol{R}_{SS}$ can be found in [49] and [106].

For a group of *L* coherent signals, the minimum number of receivers in each subarray is *L*+1, thus the forward spatial smoothing method requires at least 2*L* receivers in a phased array and the maximal number of estimable signals in a coherent group is $\min(N, K/2)$, more discussion can be found in [47].

To achieve better decorrelation and to reduce the minimum number of receivers to 3/2*L*, the forward/backward spatial smoothing (FBSS) approach [49] forms the subarrays by starting at the opposite ends of the linear array, i.e., the reference receiver order is reversed. The FBSS process can be expressed as

$$\boldsymbol{R}_{FB} = \frac{1}{2N}\left(\sum_{i=1}^{i=N} \boldsymbol{R}_{\boldsymbol{x}}^{(i)} + \sum_{i=1}^{i=N} \boldsymbol{R}_{\boldsymbol{xb}}^{(i)}\right). \tag{6-33}$$

An expression for the *i*-th subarray covariance matrix of the backward spatial smoothing approach is given by

$$\boldsymbol{R}_{\boldsymbol{xb}}^{(i)} = E\left\{\boldsymbol{x}_{\boldsymbol{b}}^{(i)*}\boldsymbol{x}_{\boldsymbol{b}}^{(i)T}\right\}, \tag{6-34}$$

where $\boldsymbol{x}_{\boldsymbol{b}}^{(i)}$ is the receiver output vector of the *i*-th backward subarray and given by

$$\boldsymbol{x}_{\boldsymbol{b}}^{(i)} = [x_{K-i+1} \quad x_{K-i} \quad \cdots \quad x_{N-i+1}]^T. \tag{6-35}$$

The *i*-th backward subarray covariance matrix can be also written as

$$\boldsymbol{R}_{\boldsymbol{xb}}^{(i)} = \boldsymbol{J}\boldsymbol{R}_{\boldsymbol{x}}^{(N-i+1)T}\boldsymbol{J}. \tag{6-36}$$

where $\boldsymbol{J}$ is the exchange matrix, whose components are zero except for ones on the anti-diagonal elements, and is written as

$$\boldsymbol{J} = \begin{bmatrix} \boldsymbol{0} & & & 1 \\ & & \iddots & \\ & 1 & & \\ 1 & & & \boldsymbol{0} \end{bmatrix}. \tag{6-37}$$

A schematic drawing of the forward/backward spatial smoothing algorithm is illustrated in Figure 6-6

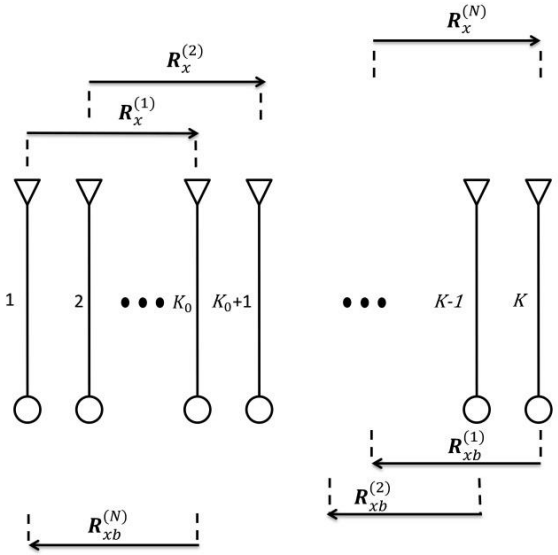

Figure 6-6: The forward/backward spatial smoothing scheme. K_0 is the number of the elements in each subarray.

Utilising the different phase shifts that occur to different incident signals on each of the subarrays, the spatial smoothing approaches recover the rank of the covariance matrix. Then, eigen-structure methods can be successfully implemented to the spatially smoothed covariance matrix at the expense of a lower angular resolution, as the aperture of each subarray is smaller than the original array. The spatial smoothing process reduces the correlation by increasing the number of averages, and the performance of optimum beamformer on the spatially smoothed covariance matrix is different from the case of independent signals; more detailed discussion for this can be found in [104].

Unfortunately, these approaches are not directly applicable to the BS coherent signal problem, since the Vandermonde structure of the ES steering vector is not present in the beam outputs; and usually no data from subarrays is available or can be formed from the beam outputs.

6.2.2 DOA Estimation for Coherent Signals in Omni-directional Transmission BS Case

As discussed in Chapter 3 and given by equation (3-2), the omni-directional transmission BS covariance matrix is a linear transformation of an invariant ES covariance matrix. If the ES covariance matrix can be reconstructed or well approximated by using both the BS covariance matrix and the transformation matrix, $\boldsymbol{V}$, which contains the steering vectors of the preformed beams, then the spatial smoothing approach can be applied to reduce the correlation, and then the DOAs can be estimated by using subspace methods.

When the number of independent beams is equal to the number of receivers, the ES covariance matrix can be exactly recovered by using the expression $\boldsymbol{R_x} = (\boldsymbol{V}^H)^{-1}\boldsymbol{R_y}(\boldsymbol{V})^{-1}$. This expression naturally suggests that when the number of beams is either less or greater than the number of receivers, an approximation for the ES covariance matrix is given by

$$\widetilde{\boldsymbol{R}}_{\boldsymbol{x}} = (\boldsymbol{V}^H)^{+}\boldsymbol{R_y}\boldsymbol{V}^{+}. \tag{6-38}$$

where $()^{+}$ denotes the Moore-Penrose pseudoinverse [98]. When $M > K$ and the rows of $\boldsymbol{V}$ are independent, its pseudo inverse is given by

$$\boldsymbol{V}^{+} = \boldsymbol{V}^H(\boldsymbol{V}\boldsymbol{V}^H)^{-1}. \tag{6-39}$$

and substituting it into (6-38) gives

$$\widetilde{\boldsymbol{R}}_{\boldsymbol{x}} = (\boldsymbol{V}\boldsymbol{V}^H)^{-1}\boldsymbol{V}\boldsymbol{V}^H\boldsymbol{R_x}\boldsymbol{V}\boldsymbol{V}^H(\boldsymbol{V}\boldsymbol{V}^H)^{-1} = \boldsymbol{R_x}. \tag{6-40}$$

Thus again the exact ES covariance matrix can be reconstructed when the number of beams, *M*, is more than the number of receivers, *K*, and the spacing of the beams ensures that there are *K* independent beams or they can be transformed to be independent.

However as most commonly happens in practice, the main interest is the case where the number of independent beams is smaller than the number of elements, and in this case the pseudoinverse matrix of $\boldsymbol{V}$ is given by

$$\boldsymbol{V}^{+} = (\boldsymbol{V}^H\boldsymbol{V})^{-1}\boldsymbol{V}^H. \tag{6-41}$$

In this case, the higher dimensional ES covariance matrix cannot be perfectly reconstructed by applying a linear transformation to the lower dimensional BS covariance matrix. However the dimension of the ES signal subspace is normally lower than the number of beams, especially when the signal subspace contains only a group of fully coherent signals, its dimension is one, and thus it may be possible to reconstruct the ES signal subspace according to the BS signal subspace. As the focus in this section is on the use of eigen-structure techniques for DOA estimation, it is important to ensure the reconstructed ES signal subspace is the same as the signal subspace determined by $\boldsymbol{R}_x$, otherwise, it could fail to find the DOAs of signal or indicate peaks at wrong angles. In the following Section 6.2.2.1 to 6.2.2.5, the process of ES signal subspace reconstruction from omni-directional transmission BS data is derived and investigated and the performance of DOA estimation based on the reconstructed ES covariance matrix is analysed.

6.2.2.1 Relationship between Omni-directional Transmission BS and ES Noise Subspaces

First consider an ES covariance matrix, $\boldsymbol{R_x}$, containing L_c ($Lc \geq 1$) groups of coherent signals and a BS covariance matrix $\boldsymbol{R_y}$, formed using M mutually orthogonal beams, i.e., $\boldsymbol{V^H V = I}$. As shown in [27] and Appendix A, the following relationship between the ES and BS noise subspace exists:

$$\boldsymbol{q}_i = \boldsymbol{V q_{yi}}, (i = Lc + 1, \cdots M), \tag{6-42}$$

where $\boldsymbol{q}_i$ and $\boldsymbol{q_{yi}}$ are the noise eigenvectors of $\boldsymbol{R_x}$ and $\boldsymbol{R_y}$ respectively. In other words, $\boldsymbol{V q_{yi}}$ $(Lc < i \leq M)$ is a noise eigenvector of $\boldsymbol{R_x}$, and the set of these vectors of $\boldsymbol{V q_{yi}}, (Lc < i \leq M)$ is a subset of the noise subspace of $\boldsymbol{R_x}$.

When $\boldsymbol{V^H V \neq I}$, the SFS method can be used to generate beams that are mutually orthogonal, where the corresponding transformation matrix and BS covariance matrix are given by (3-20) and (3-21), and the generalised SFS coherent BS steering vector is given by

$$\boldsymbol{h}'(\theta) = (\boldsymbol{V^H V})^{-\frac{1}{2}} \boldsymbol{h}(\theta). \tag{6-43}$$

6.2.2.2 Reconstruction of ES Coherent Signal Subspace from BS Covariance Matrix

The scenario in this section is restricted to a group of fully coherent signals incident on a ULA, where $|\rho_l| = 1, (1 \leq l \leq L)$ and $\text{rank}(\boldsymbol{R_s}) = 1$. In this case, a generalised steering vector in ES is a linear combination of steering vectors of the coherent signals and is denoted as

$$\boldsymbol{v_s} = \sum_{l=1}^{L} \rho_l \sigma_{sl} \boldsymbol{v}(\theta_{sl}). \tag{6-44}$$

The eigen-decomposition of the ES covariance matrix can be expressed as

$$\boldsymbol{R_x} = \lambda_1 \boldsymbol{q}_1 \boldsymbol{q}_1^H + \sum_{i=2}^{K} \lambda_i \boldsymbol{q}_i \boldsymbol{q}_i^H, \tag{6-45}$$

where $\lambda_1 = \sigma_s^2 + \sigma_n^2$, $\lambda_i = \sigma_n^2$ $(2 \leq i \leq K)$ and $\boldsymbol{q}_1 = \frac{e^{i\varphi}}{\|\boldsymbol{v_s}\|} \boldsymbol{v_s}$, where σ_s^2 is the combined power of the coherent signals and is given by $\sigma_s^2 = \|\boldsymbol{v_s}\|^2$. The above equation can be rewritten as

$$\boldsymbol{R_x} = \frac{\sigma_s^2 + \sigma_n^2}{\|\boldsymbol{v_s}\|^2} \boldsymbol{v_s} \boldsymbol{v_s}^H + \sum_{i=2}^{M} \sigma_n^2 \boldsymbol{q}_i \boldsymbol{q}_i^H + \sum_{i=M+1}^{K} \sigma_n^2 \boldsymbol{q}_i \boldsymbol{q}_i^H. \tag{6-46}$$

When $\boldsymbol{V}^H\boldsymbol{V} = \boldsymbol{I}$, the M-1 noise eigenvectors of the middle term in (6-46) satisfy the equation

$$\boldsymbol{q}_i = \boldsymbol{V}\boldsymbol{q}_{\boldsymbol{y}i},\ 2 \le i \le M. \tag{6-47}$$

For the omni-directional transmission case, the generalised coherent steering vector in BS is denoted as $\boldsymbol{h}_{\boldsymbol{s}}$ and is given by

$$\boldsymbol{h}_{\boldsymbol{s}} = \boldsymbol{V}^H\boldsymbol{v}_{\boldsymbol{s}} = \sum_{l=1}^{L} \rho_l \sigma_{sl} \boldsymbol{h}(\theta_{sl}). \tag{6-48}$$

The BS covariance matrix can be written as

$$\begin{aligned} \boldsymbol{R}_{\boldsymbol{y}} &= \boldsymbol{V}^H\boldsymbol{R}_{\boldsymbol{x}}\boldsymbol{V} \\ &= \boldsymbol{V}^H\boldsymbol{v}_{\boldsymbol{s}}\boldsymbol{v}_{\boldsymbol{s}}^H\boldsymbol{V} + \sigma_n^2\boldsymbol{I} \\ &= \boldsymbol{h}_{\boldsymbol{s}}\boldsymbol{h}_{\boldsymbol{s}}^H + \sigma_n^2\boldsymbol{I} \end{aligned} \tag{6-49}$$

The eigen-decomposition of the BS covariance matrix is expressed as

$$\begin{gathered} \boldsymbol{R}_{\boldsymbol{y}} = \sum_{i=1}^{M} \lambda_{yi}\boldsymbol{q}_{\boldsymbol{y}i}\boldsymbol{q}_{\boldsymbol{y}i}^H, \\ \lambda_{y1} = \frac{\|\boldsymbol{h}_{\boldsymbol{s}}\|^2}{\|\boldsymbol{v}_{\boldsymbol{s}}\|^2}\sigma_s^2 + \sigma_n^2 > \sigma_n^2, \lambda_{yi} = \sigma_n^2, (i \ge 2). \end{gathered} \tag{6-50}$$

Also, according to (6-25), for a group of coherent signals, the generalised BS coherent signal steering vector $\boldsymbol{h}_{\boldsymbol{s}}$ is proportional to the principal eigenvector of $\boldsymbol{R}_{\boldsymbol{y}}$, $\boldsymbol{q}_{\boldsymbol{y}1}$, and can be written as

$$\boldsymbol{h}_{\boldsymbol{s}} = e^{-j\varphi}\|\boldsymbol{h}_{\boldsymbol{s}}\|\boldsymbol{q}_{\boldsymbol{y}1}, \tag{6-51}$$

where $e^{-j\varphi}$ is a random phase. As the eigenvectors are mutually orthogonal, thus

$$\boldsymbol{q}_{\boldsymbol{y}i}^H\boldsymbol{h}_{\boldsymbol{s}} = 0, 2 \le i \le M. \tag{6-52}$$

In Appendix A, it is shown that the vector $\boldsymbol{V}\boldsymbol{q}_{\boldsymbol{y}1}$ would be coherent with the generalised ES coherent signal steering vector $\boldsymbol{v}_{\boldsymbol{s}}$, only if the value of $\frac{\|\boldsymbol{h}_{\boldsymbol{s}}\|^2}{\|\boldsymbol{v}_{\boldsymbol{s}}\|^2}$ equals one. The value of $\frac{\|\boldsymbol{h}_{\boldsymbol{s}}\|^2}{\|\boldsymbol{v}_{\boldsymbol{s}}\|^2}$ varies when the number of beams changes. Consider an example of two coherent signals at DOAs of 8.23° and 9.44°, SNR=10 dB and 5 dB respectively, correlation ρ=e^i, and beams evenly separated in angle in a sector from 1° to 20°. The value of $\frac{\|\boldsymbol{h}_{\boldsymbol{s}}\|^2}{\|\boldsymbol{v}_{\boldsymbol{s}}\|^2}$ versus the number of beams is shown in Figure 6-7.

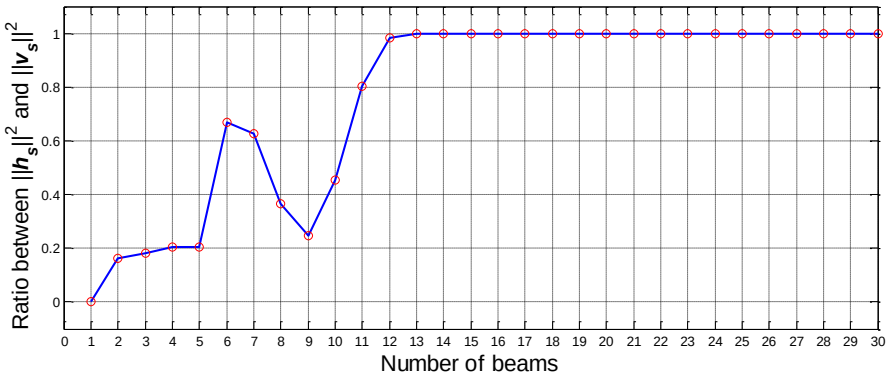

Figure 6-7: The value of $\frac{\|\boldsymbol{h_s}\|^2}{\|\boldsymbol{v_s}\|^2}$ versus the number of beams in a sector of interest.

It indicates the value of $\frac{\|\boldsymbol{h_s}\|^2}{\|\boldsymbol{v_s}\|^2}$ converges to one when the number of beams is larger than 12, in which case the spacing between the beams centres is less than half a beamwidth.

When $\frac{\|\boldsymbol{h_s}\|^2}{\|\boldsymbol{v_s}\|^2} = 1$, it is shown in Appendix A that

$$\sigma_n^2 \sum_{i=M+1}^{K} \boldsymbol{V}\boldsymbol{V}^H \boldsymbol{q}_i \boldsymbol{q}_i^H \boldsymbol{V}\boldsymbol{V}^H = 0. \tag{6-53}$$

Since $\sigma_n^2 > 0$ and $\boldsymbol{V}\boldsymbol{V}^H \boldsymbol{q}_i \boldsymbol{q}_i^H \boldsymbol{V}\boldsymbol{V}^H \geq 0$, hence,

$$\boldsymbol{q}_{M+1}^H \boldsymbol{V}\boldsymbol{V}^H = \boldsymbol{q}_{M+2}^H \boldsymbol{V}\boldsymbol{V}^H = \cdots = \boldsymbol{q}_K^H \boldsymbol{V}\boldsymbol{V}^H = 0, (M < i \leq K), \tag{6-54}$$

Substituting (6-46) and (6-47) into $\boldsymbol{R_x} \frac{\boldsymbol{V}\boldsymbol{h_s}}{\|\boldsymbol{h_s}\|^2}$, gives

$$\begin{aligned} \boldsymbol{R_x} \frac{\boldsymbol{V}\boldsymbol{h_s}}{\|\boldsymbol{h_s}\|^2} &= \left(\frac{\sigma_s^2 + \sigma_n^2}{\|\boldsymbol{v_s}\|^2} \boldsymbol{v_s}\boldsymbol{v_s}^H + \sum_{i=2}^{M} \sigma_n^2 \boldsymbol{q}_i \boldsymbol{q}_i^H + \sum_{i=M+1}^{K} \sigma_n^2 \boldsymbol{q}_i \boldsymbol{q}_i^H \right) \frac{\boldsymbol{V}\boldsymbol{h_s}}{\|\boldsymbol{h_s}\|^2} \\ &= \frac{\sigma_s^2 + \sigma_n^2}{\|\boldsymbol{v_s}\|^2} \boldsymbol{v_s} \frac{\boldsymbol{v_s}^H \boldsymbol{V}\boldsymbol{h_s}}{\|\boldsymbol{h_s}\|^2} + \sum_{i=2}^{M} \sigma_n^2 \boldsymbol{V}\boldsymbol{q}_{yi} \boldsymbol{q}_{yi}^H \boldsymbol{V}^H \boldsymbol{V} \frac{\boldsymbol{h_s}}{\|\boldsymbol{h_s}\|^2} + \sum_{i=M+1}^{K} \sigma_n^2 \boldsymbol{q}_i \boldsymbol{q}_i^H \boldsymbol{V}\boldsymbol{V}^H \frac{\boldsymbol{v_s}}{\|\boldsymbol{h_s}\|^2}. \end{aligned} \tag{6-55}$$

Substituting $\boldsymbol{V}^H\boldsymbol{V} = \boldsymbol{I}$, (6-52) and (6-54) into (6-55), then

$$\begin{aligned} \boldsymbol{R_x} \frac{\boldsymbol{V}\boldsymbol{h_s}}{\|\boldsymbol{h_s}\|^2} &= \frac{\sigma_s^2 + \sigma_n^2}{\|\boldsymbol{v_s}\|^2} \boldsymbol{v_s} \frac{\boldsymbol{h_s}^H \boldsymbol{h_s}}{\|\boldsymbol{h_s}\|^2} + 0 + 0 \\ &= \frac{\sigma_s^2 + \sigma_n^2}{\|\boldsymbol{v_s}\|^2} \boldsymbol{v_s}. \end{aligned} \tag{6-56}$$

As $\boldsymbol{R_x v_s} = (\sigma_s^2 + \sigma_n^2)\boldsymbol{v_s}$, thus $\boldsymbol{R_x v_s} = \|\boldsymbol{v_s}\|^2 \boldsymbol{R_x} \frac{\boldsymbol{V h_s}}{\|\boldsymbol{h_s}\|^2}$, because $\boldsymbol{R_x}$ is a full rank and invertible matrix, hence

$$\boldsymbol{v_s} = \frac{\|\boldsymbol{v_s}\|^2}{\|\boldsymbol{h_s}\|^2} \boldsymbol{V h_s}, \tag{6-57}$$

and by substituting (6-51),

$$\boldsymbol{v_s} = \frac{\|\boldsymbol{v_s}\|^2}{\|\boldsymbol{h_s}\|} \boldsymbol{V q_{y1}} e^{-j\varphi}. \tag{6-58}$$

For the case that the formed beams are not mutually orthogonal, the SFS method can be applied, then the corresponding SFS BS transformation matrix and the generalised coherent SFS BS steering vector are given by

$$\begin{aligned} \boldsymbol{V'} &= \boldsymbol{V}(\boldsymbol{V}^H \boldsymbol{V})^{-\frac{1}{2}} \\ \boldsymbol{h_s'} &= \boldsymbol{V}(\boldsymbol{V}^H \boldsymbol{V})^{-\frac{1}{2}} \boldsymbol{h_s}, \end{aligned} \tag{6-59}$$

and the reconstructed ES generalised coherent signal steering vector is given by

$$\begin{aligned} \boldsymbol{v_s} &= \frac{\|\boldsymbol{v_s}\|^2}{\|\boldsymbol{h_s'}\|^2} \boldsymbol{V'} \boldsymbol{h_s'} \\ &= \frac{\|\boldsymbol{v_s}\|^2 \boldsymbol{V}(\boldsymbol{V}^H \boldsymbol{V})^{-\frac{1}{2}} (\boldsymbol{V}^H \boldsymbol{V})^{-\frac{1}{2}} \boldsymbol{h_s}}{\left\| \boldsymbol{h_s}^H (\boldsymbol{V}^H \boldsymbol{V})^{-\frac{1}{2}} \boldsymbol{V}^H \boldsymbol{V} (\boldsymbol{V}^H \boldsymbol{V})^{-\frac{1}{2}} \boldsymbol{h_s} \right\|^2} \\ &= \frac{\|\boldsymbol{v_s}\|^2}{\|\boldsymbol{h_s}\|^2} \boldsymbol{V}(\boldsymbol{V}^H \boldsymbol{V})^{-1} \boldsymbol{h_s} \\ &= \frac{\|\boldsymbol{v_s}\|^2}{\|\boldsymbol{h_s}\|} \boldsymbol{V}(\boldsymbol{V}^H \boldsymbol{V})^{-1} \boldsymbol{q_{y1}} e^{-j\varphi}. \end{aligned} \tag{6-60}$$

Notice that the phase factor $e^{-j\varphi}$ and the scalar $\frac{\|\boldsymbol{v_s}\|^2}{\|\boldsymbol{h_s}\|}$ are unknown, but they do not affect separating the signal and noise subspaces and the result of DOA estimation. Thus they can be ignored without loss of generality and a vector $\tilde{\boldsymbol{v}}_{\boldsymbol{s}}$, which is coherent with the ES generalised coherent signal steering vector $\boldsymbol{v_s}$, can be reconstructed or approximated as

$$\begin{aligned} \tilde{\boldsymbol{v}}_{\boldsymbol{s}} &= \boldsymbol{V q_{y1}}, \text{ (for mutually orthogonal beams)} \\ \tilde{\boldsymbol{v}}_{\boldsymbol{s}} &= \boldsymbol{V}(\boldsymbol{V}^H \boldsymbol{V})^{-1} \boldsymbol{q_{y1}}. \text{ (for non-orthogonal beams)} \end{aligned} \tag{6-61}$$

Using the same example in Figure 6-7 , the absolute value of the correlation coefficient between $\tilde{\boldsymbol{v}}_{\boldsymbol{s}}$ and $\boldsymbol{v_s}$ (or $\boldsymbol{q}_1$) is shown in Figure 6-8. It proves that with a sufficient number of beams, the 1-D signal subspace of the reconstructed ES covariance matrix is identical to that of the original ES covariance matrix.

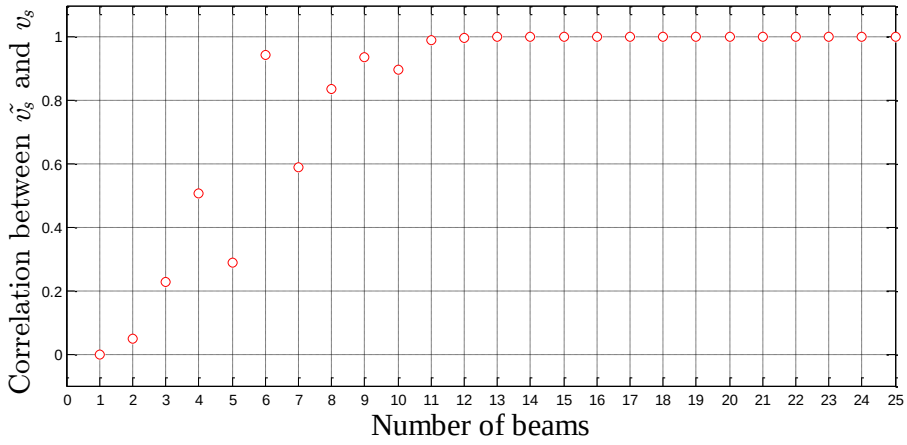

Figure 6-8: The absolute value of the correlation coefficient between $\tilde{\boldsymbol{v}}_s$ and $\boldsymbol{v}_s$ versus number of beams in the sector of interest.

In summary, an ES generalised coherent steering vector can be estimated from the principal eigenvector of the omni-directional transmission BS covariance matrix. In terms of covariance, a matrix containing the generalised coherent signal steering vector can be reconstructed as

$$\begin{aligned}\tilde{\boldsymbol{R}}'_{\boldsymbol{x}} &= \tilde{\boldsymbol{R}}_{\boldsymbol{xc}} + \tilde{\boldsymbol{R}}_{\boldsymbol{n}} \\ &= \tilde{\sigma}_s^2 \tilde{\boldsymbol{v}}_{\boldsymbol{s}} \tilde{\boldsymbol{v}}_{\boldsymbol{s}}^H + \tilde{\sigma}_n^2 \boldsymbol{I}.\end{aligned} \tag{6-62}$$

For mutually orthogonal beams, the above equation can be written as

$$\tilde{\boldsymbol{R}}'_{\boldsymbol{x}} = \tilde{\sigma}_s^2 \boldsymbol{V} \boldsymbol{q}_{\boldsymbol{y1}} \boldsymbol{q}_{\boldsymbol{y1}}^H \boldsymbol{V}^H + \tilde{\sigma}_n^2 \boldsymbol{I}. \tag{6-63}$$

Note that for both cases considered in (6-61), the reconstructed ES signal subspace is obtained by multiplying the Moore-Penrose pseudoinverse of the BS transformation matrix to the BS signal subspace. An ES noise subspace could also be constructed in a similar manner but an alternative approach is adopted here. This approach is based on one assumption and one property of MUSIC DOA estimation algorithm. The assumption is that the noise output of receiver elements is spatially white, i.e., uncorrelated between receivers and so the reconstructed ES noise covariance matrix can be assumed to be a $K \times K$ diagonal matrix. The used property is that for MUSIC the only way noise power affects the algorithm is in setting the threshold for determining the dimension of the signal subspace, i.e., the number of signals. Thus for DOA estimation using the subspace method, the exact signal and noise power values $\tilde{\sigma}_s^2$ and $\tilde{\sigma}_n^2$ are not required, as they will not affect the result of DOA estimation. Therefore, the choice of $\tilde{\sigma}_s^2$ and $\tilde{\sigma}_n^2$ is quite arbitrary, but in order to show the DOAs as very sharp peaks in the output of eigen-structure methods, $\tilde{\sigma}_s^2 > \tilde{\sigma}_n^2$ can be used.

Then the spatial smoothing and the subspace algorithms can be applied to $\tilde{\boldsymbol{R}}'_{\boldsymbol{x}}$ to estimate the DOAs of the coherent signals, the process is the same as the details described in Section 6.2.1 and [49].

6.2.2.3 An Example of Applying Spatial Smoothing and MUSIC to Estimated ES Covariance Matrix

The example in Figure 6-7 was used again, i.e., two coherent signals are incident on the array in directions of 8.23° and 9.44°(two random but closely spaced angles), with SNRs equal to 10 dB and 5 dB at any single receiver respectively, and the correlation coefficient between the two signals $\rho = e^{i}$. The array has 64 receivers, $d = 0.5\lambda$, with a variable number (10, 14 and 20) of equally spaced beams in a sector of [1°, 20°]. The BS covariance matrix was modelled as (6-12), by applying the SFS transformation, the reconstructed ES generalised coherent signal steering vector and covariance matrix are given by (6-61) and (6-62) respectively, where $\tilde{\sigma}_s = 1$ and $\tilde{\sigma}_n = 0.1$. Then, forward spatial smoothing was applied to $\widetilde{\boldsymbol{R}}_{\boldsymbol{x}}'$ with one average and ES MUSIC algorithm was then applied. The outputs of MUSIC for using different numbers of beams are shown in Figure 6-9, where the true DOAs are plotted as magenta spots. It shows that DOA estimation is very difficult using a small number of beams whose separation is larger than half of 3 dB beamwidth, whilst the MUSIC output peaks appear at the correct DOAs with increasing the number of beams and become sharp peaks when a sufficient number of beams are used.

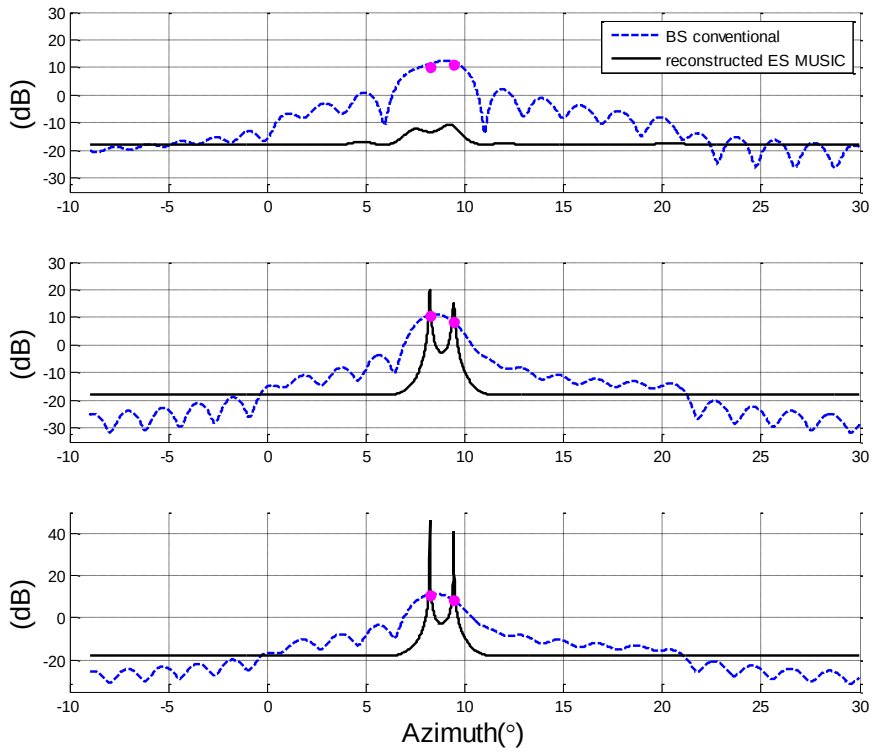

Figure 6-9: An example of applying spatial smoothing and MUSIC algorithms to a reconstructed ES covariance matrix of a model containing two coherent signals. The numbers of beams are 10, 14 and 20 respectively.

The same scenario with 20 beams at 1° separation was simulated and 1024 independent samples were generated for each beam. After reconstructing the ES covariance matrix $\widetilde{\boldsymbol{R}}_{\boldsymbol{x}}'$

and applying forward spatial smoothing with one average, the output of MUSIC versus azimuthal angle is plotted in Figure 6-10. Similar to the theoretical numerical analysis, the DOAs of coherent signals can be estimated accurately but the output peaks are not as sharp as the theoretical analysis due to the high sensitivity of MUSIC algorithm. The output of the BS conventional beamformer and MUSIC are also plotted for comparison. Neither the conventional beamformer nor the BS MUSIC approaches can separate the two DOAs and the output values of the latter one are very small.

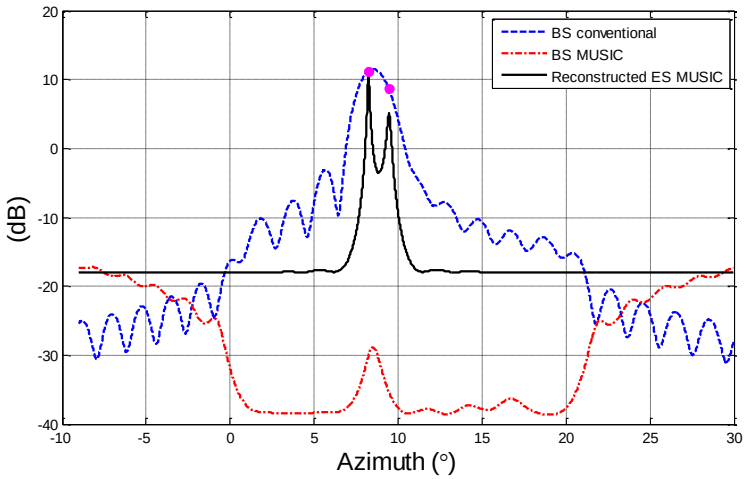

Figure 6-10: A simulation example of applying spatial smoothing and MUSIC algorithms to the reconstructed ES covariance matrix containing two coherent signals. 20 beams at 1° separation and 1024 samples were simulated for each beam.

6.2.2.4 DOA Estimation of a Mixture of Uncorrelated and Coherent Signals

When a mixture of incoherent (uncorrelated and partially correlated) and a group of coherent (fully correlated) signals are incident on a ULA, the BS covariance matrix can be written as

$$\begin{aligned} \boldsymbol{R_y} &= \boldsymbol{V}^H \boldsymbol{R_x} \boldsymbol{V} \\ &= \boldsymbol{H}(\Theta_s)\boldsymbol{R_{sc}}\boldsymbol{H}^H(\Theta_s) + \boldsymbol{H}(\Theta_{su})\boldsymbol{R_{su}}\boldsymbol{H}^H(\Theta_{su}) + \boldsymbol{V}^H\boldsymbol{V}\sigma_n^2, \end{aligned} \tag{6-64}$$

where Θ_{sc} is the set of DOAs of the coherent signals, Θ_{su} is the set of DOAs of the uncorrelated signals; $\boldsymbol{R_{sc}}$ and $\boldsymbol{R_{su}}$ denote the for coherent and incoherent source signals covariance matrices respectively; $\boldsymbol{H}(\Theta_s)$ and $\boldsymbol{H}(\Theta_{su})$ are two matrices containing the steering vectors of coherent and incoherent signals respectively. The coherent signal part in $\boldsymbol{R_y}$, $\boldsymbol{H}(\Theta_s)\boldsymbol{R_{sc}}\boldsymbol{H}^H(\Theta_s)$, can be denoted as $\boldsymbol{h_{sc}}\boldsymbol{h_{sc}^H}$, where $\boldsymbol{h_{sc}}$ is the generalised BS coherent signal steering vector. Notice $\boldsymbol{h_{sc}}$ is the same as $\boldsymbol{h_s}$ here, but this problem can be extended to multiple groups of coherent signals, so a new variable is used here. Also, only the uncorrelated signals and fully coherent signals are considered, whilst the low partially correlated signals can be treated as the uncorrelated case in DOA estimation and the highly correlated signals are similar to the coherent case.

The BS signal subspace is spanned by the generalised BS coherent steering vector and the uncorrelated signal steering vectors as following equation

$$\boldsymbol{R_{ys}} = span\{\, \boldsymbol{h_{sc}} \quad \boldsymbol{H}(\Theta_{su})\}. \tag{6-65}$$

A similar problem in ES processing has been discussed in the literature, such as [74], [75]. The basic idea is to separate the coherent and uncorrelated signal subspaces and to process each one separately. Here this idea is extended to the BS processing case, and the developed approach of reconstructing the ES signal subspace is implemented. The first step is to estimate the DOAs of the uncorrelated signals. For example, strong peaks at Θ_{su}—the DOAs of the uncorrelated signals can be found in the output of BS MUSIC. Then oblique projection is used to extract the generalised BS coherent signal steering vector, $\boldsymbol{h_{sc}}$, more specifically, the principal eigenvector of the BS coherent signal covariance matrix, $\boldsymbol{q_{yc1}}$, whilst nulling the uncorrelated signal steering vectors $\boldsymbol{H}(\Theta_{su})$; then $\tilde{\boldsymbol{v}}_{\boldsymbol{s}}$ can be estimated according to (6-61). Finally, the spatial smoothing approach can be applied to recover the rank of the coherent signal subspace and the DOAs of the coherent signals can be estimated by using ES subspace approaches. A flow diagram of the procedure of DOA estimation for a mixture of uncorrelated signals and a group of coherent signals is shown in Figure 6-11.

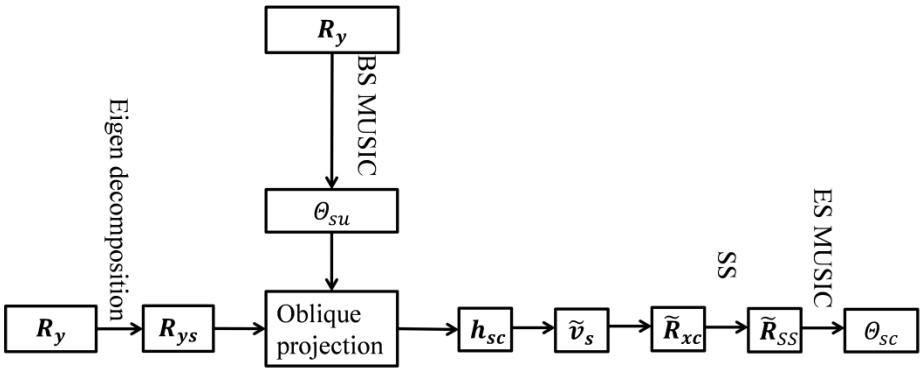

Figure 6-11: The flow diagram for estimating DOAs of a mixture of coherent and uncorrelated signals.

In the process of extracting the coherent signal subspace, as shown in equation (5-22), the oblique projection requires both $\boldsymbol{H}(\Theta_{su})$ and $\boldsymbol{h_{sc}}$. Θ_{su} can be easily obtained by using subspace methods, but obviously $\boldsymbol{h_{sc}}$ is unknown, thus the oblique projection is not able to be applied directly. As being proved in [74], the power values of the uncorrelated signals can be estimated accurately and by extending the result for ES case in [74] to the BS problem, the coherent signal subspace can be estimated as

$$\boldsymbol{h}^H(\Theta_{sc})\boldsymbol{R_{sc}}\boldsymbol{h}(\Theta_{sc}) = \boldsymbol{R_{ys}} - \boldsymbol{H}(\Theta_{su})\left(\boldsymbol{H}^H(\Theta_{su})\boldsymbol{R}_{\boldsymbol{ys}}^{+}\,\boldsymbol{H}(\Theta_{su})\right)^{-1}\boldsymbol{H}^H(\Theta_{su}), \tag{6-66}$$

where the signal subspace $\boldsymbol{R_{ys}}$ can be estimated by

$$\boldsymbol{R_{ys}} = \boldsymbol{R_y} - \boldsymbol{V}^H\boldsymbol{V}\sigma_n^2. \tag{6-67}$$

The above method was applied to an example containing uncorrelated signals and two coherent signals and the result is shown here. Two uncorrelated signals with DOAs of 5.3° and 10.67°, both with the same SNR of 10 dB at any single receiver were added into the previous example used in Figure 6-9 and Figure 6-10, whilst 20 beams in a sector of [1°, 20°] with 1° separation were formed. The eigen-spectrum of $\boldsymbol{R}_{\boldsymbol{y}}$ is plotted in Figure 6-12. Only three large eigenvalues appear and their corresponding eigenvectors span the signal subspace.

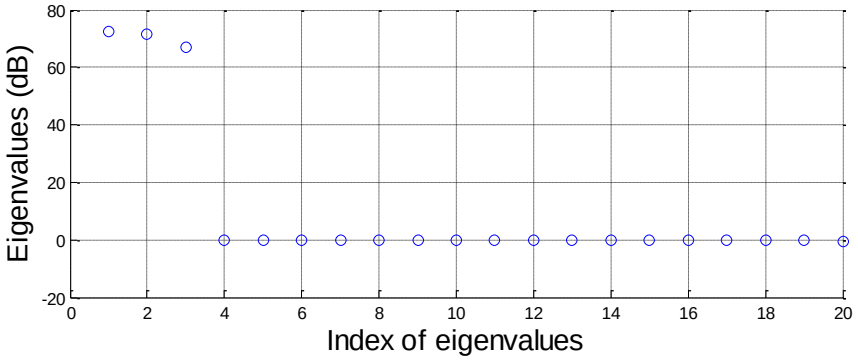

Figure 6-12: An example of eigenvalues of BS covariance matrix mixed with two coherent signals and two uncorrelated signals.

BS conventional beamformer and MUSIC outputs versus azimuthal angle are showed in Figure 6-13 and it shows that the coherent signals do not affect the DOA estimation for the uncorrelated signals.

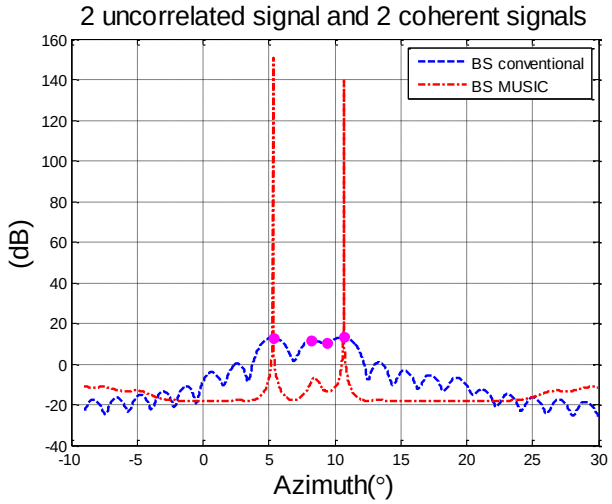

Figure 6-13: An example of BS conventional beamforming and MUSIC outputs for two coherent signals and two uncorrelated signals.

To null the BS uncorrelated signal component but keep the coherent signal component unchanged, the formula (6-66) and (6-67) were used, where the noise power was estimated according to the small eigenvalues in Figure 6-12. After extracting the coherent signal subspace, the process of reconstructing the ES coherent signal subspace

as described in Section 6.2.2.2, spatial smoothing and ES subspace techniques were carried out and the result is shown in Figure 6-14. It shows that the DOAs of coherent signals can be estimated accurately and together with the previous estimated DOAs of the uncorrelated signals, the result of DOA estimation is satisfactory.

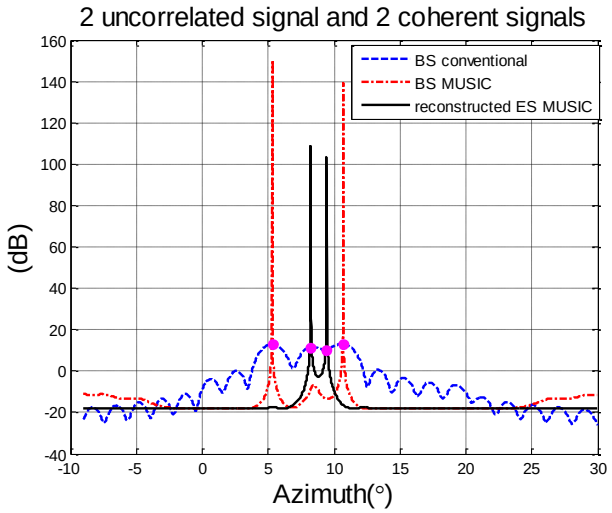

Figure 6-14: An example of DOA estimation for a mixture of uncorrelated and coherent signals. The DOAs of two uncorrelated signals are estimated using BS MUSIC and the DOAs of two coherent signals are estimated by ES MUSIC with applying spatial smoothing to the reconstructed ES covariance matrix.

In some cases, the received signals can be a mixture of several groups of coherent signals but uncorrelated among those groups. Similar to the scenario containing one group of coherent signals, the same algorithm can be used whilst more generalised coherent signal steering vectors or corresponding eigenvectors are used together. An example of such a problem in BS processing is shown in Appendix E.

6.2.2.5 The Number of Coherent Signals

To focus on subspace methods, it is common to assume the number of signals is known in advance, such as those examples in Section 6.2.2.3 and 6.2.2.4. However, this information is not always available in practice and needs to be estimated in advance. When the estimated number of signals is different from the actual number, the chosen signal subspace would have the wrong dimensions and signals could either be missed or false peaks may appear in the output. The common methods for estimating the number of independent source signals such as Akaike information criterion (AIC) and minimum description length (MDL) would not work for the case of coherent signals and need some modification such as [73]. Other methods, such as [64] and [65], have been suggested to estimate the number of coherent signals, and they carry out the MDL process after each spatial smoothing then compare the results of the MDL with increasing the number of subarrays used for spatial smoothing to decide the number of signals.

6.2.3 DOA Estimation for Coherent Signals in Directional Transmission BS Case

As shown in Chapter 4, the directional transmission BS model is different from the omni-directional transmission case; the ES covariance matrices are different for each transmit beam and the BS covariance matrix is a linear transformation of the stacked ES covariance matrix, which is given by equation (4-25). Due to the way that the different beam patterns of transmitted beams affect the ES covariance matrices, even if the number of beams exactly equals the number of receivers, it is difficult to reconstruct the ES covariance matrix. In this section, a new expression of coherent signals for the directional transmission BS case is investigated.

6.2.3.1 Spatial Decorrelation of Directional Transmission Coherent Signals in ES

First consider the problem of estimating DOAs of coherent signals in the directional transmission ES case. When receiver outputs are available, the coherence between the signals can be removed by applying a spatial smoothing approach to the ES covariance matrix for each transmit beam. In this way, coherence can be removed but some signals whose DOAs occur at nulls in the beam pattern of a particular beam would not be detected. To overcome this limitation, the results of different beams can be merged to find all the DOAs.

For the directional transmission case, as the beam pattern changes for each transmit beam, both the phase and amplitude of a signal transmitted into a certain direction vary for each beam. The average of the ES covariance matrices for all M beams is given by

$$\begin{aligned}\bar{\boldsymbol{R}}_{\boldsymbol{x}} &= \frac{1}{M}\sum_{m=1}^{M}\boldsymbol{R}_{\boldsymbol{x}}(\theta_m) \\ &= \frac{1}{M}\sum_{m=1}^{M}\boldsymbol{V}_{\boldsymbol{s}}(\Theta_s)\boldsymbol{R}'_{\boldsymbol{s}}(\theta_m)\boldsymbol{V}_{\boldsymbol{s}}^{H}(\Theta_s)+\sigma_n^2\boldsymbol{I},\end{aligned} \tag{6-68}$$

where the source signal covariance matrix weighted by the beam patterns of the m-th transmission beam is denoted as $\boldsymbol{R}'_{\boldsymbol{s}}(\theta_m)$ and given by

$$\boldsymbol{R}'_{\boldsymbol{s}}(\theta_m) = \begin{bmatrix} bp_1(\theta_m)bp_1^*(\theta_m)\sigma_{s1}^2 & \rho_{12}bp_1(\theta_m)bp_2^*(\theta_m)\sigma_{s1}\sigma_{s2} & \cdots & \rho_{1L}bp_1(\theta_m)bp_L^*(\theta_m)\sigma_{s1}\sigma_{sL} \\ \rho_{12}^*bp_2(\theta_m)bp_1^*(\theta_m)\sigma_{s1}\sigma_{s2} & bp_2(\theta_m)bp_2^*(\theta_m)\sigma_{s2}^2 & \cdots & \rho_{2L}bp_2(\theta_m)bp_L^*(\theta_m)\sigma_{s2}\sigma_{sL} \\ \vdots & \vdots & \ddots & \vdots \\ \rho_{1L}^*bp_L(\theta_m)wb_1^*(\theta_m)\sigma_{s1}\sigma_{s2} & \rho_{2L}^*bp_L(\theta_m)bp_2^*(\theta_m)\sigma_{s1}\sigma_{s2} & \cdots & bp_L(\theta_m)bp_L^*(\theta_m)\sigma_{sL}^2 \end{bmatrix}, \tag{6-69}$$

where $bp_l(\theta_m)$ is the un-normalised beam pattern of the m-th transmitted beam in the

direction of the *l*-th signal and is given by

$$bp_l(\theta_m) = \boldsymbol{v}^H(\theta_m)\boldsymbol{v}(\theta_{sl}). \tag{6-70}$$

As $bp_l(\theta_m)$ varies at each beam, it adds different weights to each correlation coefficient and $\boldsymbol{R}_s'(\theta_m)$ changes at each beam. This processing of forming $\bar{\boldsymbol{R}}_{\boldsymbol{x}}$ is similar to the case of averaging M covariance matrices for a moving array at different positions, and the coherence can be effectively removed.

An example is shown here, three directionally transmitted coherent signals are incident on an array in directions of 8.23°, 9.67° and 15°, with SNRs equal to 10 dB, 5 dB and 10 dB at any single receiver respectively, with correlations between the signals as $\rho_{12} = e^{i}$, $\rho_{13} = 1$ and $\rho_{23} = e^{-i}$. The ULA consists of 64 receivers, d=0.5λ , and 20 directionally transmitted beams equally spread in a sector of [1°, 20°]. Without decorrelation, coherence would cause ES eigen-structure methods to fail. The average over these ES covariance matrices from different beams removes the coherence and the result of applying MUSIC algorithm is plotted in Figure 6-15. Three sharp peaks appear on the correct azimuthal angles and indicate the correct DOAs.

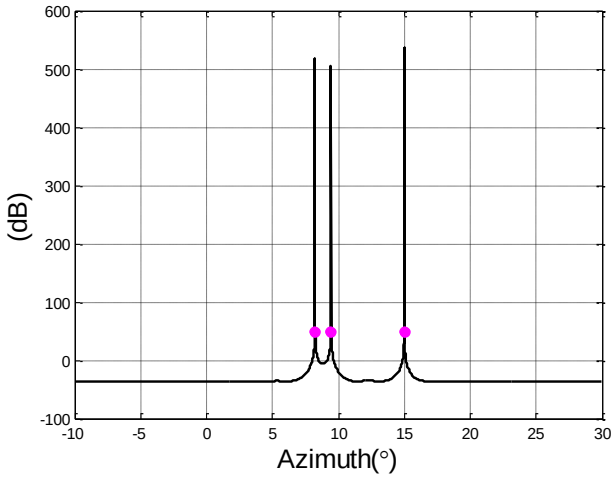

Figure 6-15: An example of applying MUSIC algorithm to the average over the ES covariance matrices for different directionally transmitted beams.

This averaging process is different from the common spatial smoothing methods, as the idea of subarrays is not used, but different weights are applied to the source signals for each transmit beam. In this way, the maximum number of signals that can be estimated for a coherent group is the smaller of the number of beams or receivers, i.e., $\min(M, K)$, which can be more than the spatial smoothing method. Additionally, unlike the subarrays methods, the array aperture is not reduced, and thus it is able to provide a better angular resolution for DOA estimation.

6.2.3.2 Feasibility of Reconstructing ES Signal Subspace for Directional Transmission BS Case

As described in Section 6.2.3.1, the coherence can be easily removed by averaging the ES covariance matrices from different beams, however, in many cases the ES receiver outputs are not available. Intuitively, the same method of reconstructing the omni-directional transmission ES covariance matrix used in Section 6.2.2.2 was first considered. Using formula (6-61) but for the stacked ES covariance matrix as (4-22), the corresponding stacked *MK*×*1* ES coherent signal steering vector is reconstructed as

$$\tilde{\boldsymbol{v}}_{ss} = \boldsymbol{U}\boldsymbol{q}_{y1} = \boldsymbol{U}\boldsymbol{U}^H\boldsymbol{q}_{1s}, \tag{6-71}$$

where $\boldsymbol{U}$ has been given by (4-24) and here $\boldsymbol{q}_{1s}$ denotes the principal eigenvector of the stacked ES covariance matrix.

Similar to the omni-directional case discussed earlier, ideally, if $\tilde{\boldsymbol{v}}_{ss}$ is coherent with $\boldsymbol{q}_{1s}$, then the ES signal subspace can be well reconstructed. By applying the approach in Section 6.2.2.2, the reconstructed stack ES covariance matrix is an *MK*×*MK* matrix and can be denoted as an *M*×*M* block matrix, each block is a *K*×*K* matrix. The block matrices on the main diagonal are the reconstructed ES covariance matrices for the different transmit beams. A question arises that whether the coherence can be removed by using the approach in Section 6.2.3.1—averaging over the reconstructed *M* covariance matrices for different beams.

To recall (4-24), $\boldsymbol{U}$ is a diagonal block matrix and $\boldsymbol{U}\boldsymbol{U}^H$ is a projection operator and it projects the one dimension BS signal subspace, $\boldsymbol{q}_{y1}$, to each beam, so $\tilde{\boldsymbol{v}}_{ss}$ is a stack of *M* vectors, each of which is a weighted ES steering vector for one of the beam directions. For example, the *m*-th vector is given by $\boldsymbol{v}(\theta_m)\boldsymbol{v}^H(\theta_m)\boldsymbol{q}_1(\theta_m)$, where $\boldsymbol{q}_1(\theta_m)$ is the principal eigenvector of $\boldsymbol{R}_{\boldsymbol{x}}(\theta_m)$. Obviously, for the case that a group of coherent signals are incident, $\boldsymbol{q}_1(\theta_m)$ is not coherent with $\boldsymbol{v}(\theta_m)$ and so $\boldsymbol{v}(\theta_m)\boldsymbol{v}^H(\theta_m)\boldsymbol{q}_1(\theta_m)$ is not coherent with $\boldsymbol{q}_1(\theta_m)$. Thus, if $\tilde{\boldsymbol{v}}_{ss}$ is used to reconstruct $\boldsymbol{R}_{\boldsymbol{x}}(\theta_m)$, only a term of the form $\boldsymbol{v}(\theta_m)\boldsymbol{v}^H(\theta_m)$ weighted by $\|\boldsymbol{v}^H(\theta_m)\boldsymbol{q}_1(\theta_m)\|^2$ can be formed, which does not contain the form of the incident signals from Θ_s. Then the principal eigenvector of the reconstructed ES covariance matrix is coherent with $\boldsymbol{v}(\theta_m)$ and the subspace method only works for the case where the DOAs of the coherent signals are coincidently located at the MRAs of beams; otherwise it does not indicate the correct DOAs and peaks would appear at or near to the beam centres close to the DOAs.

For example, this method was applied to the same scenario as in Figure 6-15 but the ES outputs were not available, the estimated DOAs were 8°, 9.88° and 15°. Only for the last signal, whose DOA coincides with the beam centre (15°), the estimated DOA is correct, and the accuracy depends on the spacing between MRAs. A more detailed analysis is shown in Appendix F. Increasing the number of evenly distributed beams only increases the resolution as beam centres are closer to the actual DOAs, but it is still not able to

work out the exact DOAs when they do not coincide with MRAs. Therefore, the method of reconstructing the ES coherent signal subspace for the omni-directional transmission BS case is not feasible for the directional transmission case.

6.2.3.3 DOA Estimation for Coherent Signals in Directional Transmission BS Case Using a newly Derived Matrix

The covariance matrix is the most common way to represent the signal model for use in array processing, but it is not the only way. For example, beam outputs can be represented in a vector as (3-1) and the fourth-order cumulants have been used as the expression of signals in [112], [113] and [114].

For a scenario containing L coherent signals, the m-th directional transmission beam output is given by

$$\begin{aligned} y_m &= \boldsymbol{v}^H(\theta_m)\boldsymbol{x}(\theta_m) \\ &= \sum_{l=1}^{L} s_l \boldsymbol{v}^H(\theta_m)\boldsymbol{v}(\theta_{sl})\boldsymbol{v}^H(\theta_m)\boldsymbol{v}(\theta_{sl})/K + \boldsymbol{v}^H(\theta_m)\boldsymbol{n}(\theta_m). \end{aligned} \tag{6-72}$$

As these signals are coherent, ignoring the propagation delay, the l-th signal can be denoted as $s_l = \rho_l \frac{\sigma_{sl}}{\sigma_{s0}} s_o$, where s_o is the unit amplitude ($\sigma_{s0} = 0$) narrowband transmitted signal, $\boldsymbol{v}^H(\theta_m)\boldsymbol{v}(\theta_{sl})$ is a complex scalar, thus its transpose is itself:

$$\boldsymbol{v}^H(\theta_m)\boldsymbol{v}(\theta_{sl}) = (\boldsymbol{v}^H(\theta_m)\boldsymbol{v}(\theta_{sl}))^T = \boldsymbol{v}^T(\theta_{sl})\boldsymbol{v}^*(\theta_m), \tag{6-73}$$

and the above equation (6-72) can be written as

$$\begin{aligned} y_m &= 1/K \sum_{l=1}^{L} \rho_l \sigma_{sl} s_o \, \boldsymbol{v}^H(\theta_m)\boldsymbol{v}(\theta_{sl})\boldsymbol{v}^T(\theta_{sl})\boldsymbol{v}^*(\theta_m) + \boldsymbol{v}^H(\theta_m)\boldsymbol{n}(\theta_m) \\ &= \frac{1}{K}\boldsymbol{v}^H(\theta_m)\left(\sum_{l=1}^{L} \rho_l \sigma_{sl}\boldsymbol{v}(\theta_{sl})\boldsymbol{v}^T(\theta_{sl})\right)\boldsymbol{v}^*(\theta_m)s_o + \boldsymbol{v}^H(\theta_m)\boldsymbol{n}(\theta_m). \end{aligned} \tag{6-74}$$

Define a matrix $\boldsymbol{Q_s}$ as the summation of weighted self-outer product of ES signal steering vectors and given by

$$\begin{aligned} \boldsymbol{Q_s} &= \sum_{l=1}^{L} \rho_l \sigma_{sl}\boldsymbol{v}(\theta_{sl})\boldsymbol{v}^T(\theta_{sl}) \\ &= \boldsymbol{V_s}(\Theta_s)\begin{bmatrix} \rho_1\sigma_{s1} & & \boldsymbol{0} \\ & \rho_2\sigma_{s2} & \\ \boldsymbol{0} & & \ddots \\ & & & \rho_L\sigma_{sL} \end{bmatrix}\boldsymbol{V_s^T}(\Theta_s). \end{aligned} \tag{6-75}$$

For a ULA, the Vandermonde structure of $\boldsymbol{v}(\theta_{sl})$ implies that $\boldsymbol{v}(\theta_{sl})\boldsymbol{v}^T(\theta_{sl})$ and hence $\boldsymbol{Q_s}$ are Hankel matrices. $\boldsymbol{Q_s}$ is closely related to an ES signal covariance matrix for L independent signals, and its rank equals to L—the number of coherent signals.

The singular value decomposition (SVD) of $\boldsymbol{Q_s}$ is represented as

$$\begin{aligned}\boldsymbol{Q_s} &= \boldsymbol{U_{sv}}\boldsymbol{\Sigma}\boldsymbol{V_{sv}} \\ &= [\boldsymbol{U_{sv}}(L) \quad \boldsymbol{U_{sv}}(K-L)]\begin{bmatrix}\boldsymbol{\Sigma}(L) & \boldsymbol{0} \\ \boldsymbol{0} & \boldsymbol{\Sigma}(K-L)\end{bmatrix}\begin{bmatrix}\boldsymbol{V_{sv}}(L) \\ \boldsymbol{V_{sv}}(K-L)\end{bmatrix},\end{aligned} \tag{6-76}$$

where the non-zero singular values are the diagonal elements of $\boldsymbol{\Sigma}(L)$; the columns of left singular vectors correspond to the non-zero singular values, i.e. $\boldsymbol{U_{sv}}(L)$, span the dominant (signal) subspace, and the remaining columns of $\boldsymbol{U_{sv}}$ correspond to the zero singular values, i.e., $\boldsymbol{U_{sv}}(K-L)$, span the subdominant(noise) subspace. These two subspaces are orthogonal to each other. Since the steering vectors in the array manifold are linearly independent, thus these steering vectors at the DOAs of the signals, i.e., $\boldsymbol{v}(\theta_{sl}), l = 1,2,\cdots L$ and the columns of $\boldsymbol{U_{sv}}(L)$ span the same subspace, i.e., $\boldsymbol{U_{sv}}(L)$:

$$span\{\boldsymbol{v}(\theta_{s1}) \quad \boldsymbol{v}(\theta_{s2}) \quad \cdots \quad \boldsymbol{v}(\theta_{sL})\} = span\{\boldsymbol{U_{sv}}(L)\}, \tag{6-77}$$

thus $\boldsymbol{v}(\theta_{sl})$ is orthogonal to $\boldsymbol{U_{sv}}(K-L)$ and the DOAs of signals can be estimated by directly applying the subspace method, such as MUSIC:

$$p_{MUSIC-Q_s}(\theta) = \frac{1}{\sum_{i=L+1}^{K}|\boldsymbol{v}^H(\theta)\boldsymbol{U_{sv}}(K-L)|^2}. \tag{6-78}$$

Notice the singular vectors are used here rather than the eigenvectors and the output peaks indicate the DOAs of signals. Theoretically, the elements in $\boldsymbol{\Sigma}(K-L)$ are zeros, but in practice they can be very small values close to zero, due to issues of numerical computation, noise and estimation errors.

6.2.3.4 Estimating Q_s from Directional Transmission BS Data

For the directional transmission BS case, assuming the noise components are both spatial and temporal white, the noise in different beams are completely uncorrelated, thus

$$\begin{aligned}E\{\boldsymbol{v}^H(\theta_m)\boldsymbol{n}(\theta_m)\boldsymbol{n}^H(\theta_m)\boldsymbol{v}(\theta_m)\} &= K\sigma_n^2, \\ E\{\boldsymbol{v}^H(\theta_m)\boldsymbol{n}(\theta_m)\boldsymbol{n}^H(\theta_i)\boldsymbol{v}(\theta_i)\} &= 0, \text{ when } i \neq m.\end{aligned} \tag{6-79}$$

The directional transmission BS covariance matrix containing a group of coherent signals can be written as

$$\boldsymbol{R}_y = \boldsymbol{v_{ys}}\boldsymbol{v_{ys}^H} + K\sigma_n^2\boldsymbol{I}_{M\times M}, \tag{6-80}$$

where $\boldsymbol{v_{ys}}$ is the generalised coherent signal BS steering vector and given by

$$\boldsymbol{v_{ys}} = \sum_{l=1}^{L} \rho_l \sigma_{sl} \boldsymbol{v_y}(\theta_{sl}). \tag{6-81}$$

Substituting (4-8), (6-73) and (6-75) in the above expression and it is can be written as

$$\boldsymbol{v_{ys}} = \begin{bmatrix} \boldsymbol{v}^H(\theta_1)\boldsymbol{Q_s}\boldsymbol{v}^*(\theta_1) \\ \boldsymbol{v}^H(\theta_2)\boldsymbol{Q_s}\boldsymbol{v}^*(\theta_2) \\ \vdots \\ \boldsymbol{v}^H(\theta_M)\boldsymbol{Q_s}\boldsymbol{v}^*(\theta_M) \end{bmatrix}. \tag{6-82}$$

Applying vectorisation to each element of $\boldsymbol{v_{ys}}$ yields

$$\begin{aligned} \boldsymbol{v_{ys}}(m) &= vec\left[\boldsymbol{v}^H(\theta_m)\boldsymbol{Q_s}\boldsymbol{v}^*(\theta_m)\right] \\ &= \boldsymbol{v}^H(\theta_m) \otimes \boldsymbol{v}^H(\theta_m) vec\left[\boldsymbol{Q_s}\right], \end{aligned} \tag{6-83}$$

and then stacking all the elements in $\boldsymbol{v_{ys}}$:

$$\boldsymbol{v_{ys}} = \begin{bmatrix} \boldsymbol{v}^H(\theta_1) \otimes \boldsymbol{v}^H(\theta_1) \\ \boldsymbol{v}^H(\theta_2) \otimes \boldsymbol{v}^H(\theta_2) \\ \vdots \\ \boldsymbol{v}^H(\theta_M) \otimes \boldsymbol{v}^H(\theta_M) \end{bmatrix} vec[\boldsymbol{Q_s}]. \tag{6-84}$$

Then, the least square error method can be used to estimate the vectorisation of $\boldsymbol{Q_s}$ as

$$vec\left[\widetilde{\boldsymbol{Q}}_{\boldsymbol{s}}\right] = \begin{bmatrix} \boldsymbol{v}^H(\theta_1) \otimes \boldsymbol{v}^H(\theta_1) \\ \boldsymbol{v}^H(\theta_2) \otimes \boldsymbol{v}^H(\theta_2) \\ \vdots \\ \boldsymbol{v}^H(\theta_M) \otimes \boldsymbol{v}^H(\theta_M) \end{bmatrix}^{+} \boldsymbol{v_{ys}}. \tag{6-85}$$

Similar to the process in Section 6.1.4, it is easy to verify the following relationship between the principal eigenvector of the BS covariance matrix, $\boldsymbol{q_{y1}}$, and $\boldsymbol{v_{ys}}$:

$$\boldsymbol{q_{y1}} = \frac{\boldsymbol{v_{ys}}}{|\boldsymbol{v_{ys}}|} e^{j\varphi}, \tag{6-86}$$

where $e^{j\varphi}$ is a random phase shift and (6-85) can be written as

$$vec\left[\widetilde{\boldsymbol{Q}}_{\boldsymbol{s}}\right] = \left|\boldsymbol{v_{ys}}\right| e^{-j\varphi} \begin{bmatrix} \boldsymbol{v}^H(\theta_1) \otimes \boldsymbol{v}^H(\theta_1) \\ \boldsymbol{v}^H(\theta_2) \otimes \boldsymbol{v}^H(\theta_2) \\ \vdots \\ \boldsymbol{v}^H(\theta_M) \otimes \boldsymbol{v}^H(\theta_M) \end{bmatrix}^{+} \boldsymbol{q_{y1}}. \tag{6-87}$$

Similar to the derivation in Section 6.2.2.2, with a sufficient number of beams, $vec\left[\widetilde{\boldsymbol{Q}}_{\boldsymbol{s}}\right]$ can be coherent with $vec[\boldsymbol{Q_s}]$. Although the complex scalar $\left|\boldsymbol{v_{ys}}\right| e^{-j\varphi}$ is unknown, it

does not affect the result of DOA estimation, thus it can be ignored, and (6-85) can be replaced by

$$vec[\widetilde{\boldsymbol{Q}}_{\boldsymbol{s}}] = \begin{bmatrix} \boldsymbol{v}^H(\theta_1) \otimes \boldsymbol{v}^H(\theta_1) \\ \boldsymbol{v}^H(\theta_2) \otimes \boldsymbol{v}^H(\theta_2) \\ \vdots \\ \boldsymbol{v}^H(\theta_M) \otimes \boldsymbol{v}^H(\theta_M) \end{bmatrix}^+ \boldsymbol{q}_{\boldsymbol{y}1}. \tag{6-88}$$

The $K^2 \times 1$ vector $vec[\widetilde{\boldsymbol{Q}}_{\boldsymbol{s}}]$ can be easily recovered or converted to a $K \times K$ matrix $\widetilde{\boldsymbol{Q}}_{\boldsymbol{s}}$. Then the subspace method based on SVD which has been discussed in Section 6.2.3.3 can be applied to $\widetilde{\boldsymbol{Q}}_{\boldsymbol{s}}$ to estimate the DOAs of coherent signals. Due to the number of samples and beams, $\widetilde{\boldsymbol{Q}}_{\boldsymbol{s}}$ can be different from $\boldsymbol{Q}_{\boldsymbol{s}}$, and the subdominant (noise) singular values can be not zeros, but with a sufficient number of beams, they are still much smaller than the dominant (signal) singular values. Notice the maximum number of signals that can be detected is still *M*.

6.2.3.5 Results of Estimating DOAs of Coherent Signals Using $\widetilde{Q}_s$

The similar scenario in Figure 6-9 was used, where two coherent signals at DOAs of 8.23° and 9.44°, SNR=10 dB and 5 dB, correlation $\rho=e^{j}$, are incident on a ULA with 64 receivers, d=0.5λ, but with variable number of directional Tx/Rx beams equally spread in a sector [1°, 20°]. The matrix, $\widetilde{\boldsymbol{Q}}_{\boldsymbol{s}}$, was estimated by using the approach in Section 6.2.3.4, and then the MUSIC algorithm was applied. The outputs of MUSIC versus a different number (16, 20 and 24) of beams are shown in Figure 6-16. Comparing the true DOAs (being plotted as magenta spots), it shows that the estimated DOAs are biased for a small number of beams, but the result improves by increasing the number of beams, and eventually very sharp peaks appear at the correct DOAs of the coherent signals.

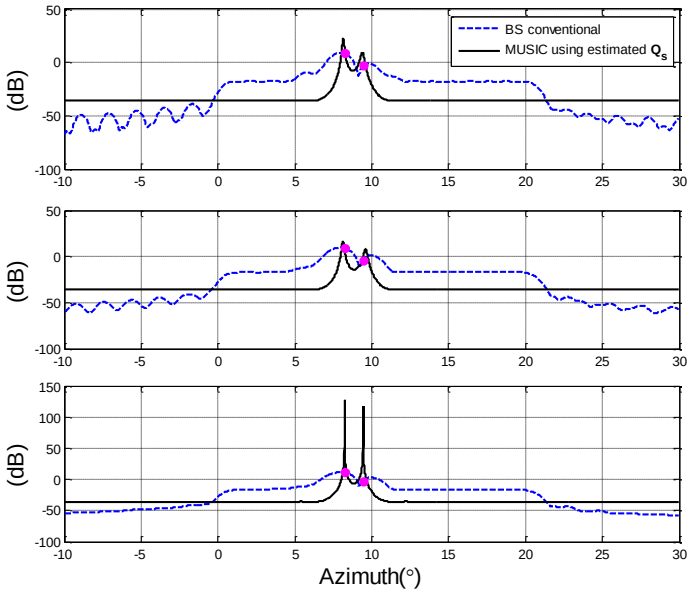

Figure 6-16: An example of applying MUSIC algorithm to estimated $\boldsymbol{Q}_{\boldsymbol{s}}$. A model containing two coherent signals was used and the numbers of beams were 16, 20 and 24 respectively.

The same scenario with 24 directional Tx/Rx beams equally spread in a sector [1°, 20°]. was simulated and 256 independent samples were generated for each beam. After estimating the matrix, $\widetilde{\boldsymbol{Q}}_{\boldsymbol{S}}$, the MUSIC using SVD method was applied and the output versus azimuthal angle is plotted in Figure 6-17. The output power of the BS conventional beamformer is also plotted for comparison and the output power values of the conventional BS beamformer at the true DOAs are marked as magenta spots. The conventional BS beamformer provides poor resolution and the output peaks are biased from the true DOAs. Similar to the omni-directional transmission case, the DOAs of the coherent signals can be estimated accurately but the output peaks are not as sharp as the theoretical analysis.

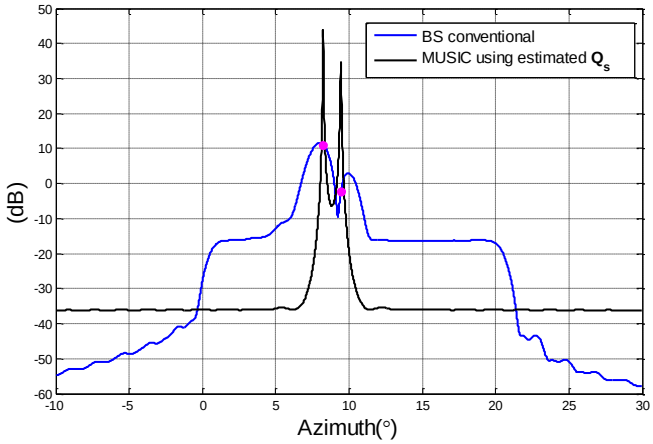

Figure 6-17: A simulation example of applying MUSIC algorithms to $\widetilde{\boldsymbol{Q}}_{\boldsymbol{S}}$. 24 directional Tx/Rx beams were used and 256 samples were simulated for each beam.

As shown in Section 6.2.2.2, for the omni-directional transmission case, an $M \times K$ matrix is used to estimate a $K \times 1$ vector representing the ES generalised coherent signal steering vector as (6-61) or a $K \times K$ matrix representing the signal subspace as (6-63). Whilst for the directional transmission case, an $M\times K^2$ matrix is used to estimate a $K^2 \times 1$ vector as (6-88). To achieve the estimation with an equivalent accuracy, more beams are required for the directional transmission case. As shown in Figure 6-16, with insufficient number of beams, the estimated DOAs can be slightly different from the true DOAs. On the other hand, due to the special structure of the directional transmission model, without any process of decorrelation, the DOAs of the coherent signals can be estimated regardless of the coherence by using $\widetilde{\boldsymbol{Q}}_{\boldsymbol{S}}$. Unlike the spatial smoothing processing for the omni-directional transmission case, the number of coherent signals is not required in advance and it is can be readily obtained as the rank or the number of the dominant singular values of $\widetilde{\boldsymbol{Q}}_{\boldsymbol{S}}$, furthermore, the array aperture is not reduced, thus a better spatial resolution can be provided.

6.2.4 Other Potential Approaches for Estimating DOAs of Coherent Signals in BS

The proposed subspace approaches for the BS coherence problem use either a reconstructed ES signal subspace for the omni-directional transmission case or an estimated matrix which is the summation of the self-outer product of ES signal steering vectors. Besides the proposed methods, other methods can be considered and extended to the problem of DOA estimation for coherent signals in BS. For example, constraint MUSIC[67], [68] or recursive MUSIC methods [69], [70] and [76] estimate DOAs using a sequence of projection operators to constrain the noise subspace to be orthogonal to a set of specified direction vectors. To select these directions, a priori information or estimation of DOAs is required. However the prior information is not always available and the estimate may be inaccurate. For example, peaks from conventional beamformer output power can indicate the DOAs only when high SNRs signals are well spatially separated, thus the number of signals can be easily estimated incorrectly. Also, the universal method—maximum likelihood (ML) [54], [55], [56] and [57] can be considered for the DOA estimation for coherent signals in BS. Those methods are either limited by the prior information or high computation, and will not be investigated in this thesis.

6.3 Optimum BS Beamformer for Coherent Signals with a Priori Knowledge of DOAs

As mentioned in Section 6.1.3, the optimum BS beamformer output can be seriously affected by the coherence (or high correlation) between incident signals. Generally, spatial smoothing reduces the correlation between signals but they are still partially correlated. Thus, applying the MVDR algorithm to the spatially smoothed covariance matrix cannot estimate the signal intensity accurately. However, with a priori knowledge or estimation of the DOAs of signals, the problem of signal intensity estimation is much easier. In the ES processing literature, this problem has been discussed, such as [19], [51], [60] and [66], the authors proposed to keep the unity response at the look angle and minimise the total power of rest of coherent signals and interferences, whilst a signal-free covariance matrix is obtained by blocking the steering vector at the DOA of the desired signal.

For optimum BS beamforming, the same method can be applied. After estimating the DOAs of L coherent signals in BS using the methods developed in Section 6.2.2 or 6.2.3, the method of linear constraints or oblique projection can be applied to null the responses at the DOAs of any correlated signals but keep a unity response at the look direction. The BS LCMV algorithm can be applied and the formula is written as

$$\boldsymbol{w}(\theta) = \boldsymbol{R}_{\boldsymbol{y}}^{-1}\boldsymbol{C}(\theta)[\boldsymbol{C}^{H}(\theta)\boldsymbol{R}_{\boldsymbol{y}}^{-1}\boldsymbol{C}(\theta)]^{-1}\boldsymbol{g}(\theta), \tag{6-89}$$

where the direction constraint $\boldsymbol{C}$ and constraint values $\boldsymbol{g}$ are given by

$$\text{If } \theta \in \Theta_s, \boldsymbol{C}(\theta) = [\boldsymbol{h}(\theta) \quad \boldsymbol{h}(\Theta_s \cap \bar{\theta})], \boldsymbol{g}(\theta) = \begin{bmatrix} 1 \\ 0 \\ \vdots \\ 0 \end{bmatrix}_{L\times 1}, \qquad \text{If } \theta \notin \Theta_s, \boldsymbol{C}(\theta) = \boldsymbol{h}(\theta), \boldsymbol{g}(\theta) = 1. \tag{6-90}$$

The output power is given by

$$p_{LCMV-BS}(\theta) = \boldsymbol{g}^H(\theta)\left(\boldsymbol{C}^H(\theta)\boldsymbol{R}_{\boldsymbol{y}}^{-1}\boldsymbol{C}(\theta)\right)^{-1}\boldsymbol{g}(\theta). \tag{6-91}$$

Notice that the above formula is for the omni-directional transmission case and a modification can be easily made for the directional transmission case, which simply replaces the steering vector $\boldsymbol{h}(\theta)$ by $\boldsymbol{v}_{\boldsymbol{y}}(\theta)$.

An example of the omni-directional transmission coherent signals in BS is shown here. Two groups of coherent signals, but uncorrelated between groups, were considered. Three coherent signals with $SNR = 10$ dB, 5 dB and 10 dB at any single receiver are incident from DOAs of 8.23°, 9.44° and 12°, and with correlations $\rho_{12} = e^{i}$ and $\rho_{13} = 1$. The second group contained two signals at DOAs of 5.3° and 10.67°, both with SNR=10 dB at any single receiver, and with correlation $\rho_{12} = e^{i\pi/3}$. The ULA contains 64 receivers, d=0.5λ and 20 beams in a sector of [1°, 20°] were evenly distributed with 1° separation. After estimating the DOAs using the method discussed in Section 6.2.2, the modified LCMV BS beamformer was applied. The conventional and LCMV BS beamformer output power values versus azimuthal angle are plotted in Figure 6-18. It shows that the output power values at DOAs of the coherent signals are almost the same as the actual signal intensities. Due to the cancellation among correlated signals, the output power values at other azimuthal angles around DOAs are suppressed as much lower values and very sharp peaks appear at DOAs.

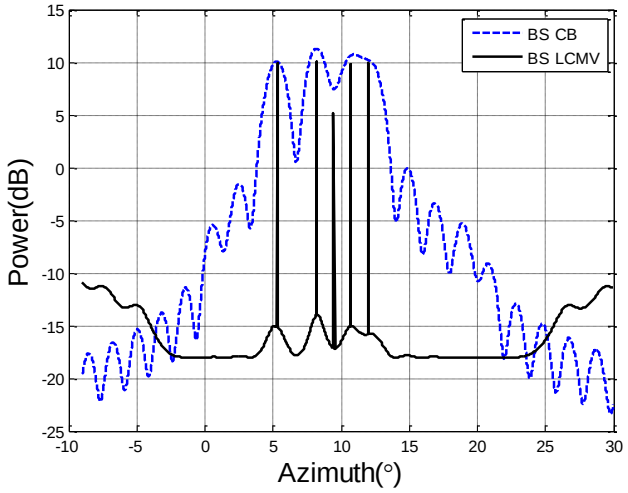

Figure 6-18: An example of BS conventional and LCVM beamformer output power values versus azimuthal angle with prior information about DOAs. The blue curve represents the conventional BS beamformer output power and the black curve is the modified BS LCMV beamformer output power.

6.4 Summary

Spatial correlation between signals can occur in both the omni-directional and directional transmission BS cases. Coherence or high correlation can seriously degrade the performance of beamformers and DOA estimation algorithms. This chapter was focused on the DOA estimation and beamforming for coherent signals in BS. In Section 6.1, the correlated signal BS model was introduced and the performance degradation for BS algorithms was analysed. In Section 6.2, with a brief introduction of spatial smoothing algorithms, the method of reconstructing ES signal subspace for the omni-directional transmission case was proposed and verified by some examples. Then, a new special matrix for the directional transmission BS was proposed. This matrix allows the DOAs of coherent signals to be estimated regardless of the coherence, and it can be estimated and constructed using the beam steering vectors and the principal eigenvector of the directional transmission BS covariance matrix. Some other potential methods for estimating DOAs of coherent signals in BS were also briefly discussed. With the DOA information, the BS LCMV beamformer with directional constraints was modified for the case of coherent signals in Section 6.3.

Chapter 7

Application of Beam Space Processing to Real Experimental Data

As mentioned earlier in this thesis, the receiver outputs of a phased array radar—phase tilt weather radar (PTWR) used in this project were not accessible and only conventional beamformer outputs were recorded for further processing. Thus commonly used ES processing methods could not be directly applied to the collected experimental data, and BS processing methods became the main technique for spatial signal processing.

In most experiments carried out by using the PTWR, beams with narrow main lobes were directionally transmitted and those beams were scanned over a sector of interest and a fixed number of pulses are transmitted and received at each beam. As shown in Chapter 4, standard BS processing methods fail for the directional transmission BS model, thus only the directional transmission BS processing algorithms developed in Chapter 4 to 6 were suitable to process the experimental data collected using the PTWR and the results of BS processing are analysed and compared in this chapter.

This radar was designed as a low cost approach for rapid weather observations, and the main benefits of using this phased array system include: low cost, portability, dual polarisation, quick electronic scanning in azimuth and high SNR gain provided by conventional beamforming. Some parameters required for weather observations, such as reflectivity and differential reflectivity, are mainly estimated by using the beam outputs. Due to the robustness of conventional beamformer, some phase errors and imperfect calibration can be tolerated and they were not significant issues for weather observations. For a rapid observation purpose, a short dwell time at each beam was preferred and thus only a small number of samples were generally collected for each beam. However, because of imperfections in the array calibration, the unavailability of system parameters, and the limited number of samples collected, the performance of the BS spatial processing algorithms was not expected to be as outstanding as the theoretical analysis or simulations based on a perfect model. Additionally, the detailed ground truth (the scatterer distribution and multipath) was often unknown, which made the verification and assessment difficult.

7.1 Description of PTWR and DSTG STF BS Experimental Data

In this section, some details about the PTWR and one selected experimental data for the application of the developed BS processing algorithms are described.

7.1.1 Details of Phase Tilt Weather Radar

The phased array system used in this project was developed by Raytheon Integrated Defence Systems and the array front-end was designed and built by First RF Corporation. It is an X-band (9.3 – 9.5 GHz) radar, with dual-linear polarisation and is comprised of 64 columns each containing 32 dipole radiating elements [94]. The aperture size of this radar is 1.5 m^2, and the elevation and azimuth beamwidths at broadside are 2.8° and 1.8° respectively. The radar can scan electronically to ±45° angles in the horizontal principal plane off broadside and mechanically tilts in elevation. For each beam, a fixed number of pulses, typically 32 – 128, are transmitted and received before the Tx/Rx beam is switched to the next direction and only the conventional beamformer output is recorded as In-phase and Quadrature (IQ) data. Both HH and VV polarised data can be recorded and the two polarisations are switched at the next pulse. More details about the radar system can be found in [119]. Photos of the front and back of the array are shown in Figure 7-1.

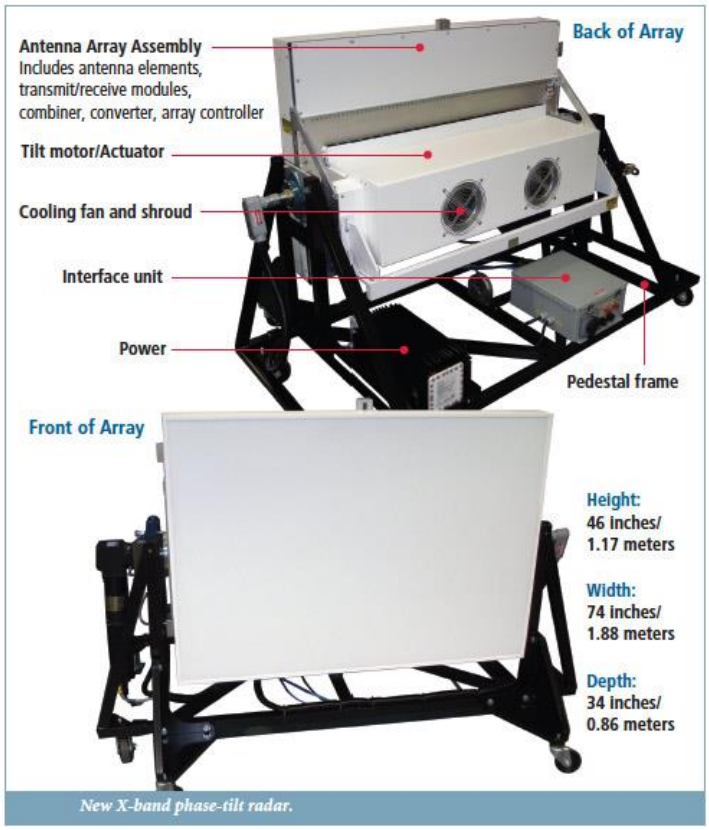

Figure 7-1: Photos of the Phase Tilt Weather Radar

7.1.2 Description of DSTG Experimental Data

In 2013, the PTWR was deployed to the University of Adelaide and used for a serious of experiments which mainly focused on weather and bushfire observations. More details about these experiments can be found in [100] and [101]. Most collected data were observations of meteorological phenomena containing quick moving volume scatterers, whilst for verifying the BS processing algorithms developed in this thesis, data including stationary targets with large RCS was highly desired.

The most suitable experiment for applying these developed BS processing algorithms was carried out at the Defence Science and Technology Group (DSTG) System Test Facility (STF) at Edinburgh, Adelaide, South Australia. The PTWR scanned over a sector by forming 20 directional Tx/Rx beams whose beamwidth was about 1.8° at broadside and the MRAs were from an azimuthal angle of -18° to 2° at steps of 1.1° and the elevation was fixed at 1°. The radar was operated at a fixed PRF of 3 kHz, with a pulse width of 1 μs and pulse compression and the sample gate spacing was about 6 m in range. 64 pulses (H and V polarisations were switched at each pulse) were transmitted/received in each beam (azimuth) direction. This scan pattern was repeated 12 times.

A metal tower at ~50 m height was located at about -8.5° in azimuth and ~ 655 m in range and a corner reflector at ~6.5 m height was deployed at about -1^{o} in azimuth and ~ 605 m in range. Returns from these two large targets are obvious in both of the two range bins because of the effect of range sidelobes. The averaged output power values of the conventional beamformer as a function of range and azimuthal angle are shown in Figure 7-2.

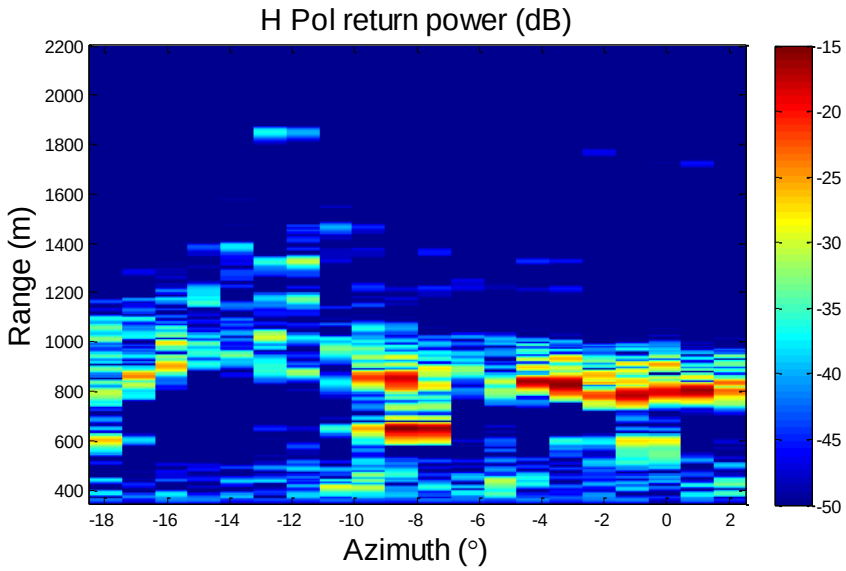

Figure 7-2: DSTG BS data H pol return power at different range and azimuthal angle

Notice that the radar receivers were switched off during the transmitting time, and no reflections were recorded in a blind range of 344.76 m. The two known targets were

easily identified in the conventional beam outputs, but may be mixed with some ground clutter. There were some vegetation features about 200 m in range behind the two experimental targets. There was an unknown but isolated target at ~2105 m in range, whose beamformed return power was only about 15 dB higher than the noise power and was not obvious in Figure 7-2. There were three targets at the range bin of ~1925 m where one of the returns was obviously stronger than the other two and its beamformed return power was at least 25 dB higher than the noise power.

Although careful calibrations were done before each experiment, there were still some unknown phased array errors; and the accuracy of the recorded MRAs of the beams was unknown. 20 transmit/receive beams were formed in a sequence and 64 pulses were recorded at each beam, thus different beams were not transmitted/received simultaneously. However those targets of main interest are almost stationary and unchanged in such a short time during one scan, thus the data in the same scan can be processed as the simultaneous beams. For a set of data from multiple scans, there were some changes among different scans, so it contains more variation but less correlation.

7.2 Results of BS Processing for PTWR Experimental Data

The developed directional transmission BS processing methods were applied and tested on the experimental data collected at the DSTG STF. In this section, the results of directional transmission BS processing for several range bins of the experimental data are presented.

7.2.1 Apply Directional Transmission Optimum BS Beamforming to PTWR Experimental Data

As discussed in Chapter 6, spatial correlation can degrade the performance of optimum BS beamformer. To avoid or reduce the effect of correlation between signals, a dataset containing a single isolated target with a strong return was highly desirable, but unfortunately, the most suitable data still contained the return from a target mixed with some other unknown weak returns. These returns were likely from ground clutter because the low elevation angle may result in the lower part of the mainlobe hitting the ground.

The chosen target was at an azimuthal angle of around -13.6° and in a range bin (294) about 2105 m away from the radar. These conventional beamformed radar returns in H polarisation for 12 repeat scans were used. As shown in (3-4), pulses in the same order but from different beams are combined as a vector, $\boldsymbol{y}(\mathrm{t})$, which represents a realisation of conventional beam outputs. The BS covariance matrix, $\widehat{\boldsymbol{R}}_y$, was estimated by averaging $\boldsymbol{y}(\mathrm{t})\boldsymbol{y}^H(\mathrm{t})$ over the 32 pulses in each scan and over the 12 scans in the assumed coherent processing interval. For H polarisation, the diagonal element of $\widehat{\boldsymbol{R}}_y$, which represent the average return power values in different beams are marked against

azimuthal angle as red spots in Figure 7-3. The directional transmission BS MVDR beamformer was applied to the estimated covariance matrix and the output power values are plotted versus azimuthal angle, the output power values of the conventional BS and standard BS MVDR are also shown for comparison.

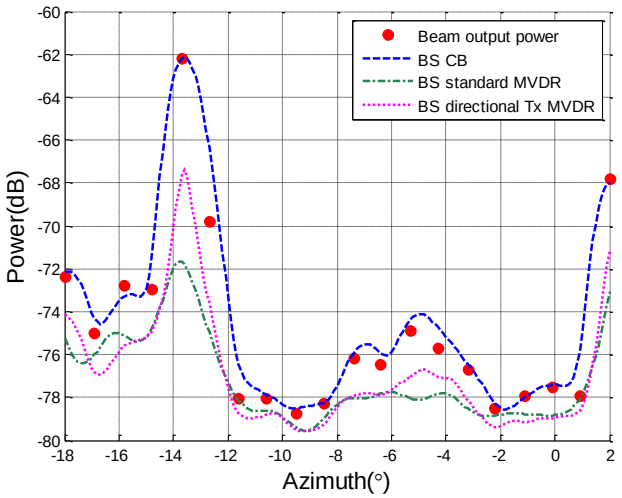

Figure 7-3: Results of applying the directional transmission BS MVDR formula to experimental BS data in the range bin (294) ~ 2105 m from the radar and comparing with the conventional and standard MVDR BS beamformers.

Similar to the theoretical analysis and performance on the simulated data in Chapter 4, the directional transmission BS MVDR formula achieved a better resolution and higher gain at the DOA of the main target (about -13.6°). Some output peaks of the standard optimum BS beamformer appear around the DOAs, but their power values are relatively small. This is because the mismatch between the omni-directional and directional transmission steering vectors causes very small outputs. The performance of the directional transmission BS MVDR formula is only slightly better than the standard BS MVDR formula and the result is unsatisfactory, as the output peak is still much lower than the conventional beamformer. Due to possible imperfect calibrations and other sources of systematic errors, the covariance matrix estimated from the experimental data is different from the theoretical model without perturbations, and taking the beam pattern of the transmitting antenna into consideration in the directional transmission BS MVDR formula reduced but could not fully solve the mismatch.

7.2.2 Apply Robust BS Beamforming to PTWR Experimental Data

As analysed in Chapter 5, different types of errors can degrade the performance of optimum BS beamformer and the example of using experimental data in Figure 7-3 showed that the optimum BS beamformer output power peak at the main target was near to 6 dB lower than the conventional beamformer. To overcome the mismatch caused by errors, the newly developed robust BS beamformer, as shown in equation (5-30), searches for the maximum output power around the processing steering vector. The result of applying the robust BS beamformer with an uncertainty set as $\epsilon(\theta) =$

$0.18\|\boldsymbol{v}_{\boldsymbol{y}}(\theta)\|^2$ to the above data in range bin 294 (~2105 m) is shown in Figure 7-4. A better SNR gain is achieved by the robust BS beamformer compared with the directional optimum BS beamformer. The robust BS beamformer has a slightly narrower "main beam" than the conventional beamformer. This is because the robust BS beamformer searches the maximum power around the processing angle (steering vector). Although this range bin was chosen because it contains an isolated target which potentially reduces the effect of signal correlation, its return was weak (considering that the SNR gain from the conventional beamforming is K) and is even hard to see in Figure 7-2. This robust optimisation technique only provides very limited improvement to the estimation of the signals whose SNRs are low and the outputs are similar to that from the conventional beamformer.

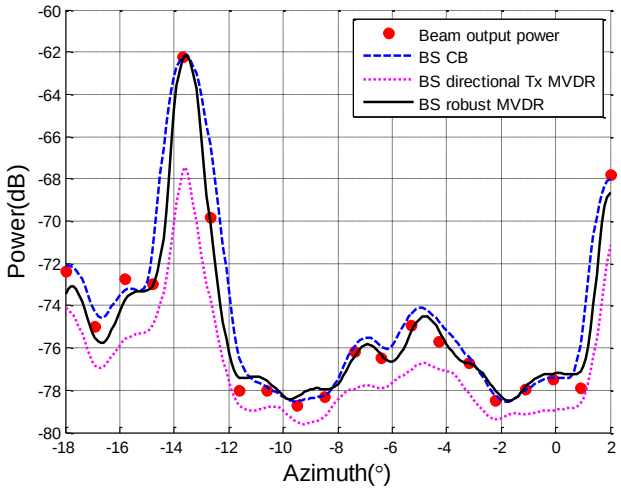

Figure 7-4: Results of applying the robust BS beamformer to experimental BS data in the range bin (294) ~ 2105 m from the radar and comparing with directional transmission conventional and optimum BS beamformers.

Another chosen target was in a range bin (264) about 1925 m away from the PTWR, and its conventional beamformed power was more than 25 dB above the noise power. There appeared to be two weaker returns located at other angles in the same range bin. In some scans, these return signals were correlated, but averaging over 12 repeat scans removed the correlation between returns in this range bin very well. Applying the developed robust BS beamformer with an uncertainty set $\epsilon(\theta) = 0.18\|\boldsymbol{v}_{\boldsymbol{y}}(\theta)\|^2$ to this data, the result is shown in Figure 7-5. For H polarisation, the average return power, are plotted as red spots and outputs of the directional transmission conventional and optimum BS beamformers are also plotted versus azimuthal angle for a comparison purpose.

By overcoming the mismatch caused by the possible phase array errors, strong peaks of the robust BS beamformer output power appeared at the DOAs of these targets. Thus the robust BS beamformer provided a much higher SNR and better resolution than the conventional and optimum BS beamformers for the main target in this range bin. For the other two targets with weaker SNRs, the robust BS beamformer output power values are similar to the BS conventional beamformer.

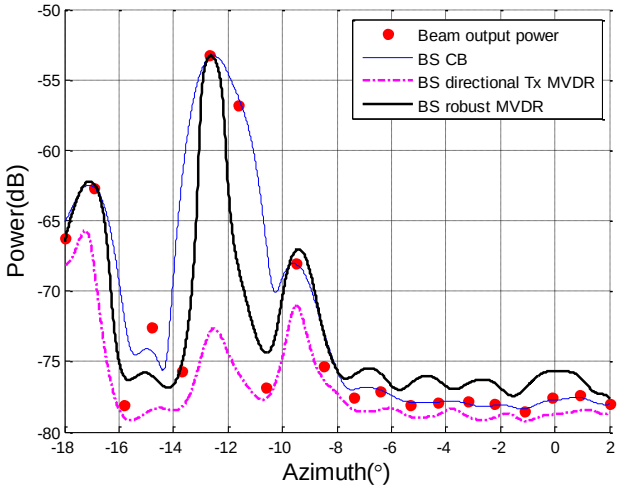

Figure 7-5: Results of applying the robust BS beamforming method to experimental BS data in the range bin (264) ~1925 m from the radar and comparing with the conventional and optimum BS beamformers.

These methods were applied to the main interest of this experiment, the metal tower located at ~ -8.5° in azimuth and ~655 m from the radar and the corner reflector was deployed at ~-1° in azimuth and ~ 605 m from the radar. The average return power values in the first scan are marked as red spots against azimuthal angle. The directional transmission conventional and optimum BS beamformer output power values, as well as the robust BS beamformer output power with an uncertainty set $\epsilon(\theta) = 0.18\|\boldsymbol{v_y}(\theta)\|^2$ are plotted in Figure 7-6 for the range bin where the corner reflector was located in.

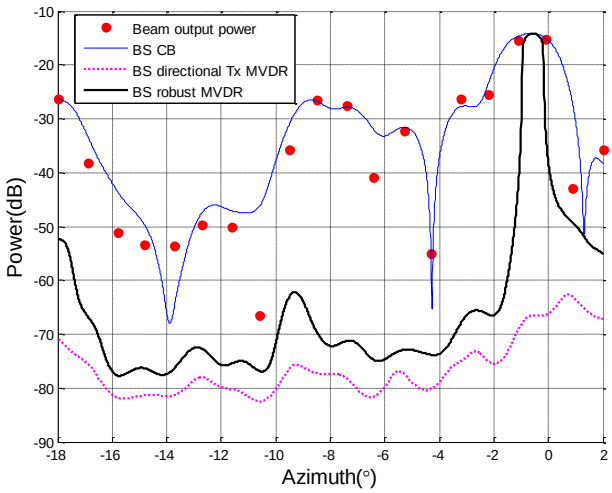

Figure 7-6: Results of applying the robust BS beamformer to the DSTG experimental data in the range bin (44) ~605 m from the radar.

The conventional BS beamformer output power values versus azimuthal angle interpolate the beam outputs well but with a low resolution. Obviously, the directional transmission BS MVDR algorithm fails to process this data, as the output power peak values are too low to be identified. The reason for its failure can be the phase array errors

and also the returns from different directions are highly correlated. A sharp and strong peak of the robust BS beamformer output power appears at the assumed DOA of the corner reflector. However the output around $-8.5°$, where the range sidelobe of the tower was located in, is very weak. The peak of the output power around this angle is 30 dB below the corresponding output peak of the conventional beamformer. The result of applying the robust BS beamformer to the data in the range bin 52 (~655 m away from the radar), where the metal tower was located in was similar to this: a strong peak appears at the assumed DOAs of the tower but the output around the assumed DOA of the corner reflector is weak. This is because the return signals from two main targets are highly correlated and multipath might occur around the same target, thus the performance of the robust BS beamformer is degraded seriously by the correlation and only a strong and sharp peak appears at the DOA of the strongest signal return in each coherent group.

In this example, only data in the first scan was used, where the signals were highly correlated. When data is averaged over multiple scans, more variations and less correlation between signals are in the BS data. For example, when all the 12 scans were averaged and used to estimate the covariance matrix, the maximal robust BS beamformer output power appeared at about the same angle, i.e., the DOA of the corner reflector, and with almost the same output power value as that using the data from the first scan; also, the maximal output power peak was not as sharp as that using the data from a single scan, but the output peaks around other DOAs were larger than that from a single scan.

In [85], the authors reported satisfactory results with different values of the parameter ϵ for the uncertainty set. However, to process the above experiment BS data with correlation issues indicated that different values of ϵ can provide different results. When ϵ was too small, the actual steering vectors could not be well approximated, but when the parameter was increased as $\epsilon(\theta) = 0.27\|\boldsymbol{v}_{\boldsymbol{y}}(\theta)\|^2$, more beamformer output power peaks appeared, which is shown in Figure 7-7.

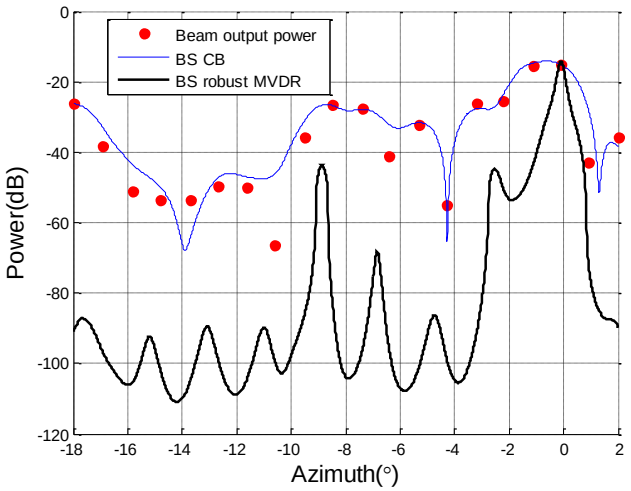

Figure 7-7: Results of applying robust BS beamformer to the DSTG experimental data in the range bin (44) ~605 m from the radar, with a large value of ϵ.

For the case of a group of coherent signals in the directional transmission BS case, the BS covariance matrix is given by (6-80) as $\boldsymbol{R}_y = \boldsymbol{v}_{\boldsymbol{ys}}\boldsymbol{v}_{\boldsymbol{ys}}^H + K\sigma_n^2\boldsymbol{I}_{M\times M},$, and the generalised coherent signal steering vector $\boldsymbol{v}_{\boldsymbol{ys}}$ is given by (6-81) as $\boldsymbol{v}_{\boldsymbol{ys}} = \sum_{l=1}^{L}\rho_l\sigma_{sl}\boldsymbol{v}_{\boldsymbol{y}}(\theta_{sl})$. Thus for any BS processing methods, an output peak would appear when the processing vector is coherent with $\boldsymbol{v}_{\boldsymbol{ys}}$. For this data, considering the factor of phased ray errors, the generalised coherent signal steering vector can be modified as

$$\acute{\boldsymbol{v}}_{\boldsymbol{ys}} = \sum_{l=1}^{L}\rho_l\sigma_{sl}\acute{\boldsymbol{v}}_{\boldsymbol{y}}(\theta_{sl}), \tag{7-1}$$

where $\acute{\boldsymbol{v}}_{\boldsymbol{y}}(\theta_{sl})$ is the actual directional transmission BS steering vector for a scatterer at an angle, θ_{sl}, and given by (5-27). As the robust BS beamformer searches for the peak power value by varying $\hat{\boldsymbol{v}}_{\boldsymbol{y}}(\theta)$ in the uncertainty set around $\boldsymbol{v}_{\boldsymbol{y}}(\theta)$, when $\hat{\boldsymbol{v}}_{\boldsymbol{y}}(\theta)$ is coherent with $\acute{\boldsymbol{v}}_{\boldsymbol{ys}}$, the optimisation processing will generate an output peak. Therefore, it is easier to find a vector coherent with $\acute{\boldsymbol{v}}_{\boldsymbol{ys}}$ at the DOA of the strongest one in a group of coherent signals; whilst with a large uncertainty set, vectors around steering vectors at other DOAs of the coherent signals or angles near to the DOA of the strongest signal can be coherent with $\acute{\boldsymbol{v}}_{\boldsymbol{ys}}$ and thus generating more output peaks.

7.2.3 Apply DOA Estimation Algorithm for Coherent Signals in Directional Transmission BS to PTWR Experimental Data

As discussed in Chapter 6, for the directional transmission BS case, the returns from different stationary targets can be highly correlated and the correlation between signals can seriously degrade the performance of BS processing. In the examples shown in Section 7.2.2, some performance losses of the optimum and robust BS beamformers were found and the correlation between signals can be the possible reason.

For the H polarisation data in the range bin 44 of the fifth scan of the DSTG STF experimental data, the eigen-spectrum of the directional transmission BS covariance matrix is plotted in Figure 7-8 and it shows only one eigenvalue is significantly larger than the other eigenvalues. The metal tower and corner reflector were known and preplaced targets, and at least two separated targets (or its range sidelobes) have been clearly shown by the conventional beamformer output power in Figure 7-2 and Figure 7-6. This indicates that the strong correlation between the signals in this range bin occurred.

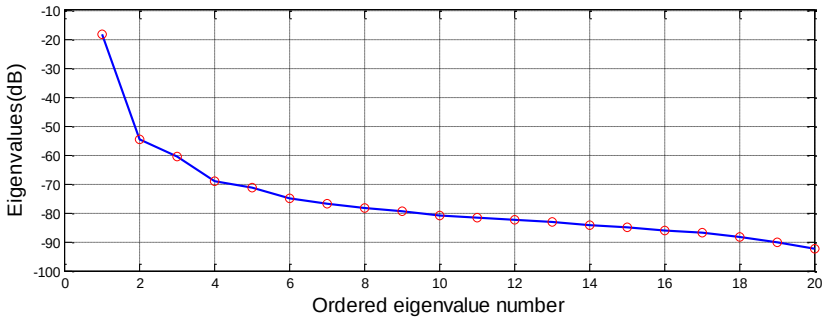

Figure 7-8: Eigenvalues of the BS covariance matrix estimated using the BS data in the range bin 44 of the fifth scan of the DSTG STF experimental data.

In Section 6.2.3, a method based on using the newly derived matrix, $\boldsymbol{Q_s}$, has been proposed for estimating the DOA of coherent signals. This matrix was estimated by using the BS data in the two range bins 44 or 52 and the results are shown in Figure 7-9 and Figure 7-10 for the two range bins respectively. In both cases it was assumed there were up to 10 correlated signals and so the maximal dimension of the signal subspace was 10. For a comparison purpose, the results of applying the conventional BS beamforming and BS MUSIC algorithm to the BS covariance matrix directly are also plotted. As expected, the performance of BS MUSIC without decorrelation was very poor, as the output peaks are weak and not obvious. The proposed DOA estimation method in Section 6.2.3 generates multiple strong peaks in both figures, and several peaks around the assumed locations of the preplaced targets appear at about the same azimuthal angles in both figures. The positions of the largest MUSIC output peak in Figure 7-9 (at ~ -1.5°) and in Figure 7-10 (at ~ -8.5°), correspond to the recorded angular positions of the corner reflector and metal tower. Additionally, the spatial separation between these two groups of peaks was calculated to be close to that recorded. The multiple peaks around the assumed DOAs of the stationary targets or range sidelobes are possibly multipath and are discussed in the next paragraph.

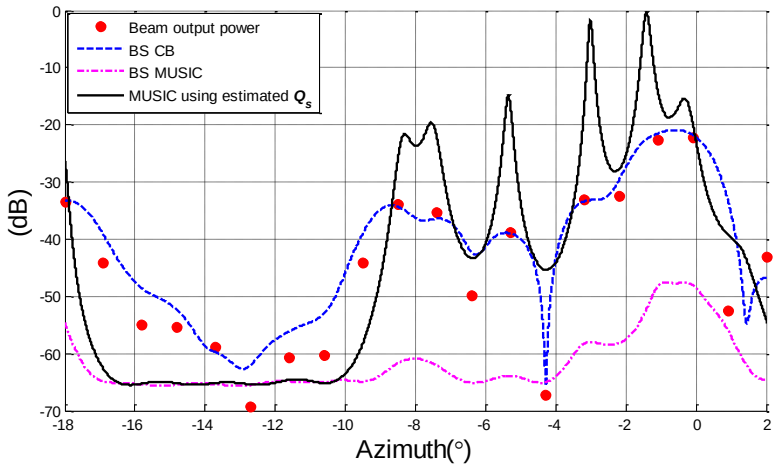

Figure 7-9: DOA estimation of returns in the range bin 44 of the fifth scan of the DSTG STF experimental data.

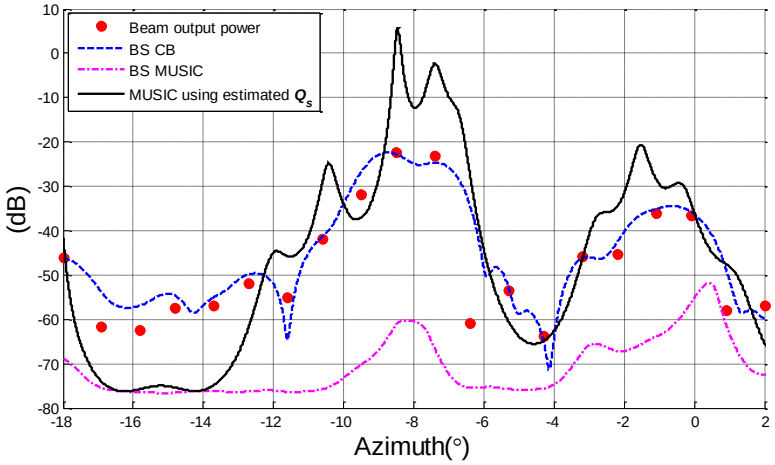

Figure 7-10: DOA estimation of returns in the range bin 52 of the fifth scan of the DSTG STF experimental data.

It was unexpected to find six or more targets in the two range bins of this experimental data, since only two targets with large RCS were preplaced, also an analysis of the experimental setup indicated that the calculation shows the corresponding physical distances between adjacent peaks of the MUSIC output were larger than the sizes of the metal tower and the corner reflector. However, the multiple strong peaks in the above two figures likely indicate the DOAs of the coherent signals, and it is possibly that some returns were caused by multipath. Considering that in order to detect the corner reflector (at about 6.5 m height), a low elevation steering angle (1°) and a relatively wide elevation beamwidth (2.8°) were used, the other returns might be signals bounced off from the main targets and then reflected by other unknown targets on the ground. Unfortunately, except for the two known and preplaced targets, the rest of the ground truth, including the exact number of signals, whether any additional targets existed, and whether multipath occurred, is unknown.

The performance of the proposed DOA estimation algorithm based on the derived matrix, $\boldsymbol{Q_s}$, is obviously better than the BS MUSIC without decorrelation. As shown in Figure 6-16, when 20 beams are used to span over a 20° angular sector, this method has limited resolution for DOA estimation, thus the above results are reasonable. As analysed in Chapter 6, increasing the number of beams would improve the accuracy of the DOA estimation and may provide sharper output peaks at the DOAs of signals, but unfortunately only 20 beams were formed in this experiment, which limits the potential for better performance. Also, possible phase array errors would degrade the performance of MUSIC and this might be another reason of that the output peaks are not very sharp. This issue about errors in subspace methods has been discussed in [102] and [103], but no solution has been suggested.

Since the accuracy of the DOA estimation for this data is not able to be verified and the phased array errors caused the actual steering vectors are unknown, the optimum LCMV BS beamformer for coherent signals, which is given in Section 6.3, will not be applied.

7.3 Summary

In this chapter, several proposed BS algorithms for the directional transmission case were tested on a set of real experimental data collected by using the PTWR. The result indicated that the directional transmission optimum BS beamformer proposed in Section 4.1.3 provided better performance than the standard optimum BS beamformer, but possibly due to phase array errors, the performance was still unsatisfactory. By applying the robust BS beamformer proposed in Section 5.4.3, promising results for signals with high SNRs were achieved. For the directional transmission case, the returns from different stationary targets can be coherent and caused poor performance of the BS processing algorithms. The DOA estimation algorithm developed in Section 6.2.3, which is based on an estimated matrix, $\widetilde{\boldsymbol{Q}}_{\boldsymbol{s}}$, was applied to the experimental data and achieved strong peaks of the MUSIC output. Some of these peaks were around the preselected azimuthal angles where the known targets were located. However, limited by the number of beams, it was not possible to check if a further improving performance would appear with a larger number of beams as described in Section 6.2.3.5. Limited by the collected data, such as the number of beams, and the lack of ground truth, i.e., the exact DOAs of known and additional unknown signals, meant that the performance of the developed algorithms could not be fully verified, but they still showed obvious superiority to existing methods and presented some promising results.

There might be better ways for further evaluating the developed BS processing techniques. Firstly, for the directional transmission optimum BS beamformer, an isolated but strong point target would avoid the issue of correlation. Secondly, if more details about the system calibration and errors were available, it might be possible to improve the evaluation of the robust BS beamformer. Thirdly, besides forming more Tx/Rx beams, if the locations of stationary scatterers were accurately surveyed and higher elevation angles were chosen to avoid returns from clutter, it would be easier to check the performance of DOA estimation for coherent signals in the BS cases.

The approaches in this thesis were developed for point targets, but obviously more complicated scenarios occurred in the experimental data. The results of applying BS processing to the experimental data revealed various issues when distributed scatters were observed. In general, for extended targets and clutter, the scatterers are angularly spread and the corresponding signal models [120], [121] and [122] are different from that being discussed in this thesis, thus the performance of the developed techniques are not guaranteed. For further analysis and research, there is the need to calibrate the returned power and relate it to the cross section per unit volume in case of weather or per unit area in case of ground clutter. Also it is worth investigating how to separate or distinguish the eigenvectors (and eigenvalues) for distributed (volume or surfaced) scatterers from those of point scatterers. This is because the proposed BS processing approaches for point scatterers could be applied to weather phased array radars for identifying returns from such scatterers and censor or filter these from weather contributions.

Chapter 8

Conclusion

In this thesis, the BS processing problem, especially for the case of directional transmit/receive beams scanned over a sector of interest, has been addressed and mainly three parts of theoretical development has been completed.

In the first part, the basic concept of phased array, ES signal processing and standard BS processing algorithms were introduced. The standard BS processing algorithms were not able to work effectively for the directional transmission BS case, due to the mismatch between the actual directional transmission steering vector and the assumed steering vector in the formulae. To solve this problem, new formulae taking account into the transmission beam pattern for the directional transmission BS model were developed and satisfactory results have been shown by theoretical analysis and evaluations using simulated data.

The second part of this thesis investigated the properties associated with the directional transmission BS processing. Problems related to the region outside the sector of interest were investigated. The optimum BS beamformer output power at the DOA of the interference outside the sector of interest was analysed, and then two methods were proposed to mitigate the high response outside the sector of interest, which is caused by the high gains of the noise components. The effect of an out of sector interference on the optimum BS beamformer output power inside the sector of interest was analysed and a method of mitigating the spurious peak inside the sector of interest was proposed. To improve the robustness of the optimum BS beamformer to different types of errors, an ES robust beamformer algorithm was extended to the directional transmission BS case and has shown strong robustness to errors. The CRB of DOA estimation was derived for the directional transmission BS case and compared with the CRBs for the omni-directional transmission ES and BS cases. Also, the performance of the directional transmission optimum BS beamformer was checked for the scenario containing a scatterer moving in the same range.

Similar to the ES case, signals in the BS model can be coherent or highly correlated. The third part of this thesis was focused on the DOA estimation techniques for coherent signals in BS. As the subarray methods are not applicable for most BS cases, a technique of reconstructing ES signal subspace from the BS signal subspace for the omni-directional transmission case was proposed. A newly derived matrix, which is the summation of the weighted self-outer products of the ES signal steering vectors, was proposed for the directional transmission BS case, and this matrix allows the DOAs of signals to be estimated regardless the coherence. A method was developed to estimate

this matrix from the BS covariance matrix. Then the power of the coherent signals can be readily estimated by a modified LCMV method.

Finally, those developed algorithms were applied to real experimental data containing stationary targets.

As the last chapter of this thesis, Section 8.1 summaries the main conclusions from each chapter and some potential future research work is discussed in Section 8.2.

8.1 Chapter Summaries

Chapter 2 Array Signal Processing Background This chapter briefly introduced basic concepts, knowledge and typical algorithms in ES spatial signal processing.

Chapter 3 Standard Beam Space Processing With a brief review of the standard BS mathematical model and spatial signal processing algorithms, the performance of standard optimum BS beamformer was checked through some examples using different numbers of beams. It showed that ES equivalent performance can be achieved by BS processing when the number of independent beams is the same as number of receivers for a full angular region, and when $\frac{\lambda}{d} < \frac{1}{2}$ provided the beams overlap at the their 3 dB beam pattern points and span the full angular sector, a smaller number of beams can be used for the optimum beamforming to achieve performance almost equivalent to that of the ES case. Also, when sufficient beams are formed in a sector of interest, signals in this subsector can be well estimated by the optimum BS beamformer. The case where the DOA of the interference lies out of the sector of interest is analysed and it showed that in most cases where signals and the interference are well spatially separated, the optimum BS beamformer output power at the DOA of in sector signals is only negligibly affected by the interference. On the other hand, to identify the interference using the optimum BS beamformer output power is complicated.

Chapter 4 Directional Transmission Beam Space Processing Due to the mismatch between the omni-directional transmission and directional transmission BS steering vectors, the performance of the standard BS formula to the model of directional transmission with relatively narrow scanning Tx/Rx beams was shown to be unsatisfactory. In this chapter, new BS algorithms specific for the directional transmission model were developed, and the optimum BS beamformer output power has been analysed theoretically and verified by numerical evaluation and simulation examples.

Chapter 5 Properties of Directional Transmission Beam Space Processing In this chapter, some properties of the directional transmission BS case were analysed. The problems related to the region outside the sector of interest were analysed in three aspects. It is difficult to identify the interference using the optimum BS beamformer output power, as the interference can be masked by the high response in the region

outside the sector of interest. Two methods were proposed to mitigate the high response caused by the high noise gain in this region. The method of virtual beams can mitigate the high response effectively but also removed the interference, whilst another proposed method – scaling beamforming removed the high response and kept the interference. However for the scaling method, the DOAs need to be estimated in advance and the method can fail at azimuthal angles far away from the sector. Additionally, an interference outside the sector of interest almost has no effect on the optimum BS beamformer output power values at DOAs inside the sector of interest, but can cause a spurious peak within the sector. To eliminate the spurious peak but keep the output power values at DOAs of signals unchanged, an oblique projection method was proposed. To deal with errors in BS processing, different array perturbations were analysed and a robust ES beamforming algorithm has been extended to the directional transmission BS case. Then, the CRB for DOA estimation in the directional transmission BS case was derived and analysed. As moving targets commonly occur in practice, to check how the motion of a scatterer affects the result of the optimum BS beamformer, its performance in a scenario containing both stationary and non-stationary scatterers was analysed.

Chapter 6 Beam Space Processing for Coherent Signals This chapter was focused on the DOA estimation and beamforming problems for coherent signals in BS. The coherence between incident signals can be caused by multipath or the same transmitted signal reflected from stationary scatterers at the same range. As the commonly used ES subarray methods cannot be directly used to remove the signal coherence in BS problem, a method of reconstructing ES signal covariance matrix for the omni-directional transmission case was proposed and verified by some examples. Then, a newly derived matrix was proposed for estimating the DOAs of coherent signals in the directional transmission BS case, since it allowed the DOAs to be estimated by existing subspace methods regardless the coherence. A method was developed to estimate the matrix from the principal eigenvector of the directional transmission BS covariance matrix. The LCMV BS beamformer was modified for the case of coherent signals and verified through an example.

Chapter 7 Application of Beam Space Processing to Real Experimental Data In this chapter, several developed BS processing algorithms for the directional transmission case were applied to a set of real experimental data collected by using the PTWR. The result indicated that the directional transmission optimum BS beamformer has better performance than the standard optimum BS beamformer. Due to phase array errors, the performance of the directional transmission optimum BS beamformer was unsatisfactory, and the robust BS beamformer was applied and it showed an improved performance. The algorithm for DOA estimation for coherent signals in the directional transmission BS case generated strong output peaks around the angular region where preselected targets were located.

8.2 Future Work

In this thesis, only the scenario that deterministic signals mixed with spatial white noise are incident on a uniform linear array has been considered for spatial processing. The developed BS methods can be extended or further developed for other scenarios, for example, other types of Tx/Rx systems, signal and noise models with some variations. Also, some other expressions of representative of BS data can be considered and a few other signal processing methods are worth to be investigated for BS processing.

Firstly, only ULA was considered in this thesis, whilst phased arrays, whose elements are placed in other geometries, have some advantages and are also commonly used in practice. For example, uniform circular arrays (UCA) have the same aperture for all beam Tx/Rx directions and can estimate DOAs in both azimuth and elevation. As shown in the literature [107], [108] and [109], BS processing can be used to map and approximate the manifold vectors for an arbitrary array onto Vandermonde ULA type steering vectors in an interpolated array concept [110]. These developed BS processing algorithms in this thesis can be extended to and further investigated for arrays of other shapes.

Secondly, BS spatial processing methods were mainly investigated for the model of stationary point scatterers. The results of applying BS processing to experimental data in Chapter 7 revealed various issues in the case of distributed scatters. For further analysis and research, there is the need to calibrate the returned power and relate it to the cross section per unit volume in case of weather or per unit area in case of ground clutter. Also it is worth investigating how to separate or distinguish the eigenvectors (and values) for distributed (volume or surfaced) scatterers from those of point scatterers. This is because the proposed BS processing for point scatterers could be applied to weather phased array radars for identifying returns from such scatterers and censor or filter these from weather contributions. Also in practice, the models containing non-stationary targets or a mixture of both stationary and non-stationary targets are common or standard, for example, fast moving aircrafts, volume scans of weather phenomenon can be mixed with stationary ground clutter returns. Similarly, phased arrays can be mounted on moving platforms, such as a ship or an aircraft, and can be used as multi-channel synthetic aperture radar. For such a moving array, the phase of returns from a stationary target changes from pulse to pulse, this adds more difficulties for array processing but also brings some extra advantages, such as the signal coherence can be easily removed. Most literature for moving arrays, such as [97], discusses this problem from robustness aspect and the result is similar to the moving interference or target problem discussed in Section 5.6. Some sophisticated techniques, such as motion composition, could be considered and incorporated into the BS processing to improve the performance. Furthermore, spatial time BS processing can be investigated for the problems of non-stationary, volume scatterers and clutter mitigation.

Thirdly, the key modification for the directional transmission BS formulae is to take the transmission beam pattern into account. If the transmission and receive beam patterns are known, the concept of developed BS processing algorithms can be potentially extended to other radar or communication systems, such as a conventional dish radar which mechanically rotates and scans over a region contains stationary scatterers, a bistatic radar whose receiver and transmitter beam patterns are different, and a multiple-input and multiple-output (MIMO) system with a distributed transmitters and receivers.

Fourthly, more work for the BS processing with noise and perturbations can be considered. Only the spatial and temporal white noise has been considered in this thesis, but coloured noise occurs naturally in many practical applications and would affect the performance of array processing methods based on the white noise model, especially for the low SNR case. Some ES array processing methods for estimating signals in coloured noise such as discussed in [43] and [111] can be extended into BS processing, whilst non-independent beams may add correlations between noises in different beams. To deal with the phased array and beam direction errors in BS processing, robust beamformer has been considered, further work of increasing robustness can be extended to other algorithms, such as BS MUSIC. Also, calibration can be potentially investigated for the BS case.

Finally, as mentioned in Chapter 6, the covariance matrix is the most common but not the only way to represent signals incident at a phased array, other expressions can be considered for BS processing, such as a higher order cumulants [112], [113] and [114]. Also in Section 6.2.3, a vector, $vec[\widetilde{\boldsymbol{Q}}_{\boldsymbol{s}}]$, was estimated using the principal eigenvector of the directional transmission BS covariance matrix, and then it was reshaped to be a matrix $\widetilde{\boldsymbol{Q}}_{\boldsymbol{s}}$. Rather than simply reshaping the vector as a matrix, generating a matrix or other expressions based on this vector and following signal processing techniques can be further investigated. Unfortunately, limited by the time, this investigation has not been carried out in this thesis. In some ES literature such as [115], ES covariance matrix is reshaped as a vector to utilise the cross correlation between elements output and expand a virtual array with a larger aperture. Additionally, some recently developed ES array processing algorithms, such as sparse signal representation [116], which provides super resolution for DOA estimation problem, can be considered and further investigated for BS processing.

Appendix A

Linear Transformation between Subspaces of Omni-directional Transmission ES and BS

Section 3.2.4 discussed the linear transformation between a subset of the noise eigenvectors of the ES covariance matrix and noise eigenvectors of the BS covariance matrix. Also in Section 6.2.2 discussed estimating the ES generalised coherent signal steering vector from the BS generalised coherent signal steering vector. This Appendix will introduce more details about the linear transformation between the ES and BS subspaces.

A.1. Independent Signals Case

The eigen-decomposition of the omni-directional ES covariance matrix is given by

$$\boldsymbol{R_x} = \sum_{i=1}^{K} \lambda_i \boldsymbol{q}_i \boldsymbol{q}_i^H = \boldsymbol{Q\Lambda Q}^H. \tag{A-1}$$

When the incident signals are independent, the signal subspace is given by

$$\boldsymbol{E_{sx}} = span\{\boldsymbol{q}_1 \quad \cdots \quad \boldsymbol{q}_L\}, \tag{A-2}$$

where L is the number of independent signals and $\boldsymbol{E_{sx}}$ is spanned by a set of eigenvectors corresponding to the largest L eigenvalues. The noise subspace is given by

$$\boldsymbol{E_{nx}} = span\{\boldsymbol{q}_{L+1} \quad \cdots \quad \boldsymbol{q}_K\}, \tag{A-3}$$

where K is the number of receivers.

The steering vectors at the DOAs of signals also span the same signal subspace, thus

$$\boldsymbol{E_{sx}} = span\{\boldsymbol{v}(\theta_{s1}) \quad \ldots \quad \boldsymbol{v}(\theta_{sL})\}. \tag{A-4}$$

Since the eigenvectors are mutually orthogonal, all the noise eigenvectors are orthogonal to any vector in the signal subspace; and this is the principle of how the subspace methods work and so

$$\boldsymbol{v}^H(\theta_{sl})\boldsymbol{q}_i = 0, l \leq L, i > L. \tag{A-5}$$

In omni-directional transmission with white noise case, the BS covariance matrix is a linear transformation of the ES covariance matrix and is given by

$$\boldsymbol{R_y} = \boldsymbol{V}^H \boldsymbol{R_x} \boldsymbol{V} = \boldsymbol{V}^H \boldsymbol{V_s}(\Theta_s) \boldsymbol{R_s} \boldsymbol{V_s}^H(\Theta_s) \boldsymbol{V} + \sigma_n^2 \boldsymbol{V}^H \boldsymbol{V}, \tag{A-6}$$

where $\boldsymbol{R_s}$ denotes the source signal covariance matrix. The eigen-decomposition of $\boldsymbol{R_y}$ is given by

$$\begin{gathered} \boldsymbol{R_y} = \sum_{i=1}^{M} \lambda_{yi} \boldsymbol{q_{yi}} \boldsymbol{q_{yi}}^H, \\ \lambda_{yi} > \sigma_n^2, (i \le L), \text{ and } \lambda_{yi} = \sigma_n^2, (i > L), \end{gathered} \tag{A-7}$$

Similar to the ES case, the BS steering vectors at the DOAs of signals also span the same signal subspace as the BS eigenvector corresponding to the largest L eigenvalues

$$\boldsymbol{E_{sy}} = span\{\boldsymbol{h}(\theta_{s1}) \quad \ldots \quad \boldsymbol{h}(\theta_{sL})\} = span\{\boldsymbol{q}_{\mathbf{y}1} \quad \cdots \quad \boldsymbol{q}_{yL}\}, \tag{A-8}$$

and any vector in this space, such as the BS steering vector at the DOA of the l −th signal, $\boldsymbol{h}^H(\theta_{sl})$, is orthogonal to those BS noise eigenvectors, and this is given by

$$\boldsymbol{h}^H(\theta_{sl}) \boldsymbol{q_{yi}} = \boldsymbol{v}^H(\theta_{sl}) \boldsymbol{V} \boldsymbol{q_{yi}} = 0, l \le L, i > L. \tag{A-9}$$

Thus it shows the K×1 vector $\boldsymbol{V q_{yi}}, (i > L)$ is orthogonal to any ES steering vectors at the DOAs of the signals. Then the following relationship exists

$$\begin{aligned} \boldsymbol{R_x V q_{yi}} &= \left(\sum_{l=1}^{L} \sigma_l^2 \boldsymbol{v}(\theta_{sl}) \boldsymbol{v}^H(\theta_{sl}) + \sigma_n^2 \boldsymbol{I} \right) \boldsymbol{V q_{yi}} \\ &= \sum_{l=1}^{L} \sigma_l^2 \boldsymbol{v}(\theta_{sl}) \boldsymbol{h}^H(\theta_{sl}) \boldsymbol{q_{yi}} + \sigma_n^2 \boldsymbol{V q_{yi}} \\ &= \sigma_n^2 \boldsymbol{V q_{yi}}. \end{aligned} \tag{A-10}$$

Obviously, $\boldsymbol{V q_{yi}}$ is one of the noise space eigenvectors of the ES covariance matrix $\boldsymbol{R_x}$.

A.2. Coherent Signals Case

For the omni-directional transmission case, a group of coherent signals are incident on a ULA phased array, the rank of the ES signal subspace is one and it can be represented as

$$\boldsymbol{V_s}(\Theta_s) \boldsymbol{R_s} \boldsymbol{V_s}^H(\Theta_s) = \boldsymbol{v_s} \boldsymbol{v_s}^H, \tag{A-11}$$

where $\boldsymbol{v}_s$ is the generalised coherent signal vector and given by

$$\boldsymbol{v_s} = \sum_{l=1}^{L} \rho_l \sigma_{sl} \boldsymbol{v}(\theta_{sl}). \tag{A-12}$$

and the ES covariance matrix is given by

$$\boldsymbol{R_x} = \boldsymbol{v_s}\boldsymbol{v_s}^H + \sigma_n^2\boldsymbol{I}. \tag{A-13}$$

The eigen-decomposition of the ES covariance matrix is given by

$$\boldsymbol{R_x} = \lambda_1\boldsymbol{q}_1\boldsymbol{q}_1^H + \sum_{i=2}^{K}\lambda_i\boldsymbol{q}_i\boldsymbol{q}_i^H, \tag{A-14}$$

where $\lambda_1 = \sigma_s^2 + \sigma_n^2$, $\lambda_i = \sigma_n^2$ $(2 \le i \le K)$ and $\boldsymbol{q}_1 = \frac{e^{i\varphi}}{\|\boldsymbol{v_s}\|}\boldsymbol{v_s}$, where σ_s^2 is the combined power of the coherent signals and is given by $\sigma_s^2 = \|\boldsymbol{v_s}\|^2$.

For a group of coherent signals in the omni-directional transmission BS case, the generalised coherent BS steering vector is denoted as $\boldsymbol{h_s}$ and is given by

$$\boldsymbol{h_s} = \boldsymbol{V}^H\boldsymbol{v_s} = \sum_{l=1}^{L}\rho_l\sigma_{sl}\boldsymbol{h}(\theta_{sl}) \tag{A-15}$$

and is proportional to the principal eigenvector of BS covariance matrix, i.e.,

$$\boldsymbol{h_s} = e^{-j\varphi}\|\boldsymbol{h_s}\|\boldsymbol{q}_{\boldsymbol{y}1}, \tag{A-16}$$

where $e^{j\varphi}$ is a phase shift. In this case, the BS covariance matrix can be written as

$$\begin{aligned}\boldsymbol{R_y} &= \boldsymbol{V}^H\boldsymbol{R_x}\boldsymbol{V}\\ &= \boldsymbol{V}^H\boldsymbol{v_s}\boldsymbol{v_s}^H\boldsymbol{V} + \sigma_n^2\boldsymbol{I}\\ &= \boldsymbol{h_s}\boldsymbol{h_s}^H + \sigma_n^2\boldsymbol{I}\end{aligned} \tag{A-17}$$

The eigen-decomposition of $\boldsymbol{R_y}$ is given by

$$\begin{gathered}\boldsymbol{R_y} = \textstyle\sum_{i=1}^{M}\lambda_{yi}\boldsymbol{q}_{\boldsymbol{y}i}\boldsymbol{q}_{\boldsymbol{y}i}^H,\\ \lambda_{y1} = \frac{\|\boldsymbol{h_s}\|^2}{\|\boldsymbol{v_s}\|^2}\sigma_s^2 + \sigma_n^2 > \sigma_n^2, \lambda_{yi} = \sigma_n^2, (i \ge 2)\end{gathered} \tag{A-18}$$

The eigenvectors are mutually orthogonal, thus

$$\boldsymbol{q}_{\boldsymbol{y}i}^H\boldsymbol{h_s} = 0, 1 < i \leqslant M. \tag{A-19}$$

It follows that

$$\begin{aligned}\boldsymbol{V}\boldsymbol{R_y}\boldsymbol{V}^H &= \sum_{i=1}^{M}\lambda_{yi}\boldsymbol{V}\boldsymbol{q}_{\boldsymbol{y}i}\boldsymbol{q}_{\boldsymbol{y}i}^H\boldsymbol{V}^H\\ &= \left(\frac{\|\boldsymbol{h_s}\|^2}{\|\boldsymbol{v_s}\|^2}\sigma_s^2 + \sigma_n^2\right)\boldsymbol{V}\boldsymbol{q}_{\boldsymbol{y}1}\boldsymbol{q}_{\boldsymbol{y}1}^H\boldsymbol{V}^H + \sigma_n^2\sum_{i=2}^{M}\boldsymbol{V}\boldsymbol{q}_{\boldsymbol{y}i}\boldsymbol{q}_{\boldsymbol{y}i}^H\boldsymbol{V}^H\end{aligned} \tag{A-20}$$

As $\boldsymbol{R_y} = \boldsymbol{V}^H \boldsymbol{R_x} \boldsymbol{V}$, the above equation can also be written as

$$\begin{aligned}
\boldsymbol{V}\boldsymbol{V}^H \boldsymbol{R}_x \boldsymbol{V}\boldsymbol{V}^H &= \sum_{i=1}^{K} \boldsymbol{V}\boldsymbol{V}^H \lambda_i \boldsymbol{q}_i \boldsymbol{q}_i^H \boldsymbol{V}\boldsymbol{V}^H \\
&= (\sigma_s^2 + \sigma_n^2)\boldsymbol{V}\boldsymbol{V}^H \boldsymbol{q}_1 \boldsymbol{q}_1^H \boldsymbol{V}\boldsymbol{V}^H + \sigma_n^2 \sum_{i=2}^{M} \boldsymbol{V}\boldsymbol{V}^H \boldsymbol{q}_i \boldsymbol{q}_i^H \boldsymbol{V}\boldsymbol{V}^H + \sigma_n^2 \sum_{i=M+1}^{K} \boldsymbol{V}\boldsymbol{V}^H \boldsymbol{q}_i \boldsymbol{q}_i^H \boldsymbol{V}\boldsymbol{V}^H \\
&= \frac{\sigma_s^2 + \sigma_n^2}{\|\boldsymbol{v}_s\|^2} \boldsymbol{V}\boldsymbol{V}^H \boldsymbol{v}_s \boldsymbol{v}_s^H \boldsymbol{V}\boldsymbol{V}^H + \sigma_n^2 \sum_{i=2}^{M} \boldsymbol{V}\boldsymbol{V}^H \boldsymbol{q}_i \boldsymbol{q}_i^H \boldsymbol{V}\boldsymbol{V}^H + \sigma_n^2 \sum_{i=M+1}^{K} \boldsymbol{V}\boldsymbol{V}^H \boldsymbol{q}_i \boldsymbol{q}_i^H \boldsymbol{V}\boldsymbol{V}^H \\
&= \frac{\sigma_s^2 + \sigma_n^2}{\|\boldsymbol{v}_s\|^2} \boldsymbol{V}\boldsymbol{h}_s \boldsymbol{h}_s^H \boldsymbol{V}^H + \sigma_n^2 \sum_{i=2}^{M} \boldsymbol{V}\boldsymbol{V}^H \boldsymbol{V}\boldsymbol{q}_{yi} \boldsymbol{q}_{yi}^H \boldsymbol{V}^H \boldsymbol{V}\boldsymbol{V}^H + \sigma_n^2 \sum_{i=M+1}^{K} \boldsymbol{V}\boldsymbol{V}^H \boldsymbol{q}_i \boldsymbol{q}_i^H \boldsymbol{V}\boldsymbol{V}^H \\
&= \frac{\|\boldsymbol{h}_s\|^2(\sigma_s^2 + \sigma_n^2)}{\|\boldsymbol{v}_s\|^2} \boldsymbol{V}\boldsymbol{q}_{y1} \boldsymbol{q}_{y1}^H \boldsymbol{V}^H + \sigma_n^2 \sum_{i=2}^{M} \boldsymbol{V}\boldsymbol{q}_{yi} \boldsymbol{q}_{yi}^H \boldsymbol{V}^H + \sigma_n^2 \sum_{i=M+1}^{K} \boldsymbol{V}\boldsymbol{V}^H \boldsymbol{q}_i \boldsymbol{q}_i^H \boldsymbol{V}\boldsymbol{V}^H.
\end{aligned} \tag{A-21}$$

Where the orthogonality of the M beams, i.e., $\boldsymbol{V}^H \boldsymbol{V} = \boldsymbol{I}_{M\times M}$, has been assumed. Comparing (A-20) and (A-21), it follows that

$$\left(\frac{\|\boldsymbol{h}_s\|^2}{\|\boldsymbol{v}_s\|^2}\sigma_s^2 + \sigma_n^2\right)\boldsymbol{V}\boldsymbol{q}_{y1}\boldsymbol{q}_{y1}^H\boldsymbol{V}^H = \frac{\|\boldsymbol{h}_s\|^2(\sigma_s^2+\sigma_n^2)}{\|\boldsymbol{v}_s\|^2}\boldsymbol{V}\boldsymbol{q}_{y1}\boldsymbol{q}_{y1}^H\boldsymbol{V}^H + \sigma_n^2\sum_{i=M+1}^{K}\boldsymbol{V}\boldsymbol{V}^H\boldsymbol{q}_i\boldsymbol{q}_i^H\boldsymbol{V}\boldsymbol{V}^H. \tag{A-22}$$

As indicated in Figure 6-7, provided a sufficient number of beams are used, $\frac{\|\boldsymbol{h}_s\|^2}{\|\boldsymbol{v}_s\|^2}$ =1. In this case it follows for (A-22) that

$$\sigma_n^2 \textstyle\sum_{i=M+1}^{K} \boldsymbol{V}\boldsymbol{V}^H \boldsymbol{q}_i \boldsymbol{q}_i^H \boldsymbol{V}\boldsymbol{V}^H = 0, \tag{A-23}$$

since $\sigma_n^2 > 0$ and $\boldsymbol{V}\boldsymbol{V}^H \boldsymbol{q}_i \boldsymbol{q}_i^H \boldsymbol{V}\boldsymbol{V}^H \geq 0$ hence,

$$\boldsymbol{q}_{M+1}^H \boldsymbol{V}\boldsymbol{V}^H = \boldsymbol{q}_{M+2}^H \boldsymbol{V}\boldsymbol{V}^H = \cdots \boldsymbol{q}_K^H \boldsymbol{V}\boldsymbol{V}^H = 0, (M < i \leq K), \tag{A-24}$$

thus $$\boldsymbol{q}_i^H \boldsymbol{V}\boldsymbol{q}_{y1} = \boldsymbol{q}_i^H \boldsymbol{V}\boldsymbol{V}^H \boldsymbol{V}\boldsymbol{q}_{y1}=0, M < i \leq K. \tag{A-25}$$

Also consider that

$$\boldsymbol{q}_i^H \boldsymbol{V}\boldsymbol{q}_{y1} = \boldsymbol{q}_{yi}^H \boldsymbol{q}_{y1} = 0, 2 \leq i \leq M \tag{A-26}$$

Combining the above two expressions gives

$$\boldsymbol{q}_i^H \boldsymbol{V}\boldsymbol{q}_{y1} = 0, i \geq 2 \tag{A-27}$$

Therefore, it means $\boldsymbol{V}\boldsymbol{q}_{y1}$ is orthogonal to the ES noise subspace and coherent with the ES generalised coherent signal steering vector.

Appendix B

Details of Perturbations in the Robust BS Beamforming Example

In Section 5.4.4, there was an example of applying robust optimum BS beamforming to a BS model with perturbations. The perturbations include random element complex gain errors, array element location errors and beam steering angle errors and the details are as follows

(a) Random array element complex gain errors μ_k ($|\mu_k|$~unif(0.75 , 1.25) and $\angle\mu_k$~unif($-\frac{\pi}{3}$, $\frac{\pi}{3}$)) were generated. These errors can be caused by different factors such as imperfect electronic components, component parameters drift with different temperature. The amplitudes and phases of the element gain errors are shown in Figure B-1 and Figure B-2 respectively.

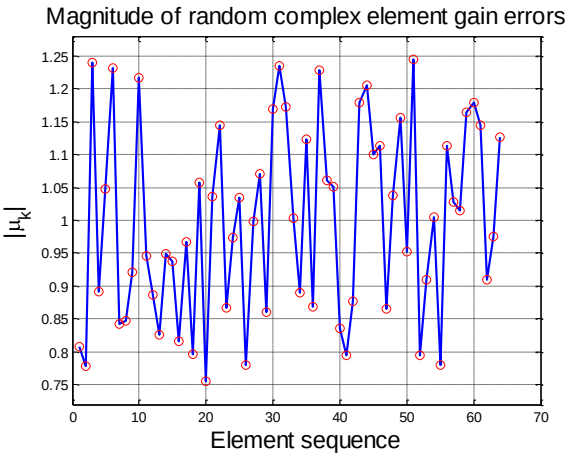

Figure B-1: Amplitudes of element gain errors

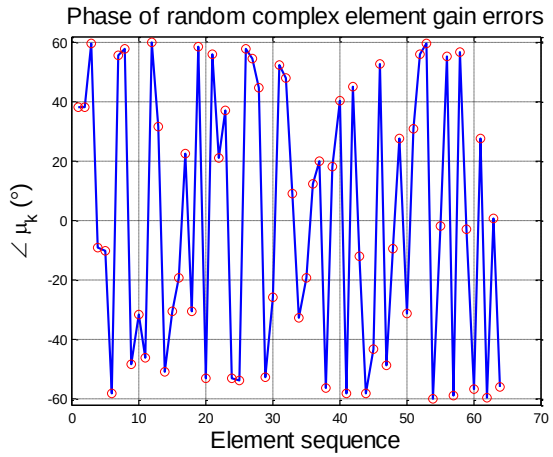

Figure B-2: Phases of element gain errors.

(b) Random array element location errors $\delta_k \sim \text{unif}(-0.1\text{d}, 0.1\text{d})$. These errors are caused by inaccurate positions in the installation and each location error is normalised as a ratio to the assumed distance between elements, *d*, which is half a wavelength.

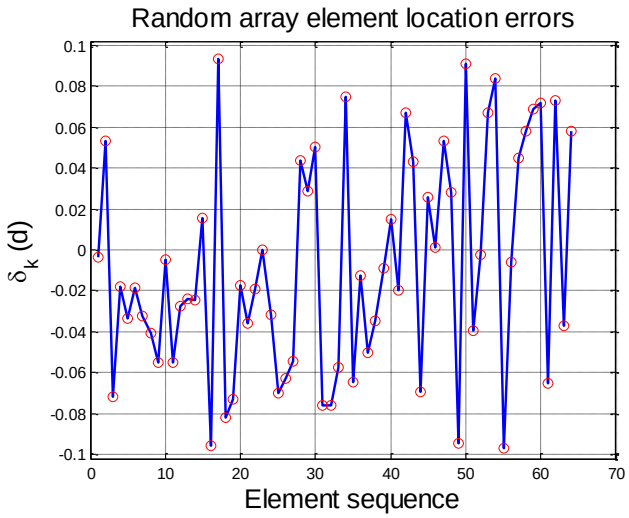

Figure B-3: Element location errors.

All the element errors in (a) and (b) are listed in Table B-1.

Table B-1: Details of the phased array element errors

Element ID	Amplitude gain error	Phase gain error (°)	Location error (d=λ/2)
1	0.81	38.21	0.00
2	0.78	38.17	0.05
3	1.24	59.53	-0.07
4	0.89	-9.25	-0.02
5	1.05	-10.26	-0.03
6	1.23	-58.15	-0.02
7	0.84	55.52	-0.03
8	0.85	57.98	-0.04
9	0.92	-48.46	-0.05
10	1.22	-31.62	0.00
11	0.95	-46.06	-0.06
12	0.89	59.97	-0.03
13	0.83	31.72	-0.02
14	0.95	-51.01	-0.02
15	0.94	-30.45	0.02
16	0.82	-19.22	-0.10
17	0.97	22.45	0.09
18	0.80	-30.43	-0.08
19	1.06	58.55	-0.07
20	0.76	-52.98	-0.02
21	1.04	55.92	-0.04
22	1.14	21.20	-0.02
23	0.87	37.25	0.00
24	0.97	-53.19	-0.03

25	1.03	-53.78	-0.07
26	0.78	57.88	-0.06
27	1.00	54.59	-0.05
28	1.07	44.71	0.04
29	0.86	-52.84	0.03
30	1.17	-25.88	0.05
31	1.24	52.54	-0.08
32	1.17	48.02	-0.08
33	1.00	8.98	-0.06
34	0.89	-32.75	0.07
35	1.12	-19.32	-0.06
36	0.87	12.33	-0.01
37	1.23	19.92	-0.05
38	1.06	-56.44	-0.03
39	1.05	18.05	-0.01
40	0.84	40.34	0.01
41	0.80	-58.15	-0.02
42	0.88	45.18	0.07
43	1.18	-12.11	0.04
44	1.21	-58.27	-0.07
45	1.10	-43.36	0.03
46	1.11	52.81	0.00
47	0.86	-48.57	0.05
48	1.04	-9.45	0.03
49	1.16	27.56	-0.09
50	0.95	-31.20	0.09
51	1.24	30.90	-0.04
52	0.79	55.91	0.00
53	0.91	59.77	0.07
54	1.01	-59.91	0.08
55	0.78	-1.80	-0.10
56	1.11	55.30	-0.01
57	1.03	-58.85	0.05
58	1.01	56.55	0.06
59	1.16	-2.88	0.07
60	1.18	-56.79	0.07
61	1.14	27.50	-0.07
62	0.91	-59.47	0.07
63	0.98	0.62	-0.04
64	1.13	-55.93	0.06

(c) For the BS case, another kind of error—random independent steering beam centres (MRAs) angle errors $\phi_m \sim \text{unif}(-0.3°, 0.3°)$ were generated. These errors can be caused by inaccurate beamforming direction parameters or an inaccurate record. The details are shown in Figure B-4 and Table B-2.

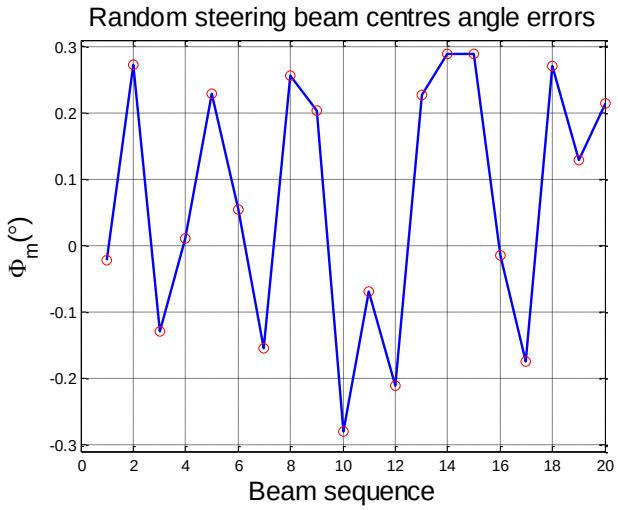

Figure B-4: Tx/Rx beam steering centre angle errors.

Table B-2: Details of a phased array beam steering centre angle errors

Beam ID	Assumed steering MRA (°)	Actual steering MRA (°)
1	1.00	0.98
2	2.00	2.27
3	3.00	2.87
4	4.00	4.01
5	5.00	5.23
6	6.00	6.06
7	7.00	6.84
8	8.00	8.26
9	9.00	9.20
10	10.00	9.72
11	11.00	10.93
12	12.00	11.79
13	13.00	13.23
14	14.00	14.29
15	15.00	15.29
16	16.00	15.98
17	17.00	16.83
18	18.00	18.27
19	19.00	19.13
20	20.00	20.21

Appendix C

Cramér–Rao Bounds for DOA Estimation in ES and BS

This appendix provides some details of the CRB derivations in Section 5.5. Consider a ULA with K receivers that receives the L far-field narrowband independent signals from different directions at $\Theta_s = \{\theta_{s1}, \theta_{s2}, \ \ldots, \ \theta_{sL}\}$. Assuming the receiver noise is both spatial and temporal white, the array receiver output vector and covariance matrix are given by

$$\begin{aligned} \boldsymbol{x}(t) &= \boldsymbol{V_s}(\Theta_s)\boldsymbol{s}(t) + n(t), \\ \boldsymbol{R_x} &= \boldsymbol{V_s}\boldsymbol{R_s}\boldsymbol{V_s}^H + \sigma_n^2 I, \end{aligned} \tag{C-1}$$

where $\boldsymbol{R_s}$ is the source signal covariance matrix and if the signals are uncorrelated, it can be expressed as

$$\boldsymbol{R_s} = diag\{\sigma_{s_1}^2, \ \sigma_{s_2}^2, \ \ldots, \ \sigma_{s_L}^2\}. \tag{C-2}$$

C.1. Cramér–Rao Bounds for DOA Estimation in ES Case

To estimate the DOAs of these signals, the probability density for a single snapshot (sample of receiver outputs) vector at time t is given by

$$p_{\boldsymbol{x}|\Theta_s} = \frac{1}{\det(\pi \boldsymbol{R_x})} \exp\left(-(\boldsymbol{x}^H(t) - \boldsymbol{m_s}^H)\boldsymbol{R_x}^{-1}(\boldsymbol{x}(t) - \boldsymbol{m_s})\right). \tag{C-3}$$

where $\boldsymbol{m_s}$ denotes the mean of signal component in the receiver outputs. With N independent snapshots vectors, $\boldsymbol{x}(t)$, the probability becomes

$$p_{\boldsymbol{x}(1),\boldsymbol{x}(2),\ldots\boldsymbol{x}(N)|\Theta_s} = \prod_{t=1}^{N} \frac{\exp\left(-(\boldsymbol{x}^H(t)-\boldsymbol{m_s}^H)\boldsymbol{R_x}^{-1}(\boldsymbol{x}(t)-\boldsymbol{m_s})\right)}{\det(\pi \boldsymbol{R_x})}. \tag{C-4}$$

The likelihood function can be written as

$$L(\Theta_s) = -Nln\{det(\boldsymbol{R_x})\} - \sum_{n=1}^{N} (\boldsymbol{x}^H(t) - \boldsymbol{m_s}^H)\boldsymbol{R_x}^{-1}(\boldsymbol{x}(t) - \boldsymbol{m_s}) - NKln\pi, \tag{C-5}$$

where the last part is a constant and can be ignored, also the parameter $\boldsymbol{m_s}$ is zero for a random signal or a constant for a deterministic signal, which is not a function of Θ_s. Therefore, the likelihood function can be simplified and rewritten as

$$L(\Theta_s) = -ln\{\det[\boldsymbol{R_x}]\} - 1/\mathrm{N}\sum_{n=1}^{N} \boldsymbol{x}^H(t)\boldsymbol{R_x}^{-1}\boldsymbol{x}(t). \tag{C-6}$$

Denoting the covariance matrix of the estimation errors by

$$\boldsymbol{C_e}(\Theta_s) = E\left\{\left(\hat{\Theta}_s - \Theta_s\right)\left(\hat{\Theta}_s - \Theta_s\right)^T\right\}, \tag{C-7}$$

and it is never smaller than the Cramér Rao bounds:

$$\boldsymbol{C_e}(\Theta_s) \geq \boldsymbol{C}_{CR}(\Theta_s) \triangleq \boldsymbol{\mathcal{F}}^{-1}, \tag{C-8}$$

where $\boldsymbol{\mathcal{F}}$ is Fisher's information matrix and is given by

$$\boldsymbol{\mathcal{F}} = -E\left\{\nabla_{\Theta_s}\left(\nabla_{\Theta_s}\left(L(\Theta_s)\right)\right)^T\right\}. \tag{C-9}$$

Using a simplified notation where an $L\times1$ vector $\boldsymbol{\varphi}$ corresponds to the set of DOAs and whose l–th element is given by $\varphi_l = \pi sin\theta_{sl}$, the elements in $\boldsymbol{\mathcal{F}}$ is given by

$$\begin{aligned}\boldsymbol{\mathcal{F}}_{ij} &= -E\left\{\frac{\partial L(\varphi)}{\partial \varphi_i}\frac{\partial L(\varphi)}{\partial \varphi_j}\right\} \\ &= -E\left\{\frac{\partial^2 L(\varphi)}{\partial \varphi_i\, \partial \varphi_j}\right\}.\end{aligned} \tag{C-10}$$

When the signal vector is a sample of Gaussian random process or deterministic, the above equation can be simplified to

$$\boldsymbol{\mathcal{F}}_{ij} = \mathrm{tr}\left[\boldsymbol{R}_{\mathrm{x}}^{-1}\frac{\partial \boldsymbol{R}_x}{\partial \varphi_i}\boldsymbol{R_x}^{-1}\frac{\partial \boldsymbol{R}_x}{\partial \varphi_j}\right], \tag{C-11}$$

where for a random white noise with power σ_n^2, $\boldsymbol{R_x}^{-1}$ is given by

$$\boldsymbol{R_x}^{-1} = 1/\sigma_n^2[\boldsymbol{I} - \boldsymbol{V_s}(\boldsymbol{V_s}^H\boldsymbol{V_s} + \sigma_n^2\boldsymbol{R_s}^{-1})^{-1}\boldsymbol{V_s}^H], \tag{C-12}$$

and the partial derivative of the ES covariance matrix is given by

$$\begin{aligned}\frac{\partial \boldsymbol{R}_x}{\partial \varphi_i} &= \frac{\partial \boldsymbol{V_s}}{\partial \varphi_i}\boldsymbol{R_s}\boldsymbol{V_s}^H + \boldsymbol{V_s}\boldsymbol{R_s}\frac{\partial \boldsymbol{V_s}^H}{\partial \varphi_i}, \\ \frac{\partial \boldsymbol{V_s}}{\partial \varphi_i} &= \frac{\partial \boldsymbol{v}(\varphi)}{\partial \varphi}|_{\varphi=\varphi_i} = \boldsymbol{d}(\varphi_\mathrm{i}).\end{aligned} \tag{C-13}$$

According to [71], [72] and [92], when the signal vector is a sample of Gaussian random process, the Cramér Rao bounds can be written as

$$\boldsymbol{C}_{CR}(\boldsymbol{\varphi}) = \frac{\sigma_n^2}{2N}\{Re[(\boldsymbol{D}^H\boldsymbol{P}_{\boldsymbol{V}}^{\perp}\boldsymbol{D}) \circ (\boldsymbol{R}_{\boldsymbol{s}}\boldsymbol{V}_{\boldsymbol{s}}^H\boldsymbol{R}_{\boldsymbol{x}}^{-1}\boldsymbol{V}_{\boldsymbol{s}}\boldsymbol{R}_{\boldsymbol{s}})^T]\}^{-1}, \tag{C-14}$$

and when the signal vector is deterministic, $\boldsymbol{s}(n)$ is a non-random L×1 complex source signal vector, then the Cramér Rao bounds can be written as

$$\begin{aligned}\boldsymbol{C}_{CR}(\boldsymbol{\varphi}) &= \frac{\sigma_n^2}{2}\left\{\sum_{n=1}^{N} Re\left[\boldsymbol{s}^H(n)\boldsymbol{D}^H\boldsymbol{P}_{\boldsymbol{V}_s}^{\perp}\boldsymbol{D}\boldsymbol{s}(n)\right]\right\}^{-1} \\ &= \frac{\sigma_n^2}{2N}\{Re\left[\left(\boldsymbol{D}^H\boldsymbol{P}_{\boldsymbol{V}_s}^{\perp}\boldsymbol{D}\right) \circ \widehat{\boldsymbol{R}}_{\boldsymbol{s}}^T\right]\}^{-1},\end{aligned} \tag{C-15}$$

where $\widehat{\boldsymbol{R}}_{\boldsymbol{s}}$, $\boldsymbol{P}_{\boldsymbol{V}_s}^{\perp}$ and **D** are given by

$$\begin{aligned}\widehat{\boldsymbol{R}}_{\boldsymbol{s}} &= \frac{1}{N}\sum_{n=1}^{N}\boldsymbol{s}(n)\boldsymbol{s}^H(n) \\ \boldsymbol{P}_{\boldsymbol{V}_s}^{\perp} &= [\boldsymbol{I} - \boldsymbol{V}_{\boldsymbol{s}}(\boldsymbol{V}_{\boldsymbol{s}}^H\boldsymbol{V}_{\boldsymbol{s}})^{-1}\boldsymbol{V}_{\boldsymbol{s}}^H] \\ \boldsymbol{D} = \dot{\boldsymbol{V}}_{\varphi} &= \left[\frac{\partial \boldsymbol{v}(\varphi_1)}{\partial \varphi_1} \quad \frac{\partial \boldsymbol{v}(\varphi_2)}{\partial \varphi_2} \quad \ldots \quad \frac{\partial \boldsymbol{v}(\varphi_L)}{\partial \varphi_L}\right]^T.\end{aligned} \tag{C-16}$$

Notice that when Θ_s is the parameter to estimate, the above $\boldsymbol{D}$ can be simply written as

$$\boldsymbol{D} = \left[\pi cos\theta_{s1}\frac{\partial \boldsymbol{v}(\theta_{s1})}{\partial \theta_{s1}} \quad \pi cos\theta_{s2}\frac{\partial \boldsymbol{v}(\theta_{s2})}{\partial \theta_{s2}} \quad \ldots \quad \pi cos\theta_{sL}\frac{\partial \boldsymbol{v}(\theta_{sL})}{\partial \theta_{sL}}\right]^T. \tag{C-17}$$

In most radar systems, the transmit waveform is known and a match filter is often used before further processing. Therefore, the recorded signals are deterministic and the second manner of CRB expression, i.e., (C-15) is normally used.

C.2. Cramér–Rao Bounds for DOA Estimation in Omni-directional Transmission BS Case

For the same scenario as above but for the omni-directional BS case, to estimate DOAs of several deterministic signals, the probability density for a single snapshot vector (one sample for each beam output) at time t , $\boldsymbol{y}(t)$,is given by

$$P_{\boldsymbol{y}|\theta_s} = \frac{1}{\det(\pi\boldsymbol{R}_{\boldsymbol{y}})}\exp\left[-\left(\boldsymbol{y}^H(t) - \boldsymbol{m}_{\boldsymbol{ys}}^H\right)\boldsymbol{R}_{\boldsymbol{y}}^{-1}\left(\boldsymbol{y}(t) - \boldsymbol{m}_{\boldsymbol{ys}}\right)\right] \tag{C-18}$$

Similar to the process in Section C.1, the simplified likelihood function for the BS case is given by

$$L(\Theta_s) = -ln\{\det[\boldsymbol{R_y}]\} - 1/\mathrm{N}\sum_{n=1}^{N}\boldsymbol{y}^H(t)\boldsymbol{R_y}^{-1}\boldsymbol{y}(t). \tag{C-19}$$

The elements of the Fisher's information matrix is given by

$$\boldsymbol{\mathcal{F}}_{ij} = tr\left[\boldsymbol{R}_{\mathbf{y}}^{-1}\frac{\partial \boldsymbol{R_y}}{\partial \varphi_i}\boldsymbol{R}_{\mathbf{y}}^{-1}\frac{\partial \boldsymbol{R_y}}{\partial \varphi_j}\right], \tag{C-20}$$

where for a random white noise with power σ_n^2, beams are mutually orthogonal and normalised to be with unit magnitude, then $\boldsymbol{R}_{\mathbf{y}}^{-1}$ is given by

$$\boldsymbol{R}_{\mathbf{y}}^{-1} = 1/\sigma_n^2[\boldsymbol{I} - \boldsymbol{H}(\boldsymbol{H}^H\boldsymbol{H} + \sigma_n^2\boldsymbol{R_s}^{-1})^{-1}\boldsymbol{H}^H], \tag{C-21}$$

where $\boldsymbol{H} = \boldsymbol{V}^H\boldsymbol{V_s}$ and the partial derivative of $\boldsymbol{R_y}$ is given by

$$\begin{aligned}\frac{\partial \boldsymbol{R_y}}{\partial \varphi_i} &= \frac{\partial \boldsymbol{H}}{\partial \varphi_i}\boldsymbol{R_s}\boldsymbol{H}^H + \boldsymbol{H}\boldsymbol{R_s}\frac{\partial \boldsymbol{H}^H}{\partial \varphi_i},\\ \frac{\partial \boldsymbol{H}}{\partial \varphi_i} &= \frac{\partial\left(\boldsymbol{V}^H\boldsymbol{v}(\varphi)\right)}{\partial \varphi}|_{\varphi=\varphi_i} = \boldsymbol{V}^H\boldsymbol{d}(\varphi_\mathrm{i}).\end{aligned} \tag{C-22}$$

When the signal vector is deterministic, $\boldsymbol{s}(n)$ is a non-random $L\times1$ complex source signal vector, then the CRB of DOA estimation in BS is given by

$$\boldsymbol{C}_{CR-\boldsymbol{h}}(\boldsymbol{\varphi}) = \frac{\sigma_n^2}{2N}\left\{Re\left[(\mathbf{D}_H^H\boldsymbol{P}_{\boldsymbol{H}}^{\perp}\boldsymbol{D}_H)\circ\widehat{\boldsymbol{R}}_{\boldsymbol{s}}^T\right]\right\}^{-1}, \tag{C-23}$$

where $\boldsymbol{P}_{\boldsymbol{H}}^{\perp}$ and $\boldsymbol{D_H}$ are given by

$$\begin{aligned}\boldsymbol{P}_{\boldsymbol{H}}^{\perp} &= \boldsymbol{I} - \boldsymbol{H}(\boldsymbol{H}^H\boldsymbol{H})^{-1}\boldsymbol{H}^H,\\ \boldsymbol{D_H} &= \dot{\boldsymbol{H}} = \boldsymbol{V}^H\boldsymbol{D}.\end{aligned} \tag{C-24}$$

A theoretical proof can be found in [92] that the CRB for DOA estimation in the omni-directional transmission BS case is never smaller than the ES CRB, and the equality appears if and only if

$$\begin{aligned}\boldsymbol{V}\boldsymbol{V}^H\boldsymbol{P}_{\boldsymbol{V_s}}^{\perp}\mathbf{D} &= \boldsymbol{P}_{\boldsymbol{V_s}}^{\perp}\mathbf{D},\\ \boldsymbol{V}\boldsymbol{V}^H\boldsymbol{V_s} &= \boldsymbol{V_s}.\end{aligned} \tag{C-25}$$

C.3. Cramér–Rao Bounds for DOA Estimation in Directional Transmission BS Case

For the directional transmission case, to estimate the DOAs of deterministic signals, the probability density function, likelihood function and even Fisher's information matrix can be represented by the same expressions in C.2,

For a random white noise with power of σ_n^2, beams with unit magnitude, $\boldsymbol{R}_{\mathbf{y}}^{-1}$ is given by

$$\boldsymbol{R}_{\mathbf{y}}^{-1} = 1/\sigma_n^2\big(\boldsymbol{I} - \boldsymbol{V}_{\boldsymbol{y}}(\boldsymbol{V}_{\boldsymbol{y}}^H \boldsymbol{V}_{\boldsymbol{y}} + \sigma_n^2 \boldsymbol{R}_{\boldsymbol{s}}^{-1})^{-1}\boldsymbol{V}_{\boldsymbol{y}}^H\big), \tag{C-26}$$

where $\boldsymbol{V}_{\boldsymbol{y}}$ is given by(4-8) and (4-14), the partial derivative of $\boldsymbol{R}_{\boldsymbol{y}}$ is given by

$$\frac{\partial \boldsymbol{R}_{\boldsymbol{y}}}{\partial \varphi_i} = \frac{\partial\, \boldsymbol{V}_{\boldsymbol{y}}(\varphi_i)}{\partial \varphi_i}\boldsymbol{R}_{\boldsymbol{s}}\boldsymbol{V}_{\boldsymbol{y}}^H + \boldsymbol{V}_{\boldsymbol{y}}\boldsymbol{R}_{\boldsymbol{s}}\frac{\partial \boldsymbol{V}_{\boldsymbol{y}}^H(\varphi_i)}{\partial \varphi_i}, \tag{C-27}$$

and the derivative of $\boldsymbol{V}_{\boldsymbol{y}}$ is given by

$$\begin{aligned}
\boldsymbol{D}_{\boldsymbol{V}\boldsymbol{y}} &= \dot{\boldsymbol{V}}_{\boldsymbol{y}}(\Theta_s) \\
&= \left[\frac{\partial\, \boldsymbol{v}_{\boldsymbol{y}}(\varphi_1)}{\partial \varphi_1} \quad \frac{\partial\, \boldsymbol{v}_{\boldsymbol{y}}(\varphi_2)}{\partial \varphi_2} \quad \ldots \quad \frac{\partial\, \boldsymbol{v}_{\boldsymbol{y}}(\varphi_L)}{\partial \varphi_L}\right] \\
&= 2\left[\boldsymbol{h}(\varphi_1)\circ\frac{\partial \boldsymbol{h}(\varphi_1)}{\partial \varphi_1} \quad \boldsymbol{h}(\varphi_2)\circ\frac{\partial \boldsymbol{h}(\varphi_2)}{\partial \varphi_2} \quad \ldots \quad \boldsymbol{h}(\varphi_L)\circ\frac{\partial \boldsymbol{h}(\varphi_L)}{\partial \varphi_L}\right] \\
&= 2[\,(\boldsymbol{V}^H\boldsymbol{v}(\theta_{s1}))\circ(\boldsymbol{V}^H\boldsymbol{d}_1) \quad (\boldsymbol{V}^H\boldsymbol{v}(\theta_{s2}))\circ(\boldsymbol{V}^H\boldsymbol{d}_2) \quad \ldots \quad (\boldsymbol{V}^H\boldsymbol{v}(\theta_{sL}))\circ(\boldsymbol{V}^H d_L)].
\end{aligned} \tag{C-28}$$

When the received signals are deterministic, $\boldsymbol{s}(n)$ is a non-random $L\times 1$ complex source signal vector, then the Cramér Rao bounds of DOA estimation in the directional transmission BS case is given by

$$\boldsymbol{C}_{CR-\boldsymbol{V}\boldsymbol{y}}(\boldsymbol{\varphi}) = \frac{\sigma_n^2}{2N}\left\{Re\left[\left(\mathbf{D}_{\boldsymbol{V}\boldsymbol{y}}^H\boldsymbol{P}_{\boldsymbol{V}\boldsymbol{y}}^{\perp}\boldsymbol{D}_{\boldsymbol{V}\boldsymbol{y}}\right)\circ\boldsymbol{R}_{\boldsymbol{s}}^T\right]\right\}^{-1} \tag{C-29}$$

where $\boldsymbol{P}_{\boldsymbol{V}_{\boldsymbol{y}}}^{\perp}$ is given by

$$\boldsymbol{P}_{\boldsymbol{V}_{\boldsymbol{y}}}^{\perp} = \boldsymbol{I} - \boldsymbol{V}_{\boldsymbol{y}}(\boldsymbol{V}_{\boldsymbol{y}}^H \boldsymbol{V}_{\boldsymbol{y}})^{-1}\boldsymbol{V}_{\boldsymbol{y}}^H. \tag{C-30}$$

Appendix D

Applying Optimum Beam Space Beamformer to Correlated Signals

Consider a scenario that two correlated signals, with a correlation coefficient, ρ_{12} and their amplitudes are σ_{s1} and σ_{s2} and DOAs are θ_{s1} and θ_{s2}. *M* mutually orthogonal omni-directional transmission conventional beams are formed. Then the BS covariance matrix is given by

$$\boldsymbol{R_y} = [\boldsymbol{h}(\theta_{s1}) \quad \boldsymbol{h}(\theta_{s2})] \begin{bmatrix} \sigma_{s1}^2 & \rho_{12}\sigma_{s1}\sigma_{s2} \\ \rho_{12}^*\sigma_{s1}\sigma_{s2} & \sigma_{s2}^2 \end{bmatrix} [\boldsymbol{h}(\theta_{s1}) \quad \boldsymbol{h}(\theta_{s2})]^H + K\sigma_n^2 \boldsymbol{I}_{M\times M}. \tag{D-1}$$

Applying the omni-directional BS optimum beamforming (MVDR) formula (3-9) to the correlated BS signals model, the output power at the first DOA, θ_{s1}, is given by

$$\begin{aligned} p_{MVDR-BS}(\theta_{s1}) &= \boldsymbol{w}^H(\theta_{s1})\boldsymbol{R_y}\boldsymbol{w}(\theta_{s1}) \\ &= [\boldsymbol{w}^H(\theta_{s1})\boldsymbol{h}(\theta_{s1}) \quad \boldsymbol{w}^H(\theta_{s1})\boldsymbol{h}(\theta_{s2})] \begin{bmatrix} \sigma_{s1}^2 & \rho_{12}\sigma_{s1}\sigma_{s2} \\ \rho_{12}^*\sigma_{s1}\sigma_{s2} & \sigma_{s2}^2 \end{bmatrix} [\boldsymbol{w}^H(\theta_{s1})\boldsymbol{h}(\theta_{s1}) \quad \boldsymbol{w}^H(\theta_{s1})\boldsymbol{h}(\theta_{s2})]^H + \boldsymbol{w}^H(\theta_{s1})K\sigma_n^2\boldsymbol{w}(\theta_{s1}) \\ &= \boldsymbol{w}^H(\theta_{s1})\boldsymbol{h}(\theta_{s1})\boldsymbol{h}^H(\theta_{s1})\boldsymbol{w}(\theta_{s1})\sigma_{s1}^2 + \boldsymbol{w}^H(\theta_{s1})\boldsymbol{h}(\theta_{s2})\boldsymbol{h}^H(\theta_{s1})\boldsymbol{w}(\theta_{s1})\rho_{12}^*\sigma_{s1}\sigma_{s2} \\ &+ \boldsymbol{w}^H(\theta_{s1})\boldsymbol{h}(\theta_{s1})\boldsymbol{h}^H(\theta_{s2})\boldsymbol{w}(\theta_{s1})\rho_{12}\sigma_{s1}\sigma_{s2} + \boldsymbol{w}^H(\theta_{s1})\boldsymbol{h}(\theta_{s2})\boldsymbol{h}^H(\theta_{s2})\boldsymbol{w}(\theta_{s1})\sigma_{s2}^2 + \boldsymbol{w}^H(\theta_{s1})\boldsymbol{w}(\theta_{s1})K\sigma_n^2. \end{aligned} \tag{D-2}$$

The MVDR optimisation criteria for the omni-directional transmission BS model can be described as

$$\min \boldsymbol{w}^H(\theta)\boldsymbol{R_y}\boldsymbol{w}(\theta), \text{ subject to } \boldsymbol{w}^H(\theta)\boldsymbol{h}(\theta) = 1. \tag{D-3}$$

Combining the function to be minimised and the constraint in (D-3) into a single equation:

$$\omega(\theta_{s1}) = \boldsymbol{w}^H(\theta_{s1})\boldsymbol{R_y}\boldsymbol{w}(\theta_{s1}) - \mu(\boldsymbol{w}^H(\theta_{s1})\boldsymbol{h}(\theta_{s1}) - 1), \tag{D-4}$$

where μ is a scalar and setting

$$\frac{\partial\omega(\theta)}{\partial w(\theta)}\Big|_{\theta=\theta_{s1}} = 0. \tag{D-5}$$

results in the following equation

$$2\boldsymbol{h}(\theta_{s1})\boldsymbol{h}^H(\theta_{s1})\boldsymbol{w}(\theta_{s1})\sigma_{s1}^2 + 2\boldsymbol{h}(\theta_{s2})\boldsymbol{h}^H(\theta_{s1})\boldsymbol{w}(\theta_{s1})\rho_{12}^*\sigma_{s1}\sigma_{s2} + 2\boldsymbol{h}(\theta_{s1})\boldsymbol{h}^H(\theta_{s2})\boldsymbol{w}(\theta_{s1})\rho_{12}\sigma_{s1}\sigma_{s2} + 2\boldsymbol{h}(\theta_{s2})\boldsymbol{h}^H(\theta_{s2})\boldsymbol{w}(\theta_{s1})\sigma_{s2}^2 + 2\boldsymbol{w}(\theta_{s1})K\sigma_n^2 - \mu\boldsymbol{h}(\theta_{s1}) = 0, \tag{D-6}$$

by substituting $\boldsymbol{w}^H(\theta_{s1})\boldsymbol{h}(\theta_{s1}) = 1$ in, it can be shown that

$$2\boldsymbol{h}(\theta_{s1})\sigma_{s1}^2 + 2\boldsymbol{h}(\theta_{s2})\rho_{12}^*\sigma_{s1}\sigma_{s2} + 2\boldsymbol{h}(\theta_{s1})\boldsymbol{h}^H(\theta_{s2})\boldsymbol{w}(\theta_{s1})\rho_{12}\sigma_{s1}\sigma_{s2} + 2\boldsymbol{h}(\theta_{s2})\boldsymbol{h}^H(\theta_{s2})\boldsymbol{w}(\theta_{s1})\sigma_{s2}^2 + 2\boldsymbol{w}(\theta_{s1})K\sigma_n^2 - \mu\boldsymbol{h}(\theta_{s1}) = 0, \tag{D-7}$$

and multiplying both sides $\boldsymbol{h}^H(\theta_{s1})/2$ gives

$$\begin{aligned}\boldsymbol{h}^H(\theta_{s1})\boldsymbol{h}(\theta_{s1})\sigma_{s1}^2 + \boldsymbol{h}^H(\theta_{s1})\boldsymbol{h}(\theta_{s2})\rho_{12}^*\sigma_{s1}\sigma_{s2} + \boldsymbol{h}^H(\theta_{s1})\boldsymbol{h}(\theta_{s1})\boldsymbol{h}^H(\theta_{s2})\boldsymbol{w}(\theta_{s1})\rho_{12}\sigma_{s1}\sigma_{s2} \\ + \boldsymbol{h}^H(\theta_{s1})\boldsymbol{h}(\theta_{s2})\boldsymbol{h}^H(\theta_{s2})\boldsymbol{w}(\theta_{s1})\sigma_{s2}^2 + \boldsymbol{h}^H(\theta_{s1})\boldsymbol{w}(\theta_{s1})K\sigma_n^2 - \frac{\mu}{2}\boldsymbol{h}^H(\theta_{s1})\boldsymbol{h}(\theta_{s1}) = 0.\end{aligned} \tag{D-8}$$

With $H(\theta) = \boldsymbol{h}^H(\theta)\boldsymbol{h}(\theta)$ as defined in (3-30), and here defining a new parameters $\alpha = \boldsymbol{w}^H(\theta_{s1})\boldsymbol{h}(\theta_{s2})$ and $\beta = \boldsymbol{h}^H(\theta_{s1})\boldsymbol{h}(\theta_{s2})$, the above equation can be written as

$$H(\theta_{s1})\sigma_{s1}^2 + \beta\rho_{12}^*\sigma_{s1}\sigma_{s2} + H(\theta_{s1})\alpha^*\rho_{12}\sigma_{s1}\sigma_{s2} + \beta\alpha^*\sigma_{s2}^2 + K\sigma_n^2 - \frac{\mu}{2}H(\theta_{s1}) = 0. \tag{D-9}$$

Then, μ can be obtained as

$$\mu = 2\left(\sigma_{s1}^2 + \frac{\beta\alpha^*\sigma_{s2}^2}{H(\theta_{s1})} + \frac{K\sigma_n^2}{H(\theta_{s1})} + \frac{(\beta\rho_{12}^* + H(\theta_{s1})\alpha^*\rho_{12})\sigma_{s1}\sigma_{s2}}{H(\theta_{s1})}\right) \tag{D-10}$$

158

Multiplying both sides of (D-7) $\boldsymbol{h}^H(\theta_{s2})/2$ gives

$$\boldsymbol{h}^H(\theta_{s2})\boldsymbol{h}(\theta_{s1})\sigma_{s1}^2 + \boldsymbol{h}^H(\theta_{s2})\boldsymbol{h}(\theta_{s2})\rho_{12}^*\sigma_1\sigma_2 + \boldsymbol{h}^H(\theta_{s2})\boldsymbol{h}(\theta_{s1})\boldsymbol{h}^H(\theta_{s2})\boldsymbol{w}(\theta_{s1})\rho_{12}\sigma_{s1}\sigma_{s2} + \boldsymbol{h}^H(\theta_{s2})\boldsymbol{h}(\theta_{s2})\boldsymbol{h}^H(\theta_{s2})\boldsymbol{w}(\theta_{s1})\sigma_{s2}^2 + K\boldsymbol{h}^H(\theta_{s2})\boldsymbol{w}(\theta_{s1})\sigma_n^2 - \frac{\mu}{2}\boldsymbol{h}^H(\theta_{s2})\boldsymbol{h}(\theta_{s1}) = 0. \quad \text{(D-11)}$$

The above equation can be simplified and written as

$$\beta^*\sigma_{s1}^2 + H(\theta_{s2})\rho_{12}^*\sigma_{s1}\sigma_{s2} + \beta^*\alpha^*\rho_{12}\sigma_{s1}\sigma_{s2} + H(\theta_{s2})\beta\rho_{12}^*\sigma_{s1}\sigma_{s2} + H(\theta_{s2})\alpha^*\rho_{12}\alpha^*\sigma_{s2}^2 + K\alpha^*\sigma_n^2 - \frac{\mu}{2}\beta^* = 0. \quad \text{(D-12)}$$

Substituting μ as (D-10) in the above gives

$$\beta^*\sigma_{s1}^2 + H(\theta_{s2})\rho_{12}^*\sigma_{s1}\sigma_{s2} + \beta^*\alpha^*\rho_{12}\sigma_{s1}\sigma_{s2} + H(\theta_{s2})\beta\rho_{12}^*\sigma_{s1}\sigma_{s2} + H(\theta_{s2})\alpha^*\sigma_{s2}^2 + K\alpha^*\sigma_n^2 - \beta^*\left(\sigma_{s1}^2 + \frac{\beta\alpha^*\sigma_{s2}^2}{H(\theta_{s1})} + \frac{K\sigma_n^2}{H(\theta_{s1})} + \frac{(\beta\rho_{12}^* + H(\theta_{s1})\alpha^*\rho_{12})\sigma_{s1}\sigma_{s2}}{H(\theta_{s1})}\right) = 0. \quad \text{(D-13)}$$

As the example in Figure 3-11 shows, the value of $H(\theta)$ is near to a constant in the sector of interest:

$$H(\theta_{s1}) \approx H$$
$$H(\theta_{s2}) \approx H. \quad \text{(D-14)}$$

Then (D-13) can be rewritten as

$$\beta^*\alpha^*\rho_{12}\sigma_{s1}\sigma_{s2} + H\alpha^*\sigma_{s2}^2 + K\alpha^*\sigma_n^2 - \frac{\beta^*\beta\alpha^*\sigma_{s2}^2}{H} - \beta^*\alpha^*\rho_{12}\sigma_{s1}\sigma_{s2} = \frac{\beta^*\beta\rho_{12}^*\sigma_{s1}\sigma_{s2} + \beta^*K\sigma_n^2 - H^2\rho_{12}^*\sigma_{s1}\sigma_{s2}}{H}, \quad \text{(D-15)}$$

and the value of α^* can be approximated as

$$\alpha^* \approx \frac{(\beta^*\beta - H^2)\rho_{12}^*\sigma_{s1}\sigma_{s2} + \beta^* K\sigma_n^2}{(H^2 - \beta^*\beta)\sigma_{s2}^2 + KH\sigma_n^2} \tag{D-16}$$

Multiplying both sides of (D-7) $\boldsymbol{w}^H(\theta_{s1})/2$ gives

$$\begin{aligned}
&\boldsymbol{w}^H(\theta_{s1})\boldsymbol{h}(\theta_{s1})\sigma_{s1}^2 + \boldsymbol{w}^H(\theta_{s1})\boldsymbol{h}(\theta_{s2})\rho_{12}^*\sigma_{s1}\sigma_{s2} + \boldsymbol{w}^H(\theta_{s1})\boldsymbol{h}(\theta_{s1})\boldsymbol{h}^H(\theta_{s2})\boldsymbol{w}(\theta_{s1})\rho_{12}\sigma_{s1}\sigma_{s2} + \boldsymbol{w}^H(\theta_{s1})\boldsymbol{h}(\theta_{s2})\boldsymbol{h}^H(\theta_{s2})\boldsymbol{w}(\theta_{s1})\sigma_{s2}^2 \\
&\quad + \boldsymbol{w}^H(\theta_{s1})\boldsymbol{w}(\theta_{s1})K\sigma_n^2 - \frac{\mu}{2}\boldsymbol{w}^H(\theta_{s1})\boldsymbol{h}(\theta_{s1}) = 0 \\
&\sigma_{s1}^2 + \boldsymbol{w}^H(\theta_{s1})\boldsymbol{h}(\theta_{s2})\rho_{12}^*\sigma_{s1}\sigma_{s2} + \boldsymbol{h}^H(\theta_{s2})\boldsymbol{w}(\theta_{s1})\rho_{12}\sigma_{s1}\sigma_{s2} + \boldsymbol{w}^H(\theta_{s1})\boldsymbol{h}(\theta_{s2})\boldsymbol{h}^H(\theta_{s2})\boldsymbol{w}(\theta_{s1})\sigma_{s2}^2 + \boldsymbol{w}^H(\theta_{s1})\boldsymbol{w}(\theta_{s1})K\sigma_n^2 - \frac{\mu}{2} = 0 \\
&\sigma_{s1}^2 + \alpha\rho_{12}^*\sigma_{s1}\sigma_{s2} + \alpha^*\rho_{12}\sigma_{s1}\sigma_{s2} + \alpha\alpha^*\sigma_{s2}^2 + \boldsymbol{w}^H(\theta_{s1})\boldsymbol{w}(\theta_{s1})K\sigma_n^2 - \frac{\mu}{2} = 0.
\end{aligned} \tag{D-17}$$

Substituting (D-10) into (D-17), the noise part is given by

$$\begin{aligned}
\boldsymbol{w}^H(\theta_1)\boldsymbol{w}(\theta_1)K\sigma_n^2 &= \frac{\mu}{2} - \sigma_{s1}^2 + \alpha\rho_{12}^*\sigma_{s1}\sigma_{s2} + \alpha^*\rho_{12}\sigma_{s1}\sigma_{s2} + \alpha\alpha^*\sigma_{s2}^2 \\
&= \sigma_{s1}^2 + \frac{\beta\alpha^*\sigma_{s2}^2}{H} + \frac{K\sigma_n^2}{H} + \frac{(\beta\rho_{12}^* + H\alpha^*\rho_{12})\sigma_{s1}\sigma_{s2}}{H} - (\sigma_{s1}^2 + \alpha\rho_{12}^*\sigma_{s1}\sigma_{s2} + \alpha^*\rho_{12}\sigma_{s1}\sigma_{s2} + |\alpha|^2\sigma_{s2}^2) \\
&= \frac{1}{H}\left((\beta\alpha^* - |\alpha|^2 H)\sigma_{s2}^2 + (\beta\rho_{12}^* - H\,\alpha\rho_{12}^*)\sigma_{s1}\sigma_{s2} + K\sigma_n^2\right).
\end{aligned} \tag{D-18}$$

The expression (D-2) can be simplified as

$$\begin{aligned}
p_{MVDR-BS}(\theta_{s1}) &= [1 \quad \alpha]\begin{bmatrix} \sigma_{s1}^2 & \rho_{12}\sigma_{s1}\sigma_{s2} \\ \rho_{12}^*\sigma_{s1}\sigma_{s2} & \sigma_{s2}^2 \end{bmatrix}[1 \quad \alpha]^H + \boldsymbol{w}^H(\theta_{s1})\boldsymbol{w}(\theta_{s1})K\sigma_n^2 \\
&= \sigma_{s1}^2 + \alpha\rho_{12}^*\sigma_{s1}\sigma_{s2} + \rho_{12}\alpha^*\sigma_{s1}\sigma_{s2} + \alpha\alpha^*\sigma_{s2}^2 + \boldsymbol{w}^H(\theta_{s1})\boldsymbol{w}(\theta_{s1})K\sigma_n^2.
\end{aligned} \tag{D-19}$$

160

Substituting (D-15) and (D-18) into above equation, then the BS optimum beamforming output at θ_{s1} can be given by

$$
\begin{aligned}
p_{MVDR-BS}(\theta_{s1}) = {} & \sigma_{s1}^2 + \alpha\rho_{12}^*\sigma_{s1}\sigma_{s2} + \rho_{12}\alpha^*\sigma_{s1}\sigma_{s2} + \alpha\alpha^*\sigma_{s2}^2 + \boldsymbol{w}^H(\theta_{s1})\boldsymbol{w}(\theta_{s1})K\sigma_n^2 \\
= {} & \sigma_{s1}^2 + \alpha\rho_{12}^*\sigma_{s1}\sigma_{s2} + \alpha^*\rho_{12}\sigma_{s1}\sigma_{s2} + |\alpha|^2\sigma_{s2}^2 + \frac{1}{H}\left((\beta\alpha^* - |\alpha|^2 H)\sigma_{s2}^2 + (\beta - H\alpha)\rho_{12}^*\sigma_{s1}\sigma_{s2} + K\sigma_n^2\right) \\
= {} & \sigma_{s1}^2 + \alpha\rho_{12}^*\sigma_{s1}\sigma_{s2} + \frac{\beta\alpha^*}{H}\sigma_{s2}^2 + \frac{\beta}{H}\rho_{12}^*\sigma_1\sigma_2 + \frac{K}{H}\sigma_n^2 \\
= {} & \sigma_{s1}^2 + \frac{\beta\sigma_{s2}^2}{H}\frac{(\beta^*\beta - H^2)\rho_{12}^*\sigma_{s1}\sigma_{s2} + \beta^*K\sigma_n^2}{(H^2 - \beta^*\beta)\sigma_{s2}^2 + KH\sigma_n^2} + \frac{(\beta^*\beta - H^2)\rho_{12}^*\sigma_{s1}\sigma_{s2} + \beta^*K\sigma_n^2}{(H^2 - \beta^*\beta)\sigma_{s2}^2 + KH\sigma_n^2}\rho_{12}\sigma_{s1}\sigma_{s2} + \frac{\beta}{H}\rho_{12}^*\sigma_{s1}\sigma_{s2} + \frac{K}{H}\sigma_n^2 \\
= {} & \sigma_{s1}^2 \\
& + \frac{1}{(H^2 - \beta^*\beta)\sigma_{s2}^2 + KH\sigma_n^2}\left(\frac{\beta\sigma_2^2}{H}\left((\beta^*\beta - H^2)\rho_{12}^*\sigma_{s1}\sigma_{s2} + \beta^*K\sigma_n^2\right) + |\rho_{12}|^2\sigma_{s1}^2\sigma_{s2}^2(\beta^*\beta - H^2) + \beta^*K\sigma_n^2\rho_{12}\sigma_{s1}\sigma_{s2}\right) \\
& + \frac{\beta}{H}\rho_{12}^*\sigma_{s1}\sigma_{s2} + \frac{K}{H}\sigma_n^2 \\
= {} & \sigma_{s1}^2 \\
& + \frac{1}{(H^2 - \beta^*\beta)\sigma_{s2}^2 + KH\sigma_n^2}\left(|\rho_{12}|^2\sigma_{s1}^2\sigma_{s2}^2(\beta^*\beta - H^2) + \frac{\beta\sigma_{s2}^2}{H}\left((\beta^*\beta - H^2)\rho_{12}^*\sigma_{s1}\sigma_{s2} + \beta^*K\sigma_n^2\right) + \beta^*K\sigma_n^2\rho_{12}\sigma_{s1}\sigma_{s2}\right. \\
& \left. + \frac{\beta}{H}\rho_{12}^*\sigma_{s1}\sigma_{s2}\left((H^2 - \beta^*\beta)\sigma_{s2}^2 + KH\sigma_n^2\right)\right) + \frac{K}{H}\sigma_n^2 \\
= {} & \sigma_{s1}^2 + \frac{1}{(H^2 - \beta^*\beta)\sigma_{s2}^2 + KH\sigma_n^2}\left(|\rho_{12}|^2\sigma_{s1}^2\sigma_{s2}^2(\beta^*\beta - H^2) + K\sigma_n^2\left(\frac{\beta^*\beta\sigma_{s2}^2}{H} + \sigma_{s1}\sigma_{s2}(\beta^*\rho_{12} + \beta\rho_{12}^*)\right)\right) + \frac{K}{H}\sigma_n^2.
\end{aligned}
\tag{D-20}
$$

Therefore, the BS optimum beamforming output at the DOAs of coherent signals are obviously different from the outputs for the model of independent signals, which is described in Chapter 3. When the SNR of the signal incident from θ_{s1} is very high ($\sigma_n^2 \ll \sigma_{s1}^2$), the output at the DOA can be simplified as

$$p_{MVDR-BS}(\theta_{s1}) \approx \sigma_{s1}^2(1 - |\rho_{12}|^2) \tag{D-21}$$

In this case, the output power depends wholly on the signal arriving from the look angle and correlation between signals. The higher correlation causes more attenuation to the output power and a relatively weak but coherent interference can fully cancel a strong signal.

When two signals are very close, β approaches H, the output is near to $\sigma_{s1}^2 + \sigma_{s2}^2 + \sigma_{s1}\sigma_{s2}(\rho_{12} + \rho_{12}^*) + \frac{K}{H}\sigma_n^2$, and the output would be similar to the conventional beamforming result. The output becomes the summation of the two signals coherently and the contribution of noise components.

Similarly, for the directional transmission BS case, when two signals are correlated, the optimum BS beamformer output power at one of the DOAs of coherent signals is given by

$$p_{MVDR-BS}(\theta_{s1}) \approx \sigma_{s1}^2 + \frac{1}{({K_y}^2 - |\beta_d|^2)\sigma_{s2}^2 + K_y K\sigma_n^2}\left(|\rho_{12}|^2\sigma_{s1}^2\sigma_{s2}^2(|\beta_d|^2 - K_y^2) + K\sigma_n^2\left(\frac{|\beta_d|^2{\sigma_{s2}}^2}{K_y} + \sigma_{s1}\sigma_{s2}(\beta_d^*\rho_{12} + \beta_d\rho_{12}^*)\right)\right) + \frac{K}{K_y}\sigma_n^2, \tag{D-22}$$

where $k_y(\theta_{s1})$ is defined in (4-20) and its value is near the constant K_y when θ_{s1} is inside the sector scanned by formed beams; $\beta_d = \boldsymbol{v}_y^H(\theta_{s1})\boldsymbol{v}_y(\theta_{s2})$, which was earlier denoted as $B(\theta_{s1}, \theta_{s2})$ in (4-34).

Appendix E

DOA estimation for Several Groups of Coherent Signals

When received signals are mixed with L_c groups of coherent signals but uncorrelated among groups, which represents a scenario of L_c independent source signals with multipath returns, the omnidirectional transmission BS covariance matrix becomes

$$\begin{aligned} \boldsymbol{R_y} &= \boldsymbol{V}^H \boldsymbol{R_x} \boldsymbol{V} \\ &= \sum_{i=1}^{Lc} \sigma_{si}^2 \boldsymbol{V}^H \boldsymbol{q}_i \boldsymbol{q}_i^H \boldsymbol{V} + \sigma_n^2 \boldsymbol{V}^H \boldsymbol{V} \end{aligned} \tag{E-1}$$

Similar to the process in Appendix A, it can be proven that with a sufficient number of beams, the ES signal subspace can be reconstructed according to the BS signal subspace and is given by

$$\sum_{i=1}^{Lc} \boldsymbol{q}_i \boldsymbol{q}_i^H = \sum_{i=1}^{Lc} \boldsymbol{V}\boldsymbol{V}^H \boldsymbol{q}_i \boldsymbol{q}_i^H \boldsymbol{V}\boldsymbol{V}^H \tag{E-2}$$

Similar to the case for one group of coherent signals, the noise subspace can be simply reconstructed as a diagonal matrix and the ES covariance matrix can be reconstructed. Then spatial smoothing and MUSIC techniques can be applied. Notice that the number of averages for spatial smoothing depends on the maximum number coherent signals in each group.

A signal model containing two groups of coherent signals, but uncorrelated between groups, are considered here. Three coherent signals at DOAs of 8.23°, 9.44° and 12°, with SNR=10 dB, 5 dB and 10 dB, and correlation $\rho_{12} = e^{i}$ and $\rho_{13} = 1$; the second group contains two signals at DOAs of 5.3° and 10.67°, with SNR=10 dB and 10 dB, and correlation $\rho_{12} = e^{i\pi/3}$. The ULA contained 64 identical receivers spaced at $d = 0.5\lambda$, and 20 omni-directional transmission beams are formed in a sector of [1°, 20°] with 1° separation. The results of applying the developed techniques are shown in Figure E-1. It shows all the DOAs can be estimated accurately and the result indicates that the technique is adequate for estimating DOAs of a mixture of multiple groups of coherent signals.

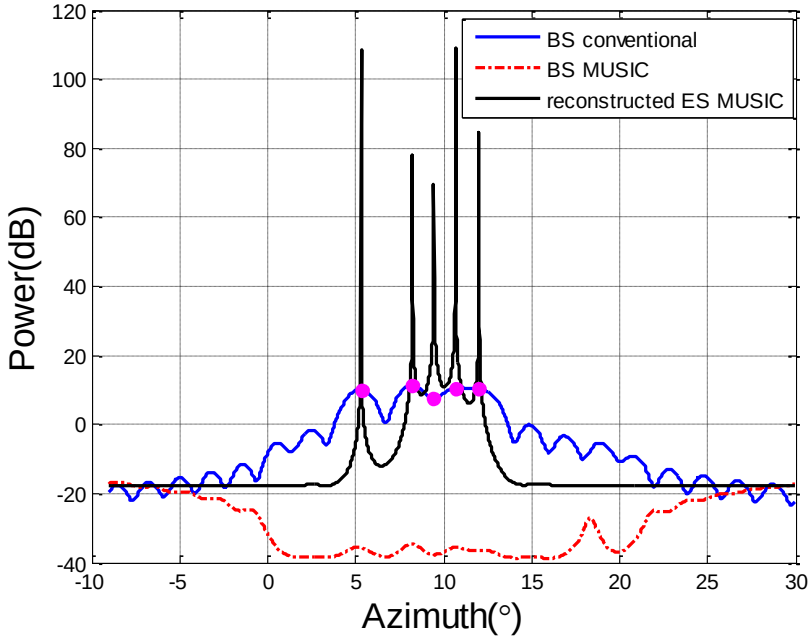

Figure E-1: An example of BS processing for two groups of coherent signals. The output of ES MUSIC with spatial smoothing to a reconstructed ES covariance matrix and compared with conventional BS beamformer and BS MUSIC without decorrelation.

Appendix F

Averaging over Reconstructed Directional Transmission ES Covariance Matrices

For the directional transmission case, as shown in Section 4.1.3, the BS covariance, $\boldsymbol{R_y}$, can be considered as a linear transformation for a stacked ES covariance matrix $\boldsymbol{R_{xs}}$.

$$\boldsymbol{R_{xs}} = E\left\{\begin{bmatrix} \boldsymbol{x}(\theta_1)\boldsymbol{x}^H(\theta_1) & \boldsymbol{x}(\theta_1)\boldsymbol{x}^H(\theta_2) & \cdots & \boldsymbol{x}(\theta_1)\boldsymbol{x}^H(\theta_M) \\ \boldsymbol{x}(\theta_2)\boldsymbol{x}^H(\theta_1) & \boldsymbol{x}(\theta_2)\boldsymbol{x}^H(\theta_2) & \cdots & \boldsymbol{x}(\theta_2)\boldsymbol{x}^H(\theta_M) \\ \vdots & \vdots & \ddots & \vdots \\ \boldsymbol{x}(\theta_M)\boldsymbol{x}^H(\theta_1) & \boldsymbol{x}(\theta_M)\boldsymbol{x}^H(\theta_2) & \cdots & \boldsymbol{x}(\theta_M)\boldsymbol{x}^H(\theta_M) \end{bmatrix}\right\},$$

$$\boldsymbol{R_y} = E\{\boldsymbol{y}\boldsymbol{y}^H\} = \boldsymbol{U}^H\boldsymbol{R_{xs}}\boldsymbol{U}, \tag{F-1}$$

$$\boldsymbol{U}=\begin{bmatrix} \boldsymbol{v}(\theta_1) & 0 & \cdots & 0 \\ 0 & \boldsymbol{v}(\theta_2) & \vdots & 0 \\ \vdots & \vdots & \ddots & \vdots \\ 0 & 0 & \cdots & \boldsymbol{v}(\theta_M) \end{bmatrix}.$$

Using the method in Section 6.2.2, the corresponding stacked *MK×1* ES coherent signal steering vector is reconstructed as

$$\tilde{\boldsymbol{v}}_{\boldsymbol{ss}} = \boldsymbol{U}\boldsymbol{q}_{\boldsymbol{y}1} = \begin{bmatrix} \boldsymbol{q}_{\boldsymbol{y}1}(1)\boldsymbol{v}(\theta_1) \\ \boldsymbol{q}_{\boldsymbol{y}1}(2)\boldsymbol{v}(\theta_2) \\ \vdots \\ \boldsymbol{q}_{\boldsymbol{y}1}(M)\boldsymbol{v}(\theta_M) \end{bmatrix}, \tag{F-2}$$

where $\boldsymbol{q}_{\boldsymbol{y}1}(m)$ is the *m*-th element in $\boldsymbol{q}_{\boldsymbol{y}1}$. It is also can be written as

$$\tilde{\boldsymbol{v}}_{\boldsymbol{ss}} = \boldsymbol{U}\boldsymbol{U}^H\boldsymbol{q}_{1s} = \begin{bmatrix} \boldsymbol{v}(\theta_1)\boldsymbol{v}^H(\theta_1)\boldsymbol{q}_{1s}(\theta_1) \\ \boldsymbol{v}(\theta_2)\boldsymbol{v}^H(\theta_2)\boldsymbol{q}_{1s}(\theta_2) \\ \vdots \\ \boldsymbol{v}(\theta_M)\boldsymbol{v}^H(\theta_M)\boldsymbol{q}_{1s}(\theta_M) \end{bmatrix}, \tag{F-3}$$

where $\boldsymbol{q}_{1s}(\theta_m)$ is the principal eigenvector of $\boldsymbol{R_x}(\theta_m)$, and the corresponding *KM×KM* ES covariance matrix can be estimated as

$$\tilde{\boldsymbol{R}}'_{\boldsymbol{xs}} = \tilde{\sigma}_s^2\tilde{\boldsymbol{v}}_{ss}\tilde{\boldsymbol{v}}_{ss}^H + \tilde{\sigma}_n^2\boldsymbol{I}_{MK\times MK}. \tag{F-4}$$

Similar to the omni-directional case discussed earlier, ideally, if $\tilde{\boldsymbol{v}}_{\boldsymbol{ss}}$ is coherent with $\boldsymbol{q}_{1s}$, then the ES signal subspace can be well reconstructed. By applying the approach in

Section 6.2.2.2, the reconstructed stack ES covariance matrix is an $MK \times MK$ matrix and can be denoted as an $M \times M$ block matrix, each block is a $K \times K$ matrix. For example, the m-th block is given by

$$\widetilde{\boldsymbol{R}}'_{\boldsymbol{xs}(m)} = \tilde{\sigma}_s^2 \left|\boldsymbol{q}_{\boldsymbol{y}1}(m)\right|^2 \boldsymbol{v}(\theta_{\mathrm{m}})\boldsymbol{v}^H(\theta_{m1}), \tag{F-5}$$

Thus the averaging processing is given by

$$\widetilde{\boldsymbol{R}}'_{\boldsymbol{x}} = \frac{1}{M}\sum_{m=1}^{M} \tilde{\sigma}_s^2 \left|\boldsymbol{q}_{\boldsymbol{y}1}(m)\right|^2 \boldsymbol{v}(\theta_{\mathrm{m}})\boldsymbol{v}^H(\theta_{m1}) + \tilde{\sigma}_n^2 \boldsymbol{I}_{K\times K}. \tag{F-6}$$

An example is shown here, three directionally transmitted coherent signals are incident on an array in directions of 8.23°, 9.44° and 15°, with SNRs equal to 10 dB, 5 dB and 10 dB at any single receiver respectively, with correlations between the signals as $\rho_{12} = e^{i}$, $\rho_{13} = 1$ and $\rho_{23} = e^{-i}$. The ULA consists of 64 receivers, $d = 0.5\lambda$, and 20 directional Tx/Rx beams equally spread in a sector of [1°, 20°] are used. The stacked ES covariance matrix estimated as (F-4) and then averaged along its main diagonal as (F-5) and (F-6). The result of applying MUSIC algorithm to the averaged matrix is plotted in Figure F-1. Three peaks appear at on are 8°, 9.88° and 15°. Only the DOA (15°) coincides with the beam centre is correct.

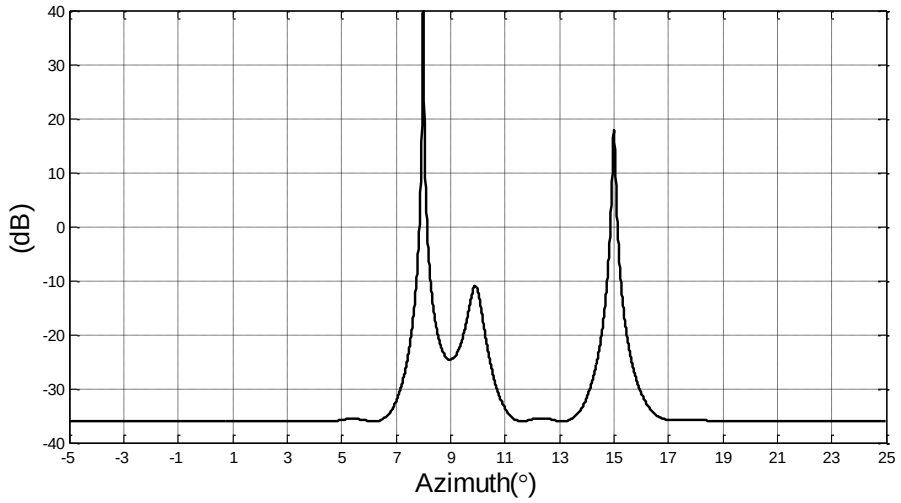

Figure F-1: An example of applying MUSIC algorithm to a matrix averaging over reconstructed directional transmission ES covariance matrices.

Recall (4-24), $\boldsymbol{U}$ is a diagonal block matrix and in (6-71), $\boldsymbol{U}\boldsymbol{U}^H$ is a projection operator and it projects the one dimension BS signal subspace, $\boldsymbol{q}_{\boldsymbol{y}1}$, to each beam, so $\widetilde{\boldsymbol{v}}_{\boldsymbol{ss}}$ is a stack of M estimated $K \times 1$ vectors, each of which is a weighted ES steering vector in each of the beam directions. For example, the m-th vector is given by $\boldsymbol{v}(\theta_m)\boldsymbol{v}^H(\theta_m)\boldsymbol{q}_1(\theta_m)$, where $\boldsymbol{q}_1(\theta_m)$ is the principal eigenvector of $\boldsymbol{R}_{\boldsymbol{x}}(\theta_m)$. Obviously, for the case that a group of coherent signals are incident, $\boldsymbol{v}(\theta_m)\boldsymbol{v}^H(\theta_m)\boldsymbol{q}_1(\theta_m)$ is not coherent with

$\boldsymbol{q}_1(\theta_m)$. Thus, if $\widetilde{\boldsymbol{v}}_{\boldsymbol{ss}}$ is used to reconstruct $\boldsymbol{R}_{\boldsymbol{x}}(\theta_m)$, the principal eigenvector of the reconstructed ES covariance matrix is coherent with $\boldsymbol{v}(\theta_m)$. Thus the subspace method only works for the case where the DOAs of the coherent signals are located at the MRAs of beams; otherwise it does not indicate the correct DOAs and peaks would appear at or near to the beam centres close to the DOAs.

Bibliography

[1] I. S. Merrill, *Radar Handbook*, 1990.

[2] R. M. Foster, "Directive diagrams of antenna arrays", Bell System Tech. J., vol. 5, pp. 292307, April 1926.

[3] H. T. Friis, and C. B. Feldman, "Multiple Unit Steerable Antenna for Short-Wave Reception," Proceedings of the Institute of Radio Engineers, 257, July 1937, pp. 841917.

[4] H. D. Griffiths, N. J. Willis, "Klein Heidelberg-The first modern bistatic radar system", *IEEE Trans*. Aerospace and Electronic Systems, vol. 46, no. 4, pp. 15711588, 2010.

[5] C. A. Fowler, "Rad Lab, Luie Alvarez, and the development of the GCA Radar Landing System: A Memoir", *IEEE Aerospace and Electronic Systems Magazine, vol. 23, no. 5*, pp. A-1A-16, May 2008.

[6] J. Hasch, E. Toprak, R. Schnabel, T. Zwick, R. Weigel, C. Waldschmidt, "Millimeter-wave technology for automotive radar sensors in the 77 GHz frequency band", *IEEE Trans. Microw. Theory Techn.*, vol. 60, no. 3, pp. 845860, Mar. 2012.

[7] G. E. Stimson, *Introduction to Airborne Radar*, NJ, Mendham: SciTech, 1998.

[8] Michael P Hayes, Peter T Gough, "Synthetic aperture sonar: a review of current status", *IEEE Journal of Oceanic Engineering*, vol. 34, no. 3, pp. 207224, 2009.

[9] P. J. Napier, A. R. Thompson, R. D. Ekers, "The very large array: Design and performance of a modern synthesis radio telescope", *Proc. IEEE*, vol. 71, pp. 12951322, 1983.

[10] S. Rost, C. Thomas, "Array seismology: Methods and applications", Rev. Geophys., vol. 40, no. 3, pp. 1008, Dec. 2002.

[11] D. S. Zrnić, V. M. Melnikov, R. J. Doviak, R. Palmer, "Scanning Strategy for the Multifunction Phased-Array Radar to Satisfy Aviation and Meteorological Needs", *IEEE Geoscience and Remote Sensing Letters*, vol. 12, no. 6, pp. 1204-1208, June 2015.

[12] W. C. Brown, "The history of power transmission by radio waves", *IEEE Trans*. Microw. Theory Tech., vol. 32, no. 9, pp. 8085, Sept. 1984.

[13] L. C. Godara, "Application of antenna arrays to mobile communications Part i: Performance Improvement Feasibility and System Considerations", *Proc. IEEE*, vol.85, pp.1031-1060, July 1997.

[14] J. L. Flanagan, J. D. Johnson, R. Zahn, G. W. Elko, "Computer-steered microphone arrays for sound transduction in large rooms", J. Acoust. Soc. Amer., vol. 78, no. 5, pp. 15081518, Nov. 1985.

[15] J. Sun, E. Timurdogan, A. Yaacobi, E. S. Hosseini, M. R. Watts, "Large-scale nanophotonic phased array", *Nature*, vol. 493, no. 7431, pp. 195199, Jan. 2013.

[16] H. Wan, P. VanBaren, E. S. Ebbini, C. A. Cain, "Ultrasound surgery: Comparison of strategies using phased array systems", *IEEE Trans*. UFFC, vol. 43, no. 6, pp. 10851098, Nov. 1996.

[17] H. Krim and M. Viberg, "Two decades of array signal processing: The parametric approach," *IEEE Signal Processing Mag*., pp. 67–94, July 1996.

[18] J. Capon, "High resolution frequency-wavenumber spectrum analysis", *Proc. IEEE*, vol. 57, no.8 pp. 14081418, Aug. 1969.

[19] O. L. Frost, "An algorithm for linearly constrained adaptive array processing", *Proceedings of the IEEE*, vol. 60, no. 8, pp. 926935, Aug. 1972.

[20] M. H. Er, A. Cantoni, "Derivative constraints for broad-band element space antenna array processors", *IEEE Trans. on ASSP*, vol. ASSP-31, pp. 13781393, Dec. 1983.

[21] M. H. Er, A. Cantoni, "An alternative formulation for an optimum beamformer with robustness capability", *Proc. Inst. Elect. Eng. Radar Sonar Navig.*, pp. 447460, Oct. 1985.

[22] R.O Schmidt. "Multiple Emitter Location and Signal Parameter Estimation", *IEEE Trans. Antennas Propagat.*, Vol. AP-34, pp. 276280, Mar. 1986.

[23] A. J. Barabell, "Improving the resolution performance of eigenstructure-based direction-finding algorithms", *Proc. ICASSP*, pp. 336339, 1983.

[24] R. Roy, T. Kailath, "ESPRIT Estimation of signal parameters via rotational invariance techniques", *IEEE Trans. Acoust. Speech Signal Processing*, vol. 37, pp. 984995, July 1989.

[25] D. A. Gray, "Formulation of the maximum signal to noise ratio array processor in beam space", *The Journal of the Acoustical Society of America*, vol. 72, no.4, pp. 11951201, Oct. 1982.

[26] D. A. Gray, "Output statistics of the sample matrix inverse beamformer implemented in beam space", *The Journal of the Acoustical Society of America*, vol. 80, no. 6, pp. 17371739, Dec. 1986.

[27] H. B. Lee and M. S. Wengrovitz, "Resolution threshold of beamspace MUSIC for two closely spaced emitters", *IEEE Trans. Acoustics, Speech and Signal Processing*, vol. 38, no. 9, pp. 15451559, Sep. 1990.

[28] P. Stoica and A. Nehorai, "Comparative performance study of element-space and beam-space MUSIC estimators", *Circuits, Systems and Signal Processing*, vol. 10, no. 3, pp. 285292, 1991.

[29] G. Xu, S. D. Silverstein, R. H. Roy, and T. Kailath, "Beamspace ESPRIT", *IEEE Trans. Signal Processing*, vol. 42, no. 2, pp. 349356, Feb. 1994.

[30] H. L. Van Trees, *Detection, Estimation, and Modulation Theory, Part IV, Optimum Array Processing*. New York: Wiley, 2002.

[31] X. L. Xu and K. M. Buckley, "An analysis of beam-space source localization", *IEEE Trans. Signal Processing*, vol. 41, no. 1, pp. 501–504, Jan. 1993.

[32] A. Hassanien, S. A. Elkader, A. B. Gershman, and K. M. Wong, "Convex optimization based beam-space preprocessing with improved robustness against out-of-sector sources", *IEEE Trans. Signal Processing*, vol. 54, no. 5, pp. 1587–1595, May 2006.

[33] A. Hassanien and S. A. Vorobyov, "A Robust Adaptive Dimension Reduction Technique With Application to Array Processing", *IEEE Signal Processing Letters*, vol. 16, no. 1, pp. 2225, Jan. 2009.

[34] D. Sidorowich and A. Gershman, "Two-dimensional wideband interpolated root-MUSIC applied to measured seismic data", *IEEE Trans. Signal Processing*, vol. 46, pp. 22632267, 1998.

[35] C.-I. C. Nilsen and I. Hafizovic, "Beamspace adaptive beamforming for ultrasound imaging," *IEEE Trans. Ultrason. Ferroelectr. Freq.Control*, vol. 56, no. 10, pp. 2187–2197, Oct. 2009.

[36] J. P.Asen, J. I. Buskenes, C.-I. C. Nilsen, A. Austeng and S. Holm, "Implementing Capon beamforming on a GPU for real-time cardiac ultrasound imaging", *IEEE Trans*actions on Ultrasonics, Ferroelectrics, and Frequency Control, vol.61, no. 1, pp. 7685, Jan. 2014.

[37] S. W. Ellingson and W. Cazemier, "Efficient multibeam synthesis with interference nulling for large arrays", *IEEE Trans.* Antennas Propag., vol. 51, pp. 503–511, Mar. 2003.

[38] R. T. Behrens and L. L. Scharf, "Signal processing applications of oblique projection operators", *IEEE Trans. Signal Processing*, vol. 42, no.6, pp. 1413–1424, Jun. 1994.

[39] X. L. Xu and K. M. Buckley, "A comparison of element and beam space spatial-spectrum estimation for multiple source clusters", *Proc. Int. Conf. Acoustics, Speech, Signal Processing (ICASSP)*, pp. 26432646 vol.5,1990.

[40] X. L. Xu and K. M. Buckley, "A statistical performance comparison of MUSIC in element-space and beam-space", *Proc. Int. Conf. Acoustics, Speech, Signal Processing (ICASSP)*, pp. 21242127, 1989.

[41] P. Forster and G. Vezzosi, "Application of spheroidal sequences to array processing", *Proc. Int. Conf. Acoustics, Speech, Signal Processing (ICASSP)*, pp. 22682271, 1987.

[42] G. Bienvenu and L. Kopp, "Decreasing high-resolution method sensitivity by conventional beamformer preprocessing", in *Proc. ICASSP '*84, pp. 33.2.14. Apr. 1984.

[43] J. Le Cadre, "Parametric methods for spatial signal processing in the presence of unknown colored noise field", *IEEE Trans. Acoust., Speech, Signal Process.*, vol. 37, no. 7, pp. 965983, 1989.

[44] H. Ye and R. D. DeGroat, "Maximum likelihood DOA estimation and asymptotic Cramér-Rao bounds for additive unknown colored noise", *IEEE Trans. Signal Processing*, vol. 43, no. 4, pp. 938949, 1995.

[45] C. Byrne and A. Steele, "Sector-focused stability for high resolution array processing", *Proc. IEEE Int. Conf. Acoustics, Speech, Signal Processing (ICASSP)*, pp. 23402343, 1987.

[46] A. K. Steele, "Performance comparison of high resolution bearing estimation algorithms using simulated and sea test data", *J. Oceanic Engineering*, vol. 18, pp. 438446, 1993.

[47] T.J. Shan, M. Wax, and T. Kailath. "On spatial smoothing for directions of arrival estimation of coherent signals", *IEEE Trans. on Acoustic, Speech and Signal Processing*, vol. 33(4):806811, April 1985.

[48] J. A. Cadzow, "A high resolution direction-of-arrival algorithm for narrowband coherent and incoherent sources", *IEEE Trans. Acoust., Speech, Signal Process.*, vol. 36, no. 7, pp. 965979, July 1988.

[49] S. U. Pillai and B. H. Kwon, "Forward/backward spatial smoothing for coherent signal identification", *IEEE Trans. Acoust., Speech, Signal Processing*, vol. 37, pp. 815, Jan. 1989.

[50] B. Widrow, K. M. Duvall, R. P. Gooch and W. C. Newman, "Signal cancellation phenomena in adaptive antennas: Causes and cures", *IEEE Trans. Antennas Propagat*., vol. AP-30, pp. 469478, May 1982.

[51] A. K. Luthra, "A solution to the adaptive nulling problem with a look direction constraint in the presence of coherent jammers", *IEEE Trans. Antennas Propagat.*, vol. 34, pp.702710, 1986.

[52] F.-M. Han and X.-D. Zhang, "An ESPRIT-like algorithm for coherent DOA estimation", *IEEE Antennas Wireless Propag. Lett.*, vol. 4, pp.443–446, Apr. 2005.

[53] Choi, Yang-Ho. "ESPRIT-based coherent source localization with forward and backward vectors", *IEEE Trans. Signal Processing*, vol.58, pp. 64166420, Dec. 2010.

[54] I. Ziskind and M. Wax, "Maximum likelihood localization of multiple sources by alternating projection", *IEEE Trans. Acoust., Speech, Signal Process.*, vol. 36, no. 10, pp. 1553–1560, Oct. 1988.

[55] P. Stoica and K. C. Sharman, "Maximum likelihood methods for direction-of-arrival estimation", *IEEE Trans. Acoust., Speech, Signal Processing*, vol. 38, pp.1132143, 1990.

[56] M. Viberg, B. Ottersten, and T. Kailath, "Detection and estimation in sensor arrays using weighted subspace fitting", *IEEE Trans. Signal Processing*, vol. 39, pp. 24362449, 1991.

[57] P. Stoica and A. B. Gershman, "Maximum-likelihood DOA estimation by data-supported grid search", *IEEE Signal Process. Lett.*, vol. 6, no. 10, pp. 273275, 1999.

[58] H. Wang and M. Kaveh, "Coherent signal-subspace processing for the detection and estimation of angles of arrival of multiple wide-band sources", *IEEE Trans. Acoust., Speech, Signal Processing*, vol. ASSP-33, pp. 823831, Aug. 1985.

[59] P. Kabal S. Valaee, "The optimal focusing subspace for coherent signal subspace processing", *IEEE Trans. Signal Processing*, vol. 44, no. 3, pp. 752–756, March 1996.

[60] LU M., HE Z.Y., "Adaptive beamforming using split-polarity transformation for coherent signal and interference", *IEEE Trans. Antennas Propag*., vol. 41, no. 3, pp. 314–324, Mar. 1993.

[61] W. F. Gabriel, "Spectral analysis and adaptive array super resolution techniques," *Proc. IEEE*, vol. 68, pp. 654-666, 1980.

[62] F. Haber and M. Zoltowski, "Spatial spectrum estimation in a coherent signal environment using an array in motion", *IEEE Trans. Antennas Propag.*, Special Issue on Adaptive Antenna Processing Systems, vol. AP-34, pp. 301310, 1986.

[63] Yang Y., Wan C., Sun C., Wang Q., "DOA estimation for coherent sources in beam space using spatial smoothing". *IEEE Trans. on ICICS-PCM*, vol.2, pp.10281032 Dec. 2003.

[64] T. J. Shan, A. Paulraj, and T. Kailath, "On smoothed rank profile tests in eigen structure methods for directions-of-arrival estimation", *IEEE Trans. Acoust. Speech Signal Processing*, vol. ASSP-35, no. 10, pp. 13771385, 1987.

[65] J. H. Cozzens and M. J. Sousa, "Source enumeration in a correlated signal environment", *IEEE Trans. Signal Processing*, vol. 42, no. 2, pp. 304317, Feb. 1994.

[66] Y.-H. Choi "Repeated blocking based robust beamforming for coherent interference cancellation", *Digit. Signal Process*., 36 (2) (2015), pp. 39–45.

[67] R. D. DeGroat, E. M. Dowling, and D. A. Linebarger, "The constrained MUSIC problem", *IEEE Trans. Signal Processing*, vol. 41, pp. 14451449, Mar. 1993.

[68] D. A. Linebarger, R. D. DeGroat, E. M. Dowling, P. Stoica, G. L. Fudge. "Incorporating a priori information into MUSIC-algorithms and analysis", *Signal Processing*. 1995; 46(1):85104.

[69] S. K. Oh and C. K. Un, "A sequential estimation approach for performance improvement of eigenstructure-based methods in array processing", *IEEE Trans. Signal Processing*, vol. 41, pp. 457–463, Jan. 1993.

[70] P. Stoica, P. Handel, and A. Nehorai, "Improved sequential MUSIC", *IEEE Trans*. Aerosp. Electron. Syst., pp. 1230–1239, Oct. 1995.

[71] P. Stoica and A. Nehorai, "MUSIC maximum likelihood and Cramer-Rao bound", *IEEE Trans. Acoust. Speech Signal Processing*, vol. 37, no. 5, pp. 720741, May 1989.

[72] P. Stoica, E. G. Larsson and A. B. Gershman, "The stochastic CRB for array processing: Textbook derivation", *IEEE Signal Processing Lett.*, vol. 8, no. 5, pp. 148150, May 2001.

[73] M. Wax and 1. Ziskind, "Detection of the number of coherent signals by the MDL principle", *IEEE Trans. Acoust. Speech Signal Processing*, vol. 37, pp. 11901196, Aug. 1989.

[74] M. L. McCloud and L. L. Scharf, "A new subspace identification algorithm for high resolution DOA estimation", *IEEE Trans. Antennas Propag*., vol. 50, pp. 1382–1390, Oct. 2002.

[75] X. Xu, Z. Ye and Y. Zhang, "DOA estimation for mixed signals in the presence of mutual coupling", *IEEE Trans. Signal Processing*, vol. 57, no. 9, pp. 35233532, Sep. 2009.

[76] R. Boyer and G. Bouleux, "Oblique projections for direction-of-arrival estimation with prior knowledge", *IEEE Trans. Signal Processing*, vol. 56, no. 4, pp. 13741387, 2008.

[77] S. S. Reddi and A. B. Gershman, "An alternative approach to coherent source location problem", *Signal Process.*, vol. 59, no. 2, pp. 221233, 1997.

[78] L. C. Godara, "The effect of phase-shift errors on the performance of an antenna-array beamformer", *IEEE J. Ocean. Eng.*, vol. OE-10, pp. 278–284, July 1985.

[79] H. Cox, R. M. Zeskind, and M. M. Owen, "Robust adaptive beamforming", *IEEE Trans. Acoust., Speech, Signal Processing*, vol. ASSP-35, pp. 1365–1376, Oct. 1987.

[80] D. D. Feldman and L. J. Griffiths, "A projection approach for robust adaptive beamforming", *IEEE Trans. Signal Processing*, vol. 42, pp. 867–876, Apr. 1994.

[81] A. B. Gershman, "Robust adaptive beamforming in sensor arrays", *Int. J. Electron. Commun*., vol. 53, no. 6, pp. 305–314, 1999.

[82] S. A. Vorobyov, A. B. Gershman, Z.-Q. Luo, "Robust adaptive beamforming using worst-case performance optimization", *IEEE Trans. Signal Processing*, vol. 51, no. 2, pp. 313324, Feb. 2003.

[83] S. Shahbazpanahi, A. B. Gershman, Z.-Q. Luo, and K. M. Wong, "Robust adaptive beamforming for general-rank signal models", *IEEE Trans. Signal Processing*, vol. 51, pp. 2257–2269, Sep. 2003.

[84] R. G. Lorenz and S. P. Boyd, "Robust minimum variance beamforming", *IEEE Trans. Signal Processing*, pp. 1684-1696, May 2005.

[85] J. Li, P. Stoica and Z. Wang, "On robust Capon beamforming and diagonal loading", *IEEE Trans. Signal Processing*, pp. 17021714, July 2003.

[86] J. Li, P. Stoica and Z. Wang, "Doubly constrained robust Capon beamformer", *IEEE Trans. Signal Processing*, vol. 52, pp. 2407–2423, Sep. 2004.

[87] A. Khabbazibasmenj, S. A. Vorobyov and A. Hassanien, "Robust adaptive beamforming based on steering vector estimation with as little as possible prior information", *IEEE Trans. Signal Processing*, vol. 60, pp. 29742987, Jun. 2012.

[88] T. Yang, T. Su, W.T. Zhu and L. Zhang, "Robust adaptive beamforming using beamspace steering vector estimation", *Electronics Letters*, vol. 49, pp. 1201-1203, September, 2013.

[89] V. Katkovnik, "A new concept of adaptive beamforming for moving sources and impulse noise environment", *Signal Process*., vol. 80, pp. 18631882, Sept. 2000.

[90] S. D. Hayward, "Adaptive beamforming for rapidly moving arrays", *Proceedings of* the CIE International Conference on Radar, pp. 480483, 1996-Oct.-8-10.

[91] Y. Jin and B. Friedlander, "Beamspace array processing for moving sources", in Conference Record of the Thirty-Sixth Asilomar Conference on Signals, Systems and Computers, vol. 1, Nov. 2002.

[92] A. J. Weiss, B. Friedlander, "Preprocessing for direction finding with minimal variance degradation", *IEEE Trans. Signal Processing*, vol. 42, pp. 14781485, June 1994.

[93] S. Anderson, A. Nehorai, "Optimal dimension reduction for array processing—Generalized", *IEEE Trans. Signal Processing*, vol. 43, no. 8, pp. 20252027, Aug. 1995.

[94] R. Palumbo, E. Knapp, K. Wood, D. J. McLaughlin, C. McCarroll, and S. J. Frasier, "Phase-tilt weather radar: Calibration and preliminary results", 2013 *International Conference on Radar*, Adelaide, SA, 2013, pp. 429433.

[95] C. D. Meyer, *Matrix Analysis and Applied Linear Algebra*, PA, Philadelphia: SIAM, 2000.

[96] A. B. Gershman, U. Nickel and J. F. Böhme (Bohme), "Adaptive beamforming algorithms with robustness against jammer motion", *IEEE Trans. Signal Processing*, vol. 45, pp. 18781885, July 1997.

[97] A. B. Gershman, E. Nemeth and J. F. Böhme, "Experimental performance of adaptive beamforming in a sonar environment with a towed array and moving interfering sources", *IEEE Trans. Signal Processing*, vol. 48, no. 1, pp. 246250, Jan. 2000.

[98] R. Penrose, "A generalized inverse for matrices", Proc. Cambridge Philosoph. Soc., vol. 51, pp. 406413, 1955.

[99] M. Sarcione, J. Mulcahey, D. Schmidt, K. Chang, M. Russell, R. Enzmann, P. Rawlinson, W. Guzak, R. Howard, M. Mitchell, "The design development and testing of the THAAD (theater high altitude area defense) solid state phased array (formerly ground based radar)", *Proc. IEEE Int. Symp. on Phased Array Syst. and Technol.*, pp. 260265, Oct, 1996.

[100] R. A. Palumbo, W. A. Al-Ashwal, B. Ferguson, C. McCarroll, and D. J. McLaughlin, "Weather and bushfire observation using low cost X-band phased array radars", in International Conference on Radar (Radar), 2013, pp. 309-314.

[101] R. A. Palumbo, W. A. Al-Ashwal, D. Gray, S. Frasier, D. McLaughlin, E. Knapp, B. Ferguson, and C. McCarroll, "Polarimetric observations of prescribed bushfires in South Australia using an X-band phased array radar", in 36th Conference on Radar Meteorology, 2013.

[102] Anne Ferreol, Pascal Larzabal, Mats Viberg, "Performance Prediction of Maximum-Likelihood Direction-of-Arrival Estimation in the Presence of Modeling Errors", *IEEE Trans. Signal Processing*, vol. 56, pp. 47854793, 2008.

[103] Anne Ferreol, Pascal Larzabal, Mats Viberg, "Statistical Analysis of the MUSIC Algorithm in the Presence of Modeling Errors Taking Into Account the Resolution Probability", *IEEE Trans. Signal Processing*, vol. 58, pp. 4156-4166, 2010.

[104] V. U. Reddy, A. Paulraj, T. Kailath, "Performance analysis of the optimum beamformer in the presence of correlated sources and its behavior under spatial smoothing", *IEEE Trans. Acoust. Speech Signal Processing*, vol. ASSP-35, pp. 927936, July 1987.

[105] M. D. Zoltowski, "On the performance of the MVDR beamformer in the presence of correlated interference", *IEEE Trans. Acoust. Speech Signal Processing*, vol. 36, pp. 945947, June 1988.

[106] S. U. Pillai, *Array Signal Processing*, Springer Verlag, pp. 5051, 1989.

[107] M. D. Zoltowski, C. P. Mathews, "Direction finding with uniform circular arrays via phase mode excitation and Beamspace Root-MUSIC", *Proc. IEEE Int. Conf. Acoust. Speech Signal Processings*, vol. 5, pp. 245248, 1992.

[108] C. P. Mathews, M. D. Zoltowski, "Eigenstructure techniques for 2-D angle estimation with uniform circular arrays", *IEEE Trans. Signal Processing*, vol. 42, pp. 23952407, Sept. 1994.

[109] F. Belloni, V. Koivunen, "Beamspace transform for UCA: Error analysis and bias reduction", *IEEE Trans. Signal Processing*, vol. 54, no. 8, pp. 30783089, Aug. 2006.

[110] B. Friedlander, "The root-MUSIC algorithm for direction finding with interpolated arrays", *Signal Process.*, vol. 30, pp. 1529, 1993.

[111] M. Viberg, P. Stoica, B. Otterston, "Array processing in correlated noise fields based on instrumental variables and subspace fitting", *IEEE Trans. Signal Processing*, vol. 43, no. 5, pp. 11871199, May 1995.

[112] M. C. Doğan, J. M. Mendel, "Applications of cumulants to array processing Part I: aperture extension and array calibration", *IEEE Trans. on Signal Processing*, pp. 12001216, May 1995.

[113] E. Gonen, J. Mendel, "Application of cumulants to array processing Part IV: Direction-finding in coherent signals case", *IEEE Trans. Signal Processing*, vol. 45, pp. 22652276, Sept. 1997.

[114] P. Chevalier, L. Albera, A. Ferreol, P. Comon, "On the virtual array concept for higher order array processing", *IEEE Trans. Signal Processing*, vol. 53, pp. 12541271, Apr. 2005.

[115] J. Yin, T. Chen, "Direction-of-arrival estimation using a sparse representation of array covariance vectors", *IEEE Trans. Signal Processing*, vol. 59, no. 9, pp. 44894493, Sep. 2011.

[116] D. Malioutov, M. Cetin, A. S. Willsky, "A sparse signal reconstruction perspective for source localization with sensor arrays", *IEEE Trans. Signal Processing*, vol. 53, no. 8, pp. 30103022, Aug. 2005.

[117] A. T. Moffet, "Minimum-redundancy linear arrays", *IEEE Trans. Antennas Propagat.*, vol. AP-16, pp. 172–175, 1968.

[118] S. Haykin, J. P. Reilly, V. Kezys, and E. Vertatschitsch, "Some aspects of array signal processing", *Proc. Inst. Elect. Eng., pt.* F, vol. 139, no. 1, pp. 1–26, 1992.

[119] Palumbo, Robert A. Jr, "Applications in Low-Power Phased Array Weather Radars", (2016). D*octoral Dissertations*.594. http://scholarworks.umass.edu/dissertations_2/594

[120] Y. U. Lee, J. Choi, I. song, S. R. Lee, "Distributed source modeling and direction-of-arrival estimation techniques", *IEEE Trans. Signal Processing*, vol. 45, pp. 960-969, Apr. 1997.

[121] O. Besson and P. Stoica, "Decoupled estimation of DOA and angular spread for a spatially distributed source," *IEEE Trans. Signal Processing*, vol. 48, pp. 1872–1882, July 2000.

[122] E. Fishler, A. Haimovich, R. Blum, L. Cimini, D. Chizhik, R. Valenzuela, "Spatial diversity in radars - Models and detection performance" ,*IEEE Trans. Signal Processing*, vol. 54, pp. 823-838, 2006.